Degradation studies of pharmaceutical drugs using fixed bed reactor incorporating dual effect of photocatalysis and photo-Fenton

Thesis

Submitted in the partial fulfillment for the award of the degree of

Doctor of Philosophy

In

CHEMICAL ENGINEERING

By:

STEFFI TALWAR

(Registration No. -901601002)

Under the guidance of

(Dr. Vikas K. Sangal)
Associate Professor
Department of Chemical Engineering
Malaviya National Institute of
Technology, Jaipur, India

(Dr. Anoop K. Verma)
Associate Professor
School of Energy & Environment
Thapar Institute of Engineering &
Technology, Patiala, India

DEPARTMENT OF CHEMICAL ENGINEERING

THAPAR INSTITUTE OF ENGINEERING AND TECHNOLOGY

(Deemed to be University)

PATIALA-147004, PUNJAB, INDIA

September, 2020

CERTIFICATE

This is to certify that the thesis entitled "**Degradation studies of pharmaceutical drugs using fixed bed reactor incorporating dual effect of photocatalysis and photo-Fenton**" that is being submitted by **Steffi Talwar**, in partial fulfillment for the award of Ph.D. in the Department of Chemical Engineering, Thapar Institute of Engineering and Technology (Deemed to be University), Patiala, India, for the award of degree of '**Doctor of Philosophy'** is a record of bonafide research work carried out by her under our guidance and supervision and has fulfilled the requirements for the submission of this thesis, which to our knowledge has reached the requisite standard.

The results embodied in this thesis have not been submitted to any other University or Institute for the award of any degree or diploma.

(Dr. Vikas K. Sangal)
Supervisor
Associate Professor
Department of Chemical Engineering
Malaviya National Institute of Technology, Jaipur, India

(Dr. Anoop K. Verma)
Supervisor
Associate Professor
School of Energy & Environment
Thapar Institute of Engineering & Technology (Deemed to be University), Patiala, India

ACKNOWLEDGMENTS

Undertaking this Ph.D. has been a truly life-changing experience for me. My experience at T.I.E.T. has been nothing short of amazing. I have been provided with new opportunities, which were advantageous to me. My Ph.D. would not have been possible without the support and guidance that I received from many people.

First of all, my heartfelt thanks to the almighty for his abundant blessing showered on me throughout this endeavor to complete this successful work of mine.

It's my pleasure to acknowledge my indebtedness to my supervisors Dr. Anoop K.Verma Associate Professor, School of Energy and Environment, TIET, Patiala and Dr. Vikas K. Sangal, Associate Professor, Department of Chemical Engineering, MNIT, Jaipur for their unflinching support & guidance regarding basic principles, constructive ideas that made it possible for me to be successful in the initiation and completion of my research work. I am thankful for their encouragement to keep going and constantly learn new things and correcting my mistakes along the way.

I would like to thank Dr. H. Bhunia, Head of the Department of Chemical Engineering and Dr. R.K. Gupta, the former Head of the Department of Chemical Engineering for providing me an opportunity to join the esteemed institution, gave access to research facilities and at all times been very supportive and accommodating. I would also express my gratitude to Dr. Amit Dhir, the Head of School of Energy and Environment for providing me lab and all the research facilities during my research work. I owe a deep sense of gratitude to Professor R. Siddique, Dean, Research and Sponsored Projects, TIET University, Patiala, India and Professor O.P. Pandey, former Dean, Research and Sponsored Projects, TIET University, Patiala, India, for their invaluable support.

I express my deepest gratitude to my doctoral committee members Dr. J. P. Kushwaha, Dr. S. Barman and Professor O.P. Pandey for their constant encouragement, insightful comments and their keen interest in me at every stage of my research work. I would also like to thank the staff of the Department of Chemical Engineering and School of Energy and Environment for their kind

cooperation and support. This research work would have not been completed without the help received from SAI Labs, Patiala. My heartfelt thanks to my seniors Dr. Palak Bansal, Dr. Jayishnu Singla, Dr. Himadri, Dr. Parminder Kaur, Dr. Ravneet Kaur, Dr. Sehaspreet, Ms. Metali Sarkar, Ms. Meenakshi for their support and guidance. I would also like to thank my lab mates Sonam, Ina Thakur, Shelly, Navneet, Alisha, Kritika for the cheerful discussion and help. I will cherish all the warmth shown by them.

Finally, I would like to express my gratitude to my parents and my brother for their unconditional affection and moral support and blessings bestowed upon me for the successful completion of my thesis. Your prayer for me was what sustained me thus far. I would at the end like to express my thanks to Buddy and Donald for providing the joy and happiness during my work.

Steffi Talwar

ABSTRACT

Developing countries, like India, has emerged as the world's third largest producer of pharmaceutical drugs. Large amount of these pharmaceuticals have been detected in the aquatic systems over the past few years. Failures of conventional technologies have prompted researchers to work in some advanced areas for handling these kinds of contaminants. The Advanced Oxidation Process (AOPs) like photo-Fenton and photocatalysis have gained wide popularity among the researchers due to their capability of treating wide range of pollutants. But certain limitations like increase in the treatment time, electron hole recombination, separation and recovery of the catalyst, high dosage of oxidant, generation of the iron sludge, suitable reactor designing have posed hurdles in the scale-up path of these techniques.

In the present study the best efforts have been made to overcome these hurdles faced by the individual AOPs (photo-Fenton and photocatalysis) by introducing a novel concept of fixed-bed in-situ dual effect. The work focuses on the incorporating the dual effect of photocatalysis and photo-Fenton using composite beads for the degradation of pharmaceutical drugs i.e. Phenazone (PHZ) and Metronidazole (MTZ) in fixed mode.

The study has been executed by fabricating a composite made up of Fuller's earth (FE) and Foundry sand (FS) with a coating of TiO_2. FE and FS being the natural source of iron has been used for the photo-Fenton reactions to take place. The leaching of iron from the composite support (in acidic conditions) along with the surface active TiO_2 layer executes the dual effect. For the study to execute two types of reactors i.e. batch reactor and continuous reactors were employed.

For the batch scale trials, two types of composite beads prepared of FE and FE+FS were employed for the degradation of PHZ. Although both type of beads showed the degradation but FE beads were not durable enough in terms of strength and stability hence, for further studies FE+FS beads were employed. These composite beads were used for the parametric optimization for the degradation of both the drugs PHZ and MTZ. Box Behnken design (BBD) has been employed for the optimization of various parameters. An artificial neural network model coupled with the genetic algorithm was employed for the optimization of various parameters for MTZ.Various parameters like the surface area covered in terms of number of beads, dosage of the oxidant, time, pH, the intensity of light were studied for the estimation of degradation efficiency. The in-situ dual

effect leads to 80% degradation of PHZ and 91% degradation of MTZ. Kinetics studies revealed the increase in the reaction rate constant (k) to 5 folds for PHZ, thus envisages degradation to be achieved at a faster pace. 81.37% of synergy was observed in the case of MTZ for the dual process. The variability in the recyclability studies varies as per the phase of the research work. As same composite beads were used for the complete study and no new composite beads were prepared during the research work. The beads were durable enough to be recycled for more than 70 recycles while maintaining their catalytic activity for both the processes. For the confirmation of catalytic activity of photocatalysis and photo-Fenton process even after recycles, various characterizations including XRD, SEM-EDS, FTIR, Raman and UV-DRS were performed.

The mineralization of the compounds PHZ and MTZ were confirmed in terms of reduction in COD, TOC and the formation of various ions like nitrates, nitrites and ammonical ions. The intermediates formed during the reaction were analyzed using GC-MS and the probable degradation mechanism was proposed for both PHZ and MTZ.

Pilot-scale fixed bed reactors employed in once-through mode were studied for the degradation of MTZ and PHZ. Same composite beads made of FE+FS were employed for encompassing the in-situ dual effect of photocatalysis and photo-Fenton. Pilot scale three reactors in series and compound parabolic concentrator (CPC) were employed for the studies. These reactors were studied in terms of approaching the plug plow for the better implementation of the process. The complete optimization studies were conducted for the pollutants (MTZ and PHZ). The extended recyclability of the beads were studied for >80 recycles and was confirmed from the characterizations. The complete mineralization of the compounds were also conducted. For the real time view of the dual process cost analysis has also been conducted. The overall cost for the treatment of 1L of solution came out to be less than 0.1 US $ which signifies its potential for commercial scale viabilities. The scale up cost analysis was also executed for real scale applications.

Further, for the authentication of the results of dual effect, the study has been extended to the real industrial wastewater. The study was conducted in batch mode and then was implemented in continuous mode. For the batch scale studies, the significant reduction in Chemical Oxygen demand (COD) (81%) along with the decrease in the treatment time by 60-70 min was observed as

compared to the exclusive processes of photo-Fenton and photocatalysis. Optimization of various parameters using continuous mode reactor has been studied in the sunlight and 75% reduction was observed after 5 h in recirculation mode.The study has also been extended to the plug flow approaching reactor in once through mode. 55% of COD removal after 45 minutes proves the effectiveness of the process using three reactors in series. Wastewater which was treated was evaluated to be non-toxic as verified from the GC-MS analysis as well as the Kirby-Bauer test. Various characterizations were performed to validate the importance of the dual effect (presence of iron as well as the activity of TiO_2). Recyclability of the catalyst even after subsequent recycles confirmed the economic efficacy of the process.

LIST OF FIGURES

LIST OF TABLES

TABLE OF CONTENTS

CHAPTER-1

INTRODUCTION

1.1. PHARMACEUTICALS AS A POLLUTANT

With a pace growing population, India is gearing up to become the foremost inhabited country by the subsequent decade surpassing China (Coale & Hoover, 2016). Increased population is causing great hindrance in the path of development and economic planning (Koumparoulis, 2015). With rising income inequality, there is an improper distribution of basic amenities like safe drinking water, proper sewage and sanitation systems, medical facilities and education (Lall, Lundberg, & Shalizi, 2008). These are the major concerns, especially in the rural and backward areas. With various health challenges and changing the epidemiological profiles of the people, India personifies an assuring international marketplace for the manufacturers of pharmaceuticals (Nag & Ghosh, 2013; K. D. Rao & Peters, 2015). India is seeming to become a strong contender of global pharmaceutical industries (Malhotra and Lofgren, 2004; Greene 2011). Indian firms are amidst the global leaders within the production of vaccines (Shah, 2012). With this increase in the development and availability of medicines, the consumption of antibiotics has increased by 103 % from 2000 to 2015 in India (Van Boeckel et al., 2014). The pharmaceuticals market of India has various characteristics, which make it more distinctive. The first includes, branded generic medicines dominating the retail market. Second, the indigenous companies have enjoyed a prevailing position driven by early investments and formulation development capabilities. Third, with increasing competition government is increasingly opening partnerships with private sectors (Saradamma, Higginbotham, & Nichter, 2000). With the launch of new programs and policies, healthcare has become one of the key priorities of the Indian Government (Abhishek, Jenamani, & Mahanty, 2017). In fact, the increased global antibiotics consumption (65%) is a major cause of the growing resistance of antibiotics, in low and middle-income countries (LMIC).

Furthermore, 50-90% of the medicines consumed do not seem to be metabolized within the body and enters into the environment through the body waste in the form of urine and feces (N. H. Tran, Reinhard, & Gin, 2018). These levels create direct risks to the health of humans via

contaminated drinking water, and that they might additionally foster conditions for pathogens to develop antibiotic resistance (Figure 1.1). Additionally, most of the medicines are discarded in their native form from hospitals, production units, and households into the municipal sewers. Increased levels of antibiotics have been measured in well water, lakes and streams situated near the pharmaceutical industries (Fick et al., 2009).

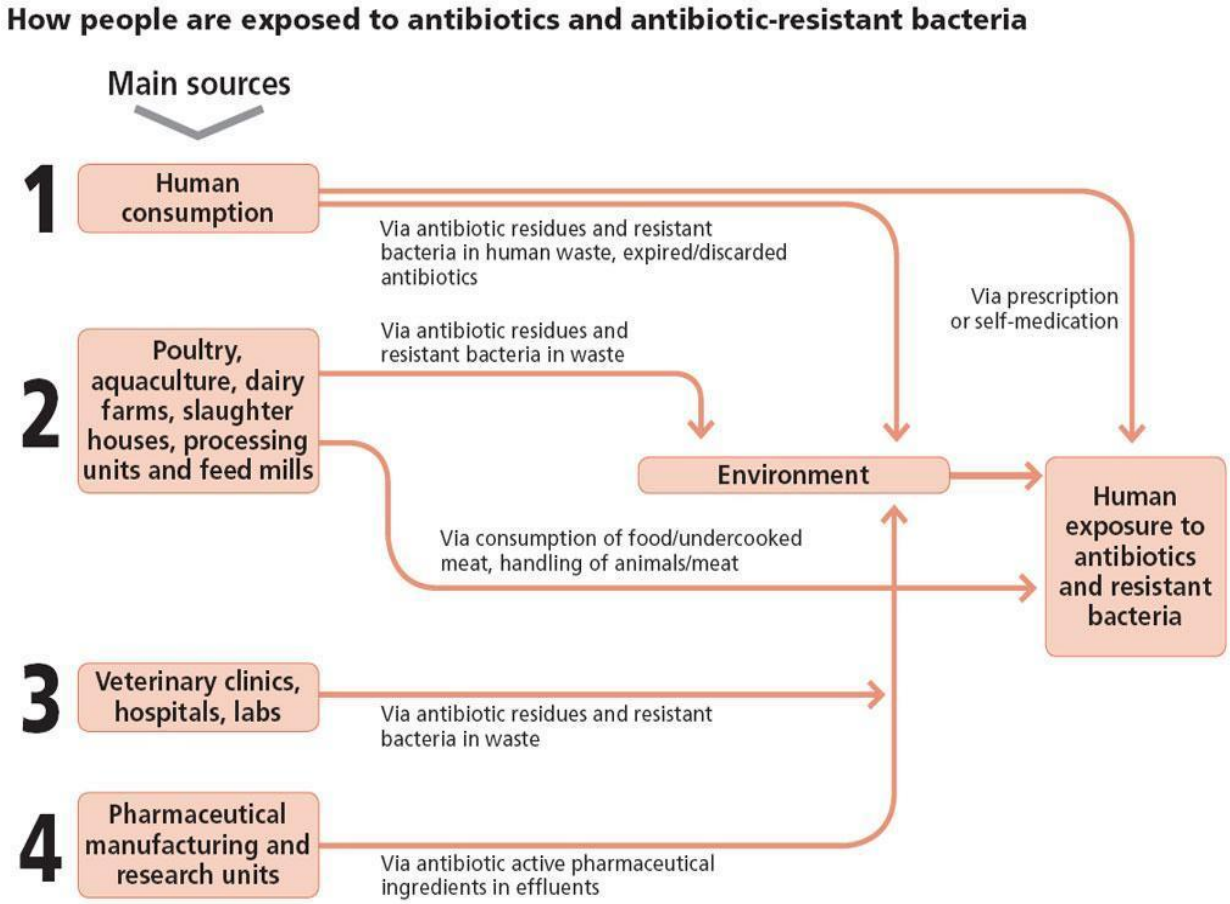

Figure 1.1: Sources of humans Exposure to antibiotic resistance bacteria (Sinha & Khurana, 2017)

Different contextual investigations demonstrated remarkably high levels (mg L^{-1}) of several pharmaceutical drugs in the effluent from a nearby wastewater treatment plant. A case study on the quality of water from Hyderabad (India) showed the emanating effluent released in the Godavari rivers Vellar, Kaveri and Tamiraparani rivers (Shanmugam et al., 2014; Gothwal and Thatikonda, 2017). The compounds like cetirizine, enoxacin, ciproflaxin, citalopram, and terbinafine were detected in various wells of the villages (Chander et al., 2016). The high amount

Zof several antibiotics were also measured in the lakes having source far away from the sewage plant (Patel et al., 2019). The presence of these kind of pharmaceuticals in drinking/surface water clearly demonstrates the inefficacies of conventional treatments. Still, 90% of the wastewater treatment plants are working on the conventional treatment options with preliminary treatment (Matamoros, Arias, Brix, & Bayona, 2009) and biological treatment (Verlicchi et al., 2012; Lefebvre et al., 2014). In the conventional wastewater treatment units, these pollutants are subjected to a succession of different reactions resulting in the formation of more complex intermediates that could adversely affect the aquatic life.

Thus, it might be concluded that conventional treatment methods like aerobic or anaerobic treatment, coagulation, adsorption, etc possess certain hindrances. These are not capable of completely eliminating a huge amount of the recalcitrant present in urban wastewaters leading to the escape of these compounds in water bodies. Progressively compelling and explicit treatments are required to decrease the natural and potential effect of effluents and comply with increasingly strict legislation. The need of an hour is to use advanced treatment methods including electro-oxidation, ozonation, microfiltration, Advanced oxidation processes (AOPs), reverse osmosis, etc applied as a pre or post-treatment options to the conventional processes for covering their inabilities to treat the wastewater (Longkai Yang et al., 2018). Taking into consideration various credentials of the advanced treatment options, AOPs have possessed wide popularity among the researchers.

1.2. ADVANCED TREATMENT TECHNIQUES

To facilitate the quality of the water and the environment's preservation, there is a need to resolve these issues using potential treatment technologies. For the treatment of a wide variety of bio recalcitrant pollutants, AOPs have proven to be the most sorted of option (Matilainen & Sillanpää, 2010; Sillanpää, Ncibi, & Matilainen, 2018). The generation of highly reactive free radicals notably the hydroxyl radical (•OH) (Haroune et al., 2014; Mohapatra et al., 2014), that can successfully attack most organic molecules to help in the degradation of the priority pollutants. AOPs have been used for the treatment of various pollutants including pesticides (Sivagami, Krishna, & Swaminathan, 2014), dyes (P. V. Nidheesh, Zhou, & Oturan, 2018), pharmaceuticals (Mirzaei, Chen, Haghighat, & Yerushalmi, 2017), phenols (Babuponnusami &

Muthukumar, 2012), chlorophenols (Elsalamony & Mahmoud, 2017), and heavy metals (Dave & Chopda, 2014). They have been used for the treatment of industrial wastewaters including paper and pulp (Ginni, Adishkumar, Rajesh Banu, & Yogalakshmi, 2014; Hermosilla, Merayo, Gascó, & Blanco, 2014), pharmaceutical industries (Deegan et al., 2011; Gadipelly et al., 2014), dye industries (P. Kaur, Kushwaha, & Sangal, 2018), petroleum refineries (Mota et al., 2009), tannery industries (Sauer, Casaril, Oberziner, José, & Moreira, 2006).

AOPs are mostly classified on the basis of the phases of the reaction taking place i.e. homogenous and heterogeneous. Commonly applied technologies like photochemical processes (e.g. UV,UV/H_2O_2), ozonation (O_3,O_3/H_2O_2), Fenton (H_2O_2/Fe^{2+}) increasingly popular photocatalytic oxidation (e.g. UV/semiconductors) have been actively investigated for water treatment (Cheng et al., 2016; Oturan & Aaron, 2014).

Compared to all the AOPs, photocatalysis has shown its popularity among the researchers in the recent past based upon benefits like (a) cost-effectiveness;(b) low-toxicity;(c) environment-friendly. Variously used photocatalysts are TiO_2, ZnO, CdS, ZnO, Fe_2O_3 and WO_3. (Prieto-Rodriguez et al., 2012; Kanakaraju et al., 2014). Among them, TiO_2 is of greater interest for photocatalytic degradations due to its inertness, having high photoreactivity, low cost, low toxicity, and chemical stability over a wide pH range (Prieto-Rodriguez et al., 2012; Pistkoviet al., 2015; Sarkar et al., 2015). In all the reported studies, TiO_2 has shown its potential in the field of semiconductor photocatalysis (Bouna et al., 2013) as electron hole pair generated can be effectively involved in oxidative and reductive reactions with pollutant molecules present at/or near the surface of the semiconductor.

Although effective, yet certain technical issues restrict their applications mostly in the laboratory scale experiments. The cumbersome separation of nano-sized catalyst from the treated solution which at the end leads to extra cost, a larger quantity of catalyst being utilized, recombination of electron-hole pairs, thus limiting its feasibility for practical applications.

For the improvement of the properties of the catalyst, various modifications have been studied. The band gap of the catalyst is needed to be decreased for the activation of catalyst in the visible range. For this purpose the modifications including doping, co-doping have been introduced. Numerous studies have also been reported regarding the doping of metal or non-

metal ions on TiO_2 (Ghosh, Chelli, Giri, & Golder, 2018; Wan, Ramakrishna, & Liu, 2018; M. Zhang, Gao, Chen, Annamalai, & Tao, 2018; Mai Zhang, Chen, Annamalai, Tao, & Gao, 2018). Doping leads to enhancement of the photoactivity of the catalyst by the generation of new energy levels below the conduction band leading to the indulgence of metal ions with TiO_2 (Lourenço & Asencios, 2018; M. B. Sarkar et al., 2017; Werapun et al., 2018). This leads to the inhibition of electron-hole recombination as well as the catalyst is capable of harness visible light. The research in the area is mostly focused upon the slurry form even after the promising results in the visible region with the various modifications. Where again the problems of costly chemicals, expensive separation of the catalyst, reusability is still not solved. Hence, to overcome these hurdles, researchers gave a solution to certain deficiencies by working on fixed-bed photocatalysis, where the catalyst is being coated on some material and subsequently used for degradation. Studies related to the fixing of catalyst on supports are extensively cited in the literature (Alinsafi et al., 2007; Chang, Huang, Shu, & Chang, 2012; Hashemi, Badii, & Abdolreza, 2010; Pan, Huang, Chen, & Shiu, 2006; Scotti, D'Arienzo, Morazzoni, & Bellobono, 2009). With the fixation of catalyst on the inert support material, this technique has gained robustness among the researchers. Different support materials used for the immobilization include alginate beads (Idris, Misran, Hassan, Jalil, & Seng, 2012), cement beads (Verma, Prakash, & Toor, 2014), glass supports (Bouarioua & Zerdaoui, 2017), pebbles (Nageswara N. Rao & Chaturvedi, 2007), polymers (Matsuzawa et al., 2008) and many more. But with the successful execution of the fixed bed catalysis, the recyclability/ durability and the inertness of support is still a big problem. Further mass transfer limitation is also a problem for the commercial-scale application of this technology.

Researchers have also focused on photo-Fenton for the removal of numerous pollutants. Being homogenous in nature, the photo-Fenton process leads to the advantage of having no mass transfer limitations which further helps in reducing the time for the treatment of priority pollutants as compared to the photocatalysis. The basic mechanism involving the redox reactions taking place between the oxides of iron for the generation of hydroxyl radicals is being well cited in the literature (Bokare & Choi, 2014a; Clarizia, Russo, Di Somma, Marotta, & Andreozzi, 2017; Vorontsov, 2019).

Most of the pilot-scale studies reported are based upon the usage of a photo-Fenton process (Varatharajan and Kanmani, 2007; Zapata et al., 2008). Again, further implications faced by this process at large scale include maintaining a high dose of H_2O_2, the formation of a high concentration of anions in the treated wastewater and large amounts of ferrous iron sludge (P. V. Nidheesh, 2015a), lower efficiency of photon utilization restricts its industrial applications. For the large scale applications, fixed bed catalysis has gained importance due to:

i) Easy separation of catalyst

ii) Reusability of the catalyst

iii) Cost-effective

Based upon all the credentials and potential of scale-up, fixed bed catalysis can provide a platform for the industries for wastewater treatment. This technology needs to revisit all the important operating parameters and best bet for the commercial-scale reactor.

1.3. SCALING UP OF FIXED BED REACTORS

For the commercial-scale applications, successful implementation of AOPs is required at the pilot plant scale using various photoreactors. The conventional reactor scaleup is comparatively more simple than the scaling up of solar reactors. Besides, the complications related to the conventional reactor system, catalyst contact, mixing, flow patterns, temperature control, and mass transfer might pose hurdles in the potential scale-up. For uniform distribution of the sunlight inside the reactor and for maximizing the exposed surface area of the reactor axial and radial scale-up are also considered essential parameters (Miyawaki et al., 2016). Numerous studies are focused on the scale-up process using TiO_2 especially in suspension form includes annular photoreactor (Autin et al., 2013), photocatalytic Taylor vortex reactor (Jia et al., 2011) parabolic trough collectors (PTCs), compound parabolic collectors (CPCs)

Numerous literature is available for the removal of pollutants using catalyst immobilized upon the inert support surface. Various reactors including packed bed photoreactor (Borges et al., 2015), coated fiber optic cable reactor, thin-film fixed-bed sloping plate reactor (Khan et al., 2012a), fluidized bed reactor (Kang et al., 2011), falling film reactor (Luna et al., 2014), corrugated plate reactor (Passalía et al., 2011) have been studied. The application of fixed bed catalysis to the field scale has not gained much popularity. This might be due to the durability

and stability of the catalyst and supports. Another hindrance includes more time consumption and mass transfer limitations also pose a problem in the scaling up. With more consumption of time, the required energy of the process increases leading to a more cost-consuming process.

The intensification of the advanced treatment process is regarded as a promising technique for the industrial processes aspiring for improvement in the efficiency of the process, cost-effectiveness, environmental safety. For the large scale implementation of the processes, various implications including the cost-effectiveness of the complete process are taken into consideration. The fixed bed reactors are mostly preferred due to the real-life applications towards plug flow approach for the field-scale applications. Plug flow reactors (PFR) being more efficient than the mixed flow reactors (MFR) are mostly preferred, as the rate of reaction is increased with the increasing concentration of the reactants. More conversion in less time makes the ideal PFR better than MFR. The major drawback of the MFR i.e. back mixing, that could be avoided in PFR, leading to continuous change in concentration. For the scaling up of the process in terms of the relevance to the advanced oxidation processes (AOPs), the study of PFR can act as an innovative approach. For the real-life applications of the AOPs at large scale, the study of the reactor is an important concern regarding the practical as well as the economic aspect of the processes. For boosting the economical considerations of the process, the utilization of solar radiation can act as a boon but various engineering prospective of these processes at a large scale would be a challenging factor. Furthermore, other hurdles for the AOPs including patterns of flow, catalyst contact, mass transfer, the reagent used, mixing and many more have posted the hurdle in successful scaling up of the processes (Sixto Malato, Blanco, Vidal, & Richter, 2002; Spasiano, Marotta, Malato, Fernandez-Ibañez, & Di Somma, 2015).

Now taking into consideration various advantages and disadvantages, a real reactor implicating the ideal PFR is mostly sorted out option. Packed bed reactor with the catalyst immobilized on the support is mostly preferred for such applications. Various obstacles like mass transfer limitations, channeling of the flow and the intactness of the coating of catalyst are hindering the process scale-up. The stability and durability of the catalyst are also an issue leading to the slower degradation along with increased time for the treatment of priority pollutants forming major hindrance to the potential scale-up. Hence in the present study, all the

concerned problems are addressed by utilizing the fixed bed packed reactors in series which approaches towards ideality.

For increasing the potential elimination of the organic pollutants present in water, recent studies have concentrated upon the development of the combined AOPs (Bejarano-Pérez & Suárez-Herrera, 2007; Kanakaraju, Glass, & Oelgemöller, 2018; Steter, Dionisio, Lanza, & Motheo, 2014; Vieira Dos Santos, Sáez, Cañizares, Martínez-Huitle, & Rodrigo, 2017). The synergistic effect of the combined process over single AOP leads to the better mineralization and degradation of pollutants. Combinations of AOPs like ozonation followed by photocatalysis (Song, Ying, He, & Chen, 2007), sonolysis combined with electro-oxidation (N. Tran, Drogui, Nguyen, & Brar, 2015), sonolysis combined with ozonation (Destaillats, Colussi, Joseph, & Hoffmann, 2000), Fenton combined with electro-oxidation (Sirés et al., 2007) have been studied. Providing high removal efficiency than the single process the combined processes is the most sorted option. The combined processes provide the treatment in the reduced time with increased production of the hydroxyl radicals to help in faster removal of the process.

1.4. DUAL PROCESS OF PHOTOCATALYSIS AND PHOTO-FENTON

Taking into consideration various shortcomings of other coupled processes, the coupling of two techniques i.e. photocatalysis and photo-Fenton can reasonably solve the implications offered by these processes when operated separately (Bansal & Verma, 2017b). The combined solar-powered AOPs possesses the promising application towards the treatment of wastewater i.e. of the capability to mineralize the toxic compounds, possessing low cost, providing a boon for the wastewater treatment.

The major challenge of this dual process is that both mechanisms (photocatalysis and photo-Fenton) shouldtake place without hindering the other process (Bouras & Lianos, 2008; Mazille, Schoettl, Klamerth, Malato, & Pulgarin, 2010).

The dual process has excellent degradation efficiency but has not been explored well yet. The cost of the process and a high dose of chemicals can be substantially reduced if the two different processes (photo-Fenton and photocatalysis) are coupled together in one system which would consequently increase the degradation as well. For the enhancement of the degradation efficiency, few studies have suggested the basic idea of the dual effect of photo-Fenton and

photocatalysis (Adish Kumar, Sree lekshmi, Rajesh Banu, & Tae Yeom, 2014; Bansal & Verma, 2017a). The generation of a sufficient amount of •OH has lead to improved degradation efficiency. The basic mechanism of the dual process involves the reaction of both, TiO_2 particles as well as the iron oxides at the same time (Figure 1.2). The TiO_2 particles, when exposed to light, leads to the photocatalysis process to take place leading to the formation of electron and hole pairs(Y. Su et al., 2015). For the photo-Fenton reactions to initiate, Fe(III) is to be converted into Fe(II) (Ruales-Lonfat et al., 2015). The electron from the photocatalysis which posed the problem of recombination helped in the conversion of Fe (III) to Fe (II). When Fe (III) ions come into contact with TiO_2, some of the Ti (IV) species are replaced due to the weakening of metal-oxygen bond and imbalance of the charge. This further leads to the formation of Ti(III) species along with the vacancies of oxygen which act as the reactive species for the degradation (Y. Zhang et al., 2019). This leads to the electron-hole pair being separated and thus helping in the oxidation of pollutants to take place (Kim, Lee, Lee, & Lee, 2012). This will contribute to more amount of •OH production and thus favoring the overall process (Asiltürk, Sayilkan, & Arpaç, 2009). The existence of Fe(II) and Ti(III) leads to the synergistic effect enhancing the oxidation and reduction thus leading to the increased degradation of wastewater (Mazille, Schoettl, & Pulgarin, 2009).

In the present study, the industrial-scale visualization of the dual process has been proposed. The present study emphasizes the novel concept of coupling two processes i.e. photocatalysis and photo-Fenton in fixed mode and both the processes taking place at the same place and same time.

In this study, the innovative novel inert composite material has been selected for TiO_2 immobilization i.e. Fuller's Earth (FE) which is also a good source of natural iron oxides. Further to make the process more lucrative from the applications' point of view, waste material of the industry i.e. Foundry Sand (FS) has been used as an alternative additional iron source.

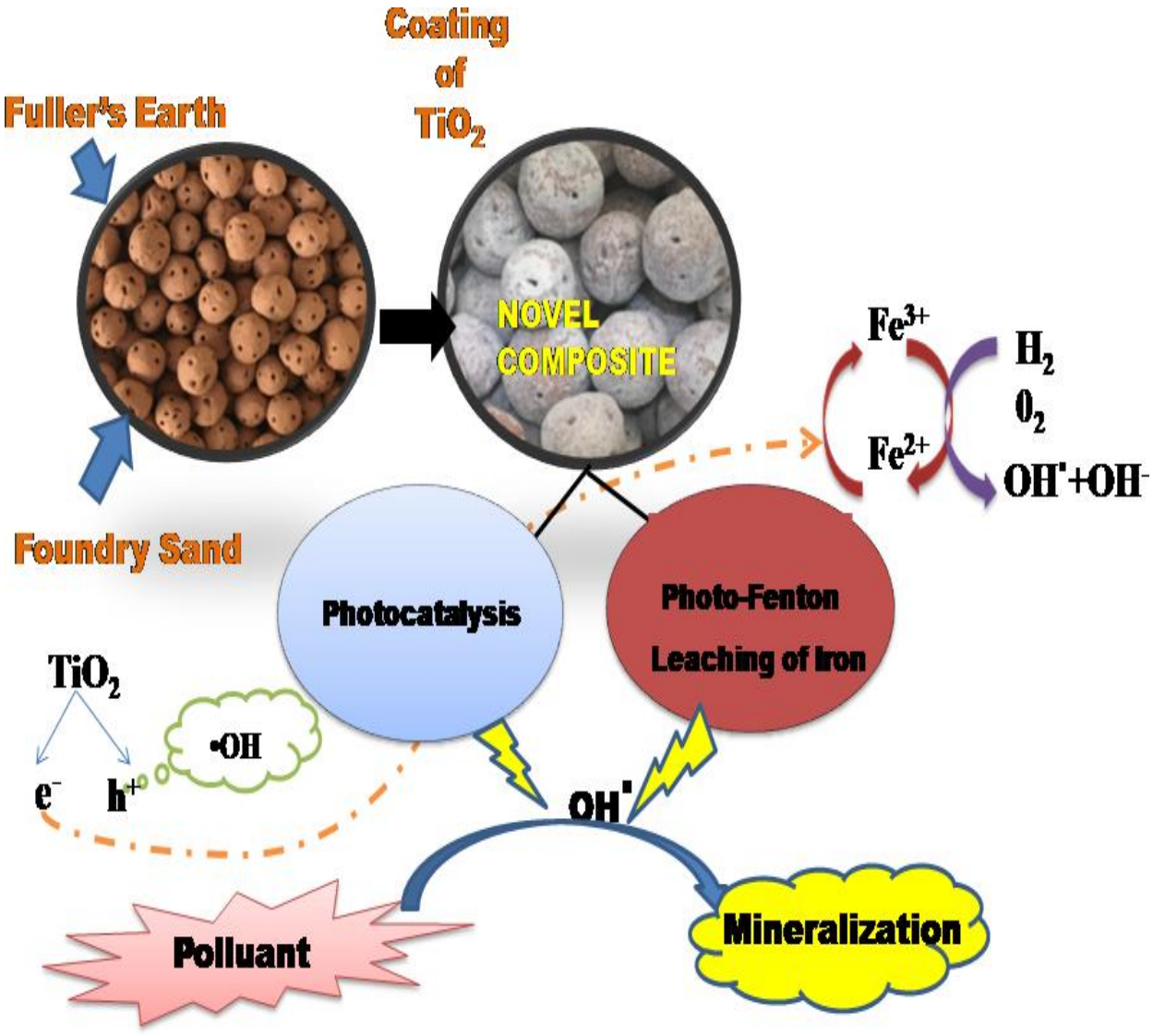

Figure 1.2: Proposed mechanism of the dual effect of photo-Fenton and photocatalysis

In this way, a novel support material has been developed capable of incorporating in-situ dual effect (photocatalysis and photo-Fenton) at the same place. For photo-Fenton process iron being the most important tool for the degradation of priority, pollutants are leaching from the support material. For the photocatalysis process to take place, support is coated with the TiO_2 layer using a dip-coating technique. Both these processes are taking place at the same time and at the same place making it more feasible and effective to use.

1.5. APPROACH USED FOR THE PROPOSED STUDY

In the present study, the novel concept of the dual process for the degradation of pharmaceutical compound Phenazone (PHZ), Metronidazole (MTZ) has been introduced. PHZ is a non-steroidal antipyretic, anti-inflammatory drug (NSAIDs) (Calza, Medana, Raso, Giancotti, & Minero, 2011) most commonly used for reduction in fever, ear infections, and skin infections and for the relief of pain. NSAIDs have been found in surface water (Zuehlke, Duennbier, & Heberer, 2007), groundwater and even in drinking water (Reddersen, Heberer, & Dünnbier, 2002). Even at a low concentration of drugs, they can pose a threat to living beings due to resistance caused by these in the bacteria and are harmful to the aquatic species. Its presence in natural waters clearly indicates the inefficacy of conventional treatment methods (Belver et al., 2017).

MTZ (2-methyl-5-nitroimidazole-1-ethanol) an antibiotic has been chosen as a model compound. MTZ has been extensively used to treat infections caused by Bacteroides, anaerobic bacteria, and protozoa. MTZ is highly soluble in water and is nonbiodegradable; hence it is accumulated in the aquatic environment. Elimination of MTZ from the water system is an important issue considering its potential mutagenicity, toxicity, and carcinogenicity.

The main aim of the present research was to develop novel support utilizing in-situ dual effect (photocatalysis and photo-Fenton) along with the novel reactor for the treatment of wastewaters. The study has been divided into different development stages comprising:

1. The synthesis and composition of the novel composite support material and utilizing them for the degradation study of pharmaceutical drug i.e. PHZ at lab-scale utilizing in-situ dual effect.
2. Optimization analysis and modeling of the degradation of MTZ at the lab scale along with mineralization studies in terms of the formation of various by-products, ions that were evaluated from the GCMS analysis.
3. The studies of the degradation of PHZ and MTZ at a large scale i.e. scale-up of the process. Assessment of the reactors in the series model for the plug flow approach. Various process parameters were optimized by utilizing the appropriate catalyst based upon the inertness, cost, and most important factor recyclability.

4. Degradation study of compounds utilizing the modified Compound parabolic concentrator.
5. The extended applications of the in-situ dual process for the treatment of real industrial pharmaceutical wastewater for substantiating the novelty of the process.

CHAPTER-2

LITERATURE REVIEW

2.1. OUTLINE

Pharmaceuticals have been highly consumed for over a century due to its major contributions in the well being of humans and for the reduction of illness and sufferings faced (Kümmerer, 2008). These compounds are most remarkably described by their low biodegradability. The vast majority of the pharmaceutical medications are disposed off in their original form or metabolites by means of toilets (humans just can use a little level of the drugs), emergency clinics, and private family units into the city sewers. Medications (pharmaceuticals products) containing active pharmaceutical ingredients (APIs) (Figure 2.1) are being designed to treat various diseases in humans as well as in animals. These APIs have been ended up in surface water, groundwater, urban wastewater and furthermore drinking water (Balakrishna, Rath, Praveenkumarreddy, Guruge, & Subedi, 2017; Shanmugam et al., 2014). Among the various accessible APIs available, a naturally significant gathering of pharmaceuticals incorporates anti-microbial, nonsteroidal anti-inflammatory drugs, antidepressants, beta-blockers (β-blockers), hormones, antihistamines, antiepileptics, and many more(Majekodunmi, 2015).

Various case studies from India have reported the higher concentration of pharmaceuticals in rivers and lakes (Dasaram et al., 2011; Subrahmanyam & Yadaiah, 2000). Meanwhile, in Hyderabad city, the pollution level has reached the toxic level to an extent that even the fishes have died due to the toxic release of various pharmaceutical industries (Fick et al., 2009). Researchers have reported the concentration of various pharmaceutical compounds including enrofloxacin, metoprolol, citalopram, enoxacin, lomefloxacin, norfloxacin, losartan, ciprofloxacin, cetirizine, ranitidine, ofloxacin in the effluent of sewage treatment plant released in rivers nearby to be ranging from 90-31,000 mg L^{-1} (Chander et al., 2016). The extreme water discharge is further leading to the global rise of drug-resistant infections. In the areas surrounded near the pharmaceutical manufacturing industries near Visakhapatnam and Hyderabad as well as in Chennai and New Delhi, the drug-resistant bacteria have been found to be in increased number (Magiorakos et al., 2012; WHO, 2014).

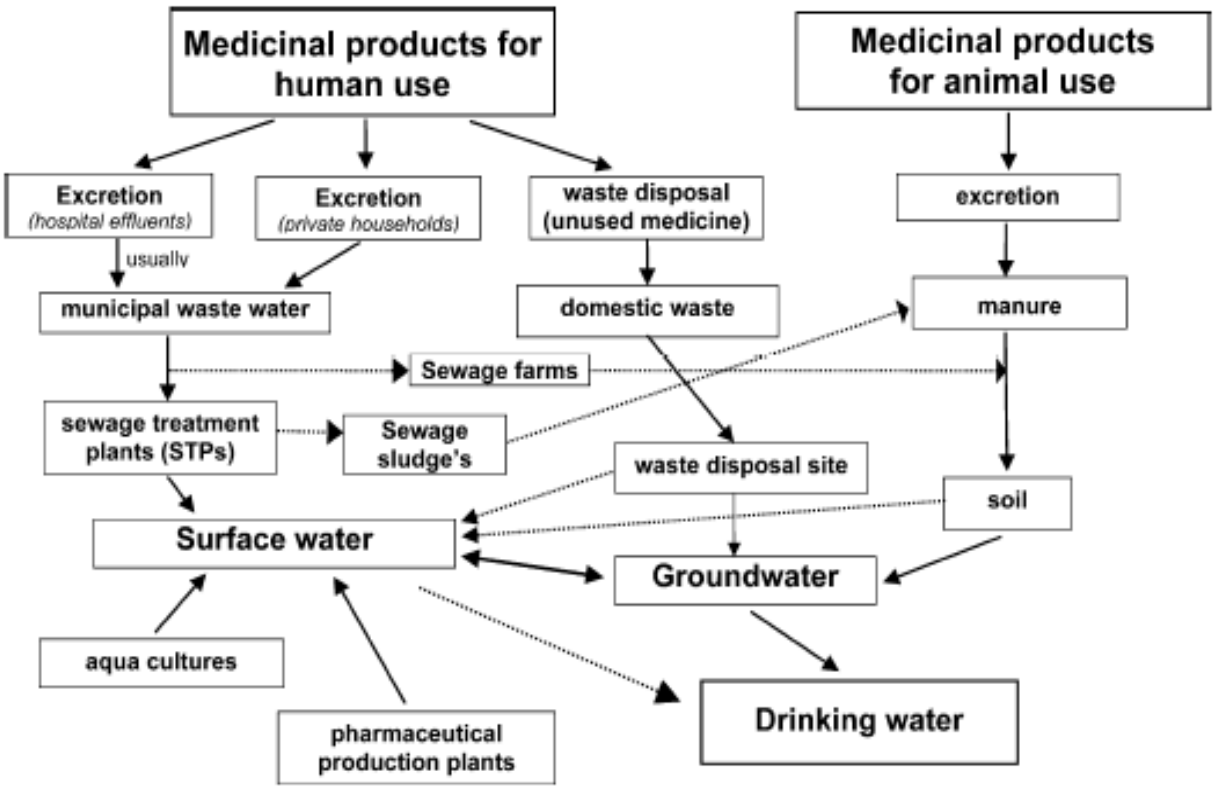

Figure 2.1: Origin and routes of Pharmaceutical Pollutants (Heberer, 2002)

At the point when released from households, hospitals, and industries, these drugs may enter wastewater treatment plants (WWTPs) (Ferro, Guarino, Castiglione, & Rizzo, 2016; Rizzo, Fiorentino, & Anselmo, 2013). Because of the extensive variation in physicochemical properties of pharmaceuticals and the design of WWTPs, the proficiency of treatment can change essentially requiring a broad range of removal protocols (Halling-Sorensen et al. 1999, Ternes 1998). The relatively high solubility and non-biodegradable nature of the APIs lead to ineffectiveness of the conventional treatment methods, which is further leading to the persistence of the parent as well as metabolites of various drugs into aquatic as well as in terrestrial environments (Dudgeon et al., 2006; Onesios, Yu, & Bouwer, 2009; Pal, Gin, Lin, & Reinhard, 2010). Veterinary medications are additionally known to legitimately build APIs levels in the ground as well as surface water (Stamatelatou et al., 2003). Thus, their high concentrations detailed in follow levels (ng L^{-1} to μg L^{-1}), can possibly harm aquatic as well as other organisms. Henceforth, APIs have been perceived as significant ecological toxins requiring the quest for

successful innovations to decrease their increasing concentration in the environment (Onesios et al., 2009).

There is presently no legitimately controlled maximum permitted concentration of pharmaceuticals disposed of to the environment, in spite of their obscure effect on nature and human wellbeing. But taking into concern the harm caused by these pharmaceuticals, European Union Water Framework Directive has produced an updated list of priority pollutants that recognizes pharmaceuticals as potential contamination. Contaminated water can, by and large, be dealt with adequately by treatment plants, utilizing adsorbents or traditional methods of treatment (ozonation, chlorination). But, these techniques are once in a while not fit for the treatment of pollutants to the levels legally necessary or basic for the resulting utilization. Antiprotozoal and antibacterial operators have restricted action against high-impact microscopic organisms. They establish a group of anti-infection agents that have been utilized in human and veterinary drugs to treat sicknesses brought about by protozoans (e.g., Giardia lamblia, Entamoeba histolicia) and bacterial contaminations (coccidiosis, hemorrhagic enteritis).

The conventional wastewater treatment plants are mostly not intended to manage polar micropollutants, for example, pharmaceuticals (J. Wang & Wang, 2016). Hence, these treatment plants containing residual pharmaceuticals discharge their waste into natural surface water bodies (stream, river or lake). Although there is widespread advancement in the biological treatment of tertiary treatment technologies (Lakatos, 2018; Lofrano, Meriç, Zengin, & Orhon, 2013; Nancharaiah, Venkata Mohan, & Lens, 2016) in various plants which has increased the efficiency of the treatment (Khandegar, Acharya, & Jain, 2018; Singh, Chauhan, Jain, & Sharma, 2017) yet the treatment of various recalcitrant compounds is still questionable.

Being a cost-intensive process tertiary treatment units are not the most favored treatment technologies. The biological treatment being the uncontrolled process as well as time consuming process is also not favored. Hence, the need of an hour is to have efficient treatment options which act as the poaching step to the existing treatment methods. Sometimes the new technologies could act as pre or post-treatment technology to the existing technology. Taking into consideration the inefficacies of the conventional wastewater treatment plants, there is a need for the research focus

to be shifted towards more efficient technologies i.e. advanced oxidation processes (AOPs) which has been a hot topic in the recent past years.

The literature was reviewed for the various advancements in the field of wastewater treatment using AOPs. Various benefits and pitfalls were examined of the AOPs in terms of their usage at the industrial level (de Araújo, Antonelli, Gaydeczka, Granato, & Malpass, 2016; De Araújo, Antonelli, Gaydeczka, Granato, & Malpass, 2016; Zhou & Smith, 2001). AOPs have been widely cited in the literature confirming the efficiency of the process (Y. Deng & Zhao, 2015; Dewil, Mantzavinos, Poulios, & Rodrigo, 2017; Kamat & Meisel, 2002; Munter, 2001). AOPs could be the better option for the pre or post-treatment option for various industries. Depending upon the technology implementation it might act as the full-fledge option for the various processes. The basic aim of the review includes the scaling up the AOPs to the industrial scale for the removal of the priority pollutants.

2.2. ADVANCED OXIDATION PROCESSES

For the removal of various recalcitrated compounds, chemical treatment involving the production of highly reactive and non-selective hydroxyl radicals (•OH) known as AOPs is used (Cheng et al., 2016; Y. Deng & Zhao, 2015; Klavarioti, Mantzavinos, & Kassinos, 2009). These processes have demonstrated profoundly productive in the treatment of various recalcitrated contaminants (Fiorentino, Rizzo, Guilloteau, Bellanger, & Merlin, 2017; Lofrano, Rizzo, Grassi, & Belgiorno, 2009; Zammit et al., 2019). AOPs can convert non-biodegradable compounds to more promptly biodegradable intermediates (De-Nasri, Nagarajan, Robertson, & Ranade, 2018; W. J. Huang, Lin, Lin, & Zheng, 2018; Zazouli & Shahmoradi, 2019).

•OH is proficient enough of oxidizing nearly all organic compounds to mineralize into carbon dioxide, water, and mineral salts. The AOP technologies fall under two general categories. The first one includes the utilization of UV combined with other chemicals including UV/Fenton, UV/O_3, UV/H_2O_2 and UV/TiO_2 (Mehrjouei, Müller, & Möller, 2015; Moreira et al., 2016; Vogna, Marotta, Napolitano, Andreozzi, & D'Ischia, 2004). The second one is without UV source which is also known as a *dark oxidative process*, such as Fenton's reagent, ozonation (O_3), microwaves and ultrasound (Rasheed, Pandian, & Muthukumar, 2011; N. Wang, Zheng, Zhang, & Wang, 2016). The photocatalytic degradation of the recalcitrant pollutants is induced

to form non-toxic and mineralized by-products. Numerous literature is available for the removal of priority pollutants using TiO_2 as a catalyst (Al-Mamun, Kader, Islam, & Khan, 2019; Awfa, Ateia, Fujii, Johnson, & Yoshimura, 2018; Q. Guo et al., 2016; Kanakaraju, Glass, & Oelgemöller, 2014b).

2.3. THE IMPORTANCE OF PARAMETRIC OPTIMIZATION IN PHOTOCATALYSIS

It has been found that the oxidation efficiency and the rate of reaction of the photocatalytic process are dependent on the operational parameters (T. Kaur, Toor, & Wanchoo, 2015; Toor, Verma, Jotshi, Bajpai, & Singh, 2005). Photo mineralization kinetics of the degradation of pollutants is governed by various factors (Poulios, Malato, & Mantzavinos, 2015; Tsoumachidou, Velegraki, & Poulios, 2016) including the nature of photocatalyst, the initial concentration of the pollutant, the catalyst's mass, pH, light wavelength, dissolved oxygen, and temperature affect the photocatalytic performance.

• *TiO_2 loading*

The concentration of TiO_2 photocatalyst in the water treatment system strongly influences the overall rate of photocatalytic reaction in accordance with true heterogeneous catalytic systems, where the rates of photodegradation are directly proportional to the catalyst loading (Ayati et al., 2014; Torres, Nieto, Combet, Pétrier, & Pulgarin, 2008). In fact, in any photocatalytic application, the optimum catalyst concentration must be determined so as to avoid the excess usage of catalyst and to ensure efficient absorption of photons. This is because, when the TiO_2 loading is in excess, an unfavorable scattering of light by the TiO_2 particles along with a reduction in its penetration into the solution is witnessed (Wenderich & Mul, 2016). Additionally, the excess titania particles can lead to a light screening effect which may reduce the surface area of TiO_2 exposed to light irradiation and hence the photocatalytic efficiency.

• *Nature of the photocatalyst*

A vital parameter that affects the performance of a photocatalyst in photo mineralization of organic contaminants is the surface morphology, namely, the particle size and agglomerate size of the photocatalyst (Dhanya & Aparna, 2016; Shahrezaei et al., 2017; Hua Yu, Zhang, Zhao, Will, & Liu, 2009). Various types of titania have been synthesized by several routes so as

to achieve a photocatalyst that exhibits desirable physical properties, activity, and stability for photocatalytic applications (Matas Adams, Marin-Beloqui, Stoica, & Palomares, 2015; Vetrivel, Rajendran, & Kalaiselvi, 2015).

• *Effect of pH*

A vital operating parameter in heterogeneous photocatalytic reactions occurring on particulate surfaces is the pH of the solution. The pH affects the charge on the photocatalyst surface as well as the size of aggregates it forms. Depending on the nature of the photocatalyst, any alteration in the operating pH is known to affect the surface charge or the isoelectric point of the photocatalyst employed (Jain, Mathur, Sikarwar, & Mittal, 2007; Rauf, Meetani, & Hisaindee, 2011). There are several studies that have used the point of zero charge (PCA) of titania for investigating the effect of pH on the PCA of the catalyst.

• *Light wavelength/source(s)*

The effect of the light sources having different wavelengths emitting ranges on the rate of photocatalytic reactions depends on the types of photocatalyst used, i.e., crystalline phase, anatase-to-rutile composition and any state of photocatalyst modifications. The light source that can be utilized for photoactivation of TiO_2 can be artificial UV lamps or solar irradiation (Natarajan, Thomas, Natarajan, Bajaj, & Tayade, 2011; Pelaez et al., 2012; Saleh & Djaja, 2014). The UVA light is sufficient for photonic activation of TiO_2 photocatalyst. A few studies have reported an enhanced catalytic efficiency with UVC radiation as compared to UVA for the degradation of certain organic materials. This observation has been attributed possibly to the direct photolysis and a higher trapping probability of e^-/ h^+ pairs with shorter wavelength excitation.

• *Effect of light intensity and irradiation time*

The dependence of the overall rate of photocatalytic process on the intensity of the light source used has been outlined due to the photonic nature of the process (Ahmed, Rasul, Brown, & Hashib, 2011; Ahmed, Rasul, Martens, Brown, & Hashib, 2010; Bhatkhande, Pangarkar, & Beenackers, 2002). The studies reporting the effect of light intensity on the kinetics of the photocatalysis process were reviewed.

• *Dissolved oxygen*

Dissolved oxygen (DO) plays a vital role in TiO_2 photocatalysis. Oxygen is necessary for the complete mineralization of contaminants as it assures the presence of sufficient electron scavengers to trap the photogenerated electrons in CB and prevent recombination (Rauf & Ashraf, 2009; J. C. Wang et al., 2017). Oxygen does not seem to be competitive with other reactants during the process of adsorption on the surface of titania, as oxidation and reduction occur at a different location. DO may also be involved with the generation of other reactive oxygen species, such as superoxide radicals and hydrogen peroxide, in the stabilization of radical intermediates.

The photostability, as well as inertness, has lead the TiO_2 to be a significant product in various applications, like food, drugs, catalyst, cosmetics, pharmaceuticals, paints and many more. Usage of TiO_2 results in simpler operation and considerable savings of the equipment involved. The large bandgap (3-3.3 eV) has prompted the TiO_2 research towards photocatalysis and extensive research is focused on the degradation of various pollutants (Ahmed et al., 2010; Chatterjee & Dasgupta, 2005; Devipriya & Yesodharan, 2005; L. Lin et al., 2013; Tanaka, Padermpole, & Hisanaga, 2000). Various compounds like aldehydes, anilines, chlorophenols, dyes, pesticides, insecticides, pharmaceuticals, herbicides, polymeric materials, herbicides have been degraded using photocatalysis (Chekir et al., 2017; L. Lin et al., 2013; Matas Adams et al., 2015; Rauf et al., 2011; Vetrivel et al., 2015). The increased efficiency and mineralization have been achieved by the researches but certain pitfalls including the catalyst separation, reusability, cost of catalyst have been faced by most of the researchers constraining its application in industrial scale (Cloteaux, Gérardin, Thomas, Midoux, & André, 2014; Manassero, Satuf, & Alfano, 2017).

Sometimes there are several other limitations associated with photocatalysis including an increase in the treatment time for degradation of priority pollutants, electron-hole recombination, separation of the catalyst, usage of the artificial lights, increased cost of energy which are inhibiting its scale-up. This is leading to the change in focus of the researchers towards the catalyst having low cost and increased photo activity.

2.4. THE EXTENDED ACTIVITY OF THE PHOTOCATALYST

For the application of AOPs in the field-scale, various literature is focused on the utilization of natural solar radiation. The usage of natural solar light in place of artificial UV lamps is an economical as well as environmentally attractive solution for photo-Fenton and photocatalysis (Chan et al., 2003). In countries like India, the applications of solar photocatalytic processes are the best option, as fit as immense solar light throughout the year is received (Tsoumachidou, Antoniadis, & Poulios, 2018). For harvesting the solar light efficiently, certain modifications in the catalyst are required. For the increased photoactivity of TiO_2 in the visible region, doping is an essential part of the study (Chanda et al., 2017; N. Kaur, Shahi, & Singh, 2015; Shahi, Kaur, & Singh, 2016). Doping is basically the modifications in the crystal lattice of the nanoparticles for the activation of the catalyst in the visible region of light. Various studies have been reported regarding the doping of various metals like Ag (Kočí et al., 2010), Cu (Fu et al., 2011), Ni (Choi, Park, & Hoffmann, 2010), Fe (J. Yu, Xiang, & Zhou, 2009), Cr (Lixia Yang et al., 2010), Au (Ayati et al., 2014), Pt (M. Huang et al., 2008). Although researchers have focused upon this technique in the lab scale, but its other liabilities restrict their large-scale applications including:

- Using costly dopants followed by the tedious methods in almost all reported studies to prepare modified TiO_2; and
- Most of the studies have used modified TiO_2 in suspension mode which further adds an expensive step of catalyst separation post-treatment.

Hence, the research is now oriented towards the cost-effective methods for the increased photoactivity of catalyst and at the low cost.

2.5. APPLICATIONS OF PHOTO-FENTON PROCESS

Homogenous photocatalysis (mostly photo-Fenton) offers certain advantages in terms of single-phase, faster reaction rate and having a wide working spectrum. The Fenton reaction described as the improved power of oxidation of H_2O_2 using a catalyst as iron (Fe) under acidic conditions (Babuponnusami & Muthukumar, 2014; P. V. Nidheesh, 2015b). The enhancement in the oxidative power was because of the •OH generation. Being homogenous in nature Fenton process has been used for the treatment of various organic pollutants including a wide variety of

industrial wastewaters (P. V. Nidheesh, Gandhimathi, & Ramesh, 2013; Meng hui Zhang, Dong, Zhao, Wang, & Meng, 2019).

Fenton reaction in the presence of UV/visible light helps in strongly accelerates the reactions (Sahoo, 2011; Sahoo & Sayoo, 2014). The major step involved is basically due to the photochemical reduction of Fe(III) back to Fe(II). Being advantageous and environmental friendly in terms of operational cost and other optimizations, the photo-Fenton process has proven its credentials for the treatment of a wide variety of pollutants (Giannakis et al., 2016; Kavitha & Palanivelu, 2004). Being homogenous in nature i.e. Iron species existing in the same phase as that of reactants as well as no mass transfer limitation leads to the faster rate of reaction. The photo Fenton reactions work mostly at lower pH range as with increased pH, the residual Fe(III) gets precipitated as iron hydroxide which leads to the formation of iron sludge (Vermilyea and Voelker, 2009; Babuponnusami and Muthukumar, 2014). These studies usually face problems in maintaining a high dose of H_2O_2, large amounts of ferrous iron sludge generation along with the formation of a high concentration of anions in the treated wastewater. These shortcomings have hindered its potential scale-up at the industrial scale (P. V. Nidheesh, 2015a).

Hence, to overcome the shortcomings of the homogeneous Fenton process, heterogeneous Fenton process has been introduced by the researchers (Kasiri, Aleboyeh, & Aleboyeh, 2008; Rodríguez, Ovejero, Sotelo, Mestanza, & García, 2010). Having various advantages over the traditional process it has also been studied well in the recent past. It basically involves the immobilization of iron catalysts within the support from where •OH could be generated after coming in contact with H_2O_2. Materials such as silicate, clay, and zeolites, etc have been proven to be used as supports (Ayoub et al., 2018; M. Blanco, Martinez, Marcaide, Aranzabe, & Aranzabe, 2014; Tekbaş, Yatmaz, & Bektaş, 2008). These helped in solving the problems of iron sludge generation as well as the recovery of catalyst for further use.

The main asset of heterogeneous processes is that the problem of iron sludge generation in case of the homogeneous process gets nullified completely. However, these processes result in a slower oxidation rate as compared to the homogeneous process (Punzi et al., 2012) owing to the existence of a smaller fraction of iron over the surface of the catalyst. Most of the problems

faced by the homogenous Fenton process have been covered up in the heterogeneous process, leading it to be feasible for large scale applications.

2.6. SCALING UP OF PHOTO REACTORS

For commercial visualization, the effective execution of photocatalytic processes at large scales, however, requires the global interdisciplinary influence of various parameters affecting the efficiency of photoreactor(Iglesias, Rivero, Urtiaga, & Ortiz, 2016). For the development of useful design procedures for industrial-scale applications, various aspects in terms of mass transfer rates as well as contacting patterns must be optimized (Motegh, Van Ommen, Appel, & Kreutzer, 2014). Scaling up of the solar photocatalytic reactors is more complex than ordinary traditional reactors. Along with the complications of the reactor involved in the traditional systems, various other implications including flow patterns, mass transfer, catalyst contact, reagent, and mixing must be optimized. For the achieve efficient exposure of the catalyst to solar irradiation, scale-up of essential parameters is required for amplifying the exposed surface areas per unit of volume of the reactor (Miyawaki et al., 2016).

AOPs have shown their potential in terms of degrading a wide variety of pollutants and proposed a strong bet for their use for commercial-scale applications using various reactors (Motegh et al., 2014). There are widespread ambiguities regarding the use of different type of reactors like step (Thu, Karkmaz, Puzenat, Guillard, & Herrmann, 2005), falling film (Mehrjouei et al., 2013), tubular (Keane et al., 2014), compound parabolic concentrator (Tian et al., 2018), parabolic trough reactor (Abdel-Maksoud, Imam, & Ramadan, 2016), thin-film reactors (Ling, Mohamed, & Bhatia, 2004) to approach plug flow behavior. The tubular packed bed is the most sought of a reactor for real-life applications (Adams, Skillen, McCullagh, & Robertson, 2013). The use of solar radiation can boost economic considerations but the engineering perspective of these processes at a large scale would be a challenging factor (Zeng, Guo, He, & Duan, 2016).

2.7. FIXED BED REACTORS

Heterogeneous photoreactors are of two types, one is the slurry form reactor where the TiO_2 is in the suspension form other the other one is the immobilized reactor where a catalyst is deposited on the solid surface. Different advantages are offered by both types of reactors.

Although the immobilized system offers less efficiency than the slurry system, the catalyst can be used recycled and reused for long use.

Different materials for supports of catalysts have been studied in literature for the degradation of wide variety of pollutants using glass beads (Chen & Cao, 2006), woven glass fabric (H. Wang, Wu, Zhao, & Guan, 2007), activated carbon (Li et al., 2008; Ping-feng et al., 2008), pumice stone (Venkata Subba Rao, Rachel, Subrahmanyam, & Boule, 2003), steel mesh (Hosseini, Borghei, Vossoughi, & Taghavinia, 2008), clay materials (Bouna et al., 2013), polymeric materials (Kumar & Bharti, 2019) and many more. Veréb et al., (2014) investigated the photocatalytic degradation of phenol (100 ppm) using TiO_2 supported Al_2O_3-based ceramic paper. A titanium alkoxide was used as a fixing agent for immobilization. The photocatalytic efficiency of the coated ceramic paper was constant up to five 2-h cycles. The use of these types of TiO_2 immobilized support materials in the photocatalytic degradation process vanishes the expensive catalyst separation step after the treatment (Gaya and Abdullah, 2008). Thus, the scale-up of the process could be visualized.

However, the prolonged use of an immobilized catalyst and the durability of support material to be used for a longer period are the major concerns to be looked at carefully for field-scale applications. On the other hand, the photocatalytic process sometimes does not completely degrade the pollutants having large structures (Ziemiańska et al., 2010). Therefore, subsequent removal of the organic compounds from the treated wastewater before discharge to water bodies is necessary.

Sometimes there are several other limitations associated with photocatalysis including an increase in the treatment time for degradation of priority pollutants, mass transfer limitations, the inertness of the support and durability. These drawbacks are not really attempting the fixed bed photocatalysis applications to work on a commercial scale.

For the industrial scale applications scaling up of the process is an important task to execute the lab-scale trial results. Various studies have reported the different types of photocatalytic reactors working under artificial illumination or solar light (Liu et al., 2012; Nickels et al., 2012; Rao, Chaturvedi and Li Puma, 2012). Photocatalytic reactors have been reported to have employed for disinfection, detoxification, hydrogen production, and various

applications (Malato et al., 2007; Alrousan et al., 2012). Photoreactors used mostly have been classified as concentrating and non-concentrating.

Solar collectors without concentrators are basically flat plates facing the equator, with a specific inclination, depending on the geographic location of use. Given that these are ideal reactors, they might also have very low concentration factors (Winston & Welford, 2008). The low cost and simplicity is the main advantage of these reactor types. The collectors which are concentrating in nature helps to focus the solar radiation and require a solar tracking system. Parabolic-trough collectors, holographic collectors, and linear Fresnel lenses are some included.

A parabolic collector has a huge area for light-harvesting but the tube area is small. only 10% –15% of total solar radiation is harvested in this case. But it could serve as a hindrance in the photocatalytic process as mostly UV solar radiation is used for photocatalysis which is approximately 4%–6% of total solar radiation. The compound parabolic concentrator (CPC) being low concentrating in nature and having the advantage of parabolic trough collector as well as one sun collector system, has been most cited for AOPs applications (Tian et al., 2018). Besides low cost these CPCs have advantages like turbulent flow conditions, absence tracking and overheating, potential to use both direct and diffuse solar radiation, weatherproof properties, and high optical and quantum efficiency (Radjenović, Sirtori, Petrović, Barceló, & Malato, 2009). Having the advantages of both non-concentrating and concentrating systems, CPCs seem to be the best option for solar photocatalytic processes.

A study involved the utilization of CPC reactors constructed in HIDROCEN, Madrid. The plant consisted of 21 CPCs connected in series for the treatment of cyanide in wastewater. After 2 hrs 76% of degradation was achieved (S. Malato et al., 2002). Experimentation was also performed for the degradation of sewage wastewater using CPC and 51% of removal was observed after 6 h with the addition of H_2O_2. Further degradation increased to 75% with the addition of sodium persulphate (Kositzi, Poulios, Malato, Caceres, & Campos, 2004). Packed bed CPC employing glass spheres have also been employed for the treatment of various pharmaceuticals (Miranda-García et al., 2011). Other studies have also reported the usage of silica beads, stones for the removal of pollutants (Martínez, Morales-mejía, Hernández, & Almanza, 2014).

Through extensive literature that exists in the area of photocatalytic reactors, the main implication that arises with almost all the configurations of reactors is the scale-up studies for commercial applications. The major pitfalls of the above discussed pilot-scale fixed-bed studies include:

- Increased treatment time;
- High energy costs;
- Poor recyclability efficiency of the immobilized catalyst;
- Film-diffusion resistance; and
- Frequent electron-hole recombination.

Thus, these drawbacks have to be nullified by one or the other way to visualize their commercial applications. For these purpose reactor approaching as ideal plug flow are mostly preferred.

2.8. PLUG FLOW APPROACH

Plug flow approaching catalytic reactors (PFR) are widely studied due to its practical advantages in the industrial scale as they exhibit better performances as compared to the continuously stirred tank reactors (CSTR) (Levenspiel, 1999). PFR thereby provides no axial mixing of the particular reactants which makes it a more desirable and efficient reactor than the mixed flow reactor (Levenspiel, 1999). PFR being better in terms of minimum residence time, as well as an increased rate of degradation, is most sought of the reactor. For implicating the advantages of the PFR in the real case, the packed bed is most commonly preferred (Abbas, Dupont, & Mahmud, 2017; Towler & Sinnott, 2013) and the support material with immobilized catalyst plays the most important role. The hurdles obstructing the scaling -up, include various complications like mass transfer resistance which could be excluded if the critical reaction rate is substantially lower than the mass transport velocity (Motegh et al., 2014). This leads, on the one hand to the need for good external mass transfer (i.e. to reasonable flow conditions in the packed bed), as well as to short diffusion paths, in catalyst particles and sufficiently large pores. The study of PFR in context to its applications in AOP can give a blooming approach where one can think about the field-scale applications. In fact, this area has not given due consideration in the literature as far as the scaling-up of the process is concerned.

2.9. COMBINATION OF PHOTO-FENTON AND PHOTOCATALYSIS

In this context, taking into concern the stumbling of both AOPs (Longkai Yang et al., 2018) the technology involving the combination of two processes is showing wide popularity among the researchers. Among these AOPs, photocatalysis (Buriak, Kamat, & Schanze, 2014; W. H. Lin, Chiu, Shao, & Hsu, 2016; Luo et al., 2017) has proven its eminence in degrading pharmaceutical active ingredients and drugs mainly in slurry mode (Maroga Mboula, Héquet, Gru, Colin, & Andrès, 2012; MiarAlipour, Friedmann, Scott, & Amal, 2018). But there are certain problems in scaling up the process like cumbersome separation of TiO_2 (Daneshvar, Salari, Niaei, Rasoulifard, & Khataee, 2005), a larger quantity of catalyst being utilized (Rastegar, Shadbad, Khataee, & Pourrajab, 2012; T. Su, Shao, Qin, Guo, & Wu, 2018; Synthesis & Zir-, 2018; L. Zhang et al., 2017) and process drawbacks like electron-hole recombination combination (Elmolla & Chaudhuri, 2010). Hence, the application of photocatalysis is mainly preferred in fixed bed mode where the catalyst is supported on the inert support material(Bansal, Verma, Aggarwal, Singh, & Gupta, 2016). But again some problems like an increase in the treatment time, mass transfer limitations and inertness of the support (Kovacic et al., 2016; Vaiano, Sacco, Sannino, & Ciambelli, 2015) pose a crunch for the large scale applications. In the case of homogeneous photocatalysis i.e. photo-Fenton (Bokare & Choi, 2014b) although the time taken for the reaction is less as compared to the other AOPs yet certain shortcomings like a larger quantity of catalyst being utilized, iron sludge production, high dose of H_2O_2 has restricted its field-scale applications. Hence, the researchers are focusing on the new innovations taking into consideration their disadvantages for the efficacious treatment of pharmaceutical compounds.

The functionalized polyvinyl fluoride films (PVF–TiO_2–Fe oxide) mediated in CPC were used for the degradation of nalidixic acid, phenol and the mixture of pesticides. Mazille et al., 2010 investigated that as the reaction proceeds the leaching of iron was less (<0.2 mg L^{-1}). The photoactivity of the PVF–TiO_2–Fe oxide was increased gradually althrough experiments. Hospital wastewater was degraded using combined heterogeneous and homogenous photo-catalytic. It was investigated that the solar/TiO_2/Fe^{2+}/H_2O_2 process displayed increased efficiency due to the synergetic effect of photocatalytic as well as photo-Fenton reactions (Adish Kumar et al., 2014). The reduction in time with increased degradation was observed in that case.

Hence, it was concluded that with the introduction of Fenton reagent in the photocatalytic system there is an increase in the production of •OH which is simultaneously generated by both the processes going side by side i.e. photo-Fenton and photocatalysis.

Best efforts would be made to reduce the treatment time by incorporating in-situ dual effect (photocatalysis and photo-Fenton). Efforts would also be made to study the dual effect in the once-through process using fixed bed reactors.

2.10. PROBABLE DUAL EFFECT MECHANISM

The basic mechanism for the dual effect of photocatalysis and photo-Fenton is explained using Figure 2.2. The surface-active TiO_2 layer would lead to photocatalysis, thus leading to the generation of •OH. Besides this, there would be subsequent leaching of iron from these composite beads. As confirmed by the characterization, the FE+FS beads have more amounts of Fe(III). Thus, for executing photo-Fenton studies, these Fe(III) ions need to be converted into Fe(II). The electron required for this reduction comes from the conduction band of TiO_2. (Kim et al., 2012). This step help in coverage of the shortcoming of the photocatalysis process of the electron-hole recombination as an electron gets involved in reduction. This will eventually lead to the generation of more number of •OH, thus increasing the reaction rate. This also helps in the oxidation of water molecules to form •OH. Moreover, Fe(II) species present in the composite are capable of changing H_2O_2 into reactive species. If the amount of Fe(II) increases in the solution, electron scavenging might take place. This could be due to the absence of H_2O_2.

Therefore, the results recommended that the binding of iron to the photo-excited TiO_2 surface might have an effect on the mechanism of the Fenton reaction to aid the •OH production (Bokare & Choi, 2014b).

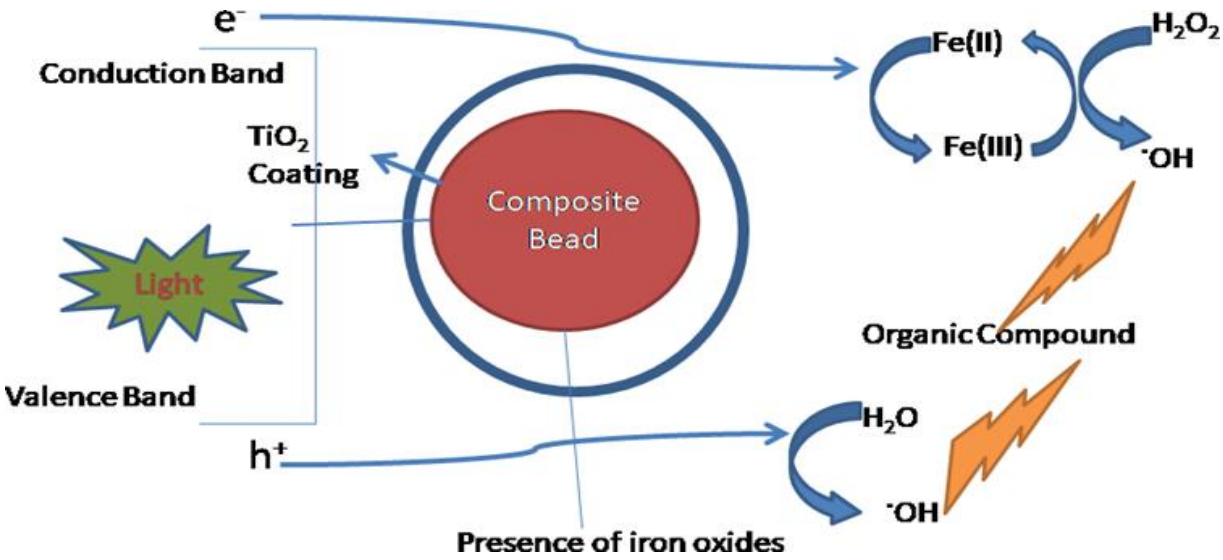

Figure 2.2: The probable mechanism of dual effect using Fe-TiO_2 composite support

The basic mechanism of the dual process taking place might be explained as shown in equations 2.1 - 2.9. The major problem of electron-hole recombination is solved in this novel effect as the electrons generated in the photocatalysis helps in the conversion of Fe^{3+} to Fe^{2+} as shown in equation 2.7 – 2.8. The scavenging effect of the H_2O_2 is explained using equation 2.9.

$$Fe_{aq}^{2+} + H_2O_2 \rightarrow \mathrm{Fe_{aq}^{3+}} + \mathrm{OH^-} + \cdot \mathrm{OH} \quad (2.1)$$

$$Fe_{aq}^{3+} + H_2O_2 + H_2O \rightarrow \mathrm{Fe_{aq}^{2+}} + \mathrm{H_3O^+} + \mathrm{HO_2^{\cdot -}} \quad (2.2)$$

$$Fe_{aq}^{3+} + H_2O \xrightarrow{h\nu} \mathrm{Fe_{aq}^{2+}} + \mathrm{H^+} + \cdot \mathrm{OH} \quad (2.3)$$

$$TiO_2 \xrightarrow{h\nu} \mathrm{e^-} + \mathrm{h^+} \quad (2.4)$$

$$TiO_2 + H_2O \rightarrow \mathrm{Ti\ OH^-} + \cdot \mathrm{OH} \quad (2.5)$$

$$\mathrm{Ti\ OH^-} + h^+ \rightarrow \mathrm{Ti - HO^{\cdot}} \quad (2.6)$$

$$TiO_2 + O_2 + e^- \rightarrow \mathrm{TiO_2} + \mathrm{O_2^-} \quad (2.7)$$

$$Fe_{aq}^{3+} + e^- + H_2O \rightarrow \mathrm{Fe_{aq}^{2+}} + \mathrm{H^+} + \cdot \mathrm{OH} \quad (2.8)$$

$$\cdot OH + H_2O_2 \rightarrow HO_2 \cdot + H_2O \quad (2.9)$$

2.11. SUMMARY EXTRACT

The AOPs have gained wide popularity among the researchers due to their capability of treating a wide variety of recalcitrant compounds. Among all the treatment technologies, TiO_2 photocatalysis has shown its potential in the field of semi-conductor photocatalysis in the context of degrading a wide variety of pollutants. But certain barriers including cumbersome separation of nano-sized catalyst from the treated solution leads to extra cost, a larger quantity of catalyst being utilized thus limiting its feasibility for practical applications and the most important is a large amount of time for treating the pollutant. To overcome this hurdle, research is now oriented towards fixed-bed photocatalysis, where the catalyst is being coated on some material and subsequently used for degradation. Studies related to fixing of catalyst on supports are extensively reported in the literature but durability, recyclability, cost of the support material have not been cited well.

Homogenous photocatalysis i.e. photo-Fenton has also provided some potential breakthroughs in the field of advanced treatment techniques. The redox reactions, taking place between the oxides of iron and H_2O_2 in the presence of light leads to the generation of •OH. But, these studies usually face problems like maintaining a high dose of H_2O_2, the formation of a high concentration of anions in the treated wastewater, large amounts of ferrous iron sludge, and their lower efficiency of photon utilization restricts its industrial applications. The literature showed the various applications of pilot-scale fixed bed reactors utilizing photo-Fenton as well as heterogeneous photocatalysis. Various reactors including concentrating and non concentrating reactors have been discussed. But various problems including the durability/recyclability of the catalyst is still a question. The prolonged usage leading to the catalyst deactivation is also a problem. Hence, extensive research is required for the fixed bed reactors for commercial-scale applications.

Taking into consideration the various advantages and limitations of the single AOP in treating the pollutants present in water, recent studies have concentrated upon the development of the techniques focusing on the combination of two AOPs. The combined process leading to the synergistic effect over the individual processes helps in better mineralization and degradation of pollutants. Moreover, the treatment time can be significantly reduced using the hybrid process. Combinations of AOPs have been studied and reported for the treatment of bio-recalcitrant

compounds. In this context, the present research work focuses on the in-situ dual effect of photocatalysis and photo-Fenton for the degradation of pharmaceutical drugs in fixed mode. For overcoming the potential drawbacks of the individual processes of photocatalysis and photo-Fenton and taking into consideration their advantages, the efforts have been made to couple both the processes.

RESEARCH GAPS

Based on the literature review, the following gaps have been identified:

- Durability and stability issues of the supported catalyst for its prolonged use are not covered effectively in literature.
- The high loss in activity of photocatalyst has been observed after few recycles of the catalyst immobilized support materials in most of the reported studies.
- The coupling of two techniques i.e. photocatalysis and photo-Fenton process in combination with fixed-bed studies is not well studied.
- Moreover in-situ dual process (photocatalysis and photo-Fenton) has not been covered effectively.
- For scale-up trials, once-through process has not been evaluated yet for in-situ dual effect.

OBJECTIVES

Hence in the present study efforts have been made to incorporate the advantages of both the processes of photocatalysis and photo-Fenton and cover up their shortcomings in a single process. The dual effect resulted in the significant degradation along with the reduction in the treatment time for the treatment of pharmaceutical drugs Phenazone (PHZ) and Metronidazole (MTZ). For field-scale visualization of the reported dual process, the studies were extended to pilot-scale reactors. Further feasibility of the process was confirmed by applying the technique for the treatment of real pharmaceutical industry wastewater. In this view, the doctoral research work was conducted with the following objectives:

- Selection of novel inert support material incorporating in-situ dual process (Photocatalysis and photo-Fenton) for the degradation of pharmaceutical drugs (Nonsteroidal anti-inflammatory drugs/Antibiotics).
- Study of fixed bed photocatalytic reactor (batch / continuous) incorporating in-situ dual effect and parametric optimization.
- Durability studies in terms of number of recycles for immobilized support incorporating dual effect.

CHAPTER -3

MATERIALS AND METHODS

The chapter includes all the materials used for the treatment of the pharmaceuticals along with the various techniques used while performing the experiments. The methodology for the analysis and the characterization of the samples has also been included.

3.1. PHARMACEUTICAL COMPOUNDS

In the study, Phenazone and Metronidazole were used as the pharmaceutical compounds for conducting the experiments. Phenazone (PHZ) is a non-steroidal antipyretic, anti-inflammatory drug (NSAIDs) (Calza et al., 2011) most commonly used for reduction in fever, ear infections, and skin infections and for relieve of pain. The structure of PHZ has been shown in Figure 3.1.

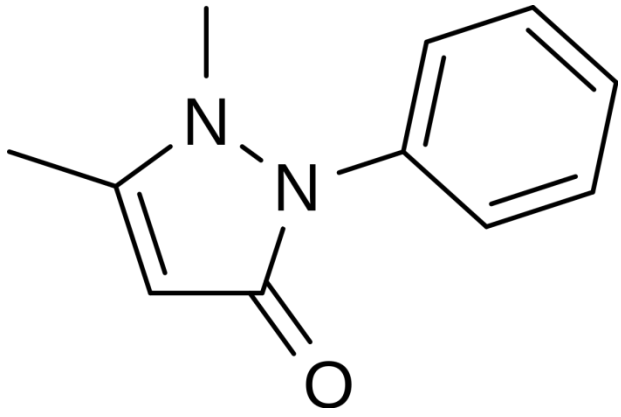

Figure 3.1: Chemical structure of PHZ

NSAIDs have been found in surface water (Zuehlke et al., 2007), groundwater and even in drinking water (Reddersen et al., 2002). Even at very low concentrations (few µg L^{-1}), drugs could pose a threat to living beings due to resistance caused by these in the bacteria and are harmful to the aquatic species. Its presence in natural waters clearly indicates the inefficacy of conventional treatment methods (Belver et al., 2017). Hence, for the present study PHZ was chosen as the targeted pollutant and was procured from TCI Chemicals, Pvt. Ltd., India.

Metronidazole (MTZ) (2-methyl-5-nitroimidazole-1-ethanol) (with its structure as shown in Figure 3.2) an antibiotic (Chua, 2017) has been extensively used to treat infections caused by bacteroides, anaerobic bacteria, and protozoa. MTZ has been detected in surface waters and wastewater in residual concentrations. MTZ is highly soluble in water and is nonbiodegradable; hence it is accumulated in the aquatic environment. Elimination of MTZ from the water system is an important issue considering its potential mutagenicity, toxicity, and carcinogenicity (Bendesky, Menéndez, & Ostrosky-Wegman, 2002). Thus, for the present study, MTZ was selected as the target pollutant. MTZ was purchased from the local industry nearby Patiala, Punjab, India.

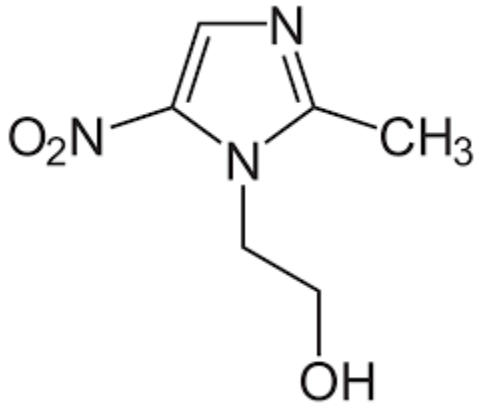

Figure 3.2: Chemical structure of MTZ

Real wastewater from the pharmaceutical industry in Barnala, Punjab, India was collected and was used as received. The characterization of the raw wastewater has been discussed in section 4.6.

3.2. CHEMICAL REAGENTS

3.2.1. CATALYSTS USED

AEROXIDE TiO_2 P25 was obtained from Evonik Degussa Corporation, Mumbai, India. Its physico-chemical properties mainly include the specific surface area of 50±15 m^2g^{-1}, the particle size of 30 nm and the appearance of fluffy white powder. The purity of the catalyst was ≥99.5%.

3.2.2. CHEMICAL REAGENTS

Hydrogen peroxide (H_2O_2) (30% *w/v*), an oxidant was bought from Ranbaxy (India). Waste foundry sand (FS) was collected as such from the local industry, Patiala (India). Fuller's earth (FE) was acquired from a local vendor, Patiala (India). Sodium acetate, >98.5% purity and acetic acid, >99.5% purity, acquired from TCI Chemicals (India) was used for preparing acetate buffer. Sodium carbonate (anhydrous), >98.5% purity was procured from Loba Chemie Pvt Ltd (India).

Potassium dichromate ($K_2Cr_2O_7$) and concentrated sulphuric acid (H_2SO_4) of analytical grade (AR), used during Chemical Oxygen Demand (COD) estimation were obtained from SD Fine Chemicals Ltd. (India). The reagents including calcium chloride ($CaCl_2$), phosphate buffer, ferric chloride ($FeCl_3$), and sodium hydroxide (NaOH), and magnesium sulphate ($MgSO_4$) of AR grade were used for the determination of BOD and were also purchased from SD Fine Chemicals Ltd. (India).

For the estimation of iron content, ferrous ammonium sulfate, 1, 10- phenonthraleine monohydrate, hydroxylamine hydrochloride, ammonium acetate, acetic acid, hydrochloric acid, potassium permanganate ($KMnO_4$) were used. All the reagents and chemicals were procured from SD Fine Chemicals Ltd. (India).

Determination of various anions like nitrate, nitrite, ammonium ions formed after the mineralization were performed using *N*-(1-Naphthyl)ethylenediamine dihydrochloride, hydrochloric acid, ammonium hydroxide, isopropyl alcohol, purchased from Loba Chemie pvt. Ltd. (India). For the preparation of all the reagents double distilled water was used.

3.3. PREPARATION OF COMPOSITE SUPPORT

FE along with FS were used as a natural sourcess of iron for composing the beads. This was confirmed from the XRD (Figure 3.3a,b) (Ref No. 00-0330-1161, 00-019-0629) as well as the SEM-EDS (Figure 3.4, 3.5) analysis of the raw materials. Along with iron source, FS provides the binding as well as compressive strength to the beads (Siddique, Schutter, & Noumowe, 2009). Composite beads made of FE (Figure 3.6a) and FE+FS (Figure 3.6b) (spherical shaped) were made manually and subsequently baked at 800°C for 2 h in a muffle

furnace for gaining the strength. These beads were subsequently cured by dipping in water for 24 h. The average diameter of the beads was 12.20 mm measured by taking the average diameter in multiple directions of randomly picked 15-20 beads using a screw gauge. These beads were used for the photo-Fenton process as the leaching of iron took place from the composite beads under acidic conditions.

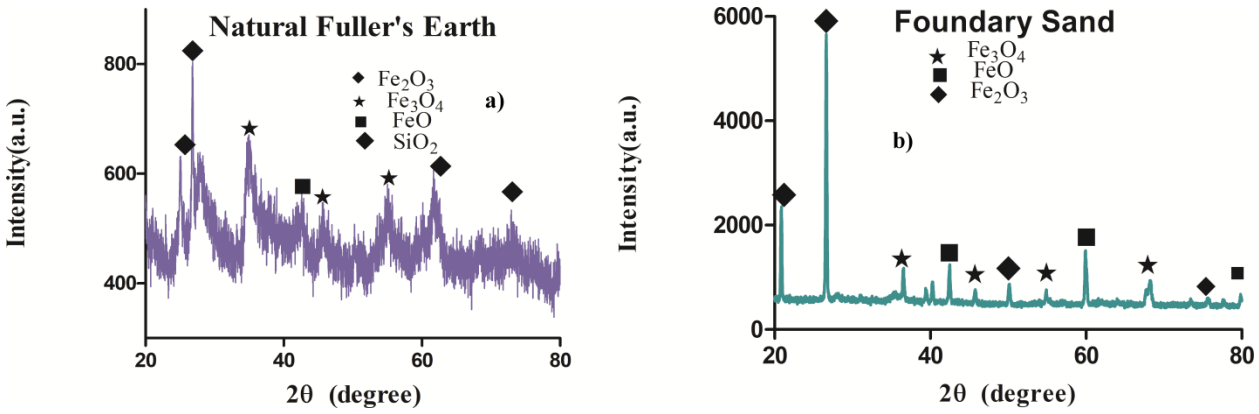

Figure 3.3: XRD pattern of a) Natural FE and b) FS

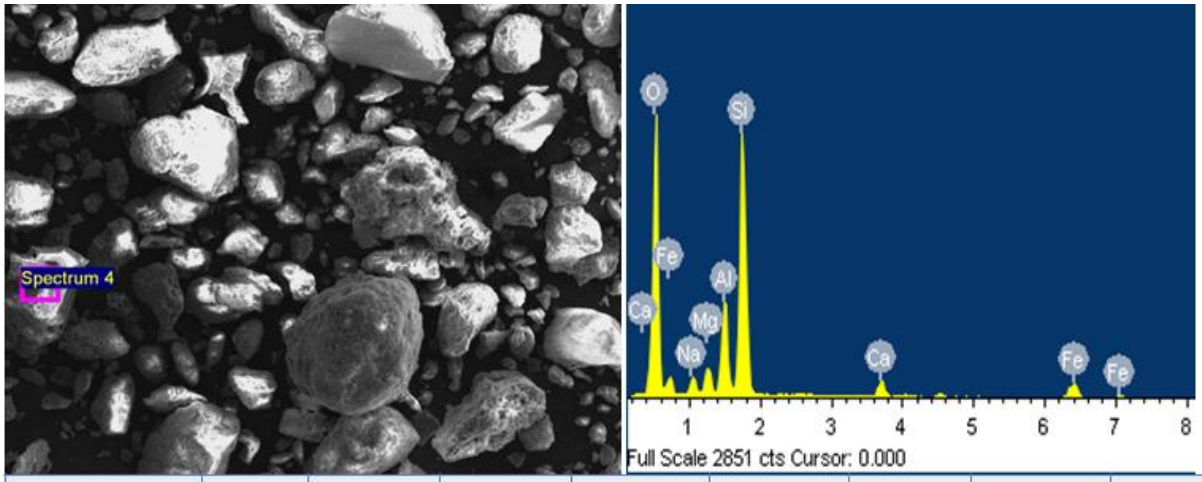

ELEMENTS	Mg K	Al K	Si K	Na K	Ca K	Fe K	O K	Total
WEIGHT%	2.25	7.27	23.24	1.79	10.81	9.26	53.55	100

Figure 3.4: SEM-EDS analysis of raw FE

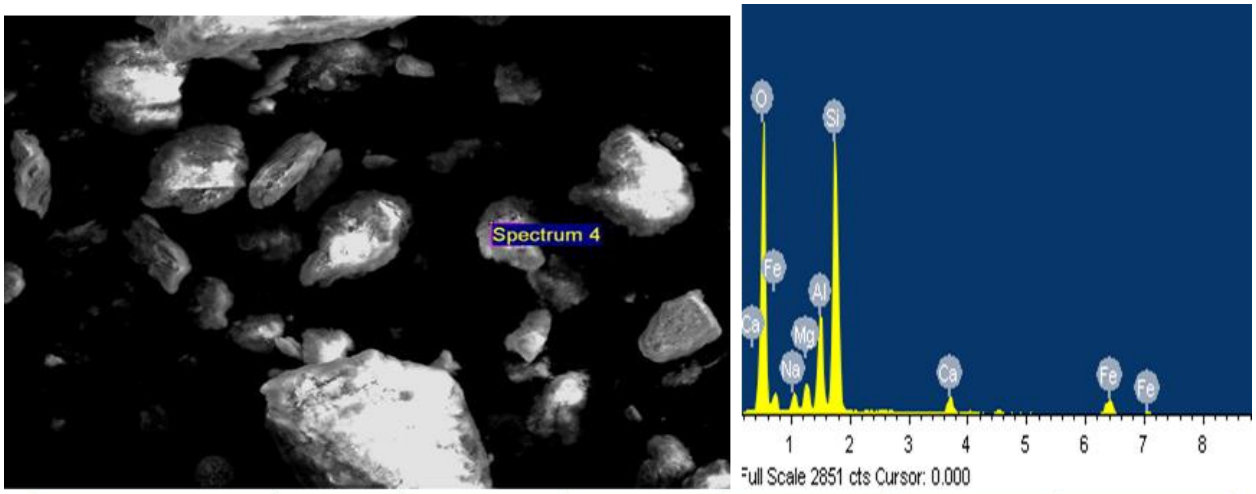

ELEMENTS	Mg K	Al K	Si K	Fe K	O K	Total
WEIGHT%	2.88	10.46	25.26	12.26	49.14	100

Figure 3.5: SEM-EDS analysis of raw FS

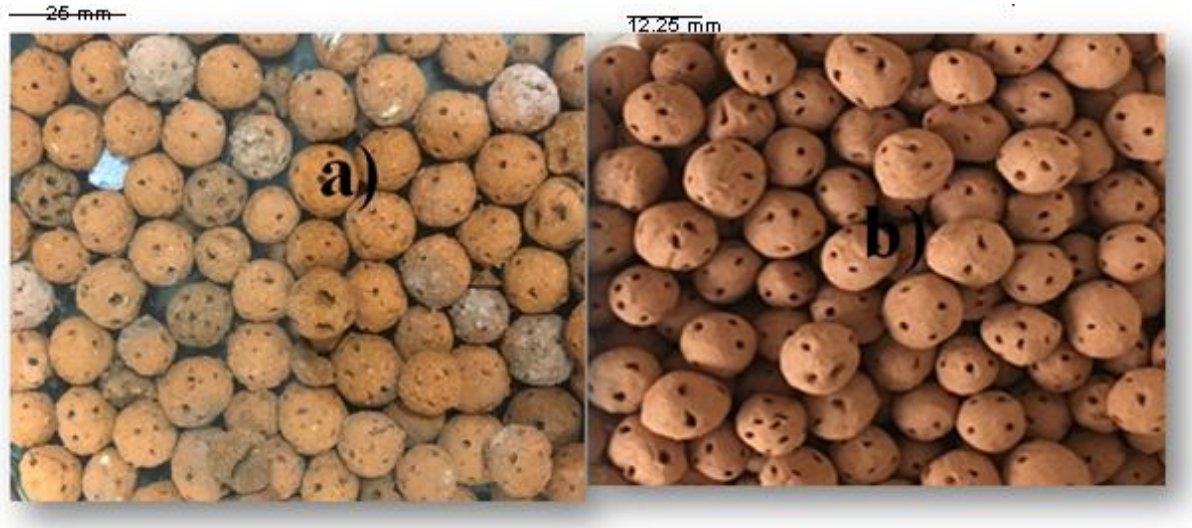

Figure 3.6: a) Actual image of the spherical beads composed of FE, b) Actual image of the spherical beads composed of FE+FS

For analyzing the morphological characteristics of the uncoated composite beads SEM analysis was carried out. The SEM analysis was combined with the EDS and mapping analysis

for the distribution of various elements present in the samples. SEM-EDS of FE beads has been shown in Figure 3.7a. SEM-EDS of FE+FS beads has been shown in Figure 3.7b. From the SEM images of the unused coated beads, it was observed that the coating was uniform without cracks and EDS confirmed the presence of Fe along with various elements including Si, Al, Mg, Ca. Mapping of the beads also confirmed the distribution of Fe, Si, Al, Mg, Ca elements on the surface of the beads (Figure 3.8).

XRD of the uncoated beads confirmed the presence of iron oxides in both FE beads (Figure 3.9a) and FE+FS beads (Figure 3.9b). Presence of Fe Oxides (JCPDs number 00-013-0534, 01-089-6466) in both types of beads along with the peaks corresponding were detected in unused beads.

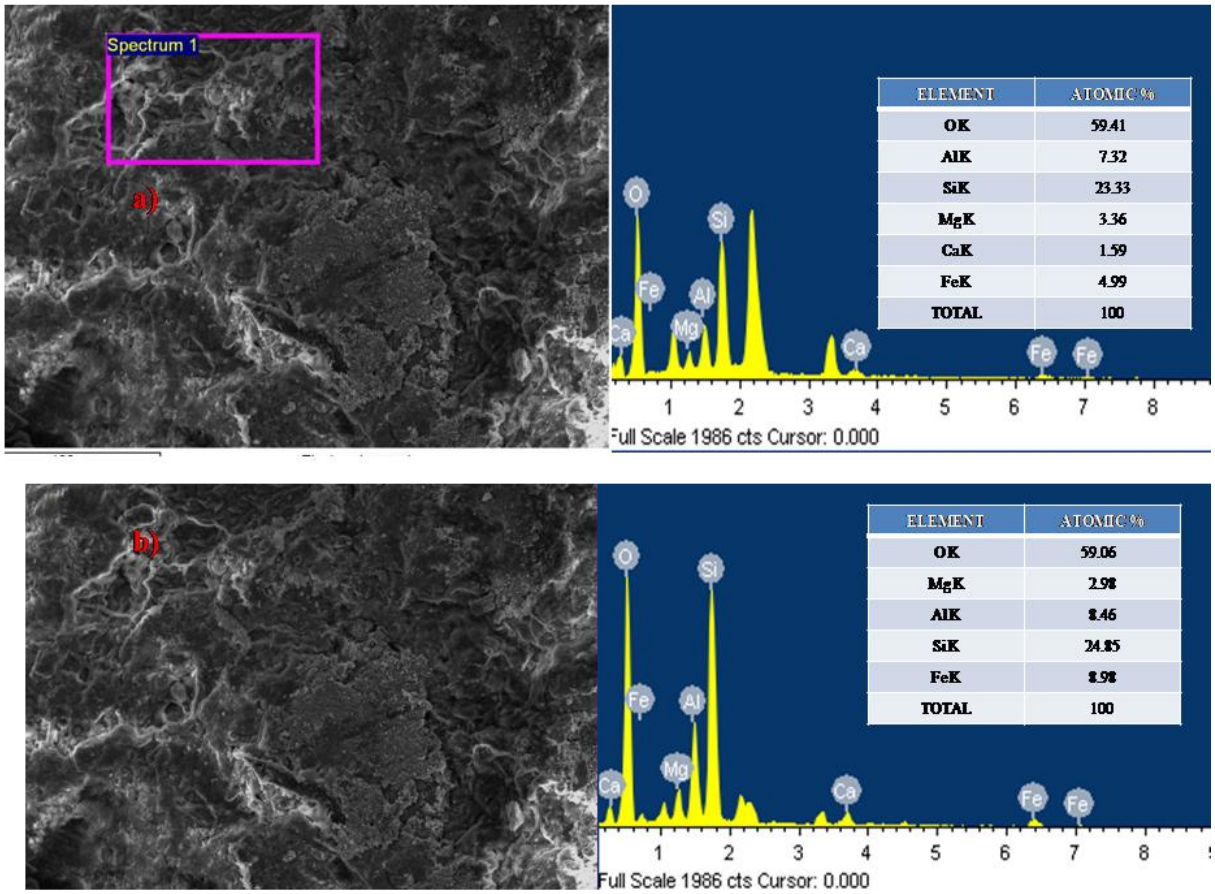

Figure 3.7: SEM-EDS analysis of uncoated a) FE beads, b) FE+FS beads

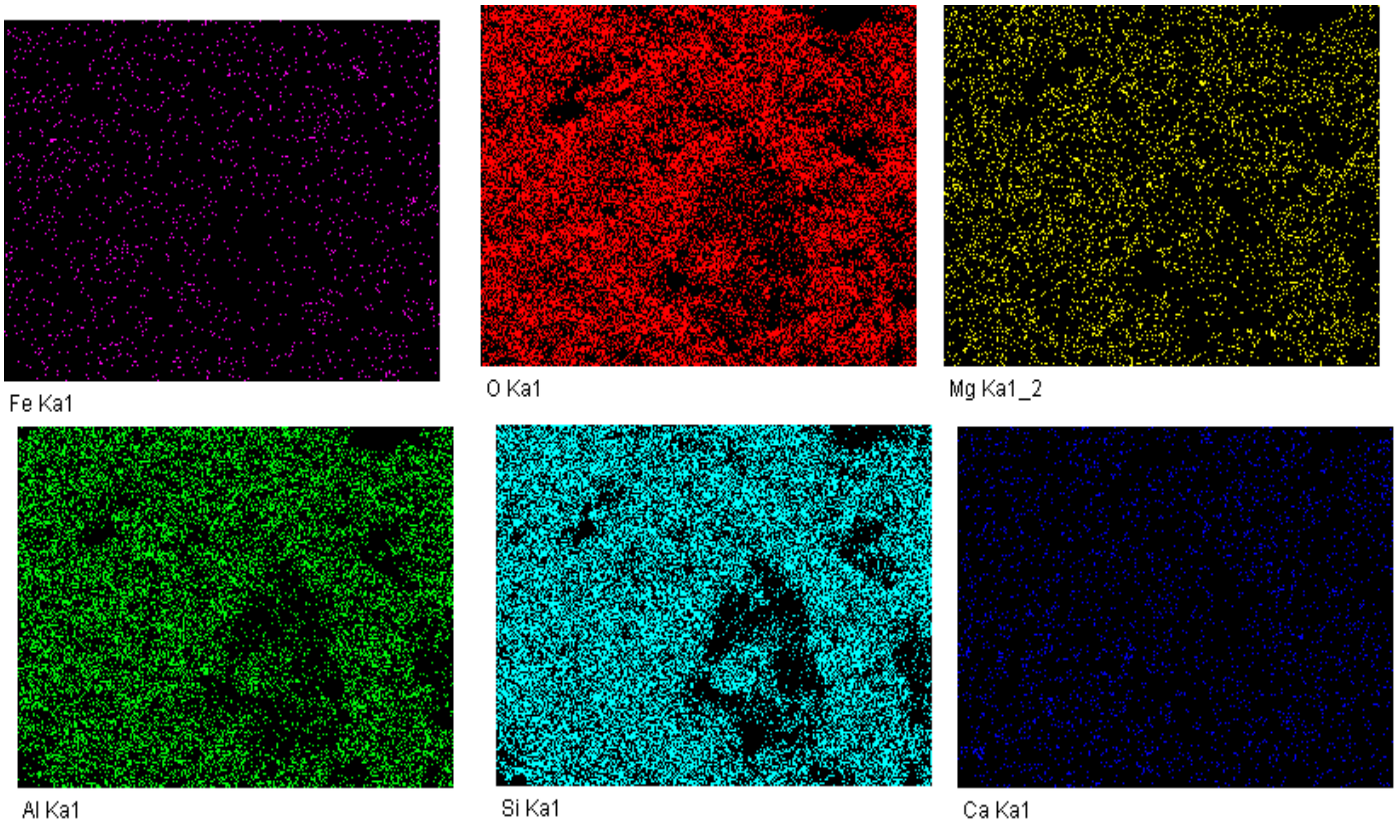

Figure 3.8: Mapping of uncoated FE+FS beads

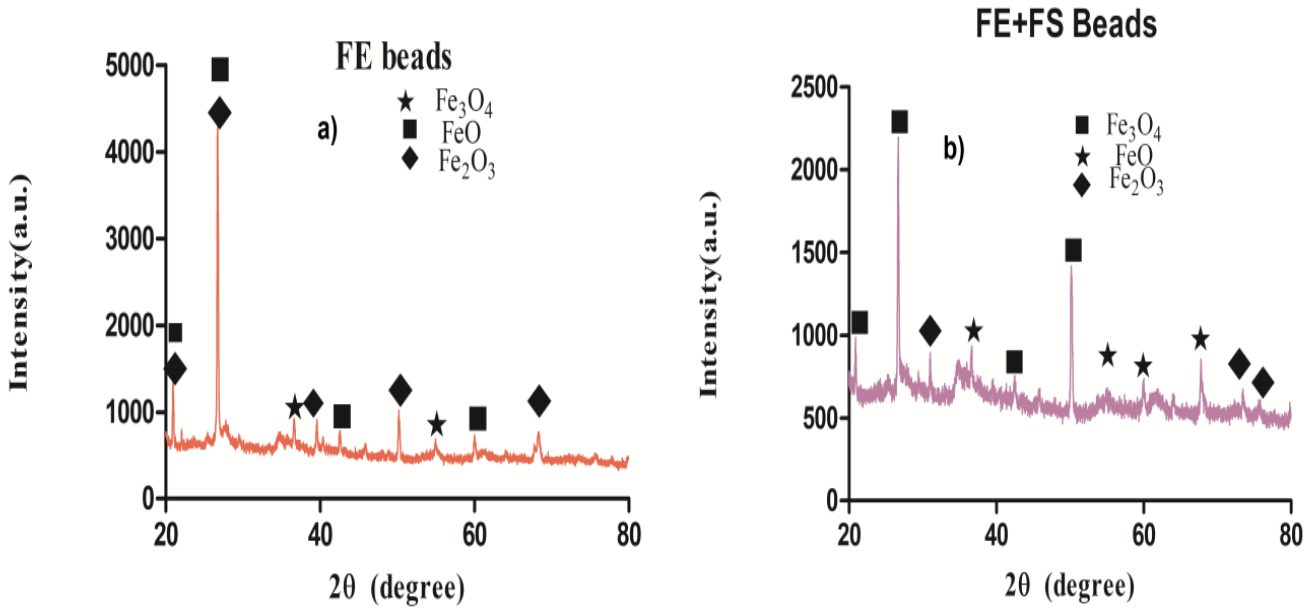

Figure 3.9: XRD pattern of a) FE beads and (b) FE+FS composite beads

3.3.1. IMMOBILIZATION OF THE CATALYST SUPPORT

For the purpose of immobilization, TiO_2 was used as a catalyst. The prepared composite beads were further used for coating the TiO_2 using a standard dip and coating method (Verma et al., 2014). 2% *(w/v)* TiO_2 slurry solution was prepared with continuous stirring for 1 h and then sonification for 30 minutes for the dispersion of particles. The prepared composites were dipped in the solution and kept for approximately 30 h with continuous quivering for the coating to be uniformly deposited. At least 2 coatings were enough for achieving the required thickness of the TiO_2 layer. These TiO_2 coated composite beads were used for in-situ dual effect studies of photocatalysis and photo-Fenton. The actual image of the FE and FS coated beads has been shown in Figure 3.10a and Figure 3.10b respectively. The thickness of the coating was 60-70µm as confirmed from the SEM analysis (Thakur, Örmeci, & verma, 2020).

Figure 3.10: a) Actual image of the TiO_2 coated composite beads composed of FE, b) Actual image of the TiO_2 coated composite beads composed of FE+FS

For analyzing the morphological characteristics of the coated composite beads SEM analysis was carried out. The SEM analysis was combined with the EDS and mapping analysis for the distribution of various elements present in the FE and FE+FS coated beads as shown in Figure 3.11a and b respectively. From the SEM images of the unused coated beads, it was observed that the coating was uniform without cracks and EDS confirmed the presence of Ti as

well as Fe elements. The mapping of the beads also confirmed the distribution of Ti and Fe elements on the surface of the bead (Figure 3.12).

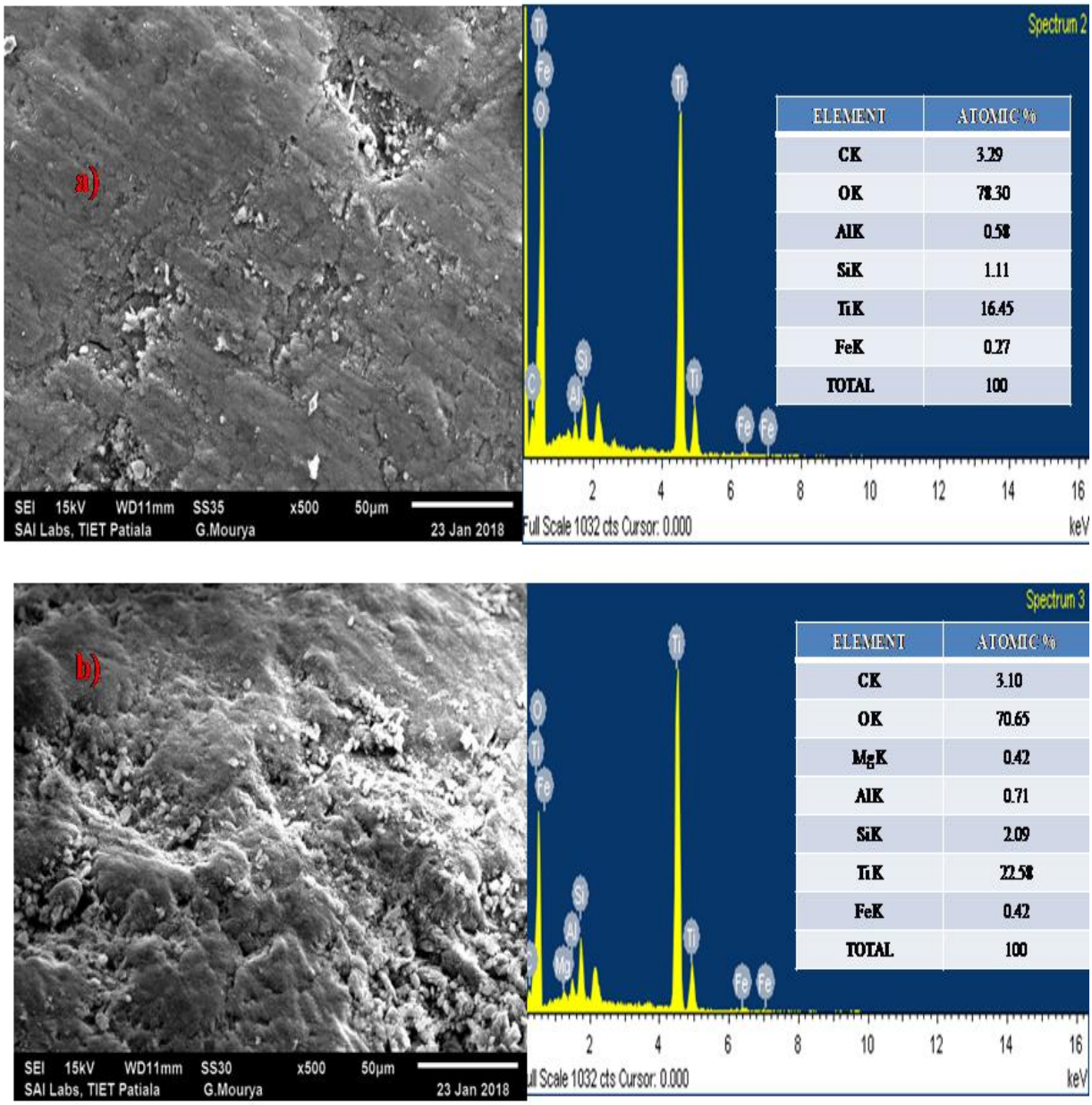

Figure 3.11: SEM-EDS image of TiO_2coated a) FE beads, b) SEM-EDS image of coated FE+FS beads

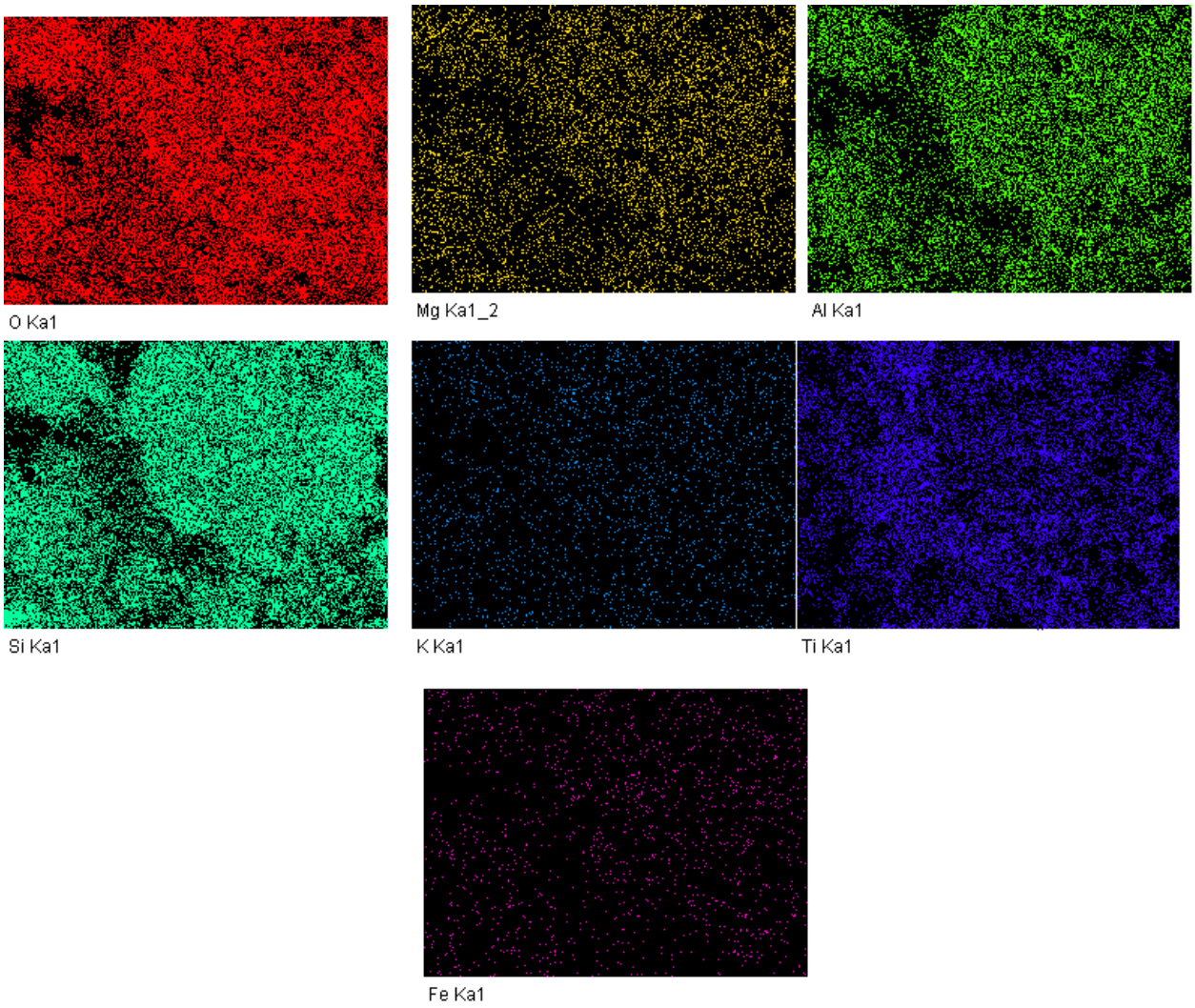

Figure 3.12: Mapping of TiO_2 coated FE+FS beads

XRD of the TiO_2 coated beads confirmed the presence of iron oxides along with TiO_2 in both types of beads (Figure 3.13a,b). Presence of Fe Oxides (JCPDs number 00-013-0534, 01-089-6466) in both types of beads along with the peaks corresponding to the basic nature of TiO_2 i.e. anatase and rutile phase (JCPDs number 01-083-2243, 01-088-1172) were detected in unused beads.

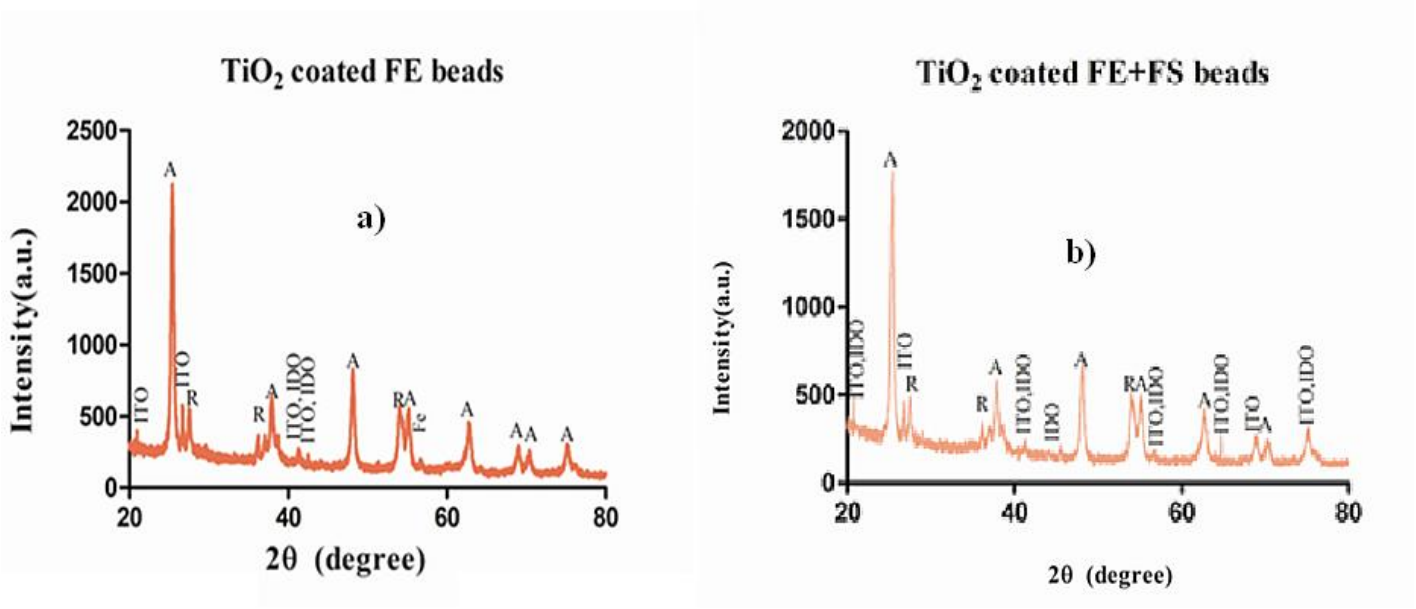

Figure 3.13: a) TiO_2 coated FE beads, b) TiO_2 coated FE+FS composite beads

3.4. EXPERIMENTAL PROCEDURE FOR CONDUCTING DUAL EFFECT EXPERIMENTS AT THE LABORATORY SCALE

For conducting the experiments, a batch reactor made of glass having dimensions (17cm×5cm) (diameter× height) was used. Experiments were performed in the closed wooden chamber with UV light (36W×7, UV-A, Philips) having λ_{max} 365 nm as shown in Figure 3.14. For measuring the intensity inside the chamber Eppley radiometer (model no.−33013) was used and during the reactions, the average intensity reported was 22 ±2 W m^{-2}. For conducting the experiments stock solution of 25 mg L^{-1} of both the drugs (PHZ and MTZ) was prepared using double distilled water.

For the degradation studies, approximately 90-100 composite beads covering the bottom surface of a cylindrical glass reactor were used with a working volume of 200 mL. For supplying the air flow continuously (3-3.5 L min^{-1}) air spargers were used. At regular intervals of time, the samples were withdrawn for numerous analyses using the syringe and were filtered using the syringe filters (Millipore, 0.45µm). The efficiency of the degradation was calculated using equation 3.1.

$$\% \, Degradation = \frac{(C_0 - C_f)}{C_0} \times 100 \qquad (3.1)$$

Where C_0 (mg L^{-1}) is the initial concentration, C_f (mg L^{-1}) is the final concentration after treatment time t (min). For reporting the results experiments were conducted in triplicates and the average was noted.

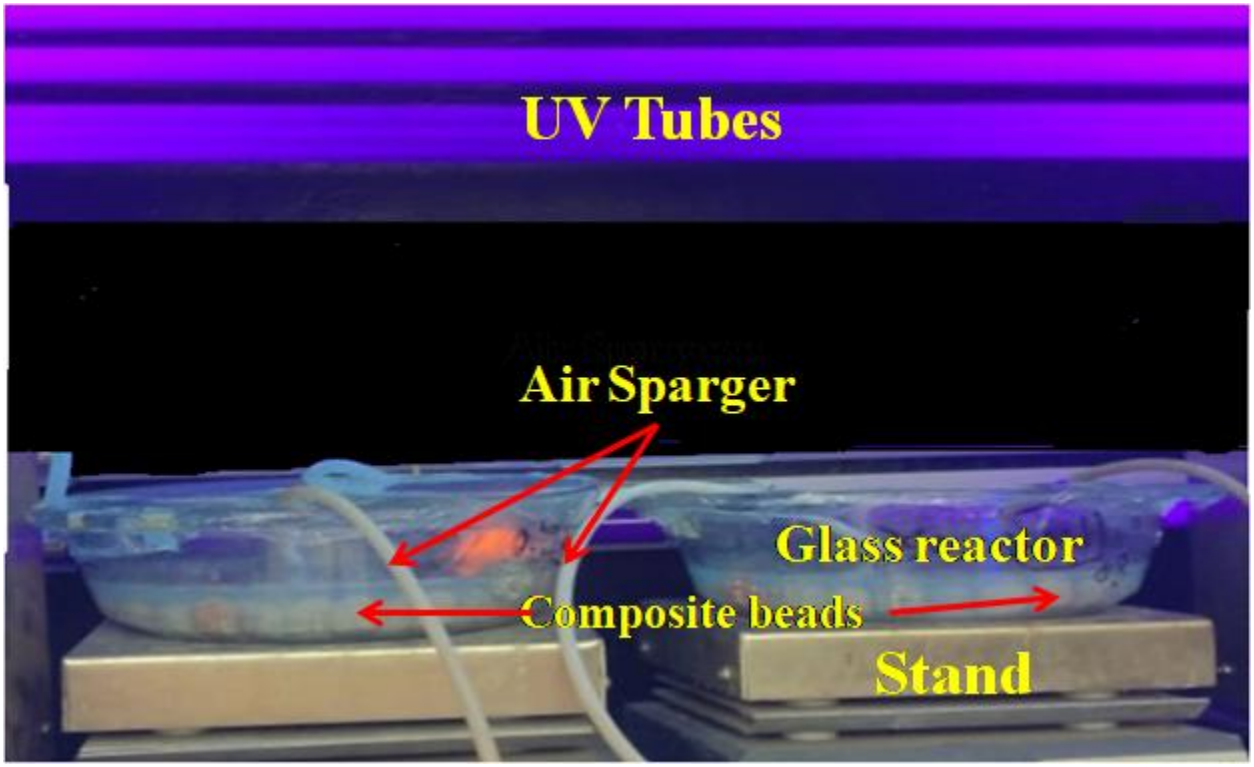

Figure 3.14: The actual photograph of the batch scale set up of reactor in UV chamber

The calibration curve for PHZ and MTZ was prepared by measuring the absorbance at 242 nm and 321 nm respectively. The curve was plotted between the known concentration and absorbance leading to the best fit (Figure 3.15).

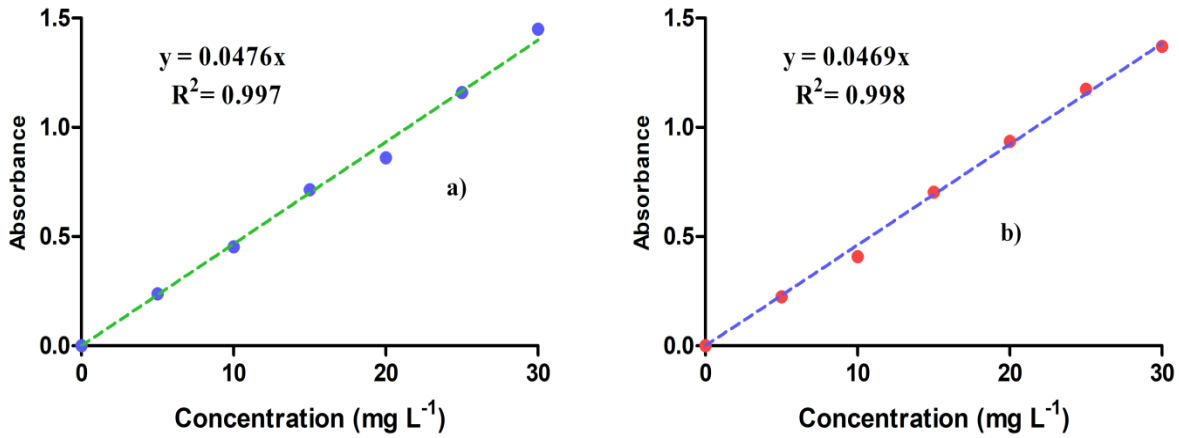

Figure 3.15: Calibration curve of a) PHZ b) MTZ

3.5. EXPERIMENTAL DESIGN AND OPTIMIZATION

For the design of experimental matrices, Response surface methodology (RSM) was used. For the statistical analysis of the operating parameter and the model developed RSM is used frequently. The basic parameters affecting the process are known as independent variables whereas the responses are the dependent variables. RSM is a collection of mathematical and statistical techniques that are useful for the modeling and analysis of problems in which a response of interest is influenced by several variables and the objective is to optimize the responses. Providing less number of experiments and being the cost inexpensive technique RSM is mostly preferred. Box-Behnken designs (BBD) comprised under RSM was utilized to optimize the process parameters. BBD has been used to optimize process parameters for a number of processes (Bhatti, Kapoor, Kalia, Reddy, & Thukral, 2011). BBD has proven to be more efficient than other factorial designs. The basic advantage of this design is that it does not allow the experiments to be performed at extreme conditions, which might lead to unsatisfactory results. It is most suited for the 3-4 factors as less number of experiments is suggested. Further BBD helps in estimating the parameters of the quadratic model, detection of lack of fit, and designing sequential designs. The statistical Design-Expert software version 6.06 (STAT-EASE Inc., Minneapolis, US) was used to design the experiments.

The output (response) Z_i which are the functions of input factors T_1, T_2 ….T_i…..T_f is obtained from the following relationship as shown in equation 3.2.

$$Zi=\phi\ (T_1,T_2,\ldots T_i\ldots T_f) \quad (3.2)$$

The above relations between input and output variables are considered to be quadratic in nature as shown in equation 3.3:

$$Z=v_0+\sum_{i=1}^{k}v_iT_i+\sum^{k}v_{ii}T_i^2+\sum\sum_{i<j}v_{ij}T_iT_j+\kappa_t \quad (3.3)$$

Where, Z is the response; υ_0 is the constant, υ_i is the linear effect of T_i, υ_{ij} is the linear by linear interaction effect among input factors T_i and T_j and υ_{ii} is the quadratic effect of input factors T_i.

Hence, multi-response process optimization with the desirability function approach could be used for the optimization of the process. The value of desirability, d_i lies between 0 and 1(Ferreira et al., 2007). Overall desirability (D_o) was estimated by combining individual desirability functions as shown in equation 3.4:

$$D_o = (d_1\times d_2\times d_3)^{1/3} \quad (3.4)$$

Where d_1, d_2, d_3 are desirability for responses respectively.

3.6. ANN MODELING

ANN model has a structural similarity with the biological neuron systems (V. K. Sangal, Kumar, & Mishra, 2014). Basically, three different layers are involved in the process i.e. input, hidden and an output layer. Certain numbers of neurons are connected with the layers (David, Arivazhagan, & Ibrahim, 2015).

A number of neurons that are present in the hidden layer are an important factor in the performance of the network (Li et al., 2017). A number of neurons can be varied to minimize the mean square error. The information from the input layer is processed by the hidden layer's neurons and after that, the processed data is summed up in the output layer using the transfer functions.

For the learning process of the database, training is necessary for the testing and validation of the developed model. Root Mean Square Error (RMSE) is used to compare the predicted and actual data results.

In this work, the backpropagation algorithm was preferred with the tan-sigmoidal transfer function applied between input and hidden layer. The input variables to the neural networks are as follows: treatment time, H_2O_2 dosage, Intensity of the UV light, pH of the solution, A/V ratio, % surface area covered by the catalyst. The output variable chosen is % degradation. All ANN calculations have been carried out using Matlab R2017 b mathematical software with ANN toolbox.

3.7. OPTIMIZATION USING GENETIC ALGORITHM

Motivated by the principle of Darwin's theory of evaluation by genetic selection i.e. the survival of the fittest theory GA is a technique to find the optimized solution (Gupta & Garg, 2013). A solution of GA is represented by a chromosome having a fitness value that confirms the solution of the particular problem to be good enough. The basic components of the GA may include a set of the population composed of genes and chromosomes, fitness, fitness function, crossover, mutation and selection (Holland, 1998). The algorithm starts with the generation of the population randomly and then the selection based on fitness to evaluate the next generation of the population (Taylor, Prabhu, Karthikeyan, & Shanmugaprakash, 2015). The selection of parent chromosomes for the recombination to produce child chromosomes is the basic process involved. With further successive iterations of generations, a good amount of fitness tends to increase until the optimum solution to the problem is reached.

GA was used to optimize the input representing the process variables, with the objective of maximizing the % degradation. For the purpose of optimization coding of GA in MATLAB, R2017 b was used.

3.8. SYNERGISTIC CALCULATIONS

The improvement in the degradation efficiency using the dual effect could also be depicted in terms of the synergy obtained. The synergy of the dual process over the individual processes was calculated using kinetic rate constant of individual processes of photocatalysis, photo-Fenton and dual process. The rate constant was evaluated using the data from the batch reactor. The synergy of the integrated system over the individual process (Madhavan, Grieser, & Ashokkumar, 2010; Rajeswari & Kanmani, 2009) was studied using the equations (3.5-3.7),

Synergy of dual over photocatalysis process:

$$\%\, Synergy = 100 \times \{(k_{dual} - k_{photocatalysis})\}/k_{dual} \quad (3.5)$$

Synergy of dual over photo-Fenton process:

$$\%\, Synergy = 100 \times \{(k_{dual} - k_{photoFenton})\}/k_{dual} \quad (3.6)$$

Synergy of dual over both photocatalysis and photo-Fenton process i.e overall synergy:

$$\%\, Synergy = 100 \times \{(k_{dual} - (k_{photocatalysis} + k_{photoFenton}))\}/k_{dual} \quad (3.7)$$

The synergy for the overall dual process has also been evaluated using % degradation as shown in equation 3.8,

$$Synergy = \frac{(\%\, degradation)_{hybrid}}{(\%degradation)_{photocatalysis} + (\%\, degradation)_{photo-Fenton}} \quad (3.8)$$

3.9. PILOT SCALE FIXED BED REACTOR

The TiO_2 immobilized FE+FS beads were used to conduct the in-situ dual effect experiments for the degradation of pharmaceuticals. Two types of reactors were used for the study. The first one includes the once-through system with three reactors connected in series and the second one includes a compound parabolic concentrator. The three reactors in series consist of baffled glass reactors. A single baffled glass reactor with dimensions (25cm×30cm×5cm) was designed to handle the total volume of 5 L as shown in Figure 3.16. Pharmaceutical wastewater containing the adequate dose of H_2O_2 was pumped from the collection tank with the help of a pump at the flow rate of 2.0 L h^{-1} to the reactor containing the FE+FS composite beads. An adequate amount of buffer was added to maintain the acidic conditions for the photo-Fenton reaction to take place. The samples were collected at the appropriate time for further degradation studies.

3.9.1. ONCE THROUGH REACTOR SYSTEM

For carrying out the once-through fixed bed studies, three glass reactors (40 cm ×20 cm ×2.5 cm) were used. The reactors were connected in series. The surface of the reactor was

covered with the required amount of the composite beads (Figure 3.16). For the reaction to take place 8 L of the pharmaceutical solution was used and the reaction was conducted under solar irradiations with an average solar intensity of 875 W m^{-2} measured using pyranometer. The pH of the solution was adjusted and the adequate amount of hydrogen peroxide (H_2O_2) was also added. The aeration was provided externally into the system using aerators. The solution was pumped to the reactor an appropriate flow rate. The experiments were performed in a once-through mode. The samples were withdrawn after the required intervals for the analysis purposes.

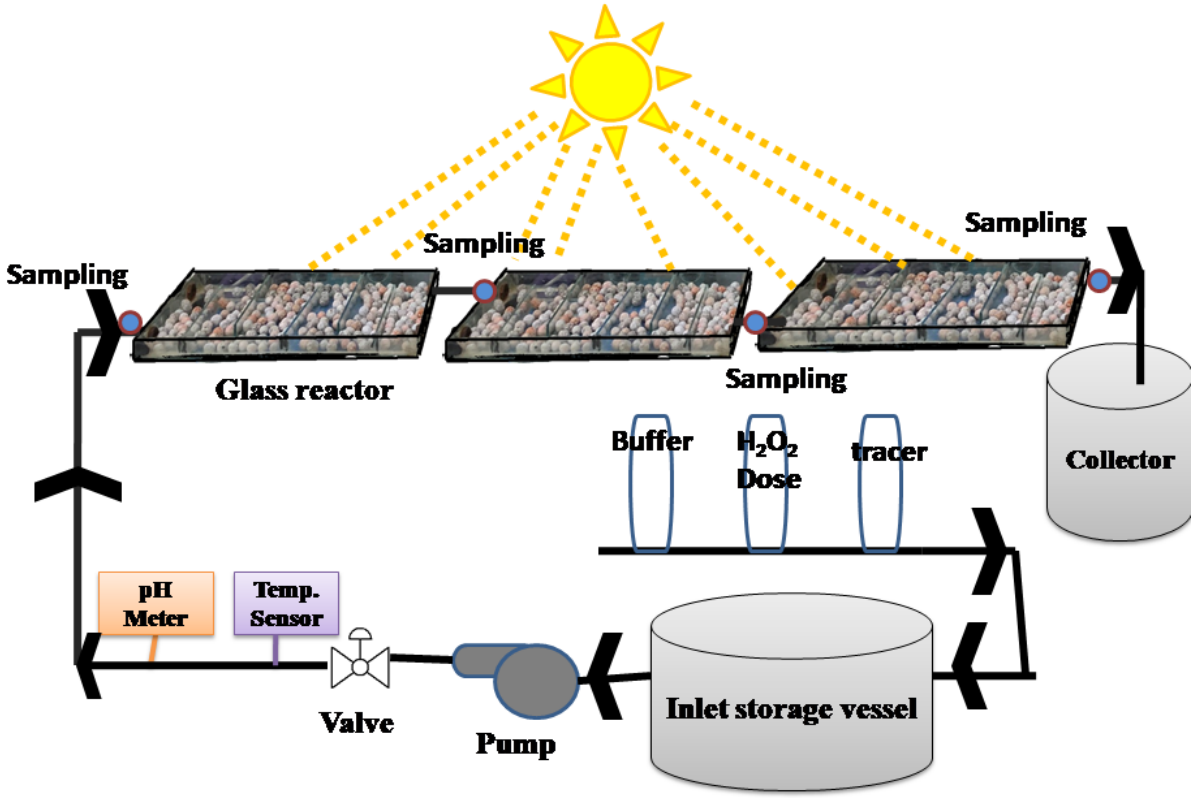

Figure 3.16: Line diagram of the pilot-scale three reactors in series showing the complete setup of the process

3.9.2. COMPOUND PARABOLIC CONCENTRATOR (CPC)

The solar CPC (10 L) was consisting of an inlet tank with continuous aeration and stirring, a peristaltic pump and the solar collector unit of area (0.24 m^2). The reactor consists of 6 borosilicate tubes attached to aluminum frame mounted on a platform placed at 30° according to the latitude (30.34° N) of Patiala (India) as shown in Figure 3.17. The glass tubes, packed

uniformly with the catalyst coated beads, were connected with the help of plastic joints and pipe line. For measuring the intensity of light, pyranometer (Apogee: MP-100) was used. The solar intensity of light was 800-900 Wm^2. For homogenization of the reaction, the wastewater was kept for 30 min at continuous stirring before irradiation. After that the CPC containing composite beads were exposed to solar radiations so as to start the reaction. Each reaction was performed three times for confirmation and average values are quoted.

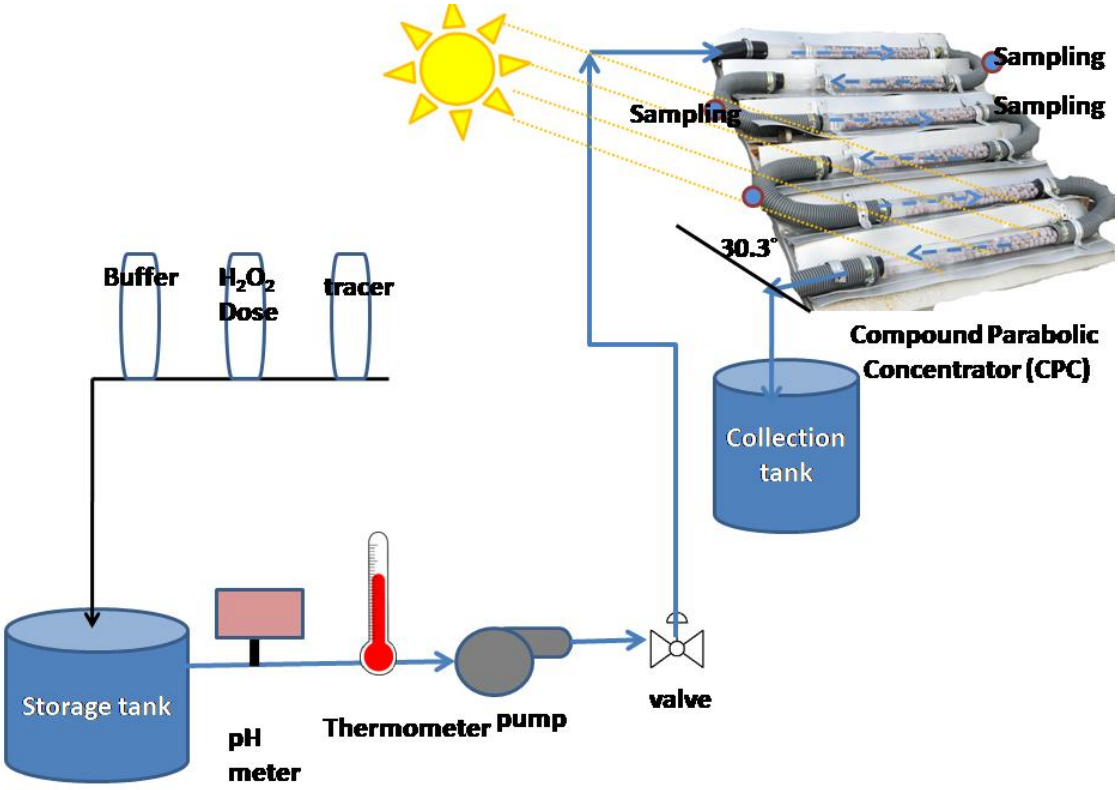

Figure 3.17: The actual image depicting the CPC with the complete setup of the process

3.10. RESIDENCE TIME DISTRIBUTION (RTD) ANALYSIS

For confirming the flow pattern and hydrodynamic behavior of the CPC reactor, RTD study was carried out. RTD being the characteristic approach for analyzing the ideal behavior of the reactor, could also be used to scale up designs at the optimized conditions for maximizing efficiency. Exit age distribution (E(t)) was used for the RTD study. The RTD software DTSPRO-V4.21 developed by PROGEPI was used for the modeling of experimental RTD curves. The distribution for E(t) was calculated using equation 3.9.

$$E(t) = \frac{S\,(t)}{\int S(t)dt} \qquad (3.9)$$

Where the tracer's concentration in (mS cm^{-1}) is denoted by S (t), and the time (min) by t.

Peclet Number (Pe) is defined as (equation 3.10):

$$Pe = \frac{\vartheta L}{D} \qquad (3.10)$$

Where ϑ is the fluid velocity of fluid (m s^{-1}), L is the characteristics length (m) and dispersion coefficient (m^2 s^{-1}) is denoted by D. The tracer used for the RTD analysis was Lithium Chloride. For modeling, the data axial dispersion model as well as tanks in series model (Abu-Reesh & Abu-Sharkh, 2003) were used.

3.11. RECYCLABILITY/DURABILITY STUDIES

For the in-situ dual to proceed for numerous cycles, continuous leaching of iron along with the catalyst layer activity and stability is a great concern. The study involves the successful recycling of the composite beads for more than 200 recycles without much loss in the degradation efficiency. The recyclability study varies as per the phase of the research going on. The same composite beads prepared in the starting of research work were used for almost 2.5 years and no new composite beads were made after that. Hence, this concludes the practical applicability of the composite beads at the industrial level for the degradation of wastewater.

3.12. ANALYTICAL DETERMINATION

The morphology of TiO_2 immobilized beads was evaluated through SEM, JSM-6510LV, JEOL (Japan) while their elemental composition was confirmed through EDS, INCAX-act, Oxford Instruments (United Kingdom). XRD (X-Ray Diffraction) was performed to confirm the crystalline structure of the different beads and catalyst prepared using X'Pert pro diffractometer (PanAlytical) in the range from 2θ = 20-80 degree. UV–visible diffuse reflectance spectrometer (DRS) was used to confirm the activity of catalyst through UV-visible diffuse reflectance spectrophotometer, UV-2600 (Shimadzu, Asia Pacific). The functional groups on the catalyst surface were investigated by FT-IR Spectrum 2 (Perkin Elmer, Japan) spectrometer in the range of 4000-200 cm^{-1}, employing KBr pellets. For recording the Raman spectrums confocal micro

Raman spectrometer, STR 500, Airix Corporation (Japan) integrated with a diode green laser (532 nm) was used.

The analysis of the samples was carried out at regular intervals of time through UV–visible absorption spectroscopy (LABINDIA, T60 U) with λmax=242nm and 321 nm and using High performance liquid chromatography (HPLC) for PHZ and MTZ respectively. The HPLC (Shimadzu, Japan) unit consists of a communication module (CBM-20A), diode array detector (SPD-M20A) and a pump (LC-20 CE). The column was C-18 and having a particle size of 5 μm. The sample was injected 20 μL for the analysis. % of Degradation was calculated in terms of absorbance.

The intermediates formed during the degradation of wastewater were identified through gas chromatography-mass spectrometry (GC–MS) analysis. The gas chromatograph, 45×–GC (Bruker, United States) was integrated with a mass detector, MSSCION- 45P (Bruker) connected with a wax column of MS (length 30 m and diameter 0.25 m). The m/z was scanned in the range from 50–410. Helium was utilized as a carrier gas with the flow rate equal to 1.0 mL $min^{-1.}$ The injection temperature was adjusted to 280 °C while the temperature for the GC oven was adjusted in the range 40-260 °C with every 10° increment in temperature. 1 μL of the sample was injected and a 1:10 split ratio was employed for GC. Standard APHA methods were followed for the monitoring and evaluation of nitrite(APHA/WEF/AWWA, 2018), nitrate (APHA, AWWA, & WEF, 2005b) and ammonium ions (APHA, AWWA, & WEF, 2005a). For the estimation of Total iron, Fe(II) and Fe(III) content leached from the beads phenanthroline method was used according to the APHA standards (APHA, 2017). Biochemical oxygen demand (BOD) was estimated by utilizing the manometric method employing WTW ‘‘Wissenschaftlich-TechnischeWerkst€atten GmbH’’, Weilheim, Germany made – Control. The working information provided by WTW was used for the determination of BOD using Oxi-Top Control. The COD was estimated according to the closed reflux stand method and analyzed using a UV-vis spectrophotometer (HACH, DR 5000, USA) (APHA, 2000). The total organic carbon (TOC) content was monitored through TOC analyzer, model- Multi N/C 2100 BU, Analytic Jena AG Corporation (Germany). H_2O_2 interference was removed prior to COD and TOC determination by adding an adequate amount of concentrated solution of sodium carbonate followed by heating at 90^oC for 1 h as reported in the literature.

CHAPTER- 4

RESULTS AND DISCUSSION

This section includes the detailed discussion about the degradation studies of pharmaceutical drugs as well as real pharmaceutical wastewater using in-situ dual effect of photocatalysis and photo-Fenton. For the evaluation of the efficiency of the process various process parameters were analyzed. This study is divided in three sections i.e. the batch mode studies, continuous mode and the application to real pharmaceutical wastewater. The overflow of the chapter is divided into three parts which has been shown in Figure 4.1.

Section 1 includes the degradation of pharmaceutical drugs PHZ and MTZ in the batch mode. the Impact of numerous parameters like treatment time, the surface area covered, H_2O_2 dose, the volume of the reactor, intensity of light were studied for the degradation of PHZ as well as MTZ. For further authentication in the perspective of the industrial scale applications of the process, the durability studies were performed using FE+FS beads. Mineralization studies in terms of reduction into various ions were also conducted along with that the reduction in COD and TOC. Various intermediates were analyzed through GC-MS and reaction mechanism was suggested.

Section 2 focuses on the continuous mode implementation of in-situ dual effect. Scale up studies including fixed bed reactors have been used employing once through process for the removal of the priority pollutants. Various reactors including once through glass reactors in series, compound parabolic reactor (CPC) were designed for the analysis of the plug flow approaching behavior and highlighting the applications of the dual effect at large scale.

Section 3 deals with the application of the process for the treatment of real industrial wastewater. The study includes the effect of various parameters on the COD reduction along with mineralization of the wastewater.

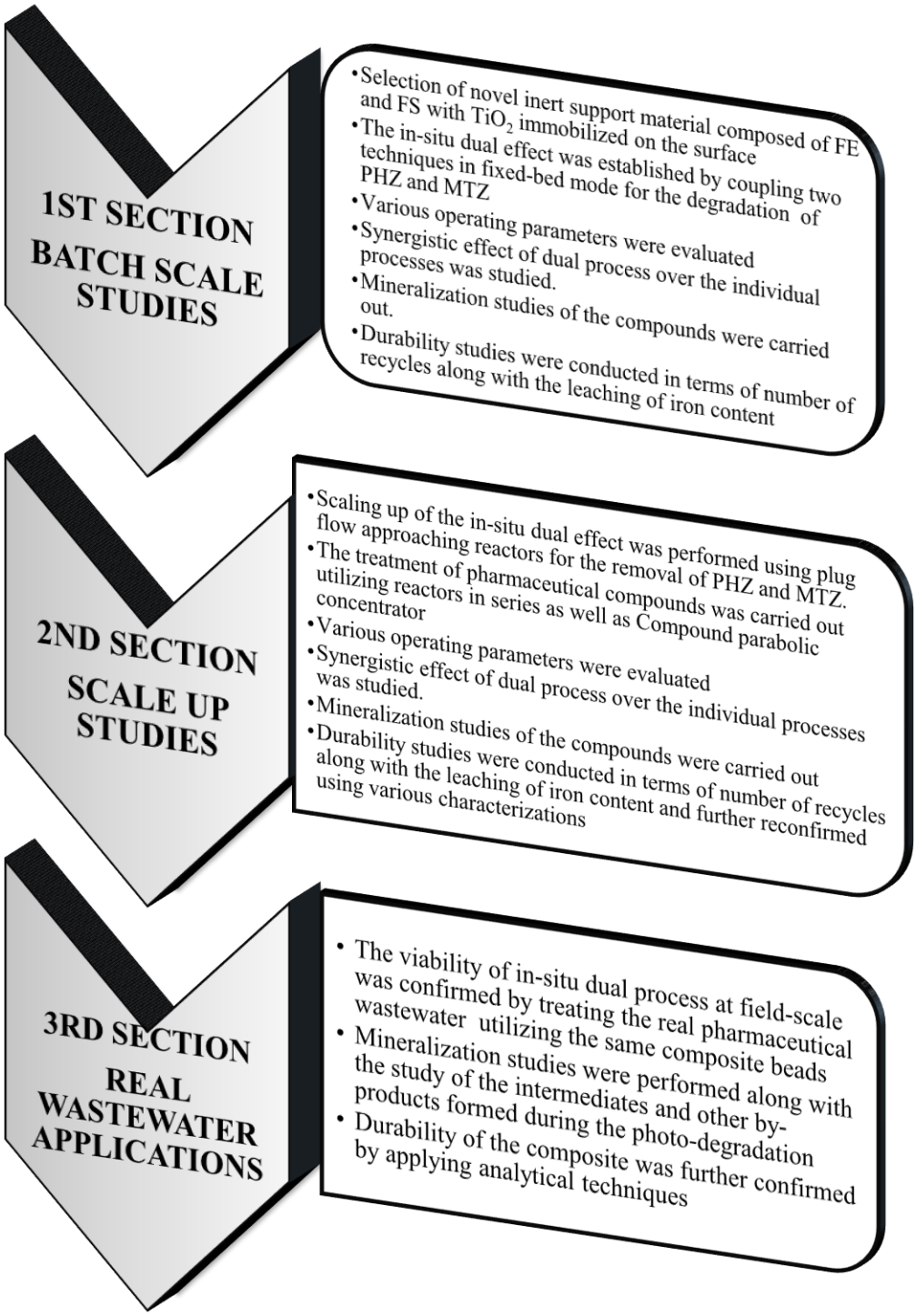

Figure 4.1: The structure of results and discussion

SECTION -1

BATCH SCALE STUDIES FOR THE DEGRADATION OF PHARMACEUTICAL DRUGS PHZ AND MTZ

The section involves the study of the application of in-situ dual process of photocatalysis and photo-Fenton for the degradation of pharmaceutical compounds PHZ and MTZ in batch mode.

4.1. DUAL EFFECT STUDIES FOR THE DEGRADATION OF PHZ

4.1.1. PRELIMINARY STUDIES

For confirming the illustriousness of dual effect (photocatalysis and photo-Fenton) various preliminary experiments was conducted including adsorption in dark using both FE and FE+FS beads. Only 4-5% reduction in the concentration of PHZ was observed even after 5 h due to the blockage of active sites by the priority pollutant. Photo-degradation of the PHZ was also carried out and only 5% reduction was obtained. Same procedure was followed for only H_2O_2 and only 6% degradation was observed owing to the unsubstantial production of •OH (Figure 4.2).

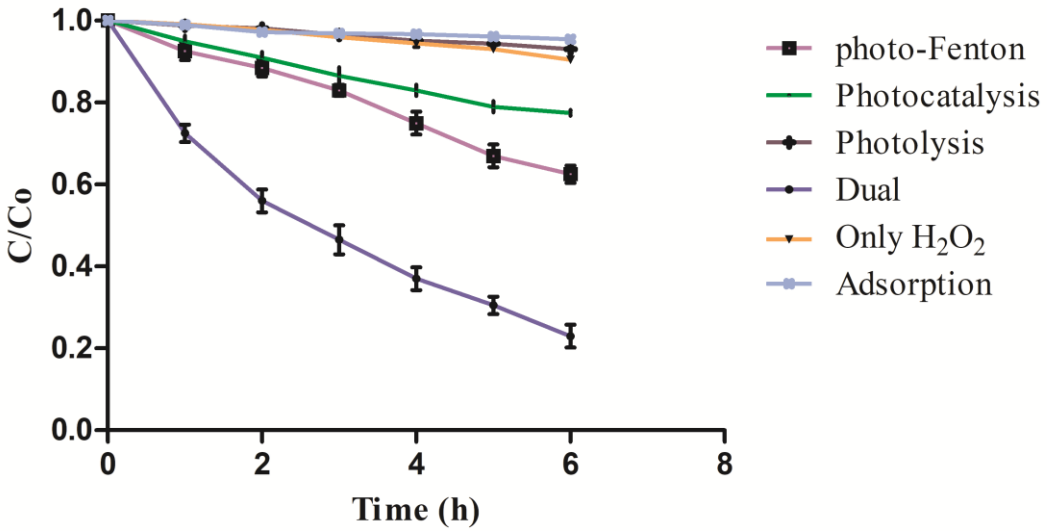

Figure 4.2: Effect of various preliminary studies on % degradation of PHZ

Photocatalysis of the pollutant was performed using coated FE and FE+FS beads and only 22% degradation was observed for both the beads even after 6h. For photo-Fenton experiments, uncoated beads (FE and FE+FS) were used with 60 mg L^{-1} of H_2O_2 and accordingly 32% (with FE) and 36% (with FE+FS) degradation was achieved in 6 h. The substantial increase in the degradation was observed with respect to the dual effect of photocatalysis and photo-Fenton using FE and FE+FS beads. Simultaneously leaching of iron from the beads leading to the photo-Fenton reaction along with surface active TiO_2 layer leading to photocatalysis, yielded 56% degradation with FE beads and 75% degradation with FE +FS beads. This was counterchecked using the production of •OH by the fluorescence spectroscopy for the three processes (Figure 4.3).

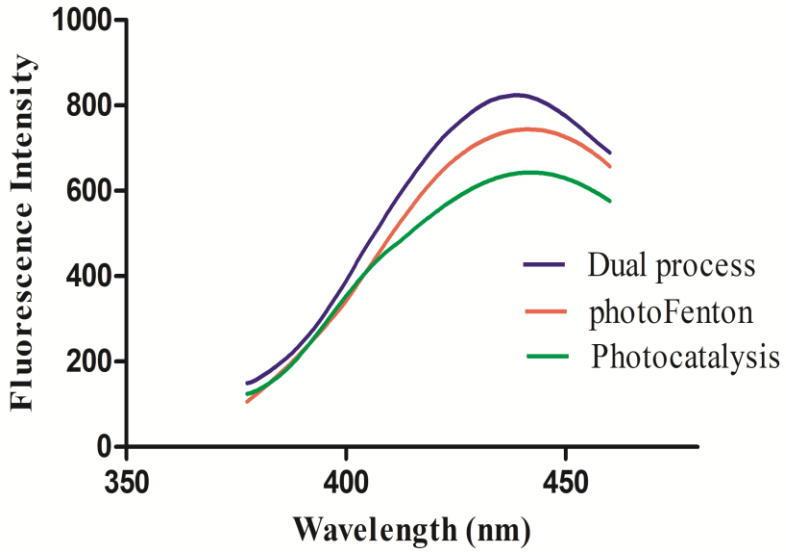

Figure 4.3: Comparison of the three processes in terms of •OH production

This effect is attributed to the presence of in-situ dual effect due to presence of leached iron from the beads (leading to photo-Fenton) along with photocatalytic active TiO_2 layer (leading to photocatalysis). Ferric and ferrous ions were determined at regular intervals of time to confirm the presence of iron in the solution (Figure 4.4) (APHA, 2017) and intactness of TiO_2 layer was subsequently confirmed by SEM-EDS as shown in Figure 3.11.

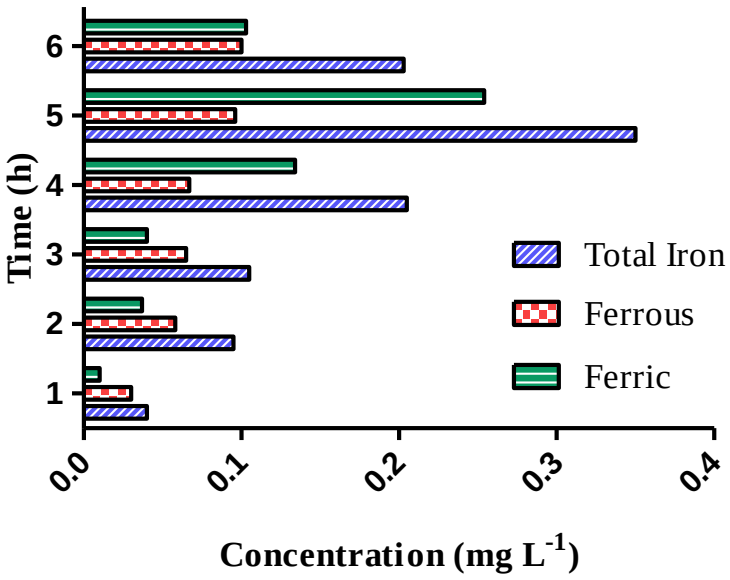

Figure 4.4: Estimation of iron content in terms of ferrous, ferric and total dissolved iron content

With simultaneous reactions using these beads, it was observed that FE beads were not durable as the strength of beads was not appropriate and the coating of TiO_2 was weathering from the surface after 5-6 recycles. Whereas, FE+FS beads were durable enough in terms of strength and retaining the TiO_2 coating. This was due to the presence of FS which provides the strength to the beads (Siddique et al., 2009). Hence, FE+FS beads were chosen for further study.

4.1.2. EXPERIMENTAL DESIGN

Three level BBD under RSM with operational parameters range as shown in (Table 4.1) H_2O_2 dose (22.5-75 mg L^{-1}), time t (1–6 h) and surface area covered by beads (50-150%) and responses as % degradation, nitrate ions and nitrite ions concentration were used for photocatalytic degradation of pharmaceutical compound PHZ.

A total set of 17 experiments were suggested by BBD as shown in Table 4.2. The quadratic model was proposed by employing other adequacy measures and sequential F-test. For better fitting of the model no transformation was used for the responses i.e. % degradation and nitrite ions concentration, but for the nitrate ions concentration log with base 10 transform was used. For the responses i.e. % degradation, Nitrate ions and nitrite ions concentration the adequate precision was found to be 22.79, 9.31, and 27.21 respectively.

Table 4.1: Experimental ranges and level of coded variables for PHZ degradation in batch reactor

	Coded levels		
Variables	-1	0	1
H_2O_2 dose (mg L^{-1})	22.5	48.75	75
Time (h)	1	3.5	6
% Surface area covered	50	100	150

Adequate precision expresses the signal to noise ratio, and adequate precision ratio above 4 indicates that the model is efficient in navigating the design space (V. K. Sangal et al., 2014).

The model summary statistics for response showed a high value of regression coefficient R^2 for all the three responses i.e. % degradation, nitrate ions and nitrite ions concentration and the values are 0.9868, 0.9448, and 0.9884 which showed a good relation between the observed and predicted values.

Table 4.3 shows the statistical analysis using ANOVA for the % degradation for the degradation of PHZ wastewater, with a model F-value of 58.50 which shows that the model is significant. For the % degradation of PHZ time was found to be highly significant variable and interaction between time and surface area covered by the beads were the significant variables.

Same could be concluded for nitrite ions concentration from the ANOVA (Table 4.4). It was observed that model F value came out to be 66.07 showing the model was significant. It was found that time, H_2O_2 dose, surface area, the interaction between H_2O_2 dose and time, interaction between time and area were significant variables.

For nitrate ions concentration ANOVA results (Table 4.5) showed that the F value for the model was 34.64 concluding the model to be significant and it could be observed that H_2O_2 dose, surface area covered and the interaction between time and surface area covered by beads were significant variables.

Table 4.2: Design of experiments suggested by BBD with observed responses for the degradation of PHZ using batch reactor

Std	H_2O_2 dose (mg L^{-1})	Time(h)	% Surface area covered	% Degradation	Nitrate ions (mg L^{-1})	Nitrite ions (µg L^{-1})
1	22.50	3.50	50.00	59.2	1.47	13
2	48.75	3.50	100.00	72.5	5.132	28
3	22.50	6.00	100.00	77.52	1.43	40.66
4	48.75	3.50	100.00	76.4	3.65	29.71
5	48.75	3.50	100.00	72.72	4.31	28.33
6	48.75	1.00	150.00	36.3	2.44	9.777
7	75.00	6.00	100.00	76.4	2.97	50
8	48.75	6.00	50.00	74.5	1.95	30.33
9	75.00	3.50	150.00	60.16	3.54	27.667
10	22.50	1.00	100.00	38.12	1.65	9.331
11	48.75	3.50	100.00	73.04	4.98	26.13
12	75.00	3.50	50.00	56.4	3.18	20.33
13	48.75	1.00	50.00	28.43	1.18	6.33
14	48.75	6.00	150.00	59.6	1.44	45.66
15	75.00	1.00	100.00	33.33	3.12	8.33
16	22.50	3.50	150.00	63.07	2.1	23.33
17	48.75	3.50	100.00	73.5	4.21	29.4

Table 4.3: ANOVA for % degradation of PHZ in batch reactor

	% Degradation					
Source	Sum of Squares	DF	Mean Square	F Value	Prob>F	
Model	4431.22	9	492.36	58.95	< 0.0001	Significant
H_2O_2 Dose	16.88	1	16.88	2.02	0.1981	
Time	2881.92	1	2881.92	345.06	< 0.0001	Highly Significant
Surface area	0.045	1	0.045	5.388×10^{-3}	0.9435	
H_2O_2 Dose ^{2}	55.93	1	55.93	6.70	0.0361	
$Time^2$	783.91	1	783.91	93.86	< 0.0001	Highly Significant
Surface area ^{2}	444.94	1	444.94	53.27	0.0002	
H_2O_2 Dose ×Time	3.37	1	3.37	0.40	0.5456	
H_2O_2 Dose ×Surface area	3.025×10^{-3}	1	3.025E-003	3.622×10^{-4}	0.9853	
Time ×Surface area	129.62	1	129.62	15.52	0.0056	
Residual	58.46	7	8.35			
Lack of Fit	48.32	3	16.11	6.35	0.0531	Not Significant
Pure Error	10.14	4	2.54			
Cor Total	4489.68	16				

Table 4.4: ANOVA Table for nitrite ions concentration

Nitrite ions concentration						
Source	Sum of Squares	DF	Mean Square	F Value	Prob>F	
Model	2636.67	9	292.96	66.07	< 0.0001	significant
H_2O_2 Dose	50.03	1	50.03	11.28	0.0121	
Time	2207.20	1	2207.20	497.77	< 0.0001	Highly Significant
Surface area	166.02	1	166.02	37.44	0.0005	
H_2O_2 Dose ^{2}	10.62	1	10.62	2.39	0.1657	
Time^2	0.53	1	0.53	0.12	0.7400	
Surface area ^{2}	134.13	1	134.13	30.25	0.0009	
H_2O_2 Dose ×Time	26.73	1	26.73	6.03	0.0438	
H_2O_2 Dose ×Surface area	2.24	1	2.24	0.51	0.5003	
Time ×Surface area	35.30	1	35.30	7.96	0.0257	
Residual	31.04	7	4.43			
Lack of Fit	23.04	3	7.68	3.84	0.1132	not significant
Pure Error	8.00	4	2.00			
Cor Total	2667.71	16				

Table 4.5: ANOVA Table for nitrate ions concentration

	Nitrate ions concentration					
Source	Sum of Squares	DF	Mean Square	F Value	Prob>F	
Model	0.68	9	0.075	34.64	< 0.0001	Significant
H_2O_2 Dose	0.17	1	0.17	76.94	< 0.0001	Highly Significant
Time	1.114×10^{-3}	1	1.114×10^{-3}	0.51	0.4969	
Surface area	0.019	1	0.019	8.55	0.0222	
H_2O_2 Dose ^{2}	0.024	1	0.024	11.27	0.0121	
$Time^2$	0.23	1	0.23	106.70	< 0.0001	Highly Significant
Surface area ^{2}	0.14	1	0.14	65.84	< 0.0001	Highly Significant
H_2O_2 Dose ×Time	4.151×10^{-4}	1	4.151×10^{-4}	0.19	0.6751	
H_2O_2 Dose ×Surface area	2.934×10^{-3}	1	2.934×10^{-3}	1.35	0.2831	
Time ×Surface area	0.050	1	0.050	23.03	0.0020	
Residual	0.015	7	2.171×10^{-3}			
Lack of Fit	8.286×10^{-4}	3	2.762×10^{-4}	0.077	0.9692	not significant
Pure Error	0.014	4	3.592×10^{-3}			
Cor Total	0.69	16				

For varying the exposed surface area of the beads, a number of beads were varied from 50 beads (50 % area) to 150 beads (150% area). It was observed that as the surface area exposure of the beads increases from 50% to 100% the degradation increases owing to the increase in the

active sites leading to the formation of appropriate •OH. When the beads were further increased to 150% the beads begin to pile up one over the other. The overlapping of the beads leads to the blockage of active sites and trapping of pollutant in the voidage between the beads, thus contributed to the decreased efficiency due to increase in the dead zones between the beads. Subsequently, the concentration of iron also increased which blocks the TiO_2 active sites leading to the decrease in the rate of degradation as shown in Figure 4.5 a.

When the H_2O_2 dose was increased from 22.5 to 48.5 mg L^{-1}, there was an initial increase in % degradation with subsequent fall in degradation as shown in Figure 4.5. This was due to the scavenging effect of •OH in presence of excess H_2O_2. From the experimental analysis, it could be observed that with the increase in treatment time and with subsequent increase in the surface area covered, % degradation increases. Accordingly, maximum degradation was observed at the surface area of 90-110% and at the treatment time of 6 h as shown in Figure 4.5b.

The best possible reasoning for the above variation could be effectively correlated with the mineralization of PHZ. It could be better correlated in terms of time and nitrate ions concentration where it first increases and then follows the decreasing trend as seen in Figure 4.5 c. The possibility of this trend is due to the conversion of nitrate ions into nitrite and ammonium ions. With the increase in H_2O_2 dose nitrate ions increases due to the mineralization of compound along with the formation of small chained compounds. Nitrite ions concentration was observed to be maximum at 100% surface area covered and treatment time of 6h as seen in Figure 4.5. From the Figure 4.5e and f, it was concluded that with the increase in time and increase in H_2O_2 dosage the nitrite ions increases. Actually it could also be correlated with plausible conversion of nitrate ions to nitrite ions with the passage of time. Further reasoning for the same has been discussed in mineralization section.

The optimized conditions suggested by BBD are the H_2O_2 dose of 45 mg L^{-1}, time of 5.3 h and surface area 95.7%. At the optimized conditions, 80% degradation and 1.97 mg L^{-1} of nitrate ions and 34.845 µg L^{-1} of nitrite ions concentration were suggested by BBD as shown in Table 4.6. To verify the adequacy of model, experiment was performed at the optimum conditions. 77.8% degradation of PHZ along with 2.02 mg L^{-1} nitrate ions and 40 µg L^{-1} of nitrite ions were observed as shown in Table 4.6. The error between the experimental verification

runs and model prediction runs for % degradation, nitrate ions and nitrite ions concentration was 2.75%, 2.53% and 8.56% respectively. Good correlation was observed between the predicted and experimental values.

Table 4.6: Predicted and experimental responses at the optimized conditions for PHZ degradation in batch reactor

Responses	Predicted value	Observed value
% Degradation	80%	77.8%
nitrate ions concentration (mg L^{-1})	1.97	2.02
nitrite ions concentration (µg L^{-1})	34.845	40

4.1.3. ELECTRICAL ENERGY CONSUMPTION

Energy consumption for the dual effect using both the composite beads was studied in term of electrical energy per order (E_{EO}) (Zisheng Zhang et al., 2004). E_{EO} is defined as the electrical energy required for the reduction in the recalcitrant compound in a cubic meter of contaminated water (Mohammadi-Aghdam, Marandi, Olya, & Mehrdad Sharif, 2014). The E_{EO} (kW h m^{-3} $order^{-1}$) has been calculated by equation 4.1:

$$E_{E0} = \frac{P \times t \times 1000}{V \times 60 \times \log\left(\frac{C_i}{C_f}\right)} \qquad (4.1)$$

Where P is the power consumed by the UV lamps (kW), t is the irradiation time (min), V is the volume (L) of the water in the reactor and C_i and C_f are the initial and final compound concentration (mg L^{-1}).

Using the equation (4.1), E_{EO} was estimated to be 16.58 (MWh m^{-3}) for FE beads and 10.78 (MWh m^{-3}) for FE+FS composite beads respectively. It was observed that electric energy consumption was less in case of FE+FS composite beads. This could be due to the faster rate of reaction in FE+FS beads. Intactness of TiO_2 coating with subsequent leaching of iron leads to the faster degradation of the compound with less consumption of energy.

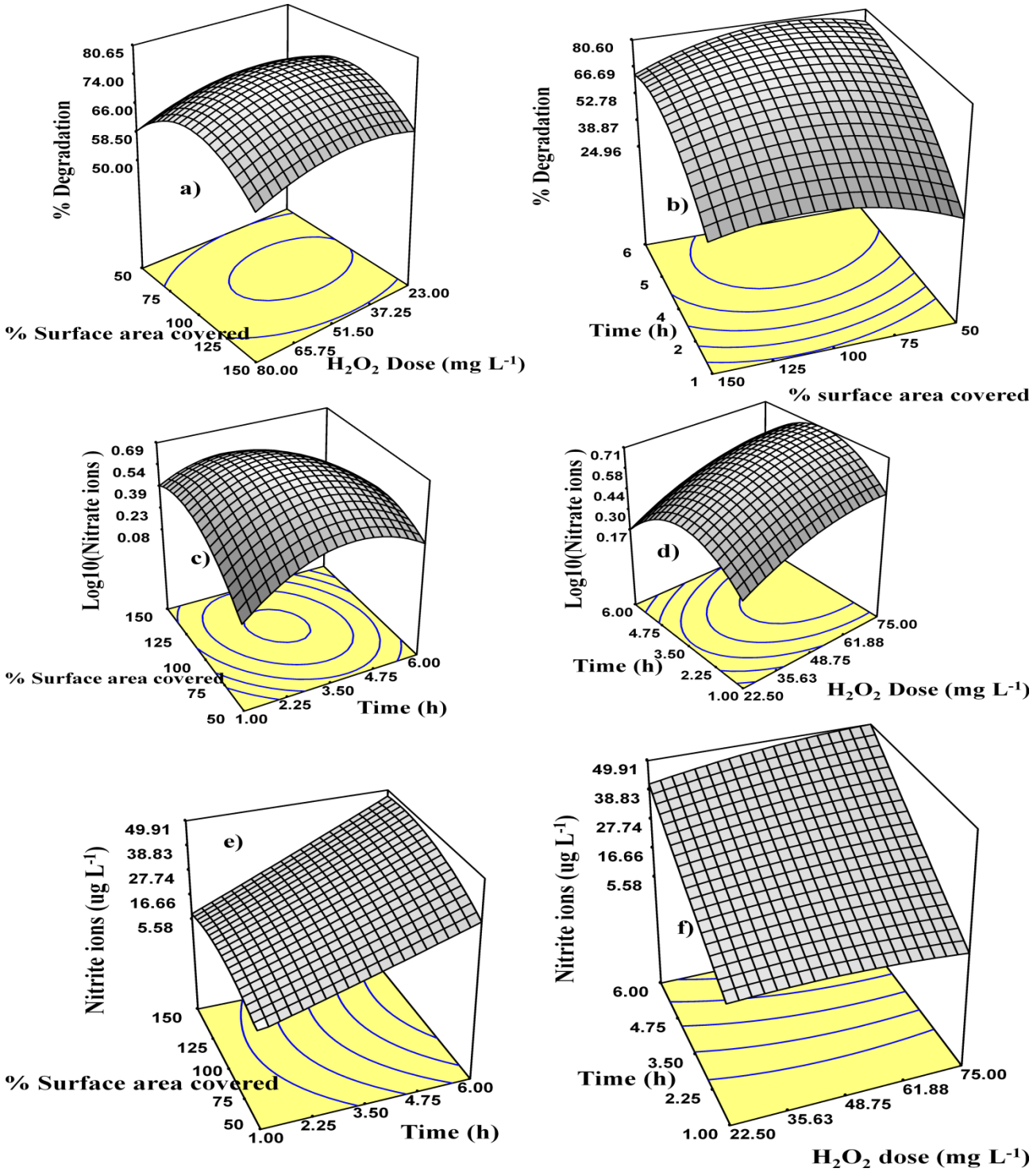

Figure 4.5: a) % Degradation 3D response surface graph of % surface area and H_2O_2 Dose, b) time and surface area, c) Nitrate ions concentration with time and % surface area covered, d) of Nitrate ions concentration time and H_2O_2 Dose, e) Nitrite ions concentration with % surface area covered and time, f) Nitrite ions concentration with time and H_2O_2 Dose

4.1.4. RECYCLABILITY/DURABILITY STUDIES

In the present study, the durability of the support was studied in terms of both leaching of iron from the support along with the intactness of the TiO_2 coating. The durability of the FE+FS composite beads was studied by subsequently recycling them for consecutive runs and then analyzing in terms of percentage degradation. Beads were successfully recycled for at-least 35 cycles (Figure 4.6a). Moreover, the catalyst activity in terms of both (photo-Fenton and photocatalysis) was retained even after 35 cycles. The various characterization techniques also proved the durability and stability of composite even after 35 recycles. Subsequently, the leaching of iron (Fe^{2+}, Fe^{3+}) was also studied after 35 recycles and presented in Figure 4.6 b.

The composite was exposed to heating in the oven at 70-80°C for almost 1 h after 5-6 reaction cycles. The composite beads were able to demonstrate a reasonable amount of degradation efficiency (70%) after 6 h of treatment. The slight loss in degradation efficiency (~10%) might be attributed to weathering-off the loose catalyst particles from the composite. The amount of catalyst loss from the surface of composite was determined by weighing the composite bead before and after recycling tests. There was almost 7-8% loss in the concentration of coated catalyst after recycling the bead for 10 runs and after that the catalyst coating got stabilized thus signifying the presence of sufficient quantity of catalyst even in the recycled composite which could contribute further in the photocatalytic experiments.

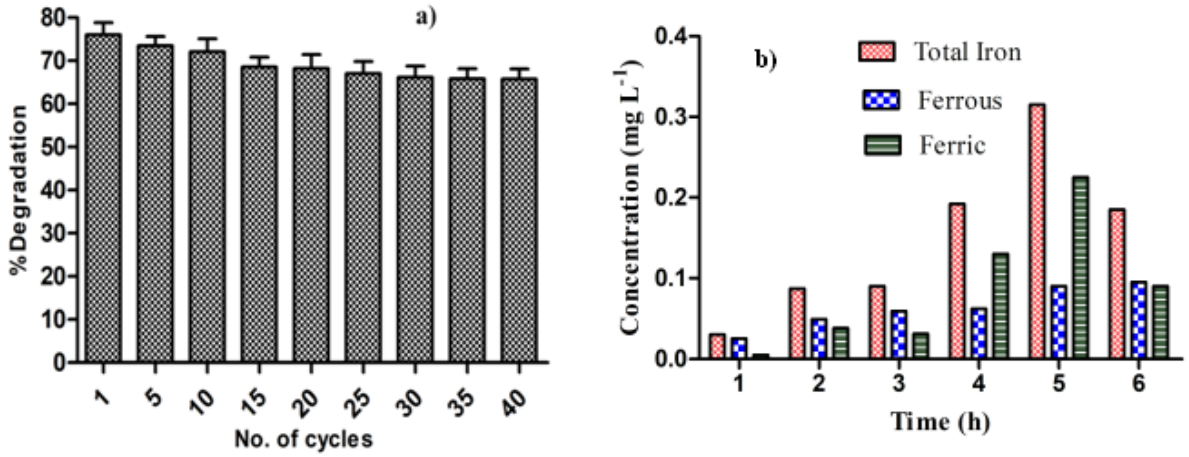

Figure 4.6: a) Recyclability studies of FE+FS composite beads for degradation of PHZ, b) Total, ferrous and ferric iron concentration with passage of time after 35 recycles

4.1.5. CHARACTERIZATION OF BEADS

The SEM/EDS images of the freshly coated FE and FE+FS, as well as recycled beads (after 35 cycles) are depicted in Figure 3.11a,b, and in Figure 4.7 respectively. The SEM images of both beads show the almost same morphology thus confirming the uniform coating of TiO_2 over the surface of beads even after recycling. The presence of Ti and Fe was further confirmed by the prominent peaks of 'Fe','Ti' and 'O' in EDS spectra. The activity of the catalyst in beads was also confirmed through XRD analysis (Figure 4.8). The diffraction peaks proved the presence of anatase and rutile phase of TiO_2 which is pointed in the Figure as 'A' and 'R' respectively. Peaks corresponding to the 'iron titanium oxides' (ITO) and iron dititanium oxides'(IDO) also confirmed the presence of iron with TiO_2 composite in the beads.

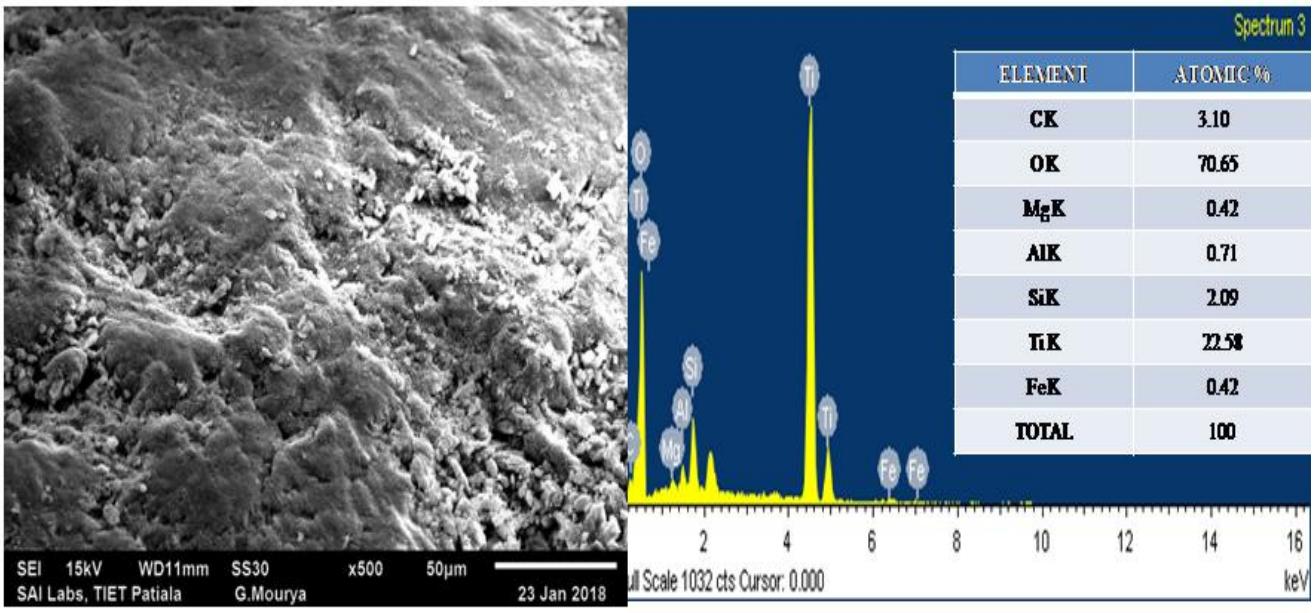

Figure 4.7: SEM/ EDS image of recycled FE+FS beads

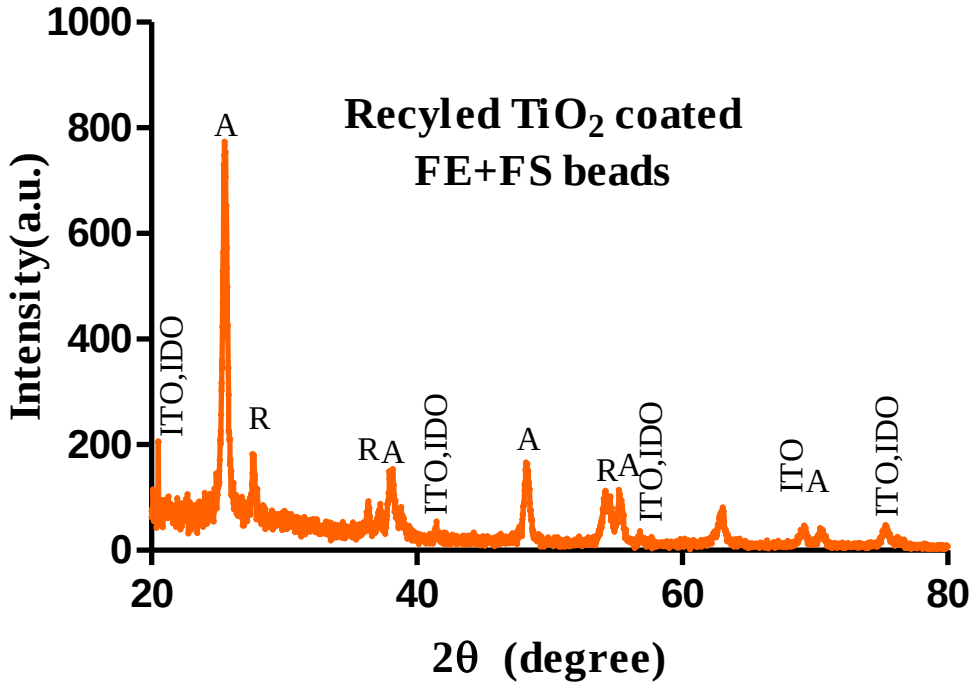

Figure 4.8: XRD of recycled TiO_2 coated FE+FS beads

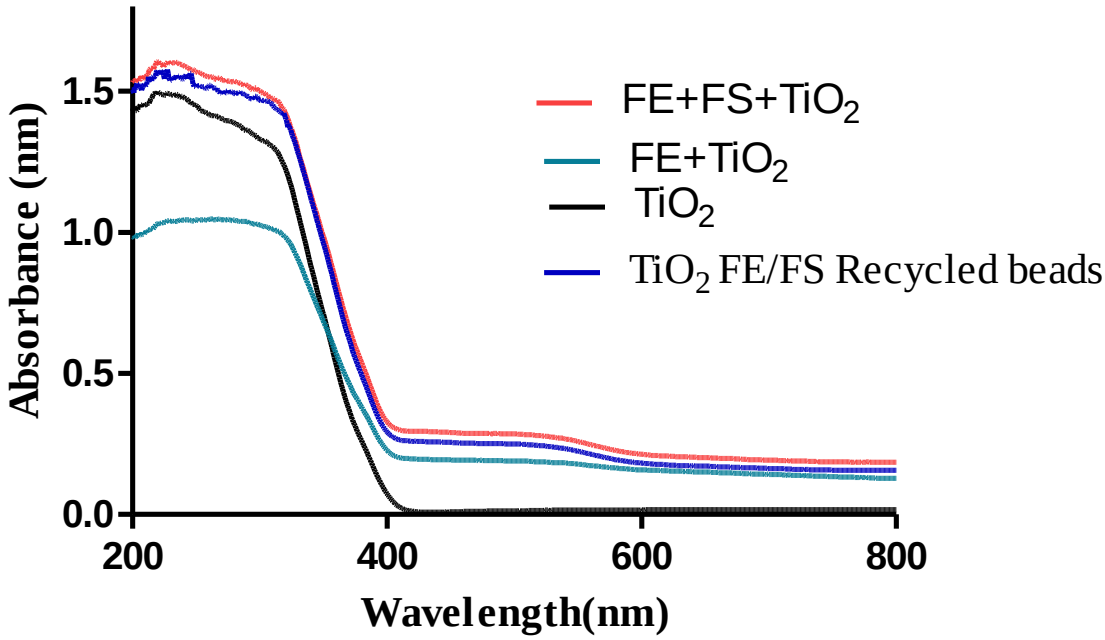

Figure 4.9: UV-DRS of TiO_2 coated FE and FE+FS material

Accordingly, the band gap energy of fresh TiO_2, FE +TiO_2 and FE+FS TiO_2 immobilized beads were also analyzed from diffuse reflectance spectrometer (DRS) (Figure 4.9). The analysis was carried out at a range of wavelength 200-800 nm. The spectra of FE +TiO_2 and FE+FS TiO_2 composite displayed the capability of absorption of light even in the visible region which clearly reflects the presence of iron in the composite. The band gap energy of TiO_2 has been calculated using photon energy equation (4.2).

$$E = h.c/\lambda \qquad (4.2)$$

Where E is band gap energy (eV), h is Plank's constant, c is the speed of light (m s^{-1}) and λ is the wavelength of absorption (nm). Hence energy for FE+FS coated beads came out to be 3.098 eV (at 401 nm) as compared to only TiO_2-P25 of 3.14 eV (395 nm).

4.1.6. KINETICS STUDY AND SYNERGISTIC CALCULATIONS

For the dual process (photocatalytic and photo-Fenton), kinetic study was performed using pseudo-first order model as shown in equation 4.3-4.4.

$$\frac{-dC}{dt} = kC \qquad (4.3)$$

$$\ln\left(\frac{C}{C_O}\right) = kt \qquad (4.4)$$

Where, C_o is the initial concentration of PHZ at t=0, C is the concentration (mg L^{-1}) of PHZ at any time, t is the degradation time (min) and k is the pseudo first order rate constant (min^{-1}).The slope of the natural log of concentrations (C_o C^{-1}) and the time for the degradation provide the rate constant (Equation 4.4). As expected, the value of the pseudo first order rate constant came higher i.e. 5×10^{-3} min^{-1} for FE+ FS beads and 1×10^{-3} min^{-1} for only FE beads. Whereas, the half life of 138.62 min for FE+FS beads was significantly lower as compared to photocatalysis (693.14 min) and photo-Fenton (693.14 min).

The synergistic effect of the dual process over individual processes and both combined was evaluated using the equations (3.5-3.7).

Synergy of dual over photocatalysis process:

$$\% \text{ Synergy} = 100 \times \{(0.005 - 0.001)\}/0.005$$

$$\% \text{ Synergy} = 80\%$$

Synergy of dual over photo-Fenton process:

$$\% \text{ Synergy} = 100 \times \{(0.005 - 0.001)\}/0.005$$

$$\% \text{ Synergy} = 80\%$$

Synergy of dual over both photocatalysis and photo-Fenton process i.e overall synergy:

$$\% \text{ Synergy} = 100 \times \{(0.005 - (0.001 + 0.001))\}/0.005$$

$$\% \text{ Synergy} = 60\%$$

Therefore, the synergetic effects of dual process over both the processes lead to the rapid increase in the rate of reaction. Hence, confirms the feasibility of the process for further applications to treat wastewater.

4.1.7. MINERALIZATION STUDIES

The mineralization studies of PHZ were carried out through reduction in the COD and TOC along with generation of anions like nitrite, nitrate, and ammonium ions. The nitrogen atoms in PHZ were found to be converted into nitrite, nitrate and ammonium ions. It was observed that nitrate ions first started to increase up to 4.7 mg L^{-1} and then decreased with time. Nitrite ions concentration was found to be increased with increase in time. Ammonical nitrogen was found to be increased from 10 mg L^{-1} to 20.9 mg L^{-1}. It is basically due to the conversion of nitrate to nitrite ions and subsequent formation of ammonical ions. There was almost 78% and 75% reduction in COD and TOC, respectively after 6 h of treatment.

The partial mineralization of PHZ might be due to the formation of several intermediate products during the degradation of PHZ. The intermediates identified through GC-MS analysis. The plausible degradation mechanism (Figure 4.10) may be explained through two different

routes ‘A’ and ‘I’. First of all hydroxylation of the compound could take place leading to the formation of 1,2-dihydro-1-(3,4-dihydroxyphenyl)-2,3-dimethylpyrazol-5-one. The fragmentation of the product leads to the formation of two different products i.e. pyrocatechol and 1,2-dihydro-2,3-dimethylpyrazol-5-one. On the route, ‘A’ further dealkylation took place leading to the formation of intermediates and finally Penta-diene. On the route, ‘B’ first of all N-N bond was deformed and then further deamination took place leading to Pent-2-enal and further dealkylation took place and formation of but-2-ene by both the routes and finally reduced to CO_2 NO_3^- and NO_2^-.

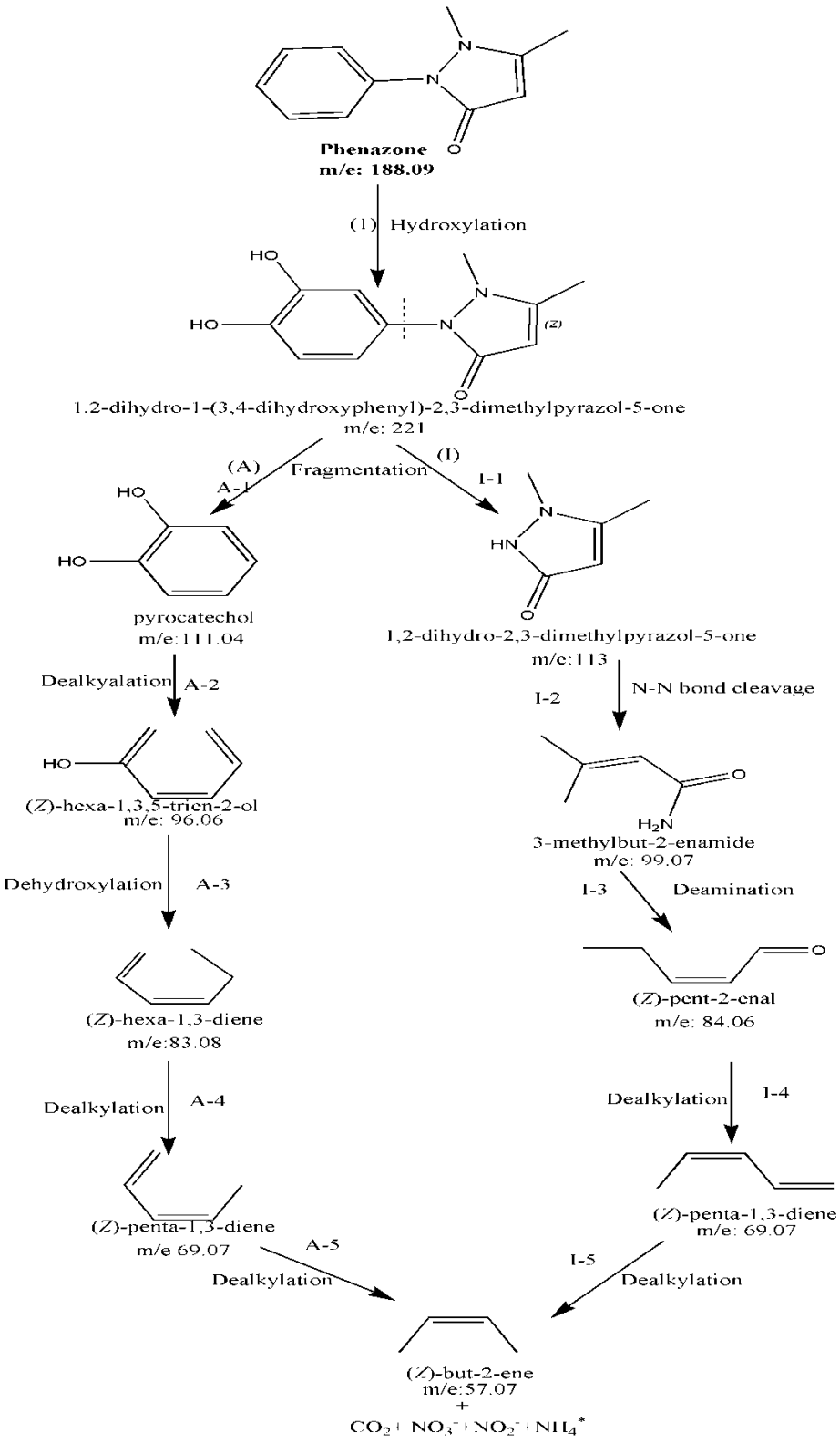

Figure 4.10: Proposed mechanism for degradation of PHZ

4.2. DUAL EFFECT STUDIES FOR COMPOUND – MTZ

Dual effect studies were further extended for the degradation of MTZ in batch mode. Various preliminary experiments were conducted including photolysis, adsorption, photocatalysis and photo-Fenton. It was noticed that there was no impact of adsorption as the solution was kept in dark for 2 h. Photolysis, as well as the effect of only H_2O_2, showed only 4% and 3% removal due to inappropriate production of •OH . Whereas in the case of photocatalysis using coated composite beads, 49.5% of removal was obtained and for the photo-Fenton process, only 34.7% of removal of MTZ was obtained after 2 h. There was a substantial increase in the degradation i.e. 75% using coated composite beads governed dual effect owing to iron leaching from the composite beads leading to the photo-Fenton process and simultaneously surface active TiO_2 layer leading to photocatalysis.

4.2.1. KINETIC STUDY

For determining the rate constants kinetic study was carried out. The degradation of MTZ followed 2nd order kinetics as shown in equation 4.5 and the rate constant (L mg^{-1} min^{-1}) has been calculated using equation 4.6.

$$-\frac{dC}{dt} = k_1 C^2 \qquad (4.5)$$

$$\frac{1}{C} - \frac{1}{C_0} = k_1 t \qquad (4.6)$$

Where C_o is the initial concentration of MTZ at t=0, C is the concentration (mg L^{-1}) of MTZ at any time, t is the degradation time (min). Where k_1 is the second order rate constant (L mg^{-1} min^{-1}). The plot between (1/C-1/C_0) and t provides the 2nd order rate constant (k_1).

4.2.2. EFFECTS OF VARIOUS PARAMETERS

4.2.2.a. EFFECT OF pH

In our study, the effect of pH has been studied in terms of the efficacy of the dual process. For the dual process to work efficiently, the low pH is preferred, owing to the large production of •OH (due to prominence of photo-Fenton). Similarly, pH also plays an important role in heterogeneous photocatalysis of any component. The •OH attack is the basic step

involved in the degradation of the pollutant. To study this, the pH of the solution was varied from 2.5 to 4 using acetate buffer.

In this study for the dual effect, the maximum degradation efficiency was obtained at pH 3.5 (Figure 4.11). It was clearly observed that 90% of MTZ degraded after 120 min in the case of pH 3.5. Results can be traced back from the inset graph (of Figure 4.11) indicating an increase in the 2^{nd} order rate constant from 0.5×10^{-3} to 2×10^{-3} L mg^{-1} min^{-1}. However, a fall in efficiency was observed if the pH was increased or decreased further. The interaction between the MTZ and the TiO_2 surface could be evaluated based on the electrostatic interactions between them. These types of interactions affect the formation of •OH (Kim et al., 2012). The surface charge on the drug also helps in deciding the degradation efficiency.

When the solution is highly acidic in nature more consumption of H_2O_2 would take place due to the capturing of •OH by H^+(Kim et al., 2012). But if the pH is too low the chances of formation of $H_3O_2^+$ are more which stabilizes the H_2O_2 and hence active sites are reduced for the generation of H_2O_2.

4.2.2.b. EFFECT OF VARIATION IN THE OXIDANT DOSAGE

Oxidant dose plays an important role in the photocatalysis and photo-Fenton process owing to its capability of generating •OH however adding to the cost of the process. But the dual effect has a capability to reduce the consumption of H_2O_2 as it is simultaneously used for both photocatalysis as well as photo-Fenton reactions, which help in increasing the production of •OH. Hence these •OH are used in both the processes owing to the reduction in the recombination of electron-hole pairs.

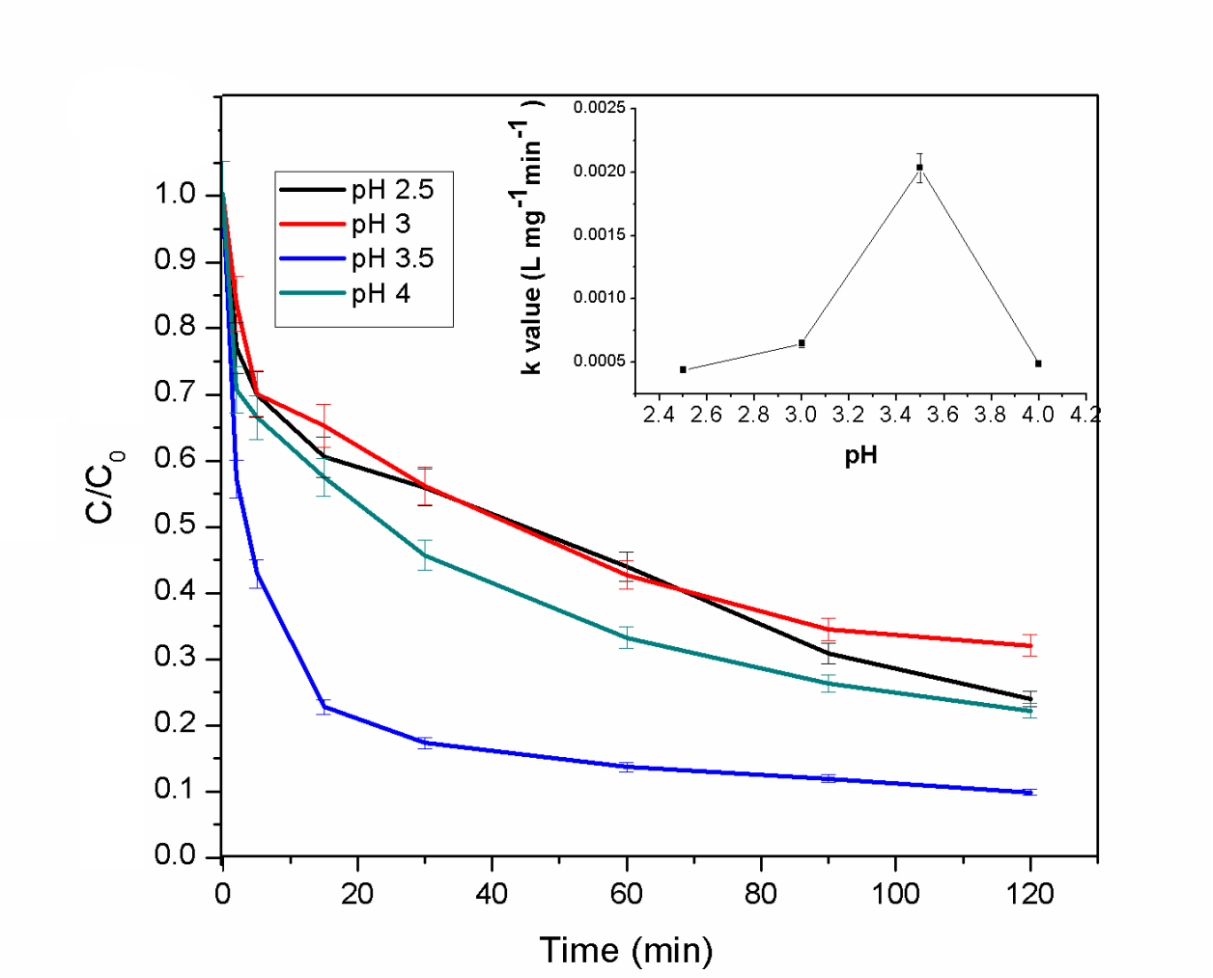

Figure 4.11: Graph showing the effect of pH on the degradation of MTZ using C/C_0 vs time (C_0=25 mg L^{-1}, H_2O_2 dose = 900 mg L^{-1}), the plot of 2nd order rate constant for the effect of the change in pH (inset)

In this perspective, the experiments were conducted with the TiO_2 coated FE+FS composite at the acidic pH by varying the dosage of the oxidant from 450 to 1350 mg L^{-1} (Figure 4.12). From the Figure 4.12, it was observed that as the amount of H_2O_2 was increased up to 1050 mg L^{-1} the degradation of the MTZ was steadily increasing as confirmed from the rate constant having a maximum value of 3.4×10^{-3} L mg^{-1} min^{-1}. With further increase in the concentration of H_2O_2, there was a slight decrease in the efficiency, this might be due to the scavenging effect at the high dose of hydrogen peroxide (Bokare & Choi, 2014b). Hence, on further optimization 1050 mg L^{-1} was chosen as the optimum dose of H_2O_2 for obtaining the

maximum degradation of the drug MTZ. Even H_2O_2 dose can be further minimized with other design considerations and scaling-up options.

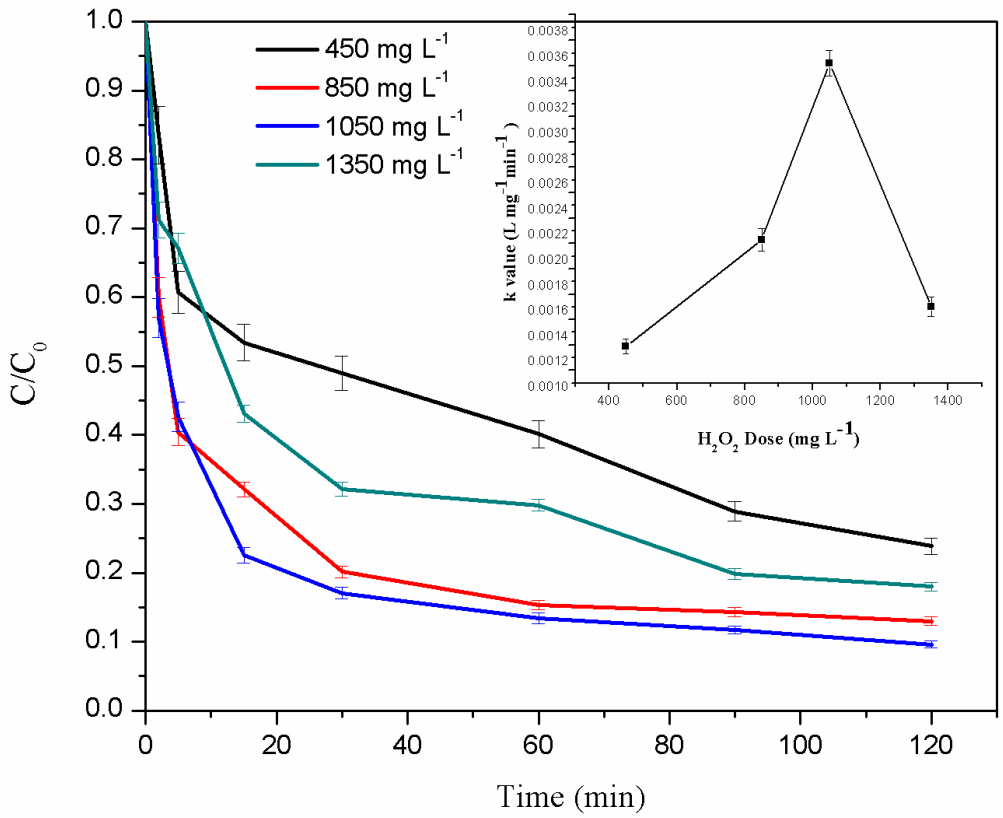

Figure 4.12: Effect of oxidant dose on the degradation of MTZ using C/C_0 vs time graph (C_0=25 mg L^{-1}, pH=3.5), a plot of 2nd order rate constant for the effect of change inH_2O_2 dose (inset)

4.2.2.c. EFFECT OF THE COVERED SURFACE AREA

In the dual process, amount of TiO_2 (required for photocatalysis) and iron concentration (required for photo-Fenton) both are prominent. As both the processes are being contained at a single place using beads, thus, it is prominent to study the effect of a number of beads i.e. surface area covered. For better contact with the priority pollutant, the available catalyst surface area is an important point of concern for the large scale applications. In this study, a number of the catalyst coated beads was varied based upon the degradation of the MTZ. The beads were varied from 50 to 150 based upon the % available surface area covered in the used glass reactor. The superlative results were obtained in the case of 100 beads (Figure 4.13). This might be due to the

increase in the exposed surface area of the beads to the MTZ solution owing to the faster degradation of the compound. By using 100 beads, the almost the whole surface of the reactor was completely covered. The active sites of the catalyst increases which help in the binding of the catalyst with the pollutant. With further increase in the number of beads, the active sites started to get block leading to decrease in the efficiency of the degradation additionally there is also a possibility of the trapping of MTZ in the void spaces. In case of the 150 beads, the reactor was covered with overlapping beads which increased the amount of TiO_2 along with the leached iron content i.e. leading to the scavenging effect, leading to the decrease in the degradation.

The systematic leaching of iron in the form of ferrous and ferric ions from the beads helps in the dual process. Covering the surface with 100 beads and keeping other conditions at optimal, the leachate total iron concentration was obtained to be 0.35 mg L^{-1}

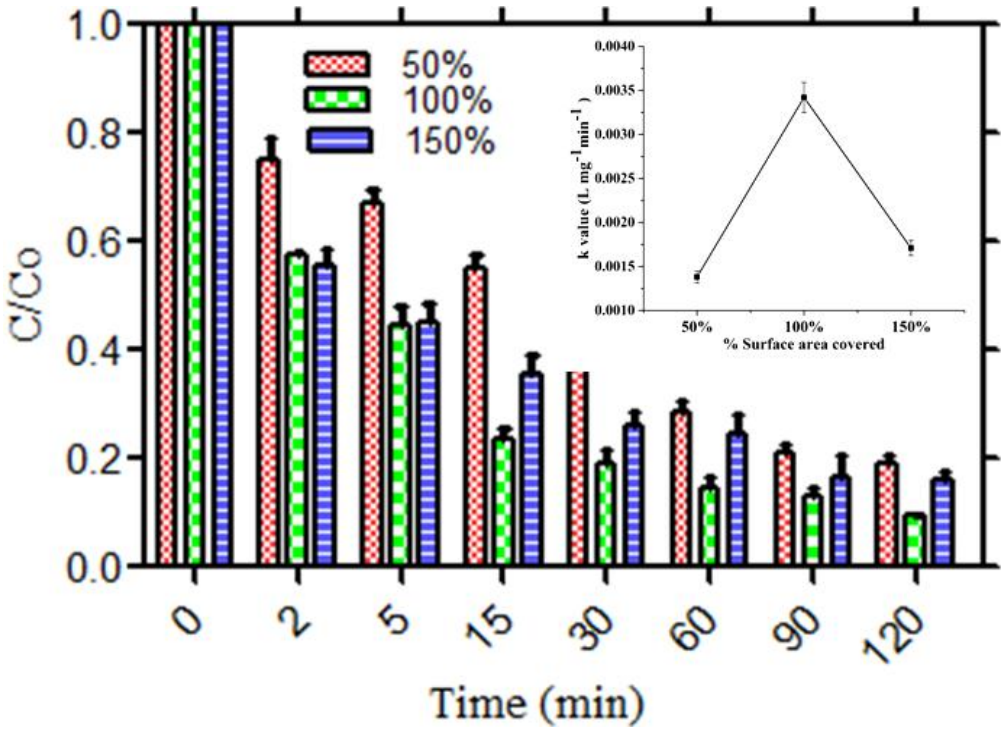

Figure 4.13: Effect of the dosage of catalyst on the degradation of MTZ using C/C_0 vs time graph (C_0=25 mg L^{-1}, pH=3.5, H_2O_2 dose=1050 mg L^{-1}), the plot of 2nd order rate constant for the effect of the change in the number of beads (inset)

4.2.2.d. EFFECT OF THE INTENSITY VARIATION

For scaling-up of the dual process at industrial scale, solar reactors play a very prominent role. As the UV intensity of the sun varies throughout the year in a particular region, thus intensity variation is an important parameter. In this context, the intensity of the UV light in our experiments was varied from 10 W m^{-2} to 25 W m^{-2} (Figure 4.14) for studying the degradation efficiency of the MTZ. From Figure 4.14, it was observed that the best degradation results were obtained at 25 W m^{-2} as the highest value of rate constant was obtained at 25 W m^{-2}. Actually, the intensity was varied by changing the distance of the reactor from UV tubes. If the reactor was placed very close to the UV tubes, it was observed that the intensity was decreased as most of the light got scattered in the lower part of the chamber and less amount reached the base of reactor hence decrease in degradation efficiency was observed.

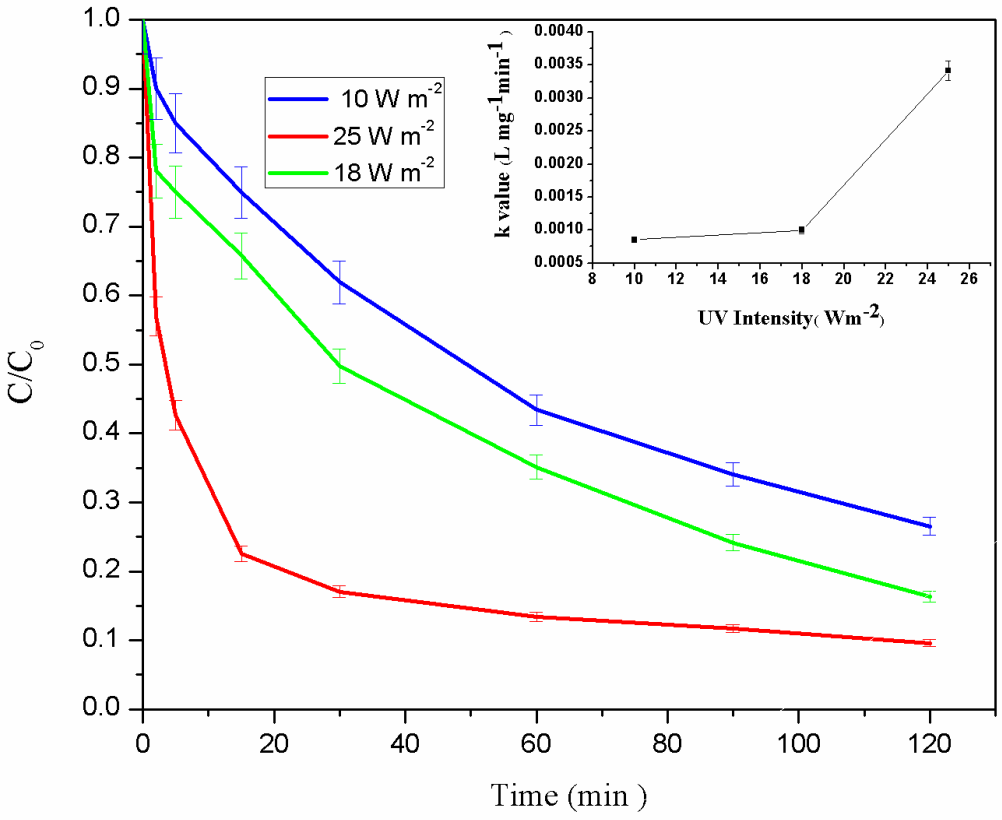

Figure 4.14: Effect of UV intensity on the degradation of MTZ using C/C_0 vs time graph (C_0=25 mg L^{-1}, pH =3.5, H_2O_2 dose=1050 mg L^{-1}, covering 100% surface area), the plot of 2nd order rate constant for the effect of the change in UV intensity (inset)

4.2.2.e. EFFECT OF THE CHANGE IN AREA BY VOLUME RATIO

The area and depth of the reactor form a major limitation in the field-scale application of the dual effect as the penetration of light should be sufficient to reach the solution. Generally, less depth and more exposed area are recommended for the better penetration of light**.** In this study, this was achieved by varying the volume of the solution and keeping the area of the batch reactor constant. Area/Volume ratio (A/V) of the batch reactor was varied in the range of 0.182 cm^2 mL^{-1} to 0.364 cm^2 mL^{-1}. Therefore, the optimum value obtained for A/V ratio was 0.273 which showed the maximum degradation which was further confirmed from the 2nd order rate constant showing the highest value of 3.4×10^{-3} L mg^{-1} min^{-1} (Figure 4.15).

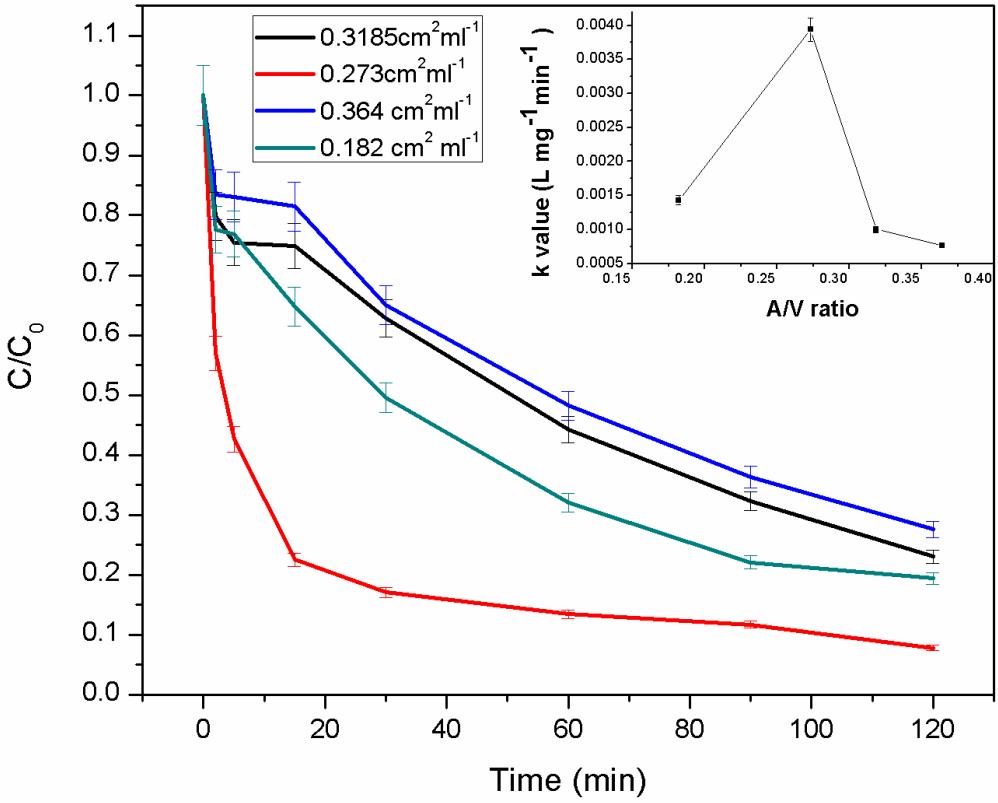

Figure 4.15: Effect of A/V on the degradation of MTZ using C/C_0 vs time graph (C_0=25 mg L^{-1}, pH=3.5, H_2O_2 dose=1050 mg L^{-1}, number of beads=100, UV intensity=25 W m^{-2}), a plot of 2nd order rate constant for the effect of the change in A/V ratio (inset)

4.2.3. MODELINIG USING ANN ALGORITHM

In the present study modeling of dual process of photocatalysis and photo-Fenton using artificial neural networks has been done. MATLAB (Mathworks 9.3.0) was used to generate the network from the data. The datasets were divided into three subsets i.e. training, validation and testing. 70%, 15% and 15% of the data were set for training, validation, and testing respectively (Talwar et al., 2018a). The topology of the network, an important part of the study gives information about the number of layers, a number of neurons and the transfer function used. In this process three-layer feed forward back propagation ANN with one hidden layer was used for the modeling of the data (Agatonovic-Kustrin & Beresford, 2000). 'Traingdx' was used as the training function which is the gradient descent with momentum and adaptive learning rate back propagation. The ranges of the input factors used for optimization is shown in Table 4.7. Figure 4.16 shows the network with one hidden layer. Inputs required for the model were treatment time, intensity, the surface area covered, A/V ratio, pH and H_2O_2 dose.

Table 4.7: Range of factors optimized by ANN for MTZ degradation in batch mode

Variables	Min. range	Max. range
H_2O_2 dose, (gm L^{-1})	450	1350
Treatment time (min)	0	120
A/V ratio	0.010	0.020
pH	2.4	4
UV intensity (W m^{-2})	10	25
No. of beads	50	150

To determine the optimum number of neurons, the number of neurons was varied from 2 to 12 and the model was repeated thrice for minimizing the mean square error. MSE was minimum for the 4 neurons as shown in Figure 4.17. With increasing the number of neurons fitting was deteriorated and the error was increasing. Hence, a network with 4 neurons was used for modeling the various parameters for obtaining the best results. After that, the training of the network was performed. The number of training was performed for the best framework and finally, after 987 iterations, the optimal network was achieved. The values of the regression

coefficient were 0.994, 0.990, 0.987 and 0.993 for training, validation, testing (Figure 4.14) and all. This gave the confirmation that the model was best suited for the simulation of the output.

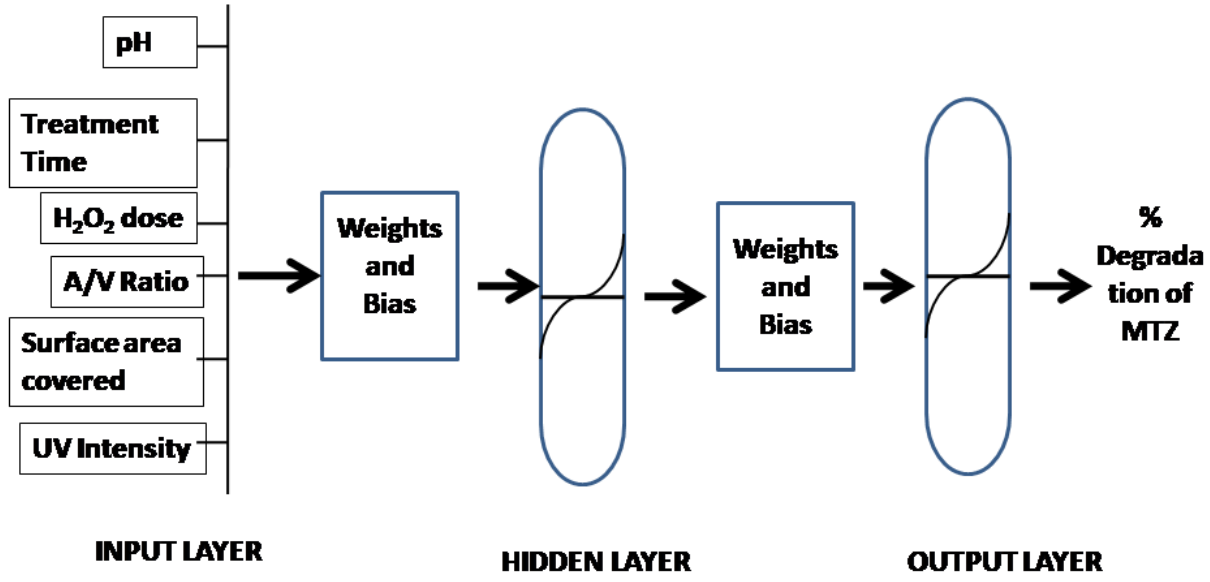

Figure 4.16: Neural network with input, hidden and output layer

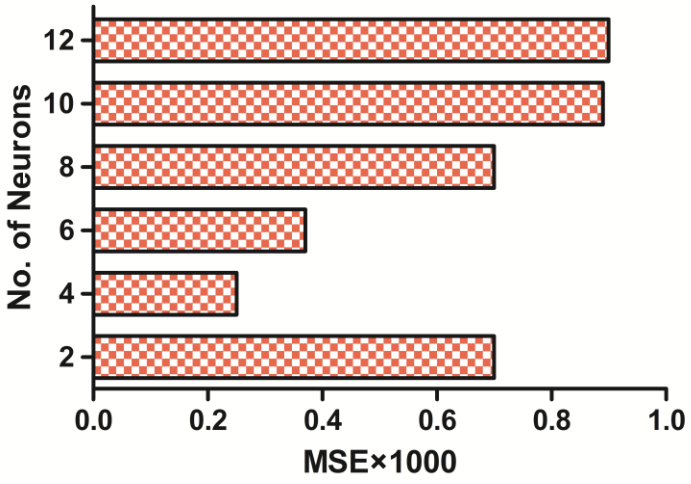

Figure 4.17: Variation in MSE with a number of neurons in a hidden layer

The sensitivity analysis was also performed for determining the impact of the input data variables on the % degradation of MTZ. For this purpose relative importance (Figure 4.18) was calculated using MSE (Shad, Nedjati, & Shafiei, 2017). Treatment time was the most important input variable as in this study; the efforts have been done to reduce the treatment time by incorporating novel in-situ dual effect of photocatalysis and photo-Fenton, along with variation of other parameters.

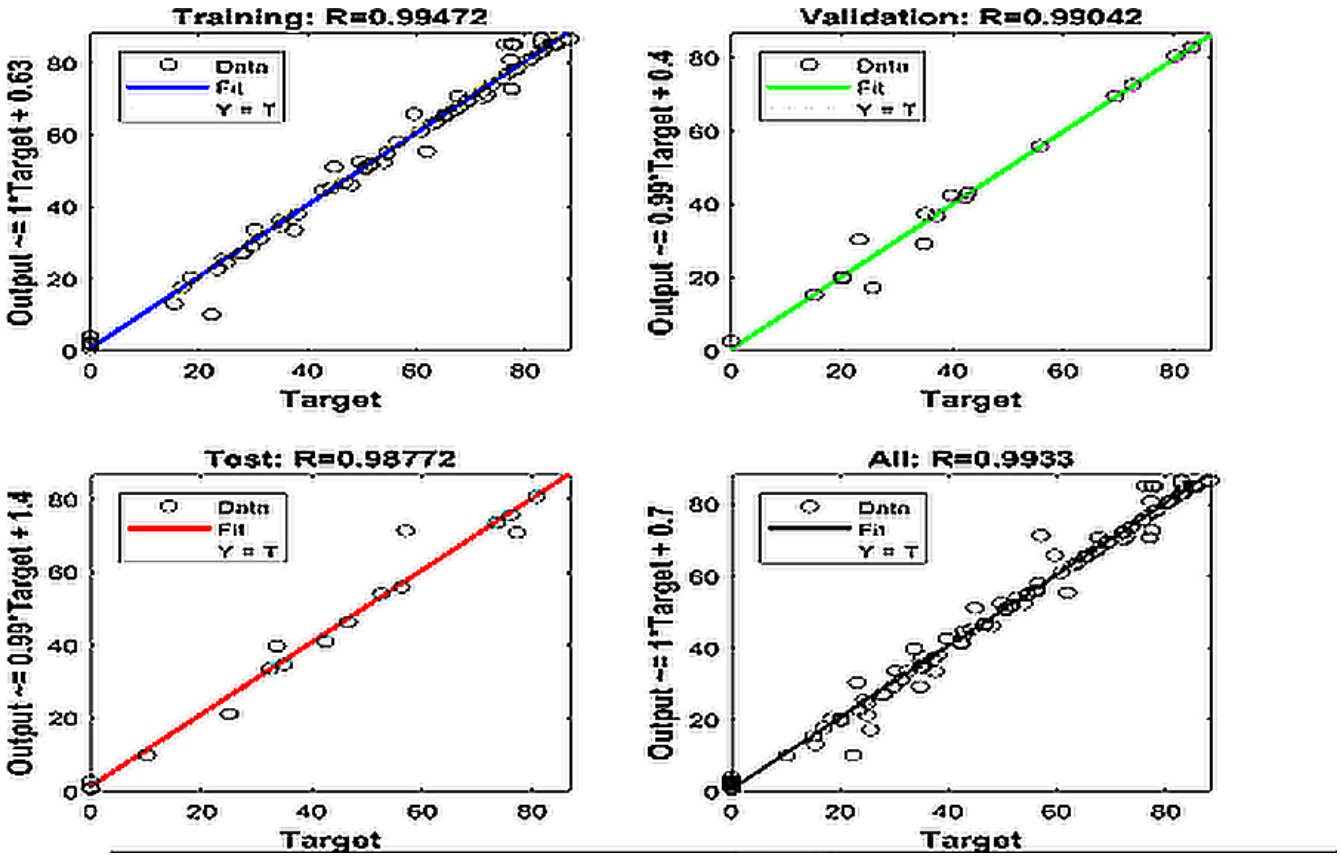

Figure 4.18: Neural network showing the regression analysis of training, validation, and target for % degradation of MTZ

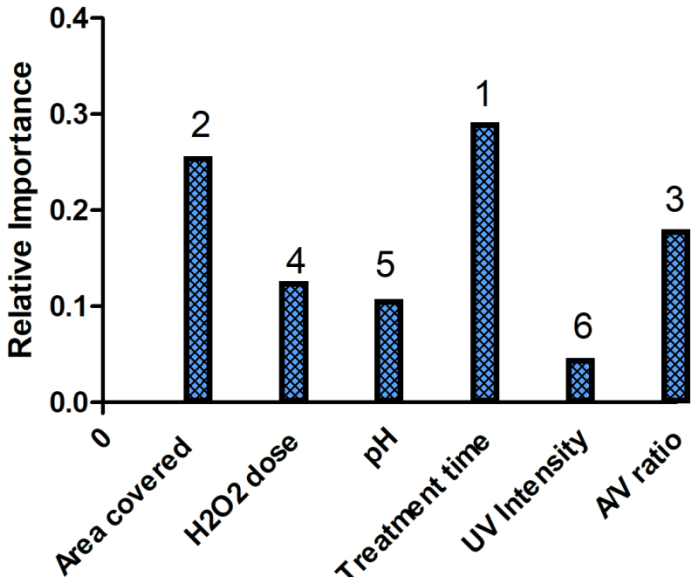

Figure 4.19: The relative importance of various parameters according to ANN

4.2.4. OPTIMIZATION USING GENETIC ALGORITHM

The advantage of modeling of dual effect data is the potential to find the optimized conditions for maximum degradation of MTZ. Hence, after the modeling, the final goal of the study was to optimize the various operating conditions used for the modeling. For this purpose, GA was used after ANN. The genetic algorithm creates a virtual environment of the operating conditions and works on the process of natural selection.

The basic rule of the optimization procedure is the use of the population for selection, crossover, and mutation (Çelekli, Bozkurt, & Geyik, 2013). The selection of the population for these functions was done randomly by the algorithm and then was used to produce children for the next generations. These new generations correspond to the optimized solution. The calculation for GA function was done using MATLAB in the command line.

The optimized output was represented as equation 4.7.

$$y = f(x_1, x_2, x_3, x_4, x_5, x_{6,}) \qquad (4.7)$$

Where y is the % degradation of MTZ, x_1, x_2, x_3, x_4, x_5, x_6 represents the pH, treatment time, dose of oxidant, the surface area covered, the intensity of light and A/V ratio.

The constraints applied were

{ 2.5 ≤ pH≤ 4; 0≤treatment time≤ 120 min; 450mg L^{-1} ≤Oxidant dose≤ 1350mg L^{-1}; 50%≤ amount of catalyst ≤ 150%; 10W m^{-2}≤Intensity of light ≤25W m^{-2}; 0.182 cm^2 mL^{-1}≤A/V ratio≤ 0.3175 cm^2 mL^{-1}}

Using the fitness function from the ANN, solutions were optimized with the help of GA. The observed error was 0.6% (Figure 4.20). The optimized conditions obtained were at the treatment time of 120 min with the oxidant dosage of 1020 mg L^{-1}, pH of 3.2, the intensity of 25 W m^{-2} and covered surface area of 100%, with the % degradation of 85%. Hence, it was further confirmed by experimental analysis at these optimized conditions.

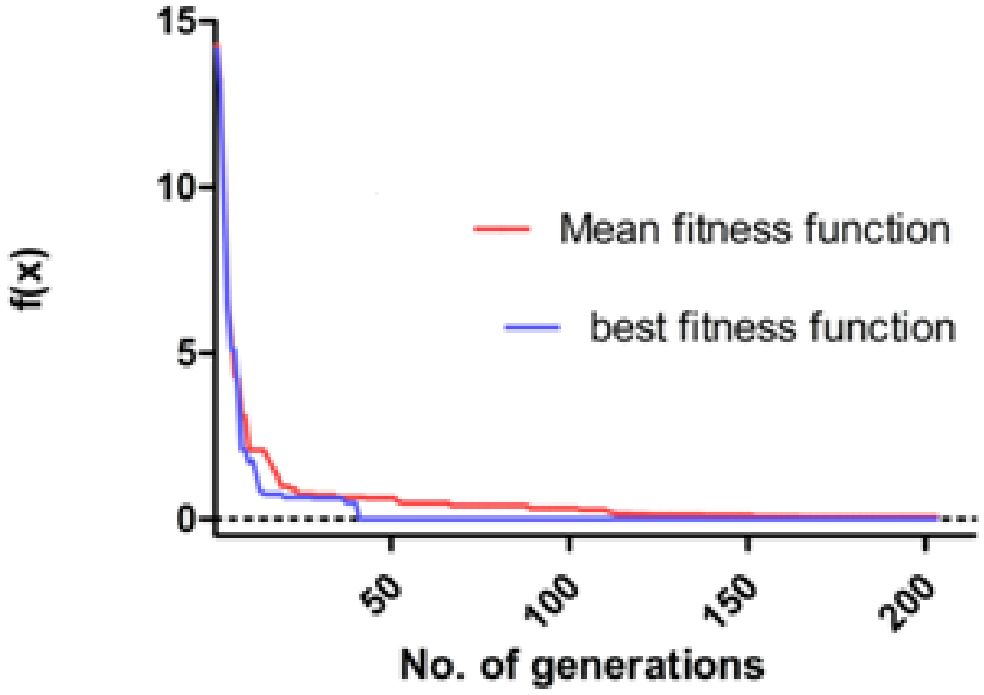

Figure 4.20: Fitness function approaching best fitness function with the number of generations

4.2.5. ELECTRICAL ENERGY CONSUMPTION

Electrical energy per order (E_{EO}) was used to compare the energy consumed by the dual process as compared with the photocatalysis and photo-Fenton (Zisheng Zhang et al., 2004). The calculation of E_{EO} was performed using the equation 4.6. It was observed that E_{E0} was 129.8

(MW h m^{-3}) for photo-Fenton, 69.1 (MW h m^{-3}) for photocatalysis and 20 (MW h m^{-3}) in case of dual effect. The rate of reaction was faster in dual effect leading to less energy consumption. With subsequent leaching of iron and Intactness of TiO_2 coating leads to the faster degradation of the MTZ with minimal energy consumption. With 70-80% less energy consumption as weighed against photo-Fenton and photocatalysis, dual process certifies its credentials for field-scale applications.

$$E_{E0} = \frac{P \times t \times 1000}{V \times 60 \times (\frac{1}{A_f} - \frac{1}{A_i})} \quad (4.8)$$

Where the power used by the UV lamps is denoted by P (kW), the time for irradiation is denoted by t (min), the volume of water is denoted by V (L) and A_i and A_f are the initial and final concentration of the compound (mg L^{-1}).

4.2.6. RECYCLABILITY OF THE BEADS

The main challenging task in using composite beads is to establish the dual effect for the continuous number of cycles. It means continuous leaching of iron from the support besides maintaining the surface activity of TiO_2. In our study, we have successfully recycled the composite beads for more than 70 runs without much decrease in the degradation efficiency. In all these recycles dual effect was maintained i.e. both iron leaching and TiO_2 activity was intact. The recyclability of the FE+FS beads in terms of retaining its catalytic activity (intactness of TiO_2 layer as shown in Figure 4.21a and appropriate leaching of iron Figure 4.21b was evaluated using the % degradation of MTZ as shown in Figure 4.21.

For further authentication in the perspective of the industrial scale applications of the process, the extended recyclability studies were conducted on the previously used FE+FS beads for at least 70 cycles and 80% of degradation was observed. Significant reduction even with used beads proposes that the dual effect could be implemented at a large scale for commercialization and for the industrial wastewater treatment purposes.

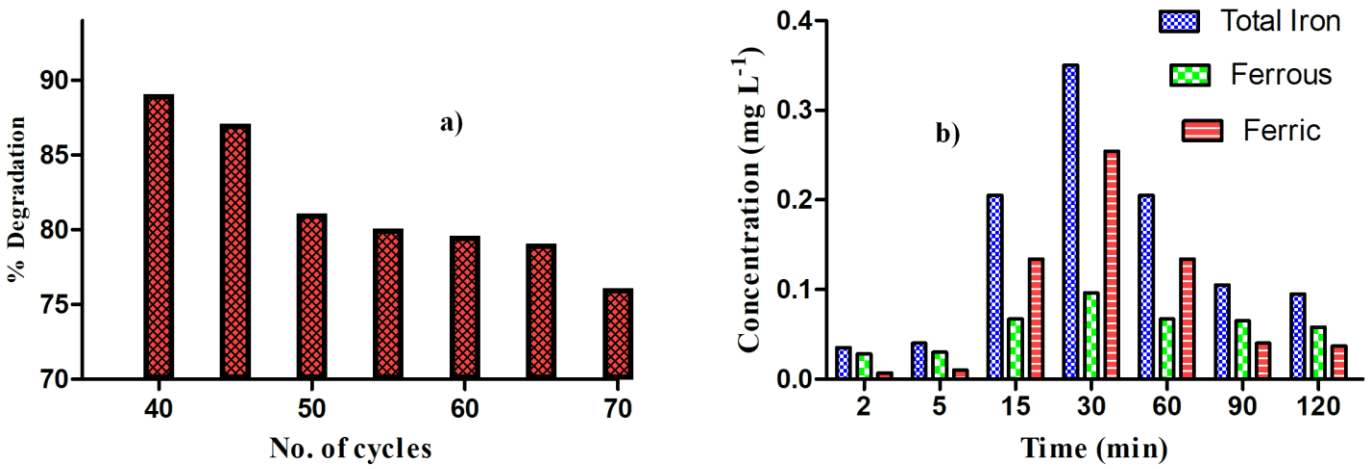

Figure 4.21: a) Recyclability studies of the Fe-TiO_2 composite, b) The concentration of iron leached after 70 recycles with the passage of reaction

4.2.7. CHARACTERIZATION OF THE COMPOSITE BEAD

In the dual process using composite beads, confirmation for the presence of TiO_2 along with Fe (even after repeated recycles) was characterized using SEM-EDS, XRD, UV-DRS, FT-IR, and Raman Spectroscopy.

4.2.7.a. SEM-EDS

The SEM-EDS of the natural raw materials (FE and FS) (Figure 3.6) confirmed the presence of 'Fe' in their native forms. Figure 4.22 shows the SEM and EDS image of the beads after 40 recycles and subsequently after 70 recycles at 500 × magnification. The coating was uniform, as very minimal cracks were observed even after 70 recycles. From the EDS confirmation of the presence of iron along with TiO_2 was done with the sharp peaks of 'Ti', 'O' and 'Fe' elements. This help in proving our fact of the dual process to succeed at the same place even after substantial recycling of the composite.

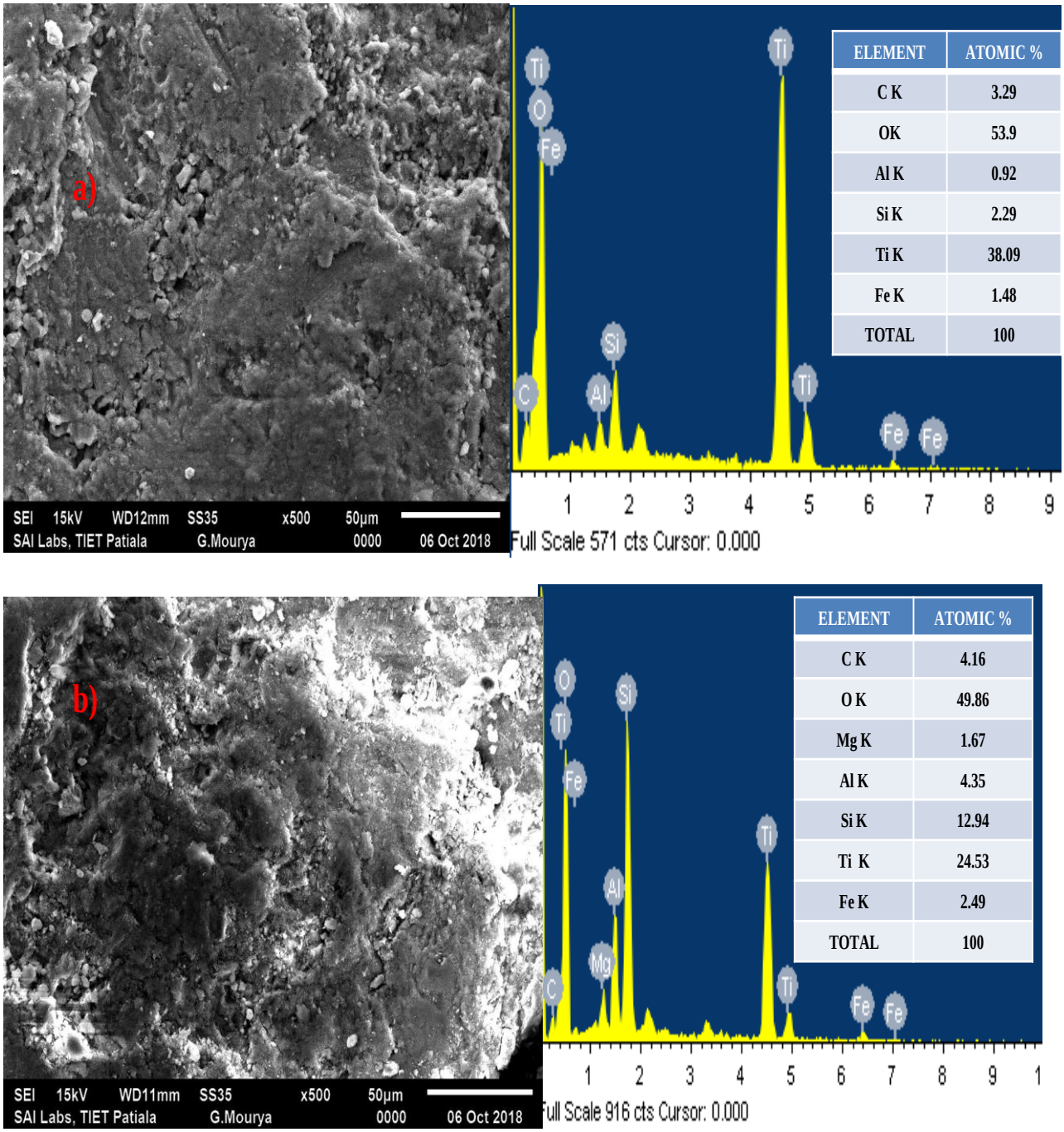

Figure 4.22: SEM-EDS analysis of coated beads after a) 40 recycles b) 70 recycles

4.2.7.b. XRD

The X-ray diffraction patterns of the 40 times recycled TiO_2 and 70 times recycled catalyst has been depicted in Figure 4.23. Basically, change in the structure of TiO_2 could be evaluated from the XRD analysis. The confirmation of both anatase (JCPDs number 01-084-1286), as well as the rutile phase and (JCPDs number 01-089-0552), confirm that there was no structural deformity in the TiO_2 catalyst. Even the peaks for the anatase phase were more as compared to rutile phase hence confirming the TiO_2 presence. The XRD of the natural raw materials (FE and FS) (Figure3.3) confirmed the presence of iron oxides in their native forms.

Additionally, there were some peaks present which confirmed the oxides of iron (JCPDs number 01-072-6233, 01-089-6466) along with titanium (JCPDs number 00-043-1011, 01-073-1631). It was observed that iron titanium oxide, as well as iron dititanium oxide, was formed. The presence of these kinds of oxides helps in authenticating our claim of both the processes to take place concurrently at the same place.Θ

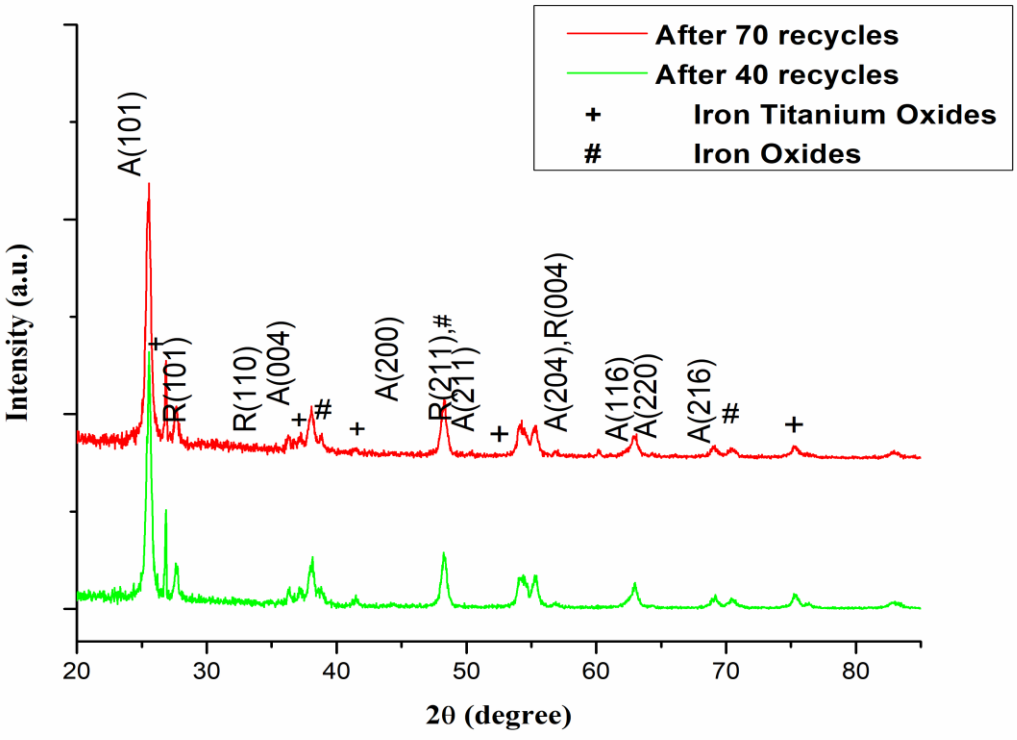

Figure 4.23: XRD analysis of the catalyst after 40 and 70 recycles

4.2.7.c. UV-DRS

For evaluating the effect of iron oxides on TiO_2, the band gap energy is also calculated from the scan of UV-VIS DRS. Observable amount of shift was noted in the recycled catalysts. The minimal quantity of the 'Fe' might be incorporated within the lattice structure of TiO_2 owing to these changes. From the Figure 4.24, it was concluded that there was a shift in the absorbed wavelength as compared to P25-TiO_2.

The band gap energy was quantified using the equation 4.9.

$$E = \frac{hc}{\lambda} \qquad (4.9)$$

Where E = band gap energy (eV), c = speed of light (3×10^8 m sec^{-1}), h = Planck's constant (6.626×10^{-34} Joules sec) and λ = absorption wavelength (nm)

There was a decrease in the band gap energy (2.89 eV for 40 recycles and 2.73 eV for 70 recycles) as compared with the original TiO_2 (3.14 eV) (Figure 4.24). This really confirms the photocatalytic activity of TiO_2 considerably under visible light irradiation.

The potential of VB and CB for the FE-TiO_2 composite were calculated using the equations 4.10-4.11.

$$E_{VB} = \chi - E^e + 0.5E_g \qquad (4.10)$$

$$E_{CB} = E_{VB} - E_g \qquad (4.11)$$

Here, χ is the absolute electronegativity of the semiconductor (χ is 5.9 eV for TiO_2), E^e is the free electrons energy on the hydrogen scale (4.5 eV), and E_g is the band gap of the composite (2.89 eV for 40 recycles and 2.73 eV for 70 recycles). The predicted CB and VB of the composite are -0.045 eV and 2.845 eV, while that of 70 recycled composites is -0.035 eV and 2.765 eV, respectively (Oladipo, 2018; Oladipo, Ifebajo, & Gazi, 2019). For the reaction to take place the holes generated get transferred from the composite to the MTZ and the electrons generated were transferred from CB to the solution. The generated electrons of the composite in CB are less negative than the potential of $O_2/ {}^{\bullet}O_2^-$ (−0.33V) hence ${}^{\bullet}O_2^-$ radicals could not be yielded.

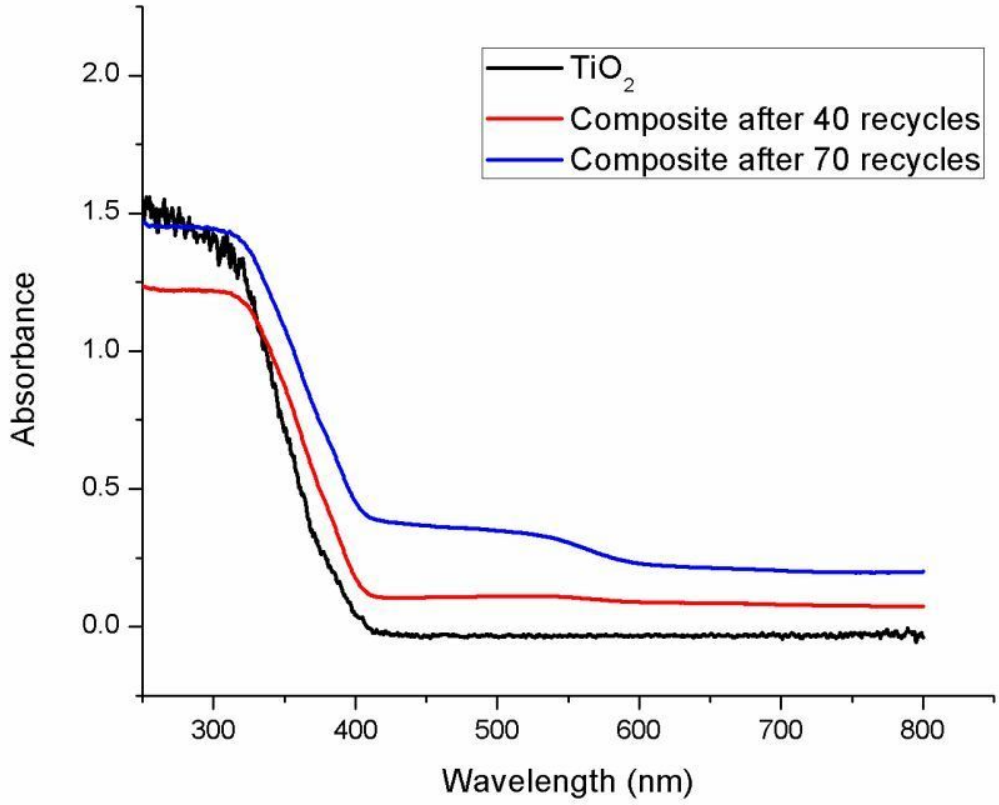

Figure 4.24: UV-DRS analysis of the catalyst after recycles

4.2.7.d. FOURIER TRANSFORM INFRARED (FTIR) SPECTROSCOPY

For further confirming the structure of the catalyst IR spectroscopy was conducted. The plot between wave number and % transmittance is depicted in Figure 4.25. The stretching band between 3330–3460 and 1610–1645 cm^{-1} were present in both the samples which might be due to the H-O-H stretching and bending respectively. This confirmed the stretching due to the presence of hydroxyl groups. For Ti-O-Ti stretching the band gap was observed at 703cm^{-1} and 784 cm^{-1}. The stretching at 450 to 550cm^{-1} (Ali et al., 2017) confirms the presence of Fe-O bonding existing in the fresh as well as recycled composite.

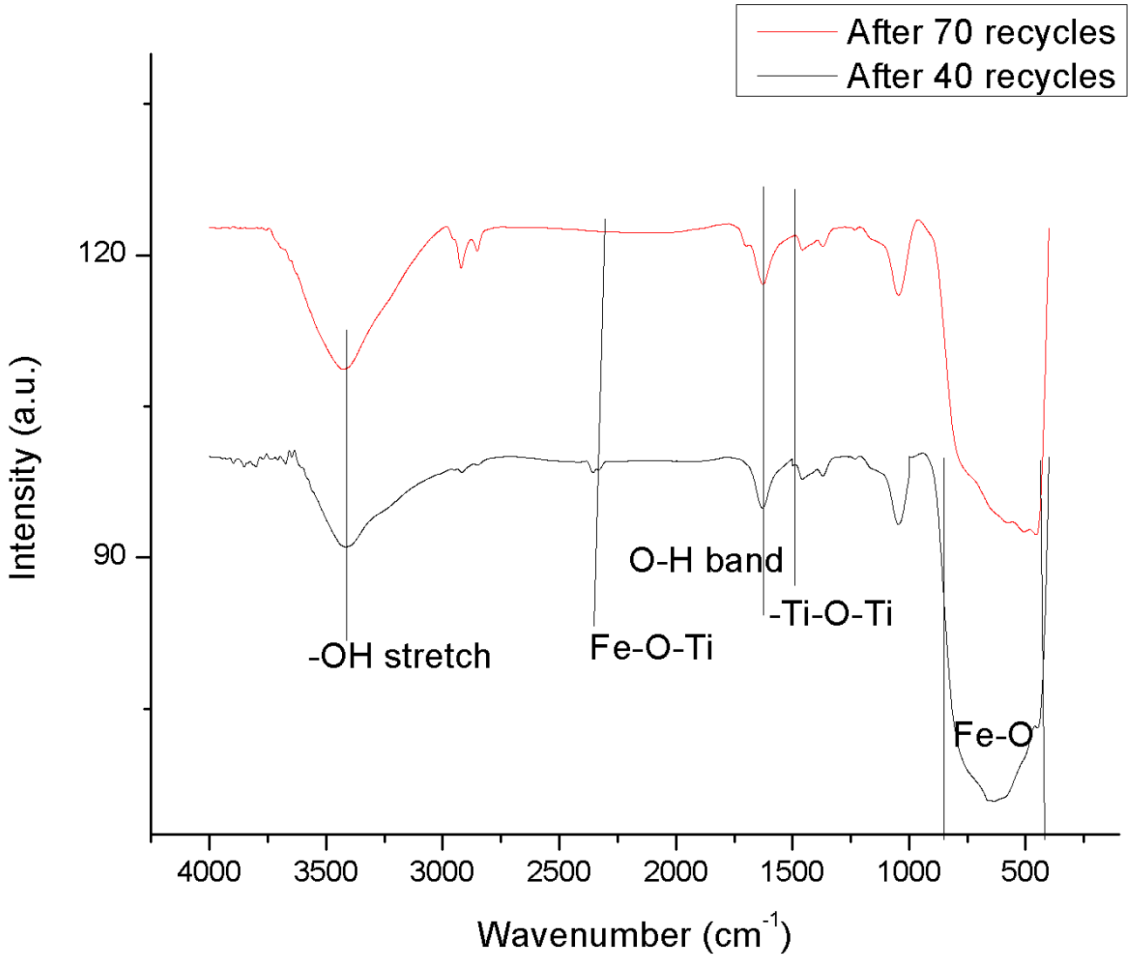

Figure 4.25: IR spectra analysis of the catalyst after recycles

4.2.7.e. RAMAN SPECTROSCOPY

For confirming the phase of the catalyst Raman spectroscopy (Figure 4.26) is used. The basic peaks in the range of 400-700 cm^{-1} are basically due to the characteristics of the TiO_2 confirming the presence of anatase as well as the rutile phase of TiO_2. Small peaks were obtained which might be due to the presence of iron oxides along with the TiO_2 (Figure 4.26). There was not much effect on the catalyst even after the introduction of iron. Structural peaks remained at the same place even after the recycles confirming the stability of the catalyst.

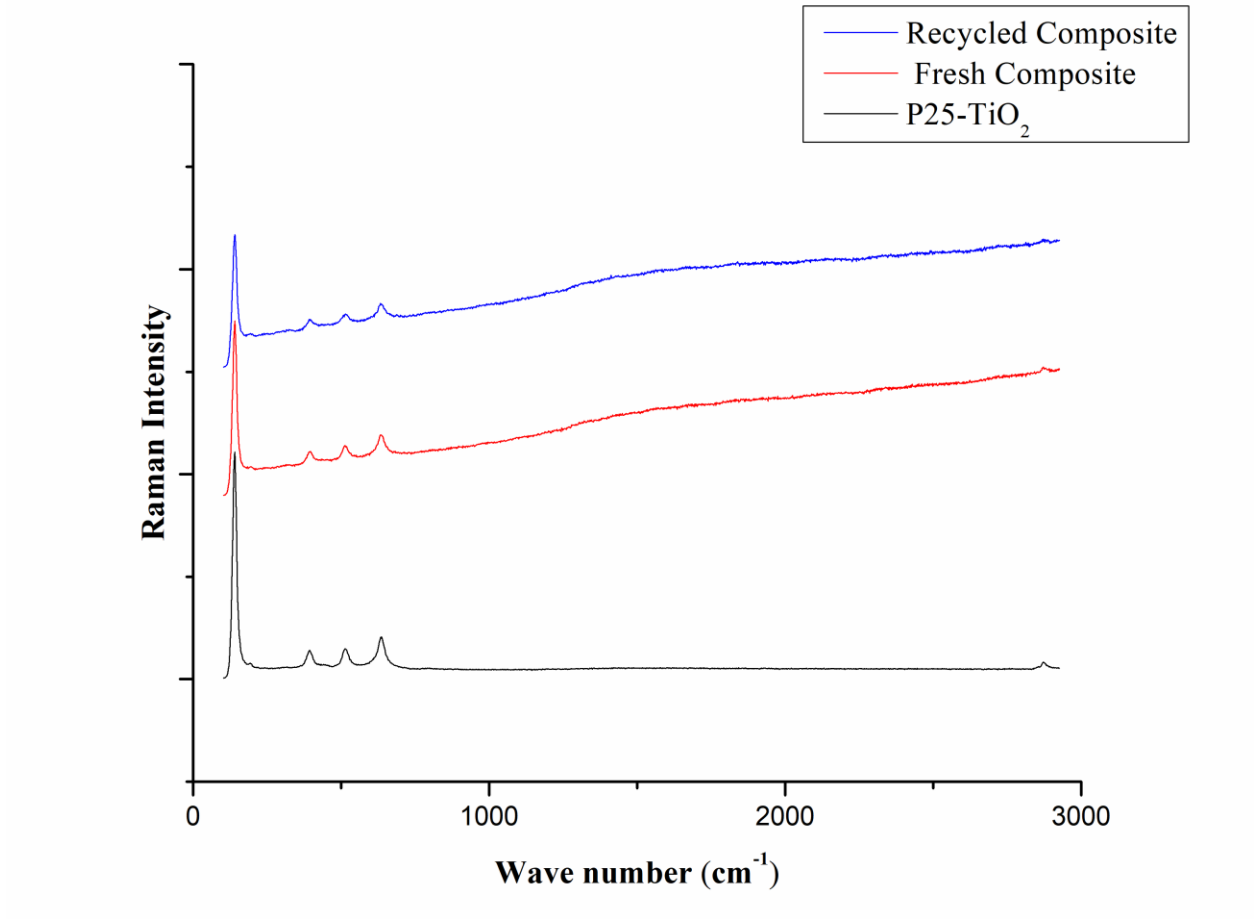

Figure 4.26: Raman spectroscopy of the catalyst after recycles

4.2.8. SYNERGISTIC EFFECT

A synergistic effect was observed in the case of dual effect as compared to the individual processes of photocatalysis and photo-Fenton. For analyzing this, second order rate constants were used as calculated from the rate equations.

There was a rapid increase in the second order rate constant for dual effect i.e. 9×10^{-3} L $mg^{-1}min^{-1}$ as compared to 0.64×10^{-3} L $mg^{-1}min^{-1}$for photocatalysis and 0.8×10^{-3} L $mg^{-1}min^{-1}$ for photo-Fenton owing to the large production of •OH (as shown in Figure 4.3) which further validates the dual effect over the individual processes. The synergy was calculated using equations 3.5-3.7.

The synergy of dual over photocatalysis process:

$$\% \text{ Synergy} = 100 \times (9 \times 10^{-3} - 0.6 \times 10^{-3})/9 \times 10^{-3}$$

$$\% \text{ Synergy} = 93.33\%$$

The synergy of dual over photo-Fenton process:

$$\% \text{ Synergy} = 100 \times (9 \times 10^{-3} - 0.8 \times 10^{-3})/9 \times 10^{-3}$$

$$\% \text{ Synergy} = 91.11\%$$

The overall synergy of the process i.e. dual over both the photo-Fenton process and photocatalysis:

$$\% \text{ Synergy} = 100 \times ((9 \times 10^{-3} - (0.6 \times 10^{-3} + 0.8 \times 10^{-3}))/9 \times 10^{-3}$$

$$\% \text{ Synergy} = 84.44\%$$

From the results, the author claims the novelty in terms of increased rate constant. In this reported study, synergy was increased to 93% as compared to photocatalysis and 91% for photo-Fenton.

4.2.9. MINERALIZATION OF MTZ

The mineralization study was carried out for MTZ at the optimum conditions obtained in terms of reduction in COD, TOC, and generation of nitrate, nitrite and ammonium ions. There was an almost 75% reduction in COD after 2 h with 57% of TOC reduction. The nitrogen atoms in MTZ might get converted into nitrate, nitrite and ammonium ions. The concentration of the nitrate ions started to increase first with time and then after 60 min, the concentration started to decrease (Figure 4.27). The concentration of the nitrite ions increased with increase in time. The concentration of the Ammonical nitrogen increased with time. It is mainly due to the oxidation of the MTZ leading to the conversion of nitrate to nitrite ions and the ensuing formation of ammonical ions. The proposed mechanism of degradation of MTZ has been shown in Figure 4.28. During the start of the reaction, MTZ with its nitroimidazole core undertook a loss of hydroxymethyl group to form a Methylfuroxancarboxamide (Tong et al., 2011) (having mass

144). Further the loss of nitro groups in the form of NO_2^- and NO_3^- due to the •OH attack lead to the formation of 1-Methylhydantoin-2-imide. The hydroxyl group attached with the structure might get converted into water molecules leading to the reduction of the 1-Methylhydantoin-2-imide. With further decarboxylation of the compound, a closed nitroimidazole structure was left. The cleavage of the ring with the loss of water and ammonium ions leads to the formation of methylenemethaneamine.

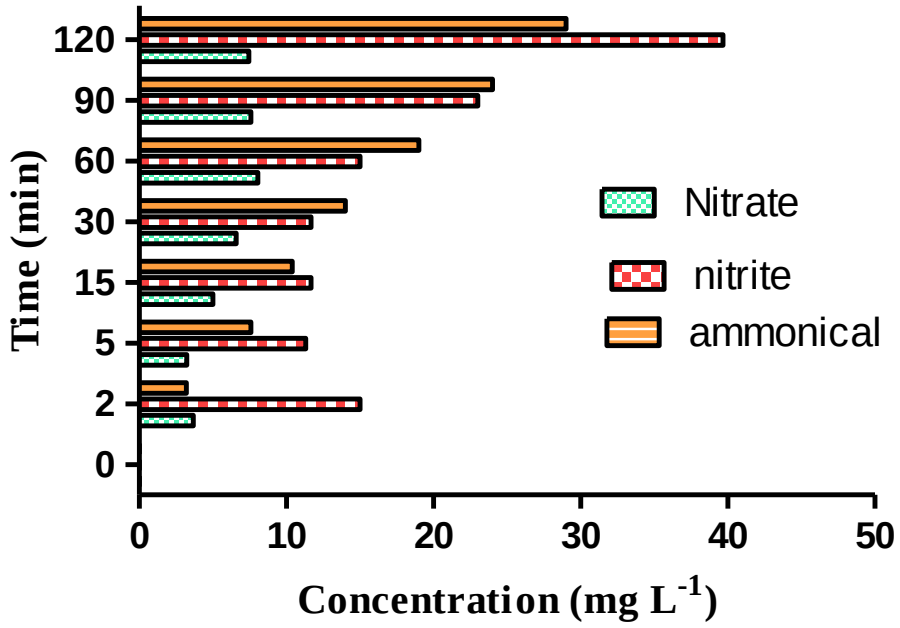

Figure 4.27: Mineralization of MTZ in the form of nitrate, nitrite and ammonical ions produced

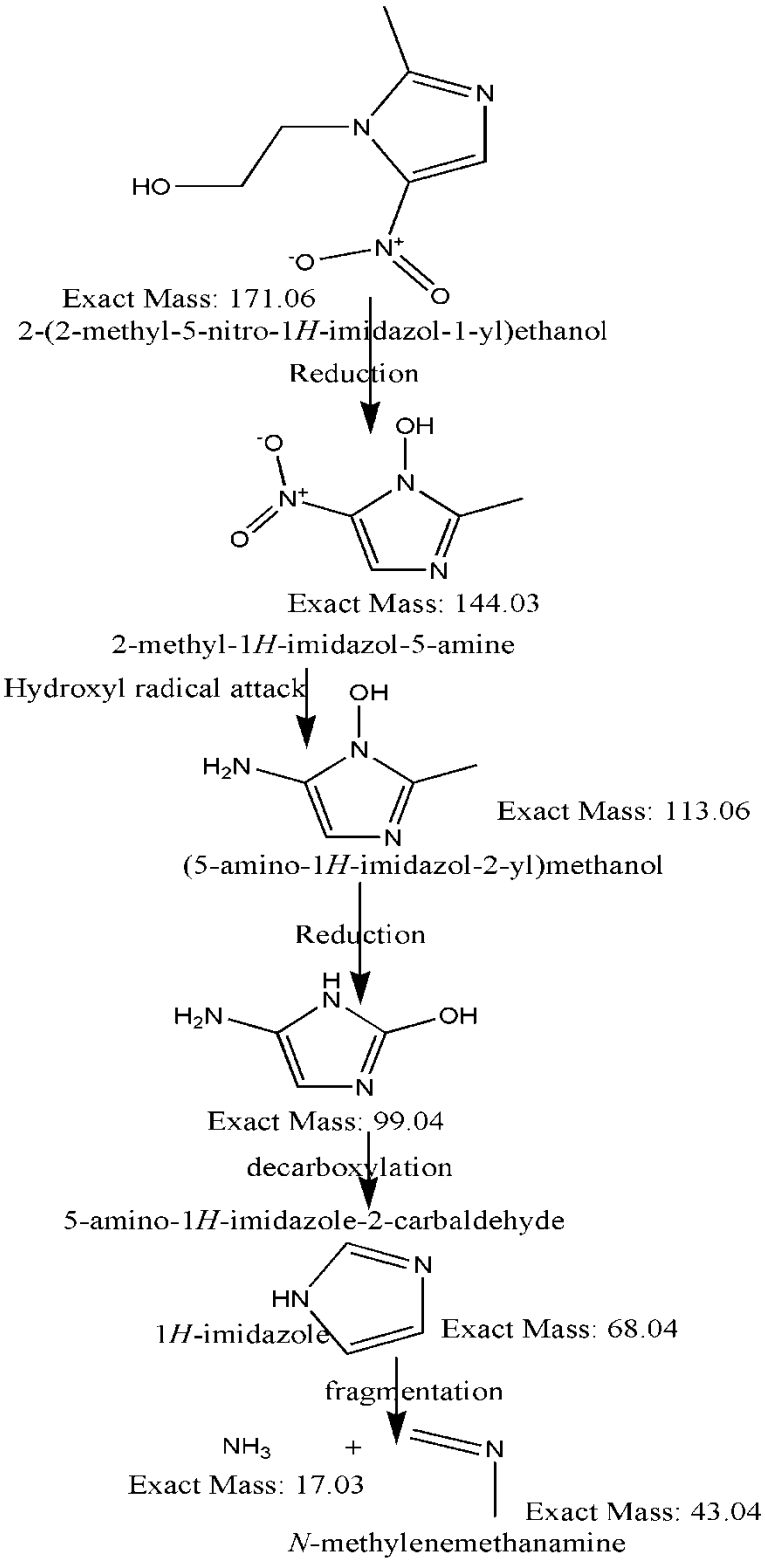

Figure 4.28: Proposed mechanism for the degradation of MTZ

SECTION 2

IN-SITU DUAL EFFECT OF PHOTO-FENTON AND PHOTOCATALYSIS IN THE CONTINUOUS MODE

The in-situ dual effect was further extended towards the continuous mode degradation of pharmaceutical drugs MTZ and PHZ in once through plug flow approaching reactors. Two types of reactors employed were fixed bed reactors in series and compound parabolic concentrator reactor.

4.3. FIXED BED REACTORS IN SERIES

In the present study, efforts have been made to approach plug flow behavior using fixed bed reactors in series employing Fe-TiO_2 composite beads, incorporating in-situ dual effect. In this study degradation of MTZ along with the mineralization has been studied at the pilot plant scale using in-situ dual effect incorporating fixed bed reactors in series. Best possible combination of flow rate, oxidant dose, and % surface area covered and number of reactors has been executed to get the desired results. In fact this is first reported study where the novel concept of fixed-bed situ dual effect has been used for the degradation of MTZ using once-through PFR approach.

4.3.1. DUAL EFFECT PRELIMINARY STUDIES

For confirming the prominence of dual effect, various preliminary studies were performed using the fixed bed reactor. Initial tests confirmed negligible adsorption using the MTZ solution performed using the TiO_2 coated beads as well as bare beads. Adsorption studies were performed using TiO_2 coated beads as well as uncoated beads kept in dark with MTZ solution. Another way round the photolysis showed approximately 10% of the oxidation of MTZ after 3.5 h. For conducting the photo-Fenton reactions uncoated beads were used at the pH of 3-3.5.The photo-Fenton reaction (only iron and •OH production by H_2O_2) showed almost 45% of degradation after 3.5 h. For carrying out the photocatalysis reaction, TiO_2 coated beads were used without maintaining the pH of the solution (thus avoids iron leaching) and only 38% of removal was obtained after 3.5 h.

Thereafter the prominence of in-situ dual effect was executed by combining both the processes. Fixed-bed in-situ dual effect confirmed the 68 % reduction in the concentration of MTZ after 2 h using the TiO_2 coated beads by maintaining the same conditions. Reduction in the

treatment time was the major achievement for the dual process as it could open new channels for its field-scale applications. Thus the primacy of in-situ dual effect was confirmed using the coated composite beads as both the processes take place at the same time, i.e. leaching of iron for photo-Fenton and TiO_2 reaction for photocatalysis.

4.3.2. EFFECT OF NUMBER OF REACTORS

A number of reactors in series would definitely affect the conversion rate of any pollutant, besides raising concerns about area required. For studying this, we have varied the number of reactors to three (Figure 4.29) and effectively measuring the concentration of pollutant after the exit of each reactor. These three reactors in the series system can handle a total volume of 8 L, with a flow rate of 4.0 L h^{-1} and H_2O_2 dose of 750 mg L^{-1}. As discussed, all the reactions were carried out in the presence of natural sunlight for keeping the process economically viable. It could be observed from Figure 4.29 that by increasing the number of reactors, the concentration of MTZ decreased. It was observed that almost 35% of the pollutant got decomposed after the 1st reactor by providing space-time of approximately 15 min. The whole process was passed once through the reactor at the specified flow rate.

Increasing the number of reactors in series along with maintaining the same conditions helped in the further degradation of MTZ. It was observed that nearly 50% of MTZ was degraded after the 2nd reactor. There was a slight loss in the degradation after the 1st reactor, which might be due to the formation of intermediates in between which slowed down the process. Further, one more reactor was adjoined to increase the degradation and with three reactors in series, 74% of the reduction in the MTZ was observed in the once-through process.

The conversion is not the only factor in determining the optimum number of reactors. The maintenance and configuration of the reactor also play an important role while optimizing the conditions. By increasing the more number of reactors, in this case, would pose difficulties in handling the whole system with increasing the maintenance cost of the process. Hence, keeping in mind all the stumbling in the process, three reactors have been optimized for the degradation of MTZ.

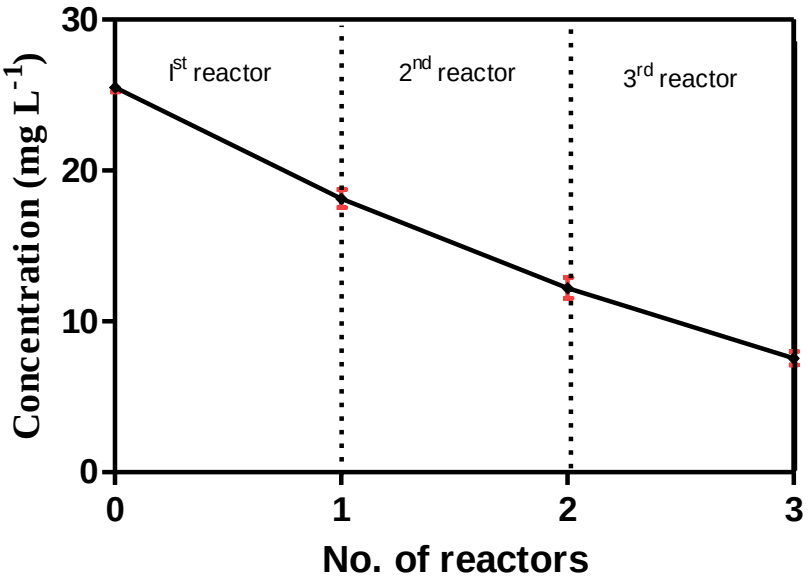

Figure 4.29: Outcome of the change in concentration of MTZ with increase in number of reactors in series during in-situ dual effect (H_2O_2 - 375 mg L^{-1}, pH-3.5, C_0 = 25mg L^{-1}, Volume =8L)

4.3.3. EFFECT OF FLOW RATE

Flow rate variations in PFR especially plays an important role in the degradation of the pollutant as the rate of turbulence and the amount of dissolved oxygen content is determined by the flow rate. Increasing the flow rate decreases the retention time in the reactor thus affecting the efficiency, whereas a low flow rate is economically not viable. In the present study, the flow rate was varied from 2.0±1.0 L h^{-1} to 40.0±1.0 L h^{-1} at the oxidant dose of 375 mg L^{-1} and under direct sunlight using three reactors in series.

It was observed that by increasing the flow rate the degradation was lowered which might be due to the less time to interact with the composite material (Figure 4.30). Similarly, with low flow rates, the overall time of the process and economy is also affected, which hinders its commercial-scale viability. At 2.0±1.0 L h^{-1} flow rate, the treatment time was 1 h 20 min with overall degradation of MTZ nearly 76.5% at the end of the third reactor. Increasing the flow rate to 8.0±1.0 L h^{-1}, there was a slight decrease in the degradation i.e. 68% but the total treatment time (45 min) was significantly reduced. Thereafter, the flow rates of 15.0±1.0 L h^{-1} and 20.0±1.0 L h^{-1} didn't contribute to the degradation pool significantly and same time treatment time was also

increased. Now from the process economics point of view, 8.0±1.0 L h^{-1} was chosen as optimized flow rate for further reactions as there was not much difference in the rate of degradation as compared to minimum flow rate i.e. 2.0±1.0 L h^{-1}. Most importantly, the time taken was nearly half in this case, without affecting the degradation significantly which really governs its commercial-scale application.

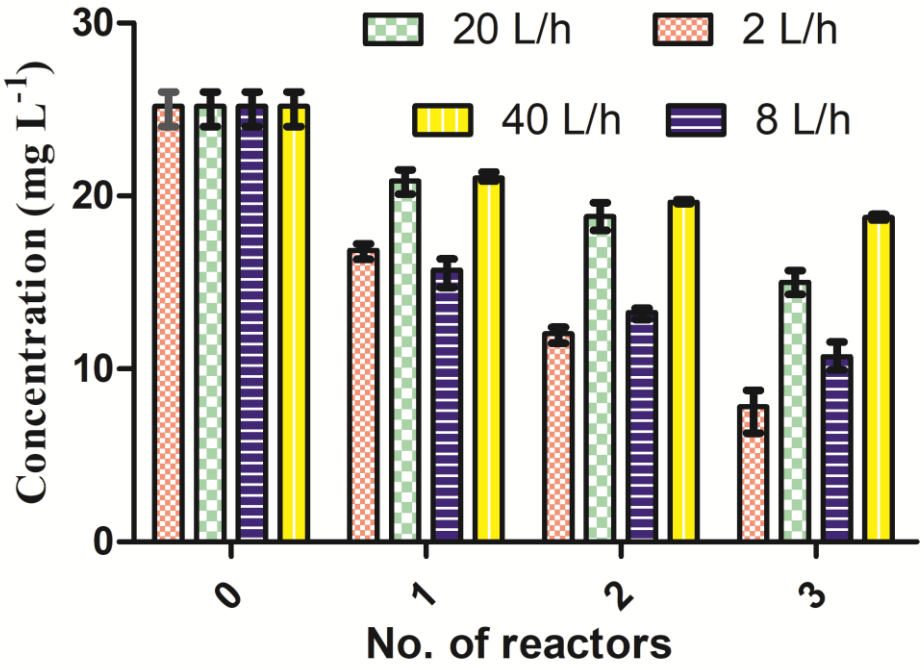

Figure 4.30: Outcome of the change in concentration of MTZ with variation in flow rate during in-situ dual effect (Number of reactors-3, H_2O_2 - 375 mg L^{-1}, pH-3.5, C_0 = 25mg L^{-1}, Volume =8L)

4.3.4. EFFECT OF SURFACE AREA COVERED

In our case, varying the number of catalyst coated beads as per the available surface area evaluates the effect of the covered surface area for the degradation of the pollutant. This effect basically studies the optimum amount of catalyst required for the degradation in the form of the number of beads. Thus, the study has been represented in the form of a percentage of area covered with varying the number of beads.

Now, as per the available surface area (exposed surface), the number of beads was increased from 25% to 100% of the reactor surface area (Figure 4.31). It was observed that with an increase in

the covered surface area from 25 to 75%, there was an increase in the degradation efficiency. This might be due to increased amount of catalyst help in the degradation and as every time the pollutant comes in contact with the new catalyst in the form of beads placed in the reactor as seen from the Figure 4.31. Thus the rate of degradation was increased as active sites were also increased, leading to the production of more •OH. Thereafter, further increasing the covered surface area from 75 to 100%, there was not much change in the rate of degradation as optimum concentration might have reached (in terms of the amount of catalyst). With an increase in covered surface area upto 100% there was a fall in the degradation, which might be due to the formation of the dead zone area along with the blocking of the active sites. Further, the concentration of iron leached also increased which also hinders the active sites of TiO_2 deteriorating its efficiency.

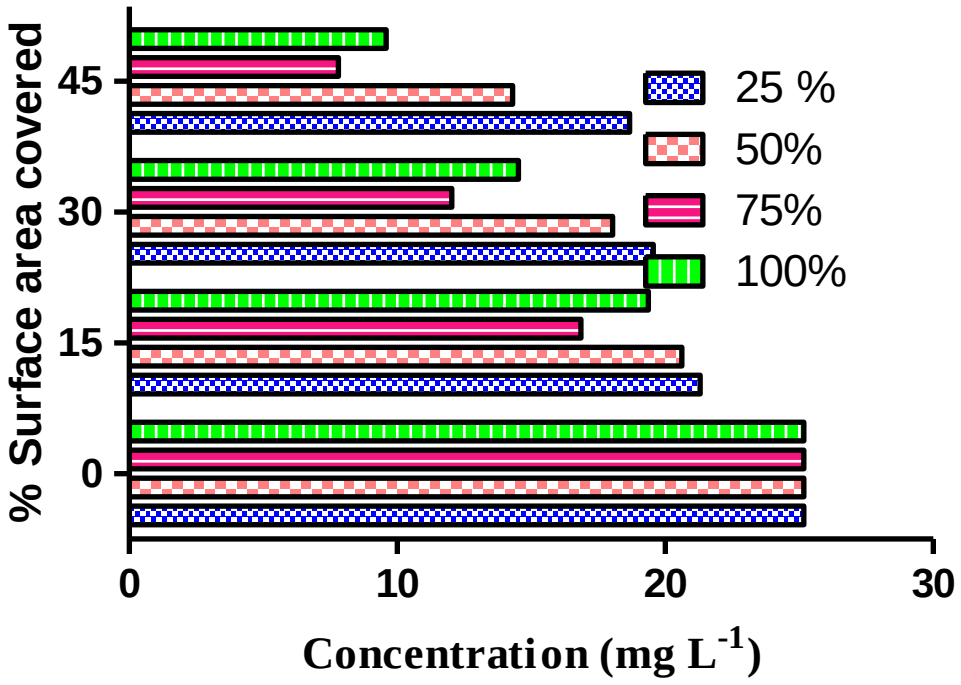

Figure 4.31: Outcome of the change in concentration of MTZ with variation in number of beads i.e. covered surface area during insitu dual effect (Flow rate- 8 L h^{-1}, number of reactors- 3, H_2O_2 - 375 mg L^{-1}, pH-3.5, C_0 = 25mg L^{-1}, Volume =8L)

4.3.5. EFFECT OF DOSE OF H_2O_2 AS AN OXIDANT

Following the once-through in-situ dual effect of photocatalysis and photo-Fenton, H_2O_2 was utilized in both the process simultaneously in the generation of •OH . The prominence of in-situ dual effect enhances the rate of reaction using H_2O_2 being an electron acceptor. In this context, the work was carried out using TiO_2 coated iron composite made up of FE and FS at the acidic conditions (maintaining pH of 3.5) with varying dose of H_2O_2. As discussed, three reactors in series were used for the process which was optimized. In this case, the dosage of H_2O_2 was varied from 187.5 to 1125 mg L^{-1} for the degradation of MTZ. From Figure 4.32, it was observed that with increasing the dosage of H_2O_2 the rate of degradation was increased upto 750 mg L^{-1}. Further, the increase in the dosage upto 937.5 mg L^{-1} the concentration was found to be constant. With further increase in the dosage upto 1125 mg L^{-1}, the decrease in the degradation of MTZ was noticed. This might be due to the scavenging effect of H_2O_2 at a higher dose. Hence, 750 mg L^{-1} was chosen as the optimum dose for the degradation of MTZ and approximately 85% of the degradation was observed. Even H_2O_2 dose can be further minimized with other design considerations and scaling-up options.

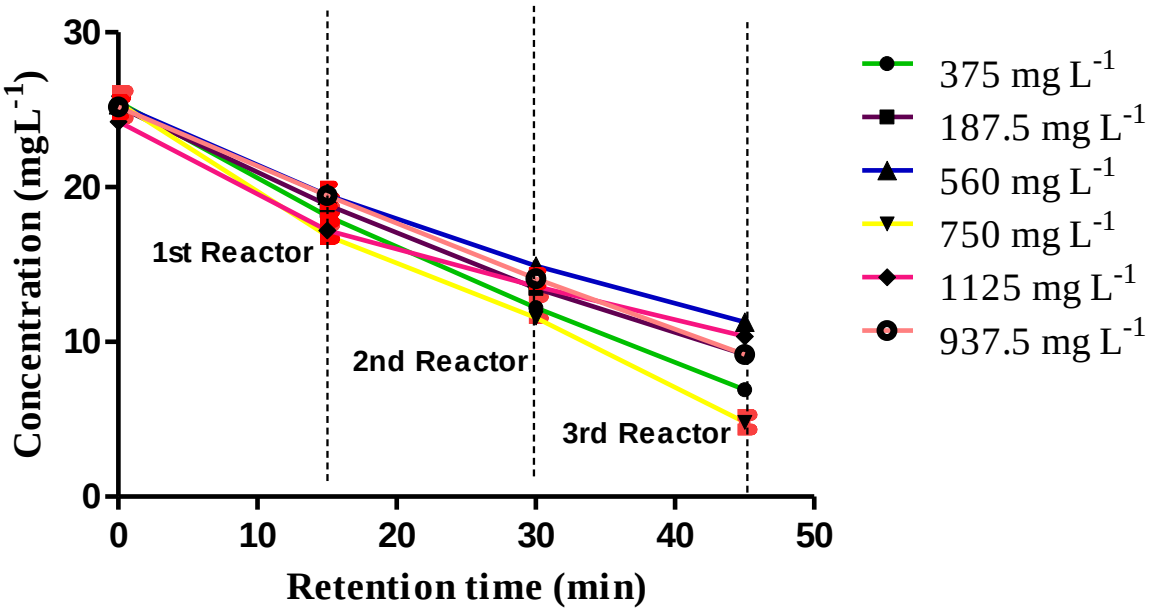

Figure 4.32: Outcome of the change in concentration of MTZ with variation in dose of H_2O_2 during in-situ dual effect (Number of reactors- 3, flow rate- 8L h^{-1}, % area covered – 75%, pH-3.5, C_0 = 25mg L^{-1}, Volume =8L)

4.3.6. SYNERGISTIC EFFECT

The synergy of the dual process over the individual processes was calculated using kinetic rate constant (Mazille, Lopez, & Pulgarin, 2009a). The rate constant was evaluated using the data from the batch reactor. In our study, the degradation of MTZ followed 2^{nd} order reaction and the value of rate constants as evaluated came out to be 6.4×10^{-4} L mg^{-1} $min^{-1}$for photocatalysis and 0.0008 L mg^{-1} $min^{-1}$for photo-Fenton and for dual effect 9×10^{-3} L mg^{-1} min^{-1}which further validates the dual effect as compared to the individual processes.

The synergy of the dual process was evaluated over the individual processes of photocatalysis and photo-Fenton using the equations 3.5-3.7.

$$\% \text{ Synergy} = 100 \times \{(0.009 - 0.0006)\}/0.009$$

$$\% \text{ Synergy} = 93.33\%$$

The synergy of dual over photo-Fenton process:

$$\% \text{ Synergy} = 100 \times \{(0.009 - 0.0008)\}/0.009$$

$$\% \text{ Synergy} = 91.11\%$$

The synergy of dual over both photocatalysis and photo-Fenton process i.e overall synergy:

$$\% \text{ Synergy} = 100 \times \{(0.009 - (0.0006 + 0.0008))\}/0.009$$

$$\% \text{ Synergy} = 84.44\%$$

Significant synergetic effect of dual process over both the processes leads to the reduction in the treatment time of reaction and thus further qualifies its applications for field-scale trails.

4.3.7. APPROACHING THE IDEAL PLUG FLOW BEHAVIOR

Theoretically, the reaction efficiency of the plug flow reactor is best as compared to the mixed flow reactor. To achieve this, the flow rate should be very low so that high conversion is obtained. But some operational problems like film diffusion resistance and mass transfer resistance might pose a problem in case of immobilized catalyst (PFR). Hence to evaluate the efficiency in the

present research, theoretical plug flow has been tried to approach with multiple reactors in series (equations 4.12-4.16).

$$\frac{V}{F_{Z0}} = \int_0^{X_Z} \frac{dx_Z}{-r_Z} \quad (4.12)$$

$$\frac{V}{\nu_0} = C_{Z0} \int_0^{X_Z} \frac{dX_Z}{-r_Z} \quad (4.13)$$

As in this case the second order reaction is being followed so,

$$-r_Z = kC_Z^2 \quad (4.14)$$

$$X_Z = \frac{(C_{Zo} - C_Z)}{C_Z} \quad (4.15)$$

And for 2nd order, $k\tau C_Z = \frac{1-X_Z}{X_Z}$

$$\frac{V}{\nu_0} = \frac{1}{kC_Z} \int_0^{X_Z} \frac{dx_Z}{(\frac{1-X_Z}{X_Z})} \quad (4.16)$$

Where the reactor's volume is depicted by V in L, volumetric flow rate by $\boldsymbol{\nu}_0$ ($Lmin^{-1}$), molar flow rate by F_{Z0} (moles min^{-1}), C_Z= final concentration (mg L^{-1}), C_{Zo}= initial concentration (mg L^{-1}), X_Z = conversion, r_Z= reaction rate (mg $L^{-1}min^{-1}$), k = rate constant ((mg $L^{-1})^{-1}min^{-1}$).

Using equation 4.16, 93.5% conversion was obtained by substituting optimized values of flow rate, i.e. 8 L h^{-1}, the total volume of 8L and with a second-order rate constant, the k value of 0.009 L $mg^{-1}min^{-1}$. At these optimized conditions, the experimental results showed 85% of conversion. There was nearly 9% of error in between theoretical as well as experimental results which might be due to experimental errors, other limitations. Hence it was concluded that three fixed bed reactors in series approached plug flow reactor.

For further confirmation, the hydrodynamic behavior of the fixed bed reactors in series residence time distribution (RTD) study was carried out. RTD is expressed in the form of exit age distribution E (t) which is calculated as equation 4.17.

$$E(t) = \frac{C\ (t)}{\int C(t)dt} \quad (4.17)$$

Where C(t) is the concentration of the tracer (mS cm^{-1}), t is the time (min). For this purpose, Lithium chloride was used as the tracer. For studying the behavior of the reactor, the axial dispersion model and CSTRs in series model were used for RTD modeling. The model used for the RTD analysis has been conceptualized as shown in Figure 4.33.

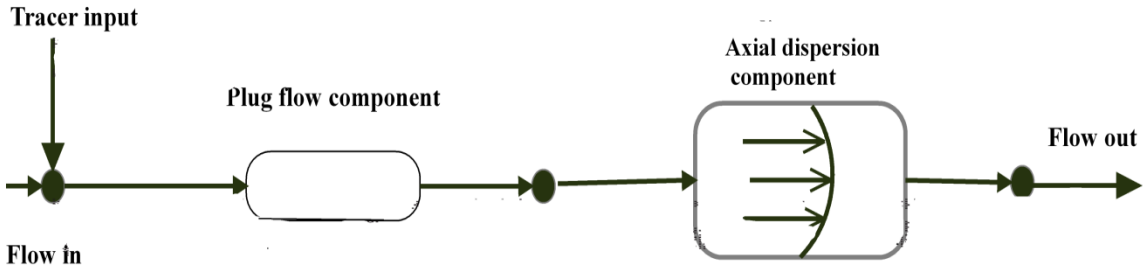

Figure 4.33: The model representation for the three tanks in series

The mean residence time of the optimized flow rate was 45 min. The mean residence time obtained from the model is 42.8 minutes, which is approximately similar to the theoretical value. The dispersion observed in Figure 4.34 is high as the three reactors were connected in series leading to the dispersion of the tracer when it passes from one reactor to the other. The value of the peclet number (Pe) was obtained as 18. This high value of Pe shows the plug flow behavior with minimum dispersion. To the best of our knowledge, this is first ever reported study confirming the plug flow approach using fixed-bed in-situ dual effect. This would help in the scaling up of the reactors and the increasing the process efficiency at an optimum rate.

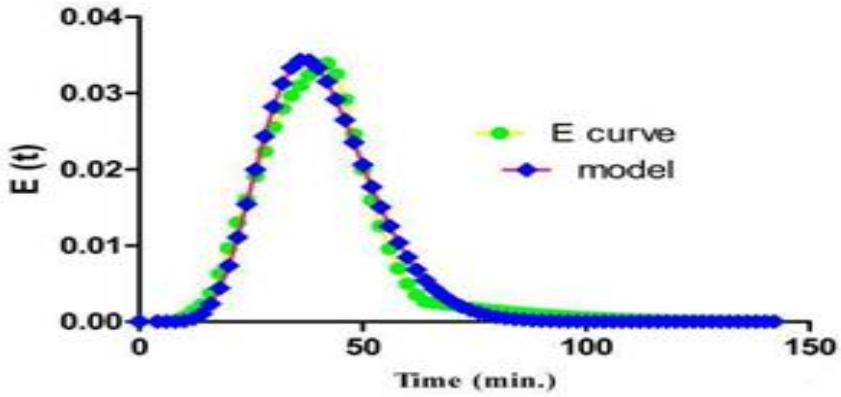

Figure 4.34: RTD curve obtained from the experimental analysis of the three reactors in series along with the fitted model of axial dispersion

4.3.8. RECYCLABILITY/DURABILITY OF THE CATALYST

In fixed-bed catalysis, the durability of the catalyst for repeated cycles would always remain a big challenge. One more challenge has been added in the durability context i.e. the stability of catalyst in the flow conditions. Even it becomes more challenging to maintain the in-situ dual effect of photocatalysis and photo-Fenton in the flow mode. For the dual effect to take place simultaneously there should be continuous iron leaching from the composite support along with photoactive TiO_2 layer intact on the surface.

In our reported study, the composite beads made up of FE+FS were recycled for more than 80 cycles (results are presented upto 80 recycles in Figure 4.35). Actually, the beads were competent enough to execute both the processes even after 80 recycles, which we claim as our novelty. The iron leaching during the operation of reactors was tested after 80 recycles (Figure 4.36) and presence of TiO_2 was confirmed through SEM-EDS. There was only (15-20%) loss in the degradation efficiency with successive recycles. Some studies have reported the thermal activation(Salaeh et al., 2017) of catalyst at high temperature for catalyst revival but in our case, the beads were dried in natural sunlight for 1-2 h. After some recycles, beads were kept in an oven at 80-90^{o}C for reactivation. This further strengthens our claim for visualizing the commercial-scale application of the process as it governs the economy of the process.

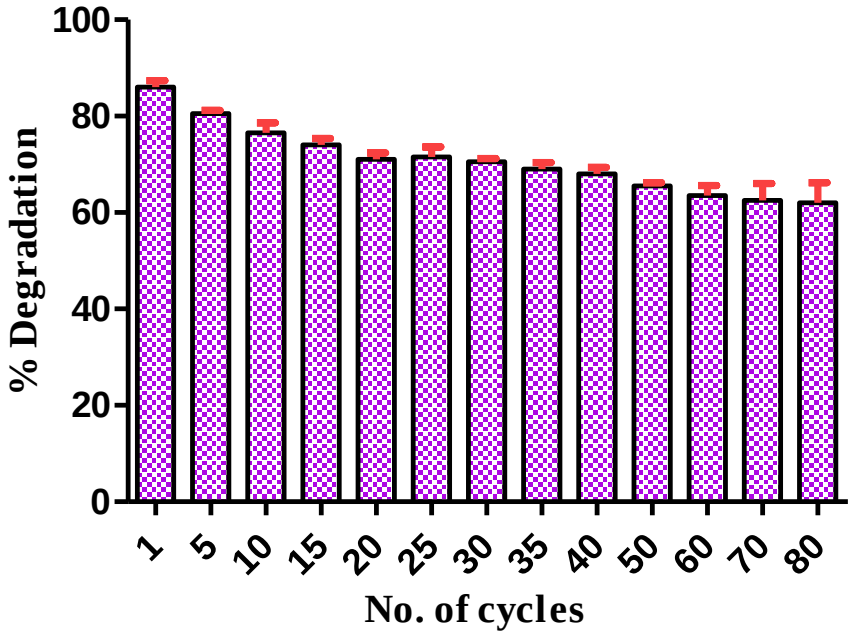

Figure 4.35: Durability of the composite beads in terms of number of recycles for the degradation of MTZ

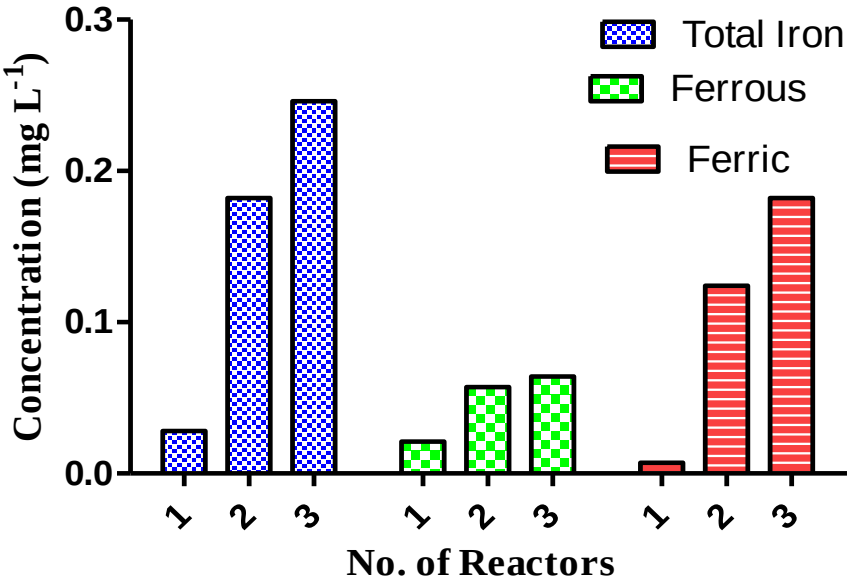

Figure 4.36: Estimation of total, ferrous and ferric ions of iron concentration leached from each reactor after 80 recycles

4.3.9. CHARACTERIZATION

4.3.9.a. SEM-EDS

For depicting the morphology of the composed composite beads, the SEM was conducted at 500 × magnification (Figure 4.37). The surface was even with fewer cracks confirming coating to be proper even after 80 recycles. The elemental composition present at the surface was depicted using EDS analysis. 'Ti' and 'O' elements were present at the surface. Some percent of 'Fe' also depicted its presence even at the surface. Even in recycled composite 'Ti', 'O' and 'Fe' were present confirming the intactness of layer of TiO_2 even after subsequent usage further substantiating our claim of in-situ dual process.

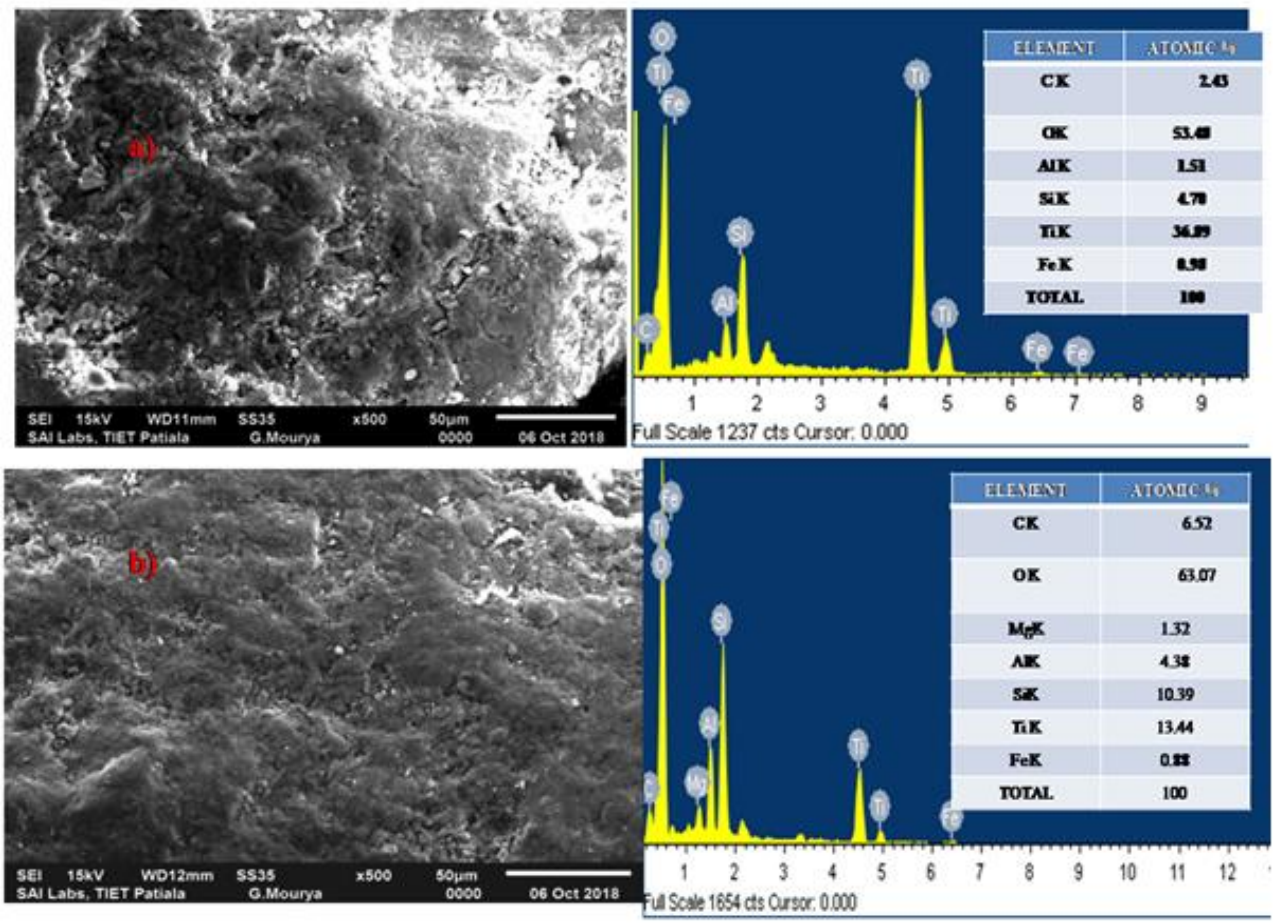

Figure 4.37: SEM-EDS images of a) freshly coated composite beads b) after 80 recycles used beads

4.3.9.b. XRD

For confirming the nature of composite after coating XRD was conducted. The basic change in the structural properties is evaluated using XRD. From the XRD analysis in Figure 4.38, it was confirmed that the basic nature of TiO_2 was maintained i.e. the presence of both anatase (JCPDs number 01-084-1286) and rutile phase (JCPDs number 01-089-0552) in the pattern. No changes in the structure were observed .In addition to TiO_2, some additional peaks corresponding to the iron oxides (JCPDs number 01-072-6233, 01-089-6466) along with titanium (JCPDs number 00-043-1011, 01-073-1631) were also observed. Iron oxides help in the photo-Fenton process to take place. The presence of this kind of oxides helps in authenticating our claim of both the processes to take place concurrently at the same place.

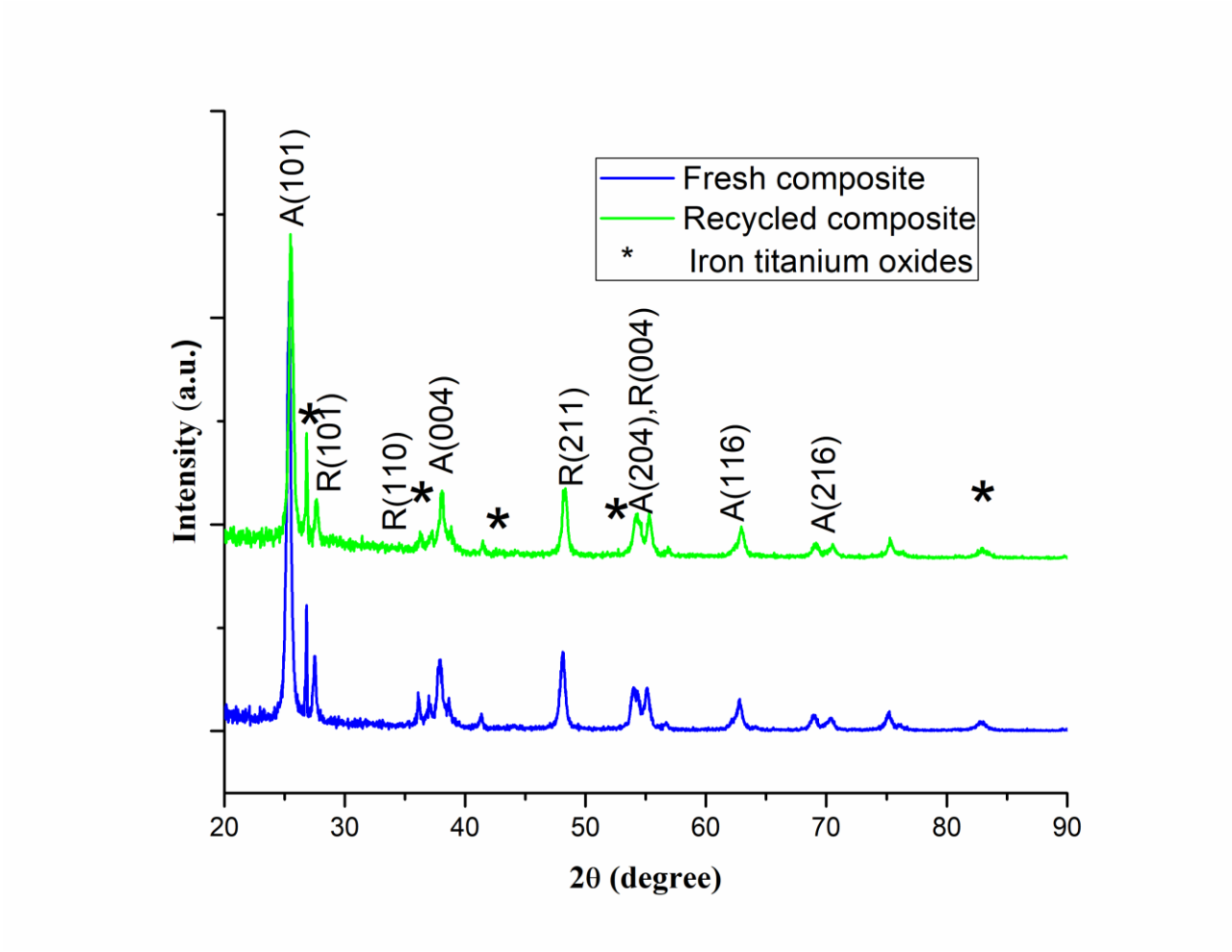

Figure 4.38: XRD pattern of fresh and recycled composite

4.3.9.c. UV-DRS

For evaluating the band gap energy of the composite material UV–DRS was conducted. The fresh and recycled composite was studied in Figure 4.39. The pattern of the light absorption was similar in case of fresh as well as a recycled catalyst.

The band gap energy was also quantified for the fresh as well as a recycled composite in comparison with the P25-TiO_2 using the equation:

$$E = \frac{hc}{\lambda} \qquad (4.18)$$

Where E = band gap energy (eV), c = speed of light (m s^{-1}), h = Planck's constant and λ = absorption wavelength (nm)

The band gap energy for the fresh and recycled composite i.e. of (Fe-TiO_2 composite) came out to be 2.8 eV and 2.77 eV respectively as compared to 3.14 eV of P25-TiO_2.

There was a decrease in the band gap energy as compared with the original TiO_2 (Figure 10). This hence confirmed that the resulting prepared catalyst is expected to be able to harvest visible light and, as a consequence, enhance the photocatalytic activity of TiO_2 considerably under visible light irradiation.

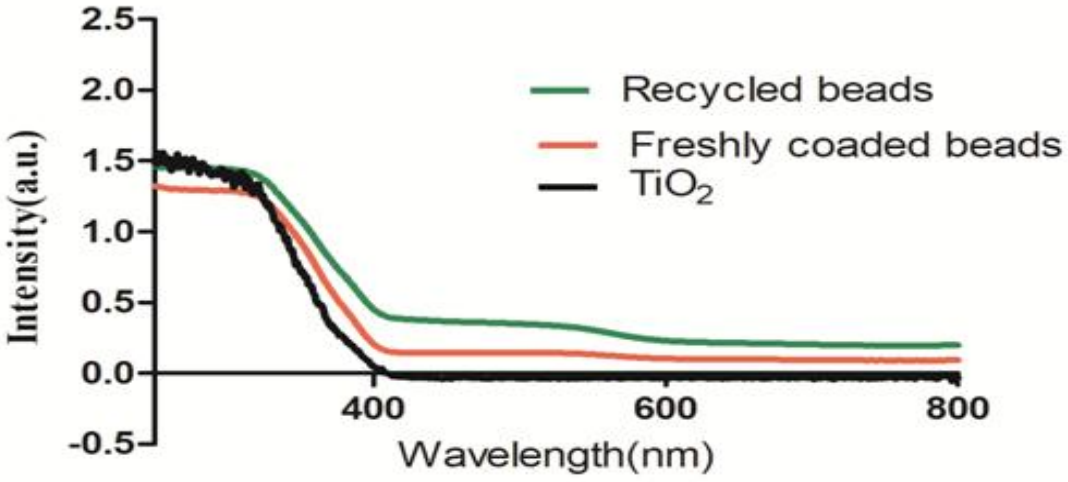

Figure 4.39: UV-DRS analysis of the fresh catalyst and catalyst after recycles

4.3.9.d. FOURIER TRANSFORM INFRARED (FTIR) SPECTROSCOPY

The characteristics of the composite were also evaluated using the Fourier transform infrared spectroscopy. The IR spectrum of the fresh as well as recycled composite, is depicted in Figure 4.40. The stretching band between the 3330–3460 and 1610–1645 cm^{-1} were present in both samples. This confirmed the stretching due to the presence of hydroxyl groups. The stretching vibrations of the O-H group confirmed the water to be adsorbed on the surface of the catalyst (J. Guo et al., 2013). Small transitions in the range of 518 cm^{-1} might attribute to the vibrations modes of TiO_2(Jaihindh, Chen, & Fu, 2018). For Ti-O-Ti stretching the band,the gap was observed at 400-100 cm^{-1}(Jaihindh et al., 2018). Further, there was a change observed in the structure of catalyst in the range of 200-2100 cm^{-1}, which might be due to the presence of Fe with the catalyst. The stretching at 450 to 550cm^{-1} (Ali et al., 2017) confirms the presence of Fe-O bonding existing in the fresh as well as recycled composite.

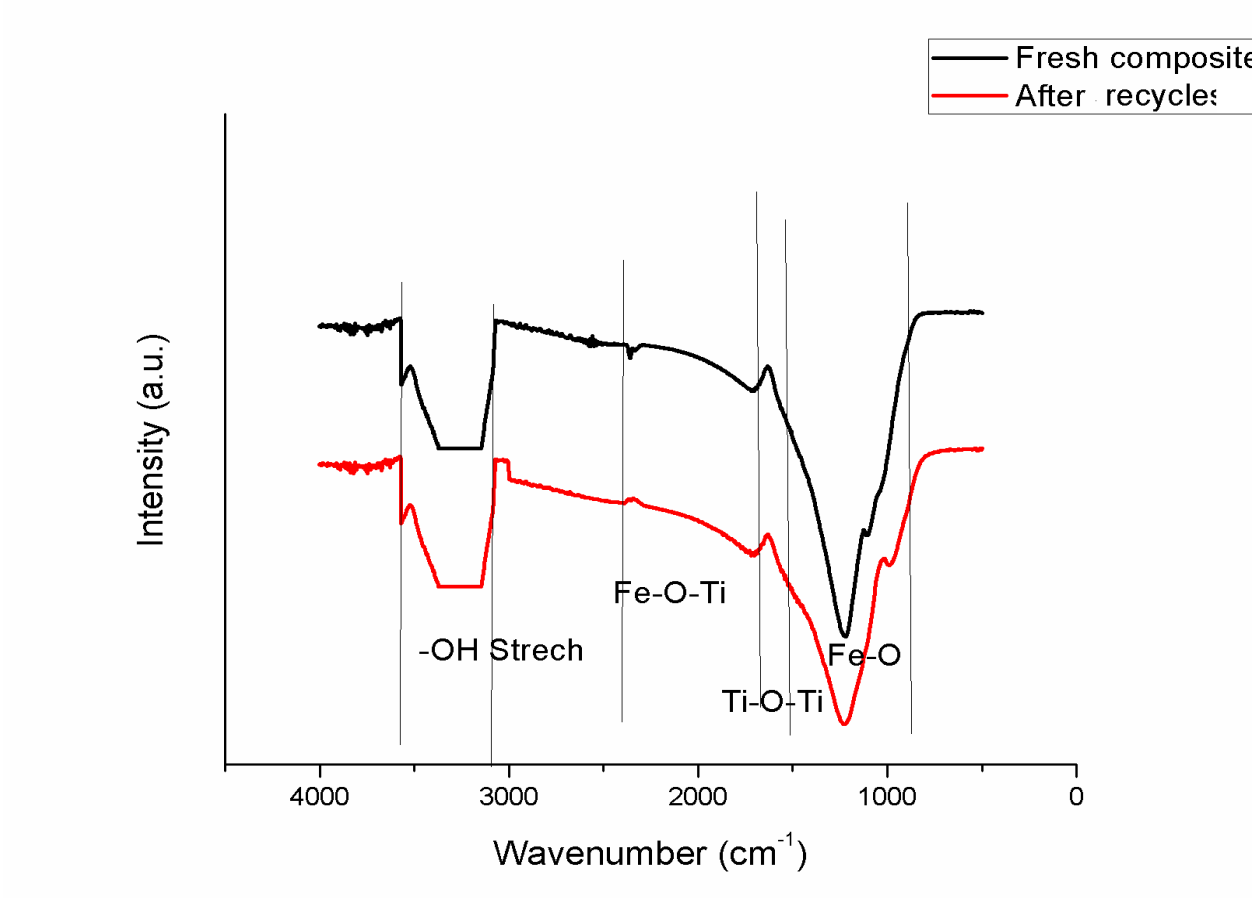

Figure 4.40: IR spectra analysis of the fresh catalyst and after recycles

4.3.10. MINERALIZATION

For confirming the mineralization of the compound MTZ reduction in COD, TOC, as well as the formation of the various ions i.e. nitrate, nitrite, and ammonium ions, have been studied. The nitrogen atoms present in the structure gets oxidized and the formation of nitrates and nitrites were observed (Table 4.8). The nitrate first increases in concentration then start to decrease which might be due to the conversion into nitrite ions. Ammonium and nitrites were found to increase in concentration at the end. It was observed that 55% of the COD was reduced at the optimum conditions with TOC removal of 36%.

The GC-MS was used to evaluate the intermediates formed during the degradation of MTZ in three reactors in a series model (Figure 4.41). MTZ might convert into methyl imidazole-amine. During the start of the reaction, MTZ with its nitroimidazole core undertook a loss of hydroxyethyl group to form a 2 methyl- 1H-imidazole-5amine (Tong et al., 2011). Further the loss of nitro groups in the form of NO_2^- and NO_3^- due to the •OH attack. The hydroxyl group attached with the structure gets converted into water molecules leading to the reduction and formation of 5-amino-1-H-imidazole-2-caraldehyde. With further decarboxylation of the compound, a closed nitroimidazole structure is left. The cleavage of the ring with the loss of water and ammonium ions leads to the formation of methylenemethaneamine.

Table 4.8: Concentration of various ions produced throughout the process for the degradation of MTZ using reactors in series

Time (min)	**Concentration (mg L^{-1})**		
	Nitrate (mg L^{-1})	**Nitrites (µg L^{-1})**	**Ammonium ions (mg L^{-1})**
15	3.73	1.66	2.1
30	5.23	2.34	3.7
45	4.31	3.45	4.6
60	4.24	3.89	6.7

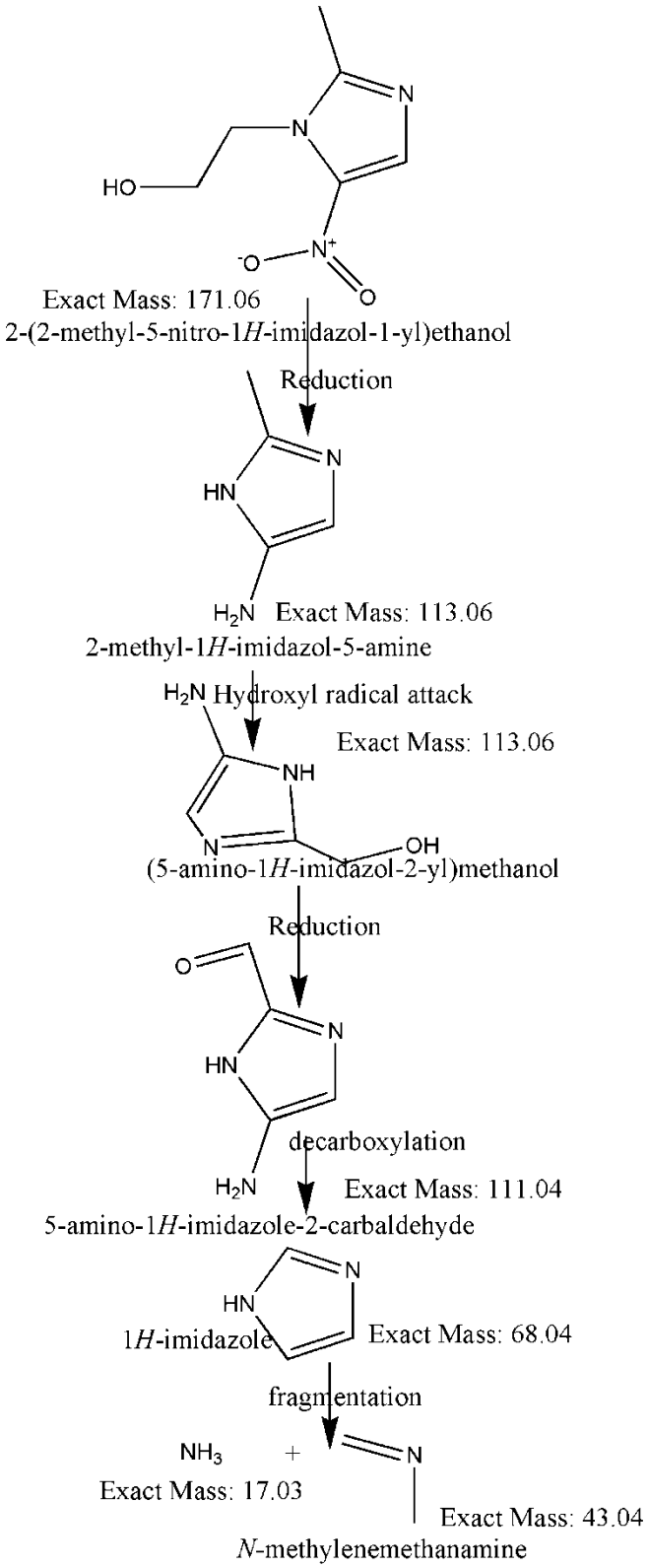

Figure 4.41: Predicted tentative pathway for the degradation of MTZ

4.3.11. COST ANALYSIS

Economics of the process always defines its viability for its commercial-scale applications and this part always remained questionable in the case of AOP. As most of the reported AOPs are not much economical in terms of their practical viability and found to be not feasible for most of the industries. The basic cost for the treatment includes the initial investment in the design of reactors, pumps, pipes and flow system. Additionally, the cost of the catalyst is also a one-time investment which could be returned after successful usages. This is one of the few studies presenting the total cost including reactor fabricating, pumping cost and all raw materials cost (Table 4.9). As the reactor was operated in sunlight the there was no extra cost energy consumption by UV lights.

Thus to treat one batch of 8L in a continuous PFR, the cost comes out to be less than one US dollar. Although best efforts have been made to incorporate all the operating parameters, yet some process variations may vary the cost. Altogether, it is a comprehensive package being provided for visualizing the commercial aspects of dual technology. The total cost approximated in this study is comparatively less as compared to other similar reports suggesting economic evaluations (Ozkal, Koruyucu, & Meric, 2016; Vishnuganth, Remya, Kumar, & Selvaraju, 2016). However for real scale-up cost analysis, effect of all the energy intensive parameters should be taken into consideration. The same has been calculated in Table 4.10 (Tribe & Alpine, 1986).

Table 4.9: Cost analysis of the in-situ dual process for the degradation of MTZ using three reactors in series

<table>
<tr><th>Cost of raw material in the market</th><th>Cost of oxidant used for the reactions</th></tr>
<tr><td rowspan="3">Fuller's Earth cost = 100$ ton^{-1}=0.1$ Kg^{-1}
Total cost of Fuller's Earth for manufacturing beads=0.2$
Cost of foundry sand=0$
Cost of TiO_2 used= 1$ gm^{-1}
Used TiO_2= 6gm
Total cost = 6 $
Electricity cost = 0.015 $ kwh^{-1}
Energy used by Muffle furnace for baking of beads at high temperature =3kwh
Cost of electricity=3×0.015=0.045$
Total cost for the beads=0.2+6+0.045=6.345$</td><td>Oxidant used for the reaction-H_2O_2
Usage of H_2O_2 = 15 mL for 5L
For 80 runs= 15×80=1200 mL =1.2 L
Cost of H_2O_2= 5$ (0.5 L)$^{-1}$
Total cost of H_2O_2 used= 12 $</td></tr>
<tr><td>Cost of the Reactor and other materials</td></tr>
<tr><td>Cost of the reactor = 14 $
Total cost of pipe fittings = 2$
Net total cost of fabrication of reactors = 44$</td></tr>
<tr><th>Cost of reactions</th><th>Pumping cost</th></tr>
<tr><td>Cost of sunlight=0$
Total reactions =80
Volume of water used in each reaction = 8L</td><td>Cost of pumping the solution = Energy consumed × cost of electricity
Energy consumed by pump = 0.11 KWh
Energy per Kg removal = 0.343 energy</td></tr>
</table>

Volume for 80 reactions= 640L=0.64m^3 Removal of MTZ= 80% (approximately) Initial concentration = 25mg L^{-1} Final concentration = 5 mg L^{-1} Total removal cost = 0.2469$ Kg^{-1}	$Volume^{-1}$ Total cost for removal = 0.262 $
Total cost: Total cost of raw materials used = Beads manufacturing + H_2O_2 used=18.345$ Cost for reactors fabrication = 44$ Cost for removal of MTZ= 0.24$ Total cost for whole operation = 62.585$ for 80 cycles Thus, cost of 1 reaction (for handling 8L solution) = 0.78 $	

Table 4.10: The scale up cost analysis for the reactor in series

Scaling up cost:
Utilizing the sixth –tenth rule of approximating costs $$\mathrm{COST_B} = \mathrm{COST_A}(\frac{\mathrm{SIZE_B}}{\mathrm{SIZE_A}})^{\mathrm{N}}$$ Scale up cost of raw material = 400.34 $ Scale up cost pumping = 32.98 $ Scale up cost of Reactions = 15.142 $ Scale up cost of oxidant= 757.08 $ Scale up cost of reactors and fittings = 4824.50 $ Total cost = 6030.04 $ (for 80 reactions handling 8000L Volume) Cost =0.075 $ L^{-1}(for 1 reaction)

4.4. DEGRADATION OF PHZ USING REACTORS IN SERIES

The fixed bed reactor in series (approaching PFR) studies has been further extended to degrade PHZ in once through mode using the hybrid technique of photocatalysis and photo-Fenton. The study involves the hydrodynamics analysis along with the optimization of various operating conditions for the degradation of PHZ.

4.4.1. REACTOR HYDRODYNAMICS

For the investigation of the flow patterns, mixing inside the reactor residence time distribution (RTD) study is carried out. Generally RTD stands for the average time a particle resides inside the reactor. Exit age distribution (E(t)) was used for studying the distribution of the fluid elements inside the reactor. RTD studies were conducted using LiCl as the tracer and recording the conditions after regular time intervals. A narrow RTD bell curve shows behavior approaching ideal plug and in contrast broader one deviates from the ideality. Empirical models were suggested for the representation of the behavior of reactors.Modeling of RTD at various conditions helped in optimizing the conditions for further studies. The flow pattern of the actual reactor was examined using the basic models of axial dispersion and stirred tank reactor model (Figure 4.42, 4.43).

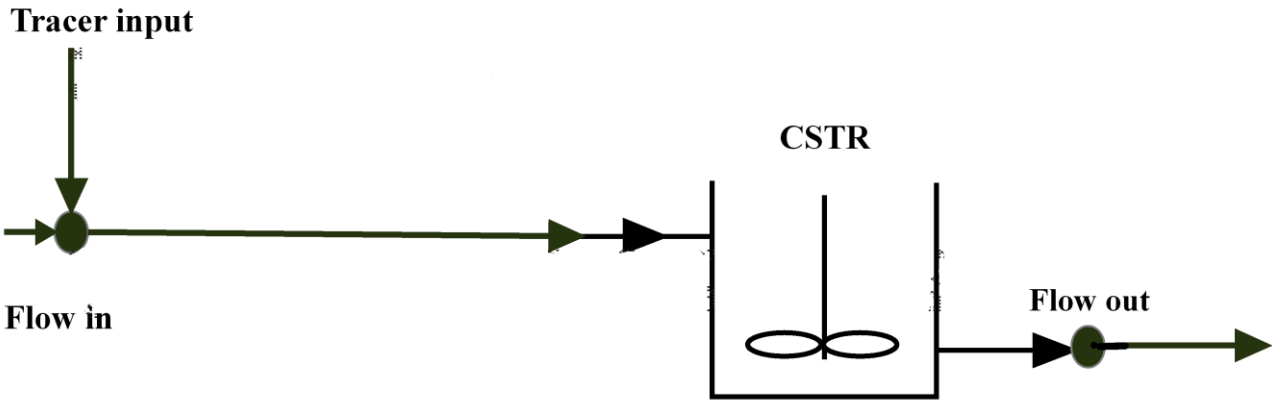

Figure 4.42: Conceptualization stirred tank model for the reactors in series

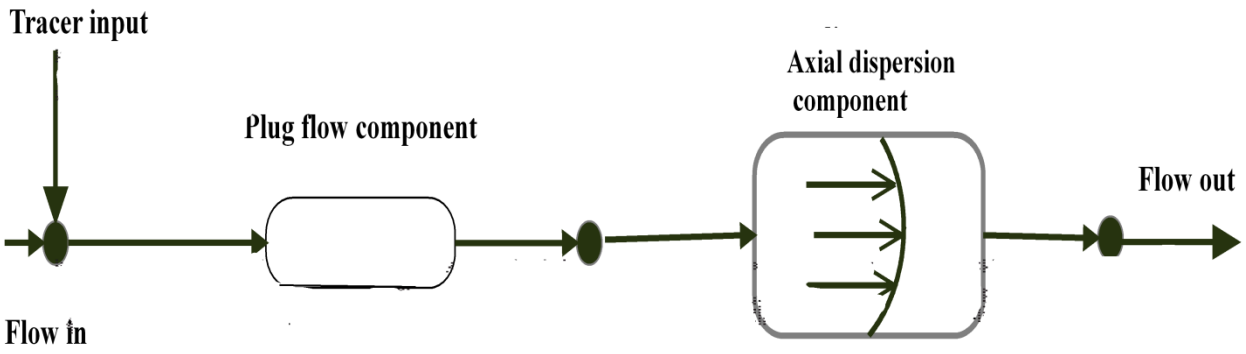

Figure 4.43: Conceptualization axial dispersion model for the reactors in series

RTD with pulse input was used to optimize the various configurations of the set up and the conditions of the experiments. In this study the reactors were optimized for behavior approaching to plug flow. PFR being more efficient than the MFR have been mostly preferred, as the rate of reaction is increased and providing high conversions. The prepared model consisted of a plug flow component and axial dispersion component attached in series. The structure of the axial dispersion model fitted closely with the flow patterns of the reactors.

For carrying out the experimentation for RTD analysis the reactors were varied from 1-3, flow rate was varied from 5.0±1.0-15.0±1.0 L h^{-1} and the covered surface area was varied from 25 to 100%. The Figure 4.44 represented the experimental E(t) curves along with the modeled CSTR and PFR E(t) curves for the various reactor configurations and parameters optimizations. Initially after noting down the concentration of LiCl the injection in the form of pulse input was given and the concentration was noted down at the outlet of the reactors. The concentration of LiCl (S) vs time (t) were convered into E(t) vs time (t) using the eq 4.19.

$$\mathrm{E(t)} = \frac{\mathrm{S(t)}}{\int_0^\infty \mathrm{S(t)dt}} \qquad (4.19)$$

Where, S(t): concentration of tracer at time t and E(t): normalized RTD curve. For calculating the mean retention time ($\bar{t}$) of the tracer inside the reactor from RTD curve, equation 4.20 was used.

$$\bar{t} = \int_0^\infty t\,E(t)dt \qquad (4.20)$$

The theoretical retention time (τ) was calculated using the equation 4.21.

$$\tau = \frac{V}{Q} \qquad (4.21)$$

Where, the V is total volume of the reactor system, Q is the flow rate of the pollutant.

The theoretical and the experimental retention time should have no difference at the normal operating conditions. If the theoretical retention time is less than the actual retention time, then it could be concluded that either the particles of the tracer might have been held back or the flow rate calculations might be rechecked. Hence, for this purpose the dead volumes (% V_d) were calculated using equation 4.22.

$$\% V_d = \left(1 - \frac{\bar{t}}{t}\right) \times 100 \qquad (4.22)$$

From the Figure 4.44a it was observed that with only one reactor, having no packing and no baffles attached, the reactor behaved mostly as the stirred tank having a long tail as in the CSTR showing some amount of dead zones present. The dead volume came out to be 76.38%. Averaged residence time inside the reactor of the particles came out to be 2.55 min with Pe as 1. The main aim of the study was to increase the residence time along with increasing Pe for the behavior to approach plug flow. After adding the packing inside the reactor (Figure 4.44b) the residence time increases to 8.5 min but Pe was 3. The dead volume percentage decreased to 15.49%. Further with the addition of baffles and beads (Figure 4.44c) the residence time increased to more than three times i.e. 28 min along with the decrease in dead volume to 0.59, confirming the more contact time of the catalyst with the pollutant. For further optimizations reactors with packing and baffles were chosen. With increasing the number of reactors the velocity profile becomes narrower confirming that there is negligible axial diffusion and approaching the PFR. With the next reactor attached (Figure 4.44d) having the same amount of packing baffles the reactors behaved as the plug flow approaching with residence time of 45 min as compared with the actual residence time of 45 min. But a tail was present at the end showing the dead zones present inside the reactor which showed 1.16% of dead zones. On addition of the third reactor (Figure 4.44e) time came upto 55 min with Pe having value high upto 85. The increased value of Pe confirms the reactor is behaving as PFR. In addition with increase in the flow rate of the pollutant (Figure 4.44f), the residence time decreased. On increasing the flow rate to 25.0±1.0 L h^{-1} residence time got almost half i.e. 30 min as compared

to 55 min. Going to the lower range i.e. at 5.0±1.0 L h^{-1} (Figure 4.44g) the residence time increased to 75 min with Pe as high as 120. Keeping the flow rate in between 5.0±1.0 L h^{-1} and 15.0±1.0 L h^{-1} could be the best option as the time was almost same and PFR was approaching. To get more accuracy in the results, more optimization in terms of packing was performed. By decreasing the packing to 25% (Figure 4.44h) of the surface area covered, and flow rate to 10.0±1.0 L h^{-1} time was almost same as that of three reactors having almost 65% area covered. But in this case the amount of catalyst reduced and the degradation of pollutant is not achieved as desired. Further on increasing the covered surface area to full i.e. 100% (Figure 4.44i) the residence time was 65 min which was close to actual residence time of 65.5 min. The Pe was very high i.e. 245 signifying the perfect plug flow. Confirming the best optimized conditions, for the degradation experiments. At these conditions TIS model was also applied and time of 65.5 min and N (number of reactors) corresponding to 200 was achieved.

Taking RTD analysis into consideration, other optimization analysis was carried out based upon increasing the removal of PHZ from the solution.

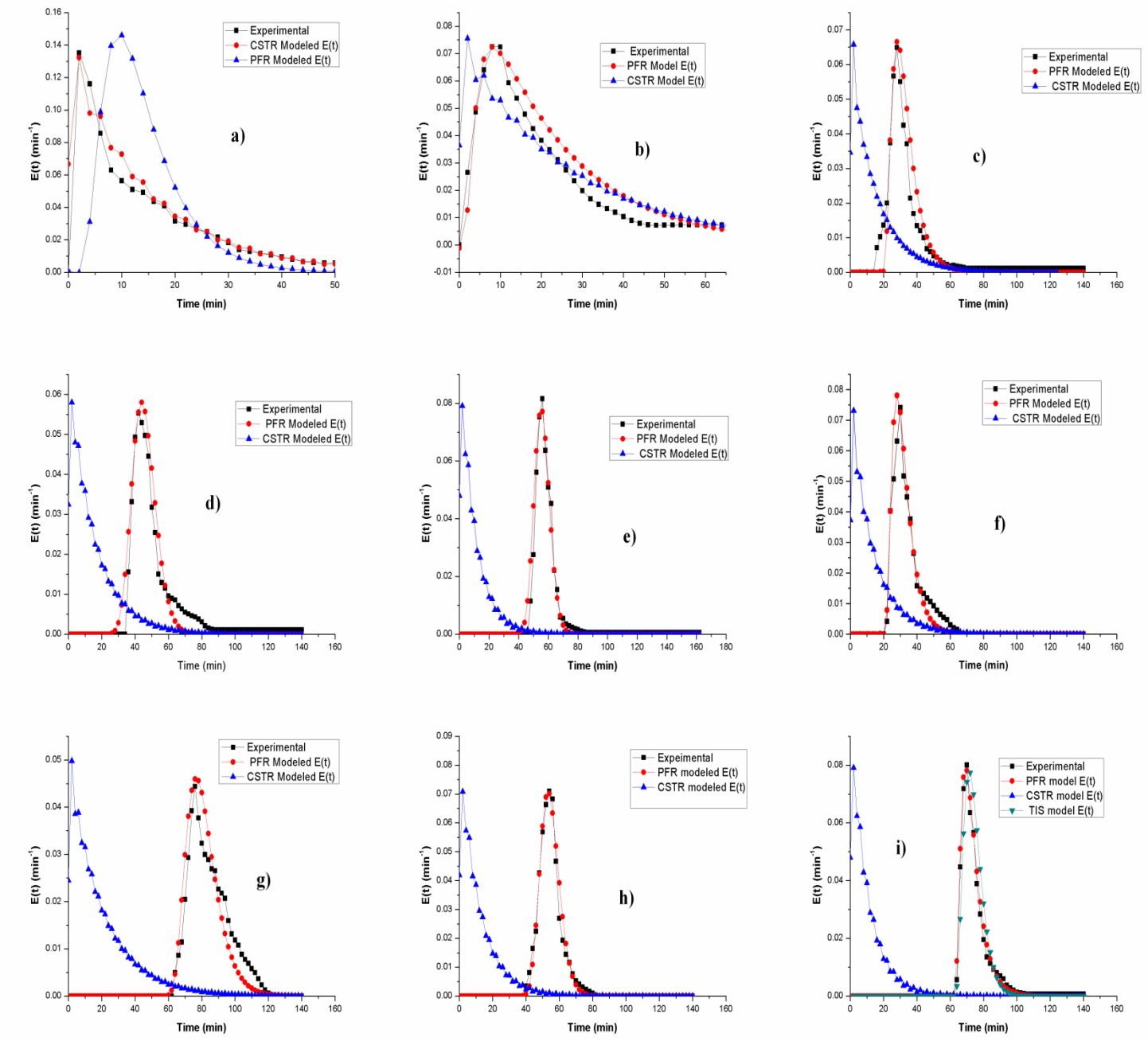

Figure 4.44: RTD curve analysis for a) having only one reactor, b) one reactor with baffles, c) one reactor with beads and baffles, d) two reactors in series, e) three reactors in series, f) three reactors in series with flow rate 25L h^{-1}, g) three reactors in series with flow rate 5L h^{-1}, h) three reactors in series with 25% area covered with the beads, i) three reactors in series with 100% area covered by the beads

4.4.2. COMPARISON OF PRELIMINARY RESULTS

The evaluation of the performance of hybrid process as well as the reactor was initially carried out using PHZ as the model pollutant. For carrying out these studies single baffled reactor with packing of composite beads was used and in recirculation. The preliminary studies revealed that PHZ did not adsorb on the catalyst surface leading to the blockage of the active sites. Photolysis also contributed negligible degradation. Photocatalysis confirmed approximately 12% of the removal of PHZ after 3 h. Whereas, photo-Fenton leaded to 15% of the removal after 3 h. The leaching of iron was also checked in terms of total, Fe(II) and Fe(III) (Figure 4.45). The degradation increased substantially when both the processes of photo-Fenton and photocatalysis were mixed, i.e. the hybrid process leaded to 30% removal in 3 h. Hence, hybrid process was chosen for all further optimizations.

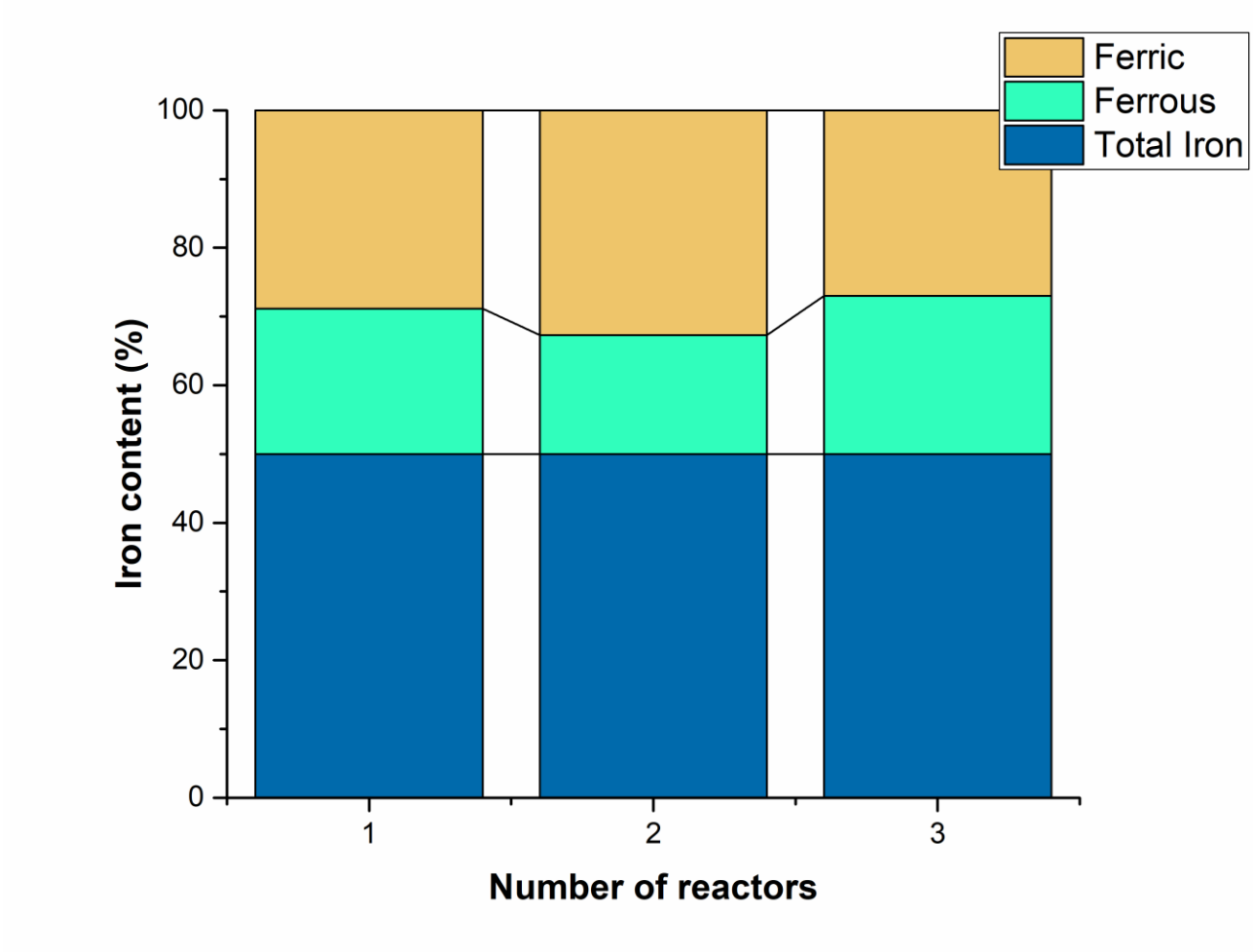

Figure 4.45: The amount of iron leached from the beads

4.4.3. PARAMETRIC CONDITIONS OPTIMIZATION

In order to determine the optimum conditions for the % degradation of PHZ BBD under RSM was used. The range of the operational parameters used were H_2O_2 dose (96-288 mg L^{-1}), number of reactors (1-3), flow rate (5.0-15.0 L h^{-1}) and % surface area covered by beads (25-100%) and response of % degradation of PHZ. The total set of 29 experiments was suggested by BBD as shown in Table 4.11. The value of R^2 obtained was 0.93 which showed good relation between predicted and observed values. The adequate precision ratio of 7.665 indicated the adequacy in signal as the ratio's value greater than 4 indicates the desirable results and the model could be used to navigate the design space.

For the analysis of the effect of the individual parameter as well as the interaction between the various parameters detailed analysis of variance (ANOVA) was studied (Figure 4.12). Low value of p and high values of F leads to the significant results. Model F value of 14.97 and p value < 0.0001 represented the model to be significant. The lack of fit also determines the model to fit. Non significance nature of the lack of fit makes the model good for fitting. Lack of fit value of 1.16 confirmed the non significance nature. The lack of fit value is derived from noise by chance as only 48% ratio. The study has number of reactors, % surface area covered, and the second order effect of oxidant dose as the highly significant variables. Wheras, the flow rate and the second order effect of number of reactors were the significant variables.

Table 4.11: The set of matrix designed by BBD for the degradation of PHZ using reactors in series

S.No	No. of reactors	% Surface area covered	H_2O_2 Dose (mg L^{-1})	Flow rate (L h^{-1})	% degradation
1	3	100.00	192	15	45
2	2	62.50	192	15	37
3	1	62.50	96	15	19.6
4	2	62.50	288	5	23.4
5	1	62.50	288	15	6.5
6	2	25.00	192	5	15.6
7	2	25.00	96	15	7.1
8	3	62.50	96	15	24.5
9	2	25.00	288	15	9.1
10	2	100.00	192	5	35.67
11	2	62.50	288	25	15.5
12	2	25.00	192	25	5.7
13	2	100.00	288	15	18.5
14	3	25.00	192	15	10.2
15	2	62.50	192	15	32
16	2	62.50	96	25	16.7
17	2	62.50	192	15	34
18	2	62.50	192	15	28
19	2	100.00	96	15	18
20	1	25.00	192	15	4
21	2	62.50	192	15	37
22	3	62.50	192	5	40.33
23	1	62.50	192	25	8
24	2	62.50	96	5	25.4
25	2	100.00	192	25	23.1
26	1	62.50	192	5	19.65
27	3	62.50	288	15	28
28	1	100.00	192	15	18.2
29	3	62.50	192	25	25

Table 4.12: The variance analysis for % degradation of PHZ for reactors in series

Source	Sum of Squares	DF	Mean Square	F Value	Prob > F	
Model	3341.71	14	238.69	14.97	< 0.0001	significant
No of reactors	785.38	1	785.38	49.26	< 0.0001	highly significant
% Surface Area covered	949.99	1	949.99	59.59	< 0.0001	highly significant
H_2O_2 dose	8.84	1	8.84	0.55	0.4688	
Flow rate	363.55	1	363.55	22.80	0.0003	
(No of reactors)^2	159.50	1	159.50	10.00	0.0069	
(% Surface area covered)^2	624.23	1	624.23	39.16	< 0.0001	highly significant
(H_2O_2 dose)^2	590.81	1	590.81	37.06	< 0.0001	highly significant
(Flow rate)^2	121.33	1	121.33	7.61	0.0154	
No of reactors×% Surface Area covered	106.09	1	106.09	6.65	0.0218	
No of reactors× H_2O_2 dose	68.89	1	68.89	4.32	0.0565	
No of reactors× Flow rate	3.39	1	3.39	0.21	0.6520	
% Surface Area covered × H_2O_2 dose	0.56	1	0.56	0.035	0.8537	
% Surface Area covered× Flow rate	1.78	1	1.78	0.11	0.7431	
H_2O_2 dose × Flow rate	0.16	1	0.16	0.010	0.9216	
Residual	223.19	14	15.94			
Lack of Fit	165.99	10	16.60	1.16	0.4809	not significant
Pure Error	57.20	4	14.30			
Cor Total	3564.90	28				

4.4.4. RESPONSE SURFACE PLOTS AND ANALYSIS

From the quadratic model 3-D response surface plots were generated showing the interactions between the parameters and finally their influence on the degradation of the PHZ. Plots of the interaction between number of reactors, H_2O_2 dose, % surface area covered and flow rate have been studied (Figure 4.46). Closer investigation on the 3-D surface plots helped in analyzing the details about the treatment of PHZ.

As confirmed from the RTD modeling, reactors in series plays an important role in approaching plug flow as well as plays the crucial part in deciding the conversion of the pollutants. For this purpose, the reactors were varied from 1 to 3 in number for studying the reactor's effect on the concentration of PHZ. From the Figure 4.46a it was observed that after the first reactor the concentration dropped down to approximately 20 %. With further increase in the same type of reactor, the degradation increased to approximately 32%. Then after that adjoining the third reactor it was approximately 45%. There was a drop in the degradation in the 2^{nd} reactor, which might be due to the formation of intermediates in between the way which were not easily degradable. The decrease in concentration is basically due to the new catalyst beads present in each reactor and when it comes in contact with the pollutant the dual action starts to play role.

For the hybrid process to take place, the catalyst coated packing plays a crucial role. The packing composed of FE+FS with TiO_2 coating acts as the dual catalyst for this process. As FE and FS being the natural sources of iron helps in iron leaching which prompts the photo-Fenton reaction along with the layer of TiO_2 helping in the photocatalysis to take place simultaneously. Being in-situ in nature the process is synergistic in nature than both the processes taking place individually. From the Figure 4.46a and b it was noticed that with the change in surface area covered by the packing the degradation changes. The exposed surface area i.e. the area covered by the packing beads was varied from 25 to 100% (Figure 4.46a). With the increase in packing from 25 to approximately 50 % the rate of degradation increased at the faster pace i.e. from 6 to 25% approx (Figure 4.46a). This is basically due to the role played by the active sites present on the surface of the catalyst along with the presence of the

leached iron content in the solution leading to increased degradation. The basic reason could also be the rate limiting step as described in equation 4.23.

$$Fe^{2+} + H_2O_2 + H^+ \rightarrow Fe^{3+} + \bullet OH + H_2O \quad (4.23)$$

$$e^- + Fe(III) \rightarrow Fe(II) \quad (4.24)$$

In the presence of TiO_2, the Fe(III) ions starts getting converted into Fe(II) (equation 4.24) and the major disadvantage of photocatalysis is solved in this hybrid effect with increased efficiency of photocatalysis process also. On further increasing the area covered upto approx 80% the degradation increased but not at the same faster rate. But on further increasing the catalyst packing the degradation begin to fall down. The reason could be the blockage of active sites with the pollutant along with the entrapment of the PHZ in the void spaces leading to the loss in efficiency. Also the increased concentration of iron could also lead to the scavenging effect on the degradation efficiency. Hence for the optimization surface area covered upto 80% was chosen.

Hydrogen peroxide (H_2O_2) being an oxidant, plays important role in both the processes i.e. in photocatalysis and in photo-Fenton simultaneously by the generation of •OH. Being electron acceptor in nature, helps in promoting the rate of reaction. For this study the dose of H_2O_2 was varied from 96-288 mg L^{-1}. From the Figure 4.46c it was observed that with increasing the H_2O_2 dose upto 195 mg L^{-1} the degradation increased to approximately 45%. This was basically due to the generation of •OH as seen from the equation 4.25.

$$H_2O_2 + \cdot O_2 \rightarrow \bullet OH + OH^- + O_2 \quad (4.25)$$

On further increasing the dose of H_2O_2, the production of less penetrative $HO_2^\bullet$ radicals was formed (equation 4.26) which reacted with the Fe^{3+} leached out of the bead and form Fe^{2+} (equation 4.27) helping in the photo-Fenton reactions to take place.

$$HO^\bullet + H_2O_2 \rightarrow HO_2^\bullet + H_2O \quad (4.26)$$

$$HO_2^\bullet + Fe^{3+} \rightarrow Fe^{2+} + O_2 \quad (4.27)$$

At the same time, surface active TiO_2 executes the production of superoxide radicals leading to the reaction with H_2O_2 to form radicals as well. But further increasing the dose of H_2O_2 the degradation falls. This was basically due to scavenging effect of H_2O_2 and the formation of hydroperoxyl radicals. These radicals have the lower oxidation capability leading to slower rate of removal.

For executing the process at the large scale, the flow rate of the pollutant plays an important role. With the flow rate variation, turbulence level as well as the dissolved oxygen concentration varies which helps in degradation. With the increased flow rate the retention time decreases as was confirmed from the RTD studies. Hence in this study flow rate was varied from 5.0±1 to 25.0±1 L h^{-1}. As expected it was observed that with decreasing the flow rate the retention time increased and the degradation increases. At very high flow rates i.e. above 20.0±1.0 L h^{-1} the degradation was falling at a greater pace. This is basically due to the pollutant not getting enough time to get contact with the catalyst coated beads. The degradation was almost similar at 5.0±1.0 and 10.0±1.0 L h^{-1}. For the economic point of view and keeping in mind the RTD analysis 10.0±1.0 L h^{-1} was chosen as the central point.

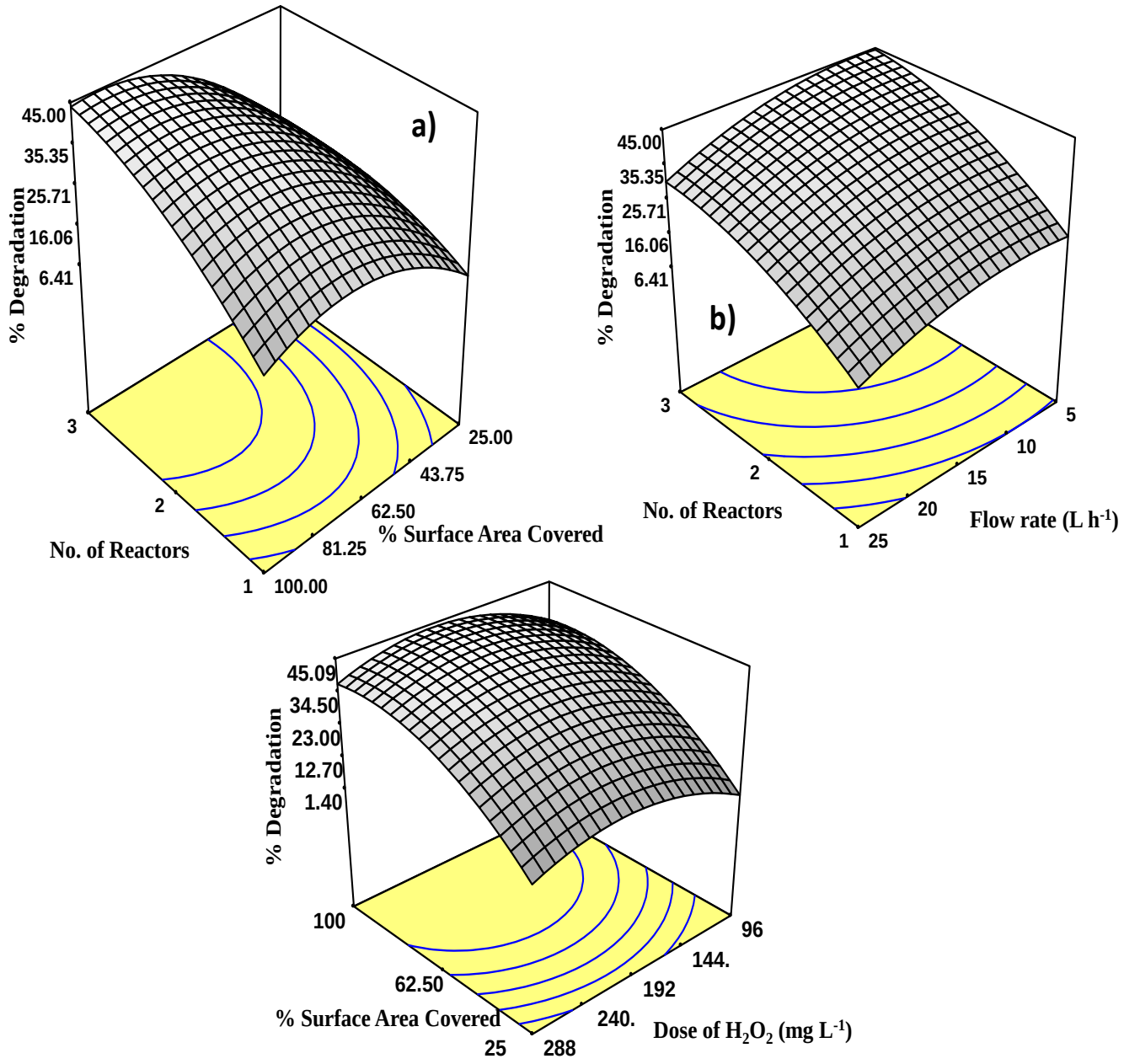

Figure4.46: a) The surface plots showing the interaction between the number of reactors and the surface area covered by the beads on % degradation of PHZ, b) The surface plots showing the interaction between the number of reactors and the rate on % degradation of PHZ, c) Surface plots showing the interaction between the surface area covered by the beads and the dose of oxidant on % degradation of PHZ

4.4.5. SYNERGISTIC EFFECT

For the evaluation of the coupling effect generated by the photocatalysis and photo-Fenton process, synergistic effect is calculated. For the calculation of synergy, % degradation data of the individual process i.e. photocatalysis and photo-Fenton alone along with the hybrid effect data were used (Babu et al., 2019). The synergy is computed using equation 3.8. Synergy of 1.67 folds was observed in the case of hybrid process as compared to the individual processes.

The basic reason for the synergistic effect in hybrid process is the generation of considerable amount of •OH reduced from both the processes. Likewise the hindrance caused by the individual processes are also solved, as the electron which recombines with the hole slowing down the process reacts with the Fe(III) ions to produce Fe(II) which proceeds the Fenton process and provides synergy. This was reaffirmed using the fluorescence spectroscopy (Figure 4.3).

4.4.6. REUSABILITY OF THE CATALYST

For the utilization of the dual effect at the industrial scale recyclability of the same catalyst coated beads is a great concern. The main confront in the process was to maintain the activity of the TiO_2 along with the adequate iron leaching for the hybrid process to take place. The major concern added to the durability is the stability of catalyst in the flow conditions. For this purpose the beads were recycled for over 200 recycles (Figure 4.47). The activity along with the iron leaching (Figure 4.48) was maintained even after these many recycles. The extended recyclability of the catalyst helps in opening new channels for the applications in industries.

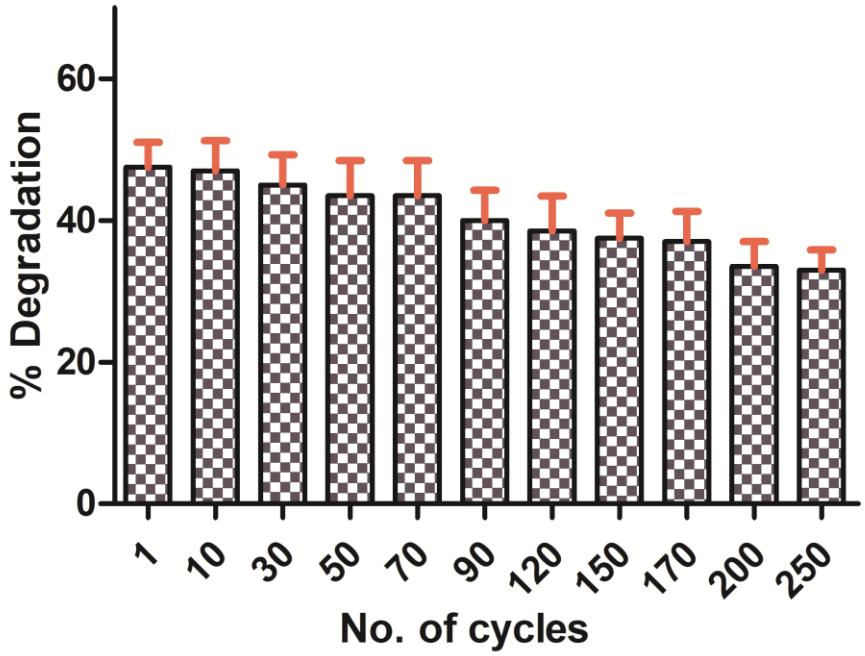

Figure 4.47: The recyclability of the composite beads

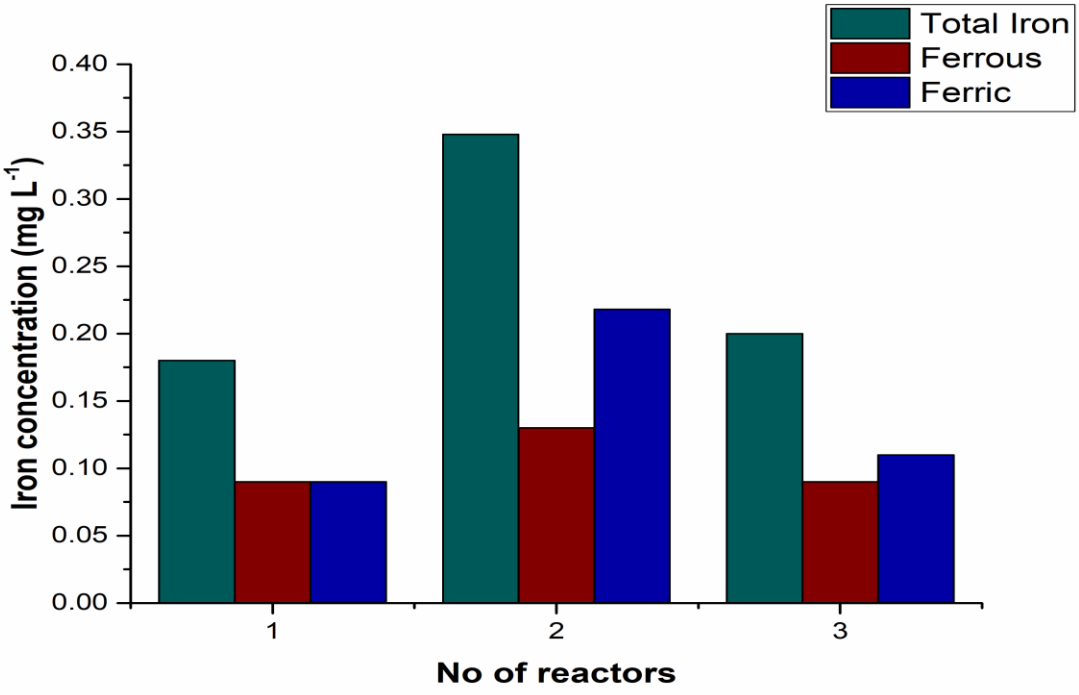

Figure 4.48: The content of iron leached even after 200 cycles

4.4.7. THEORATICALLY PFR APPROACHING REACTOR

As confirmed from the RTD modeling, the reactors in series approached ideal plug flow. For most of the cases theoretical PFR has chosen to be the best reactor among others for maximizing the conversion. Ideally the plug flow behaves well at low flow rates i.e. at laminar ranges of the flow. Ideally approaching the PFR is difficult to approach due to various constraints of mass transfer limitations, temperature control variations and film diffusion resistance. Hence to overcome such limitations hybrid effect was evaluated using reactors in series (equations 4.28-4.32).

$$\frac{V}{F_{Z0}} = \int_0^{X_Z} \frac{dx_Z}{-r_Z} \qquad (4.28)$$

$$\frac{V}{\nu_0} = C_{Z0} \int_0^{X_Z} \frac{dX_Z}{-r_Z} \qquad (4.29)$$

As in this case the first order reaction is being followed so,

$$-r_Z = kC_Z^1 \qquad (4.30)$$

$$X_Z = \frac{(C_{Z0} - C_Z)}{C_Z} \qquad (4.31)$$

And for 1st order, $k\tau = \frac{X_Z}{1-X_Z}$

$$\frac{V}{\nu_0} = \frac{1}{k} \int_0^{X_Z} \frac{dx_Z}{1-X_Z} \qquad (4.32)$$

Where the reactor's volume is depicted by V in L, volumetric flow rate by $\boldsymbol{\nu}_0$ (L min^{-1}) molar flow rate by F_{Z0} (moles min^{-1}), C_Z= final concentration (mg L^{-1}), C_{ZO}= initial concentration (mg L^{-1}), X_Z = conversion, r_Z= reaction rate (mg $L^{-1}min^{-1}$), k = rate constant ((mg $L^{-1})^{-1}min^{-1}$).

Using equation 4.32, by substituting optimized values of 10 L of the total volume, 10 L $h^{-1}$of the flow rate and the k value of 5×10^{-3} min^{-1}, 38 % of conversion was obtained. The actual trial results showed 42 % of conversion at these optimized conditions. There was nearly

8 % of error in between experimental as well as theoretical results, which is due to performance errors or due to some other limitations.

4.4.8. CHARACTERIZATION OF THE COMPOSITE

4.4.8.a. X-RAY DIFFRACTION

The crystalline nature of the prepared samples was confirmed using XRD. The results of the prepared Fe-TiO_2 composite as well as recycled composite are depicted in Figure 4.49. The peaks of the basic nature of the TiO_2 i.e. anatase and rutile phase of TiO_2 were confirmed from the analysis. Additionally the peaks appearing also corresponded to the presence of the iron oxides. Moreover these peaks are still present in the recycled composite indicating that there were no deformations in the catalyst even after 200 recycles. The presence of both Fe and TiO_2 confirms the hybrid process to take place at same place and same time. The XRD also confirms that the Fe gets successfully introduced into the TiO_2 structure for the process to take place.

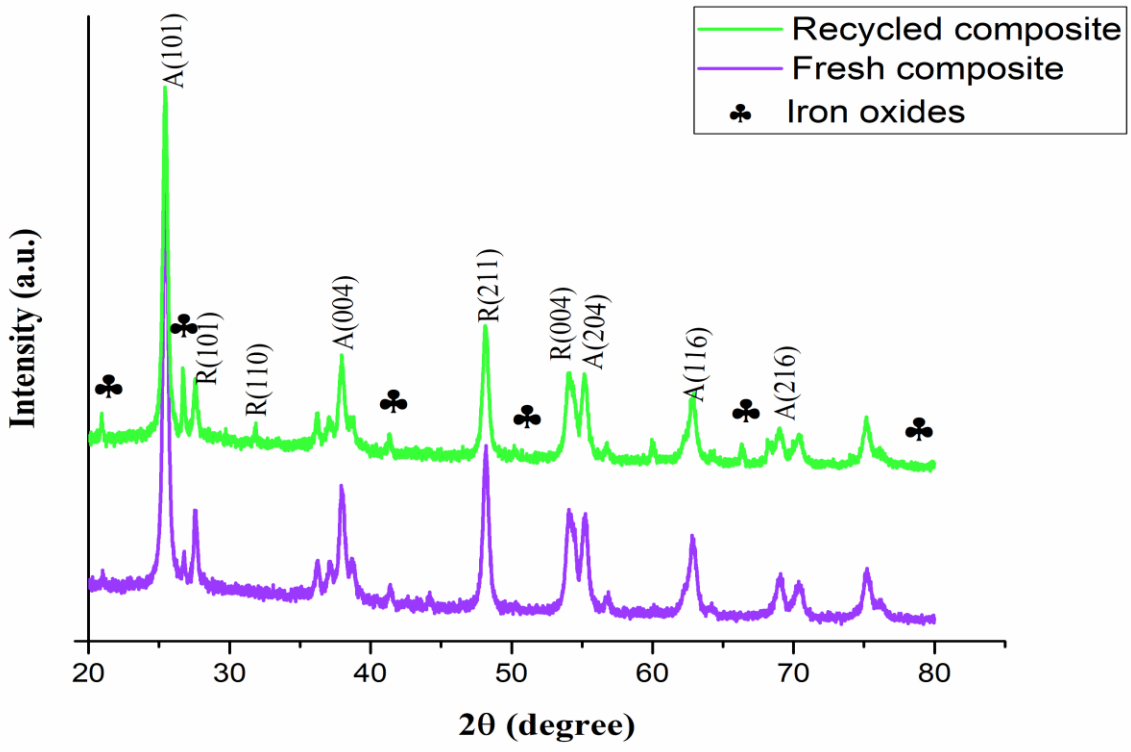

Figure 4.49: The X ray diffraction of the fresh as well as recycled composite

4.4.8.b. FTIR ANALYSIS

Figure 4.50 shows the FTIR spectra of the fresh and recycled composite. In both the samples the peak at 720 cm^{-1} corresponded to the presence of Ti-0-Ti bond. The broad band peaks obtained at 3200-3600 cm^{-1} corresponded to the H_2O molecules which get adsorbed in the catalyst. Peaks were also observed from 1000-1500 cm^{-1} due to the presence of Fe in the composite. The characteristic peaks of Si-O were also observed leading to the broadening of bond between Ti-O-Si.

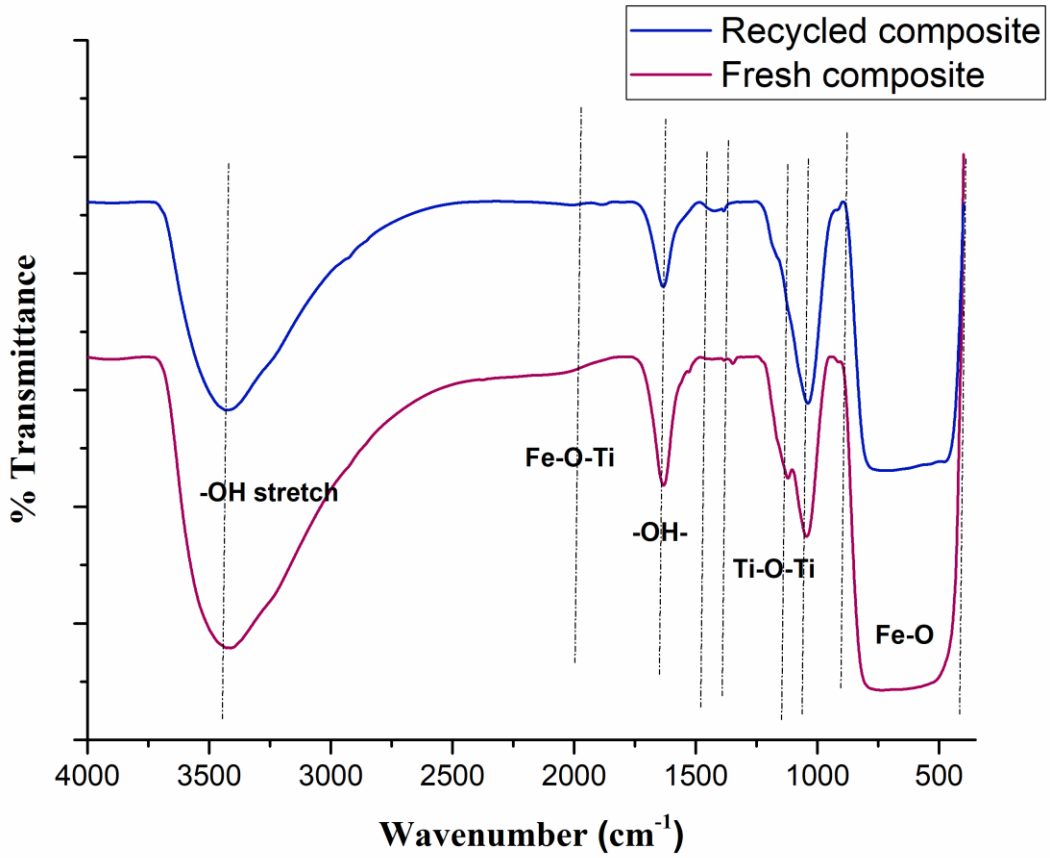

Figure 4.50: IR spectra analysis of the fresh and recycled composite

4.4.8.c. SEM-EDS ANALYSIS

For the surface morphology analysis of the packing made up of composite beads SEM was performed (Figure 4.51). The analysis of the fresh and recycled composite showed that the surface was evenly uniform without much cracks confirming the coating to be proper and

also after recycles the coating did not waved off as the surface was still uniform. The EDS analysis confirmed the presence of Ti, Fe and O elements. This further confirms the hybrid process i.e. photo-Fenton and photocatalysis to take place at the same time. Even in the recycled composite elements including Ti, Fe, and O were present. Other elements including AL, Si, Mg were also observed due to the presence of FE+FS beads which is a type of aluminum silicate.

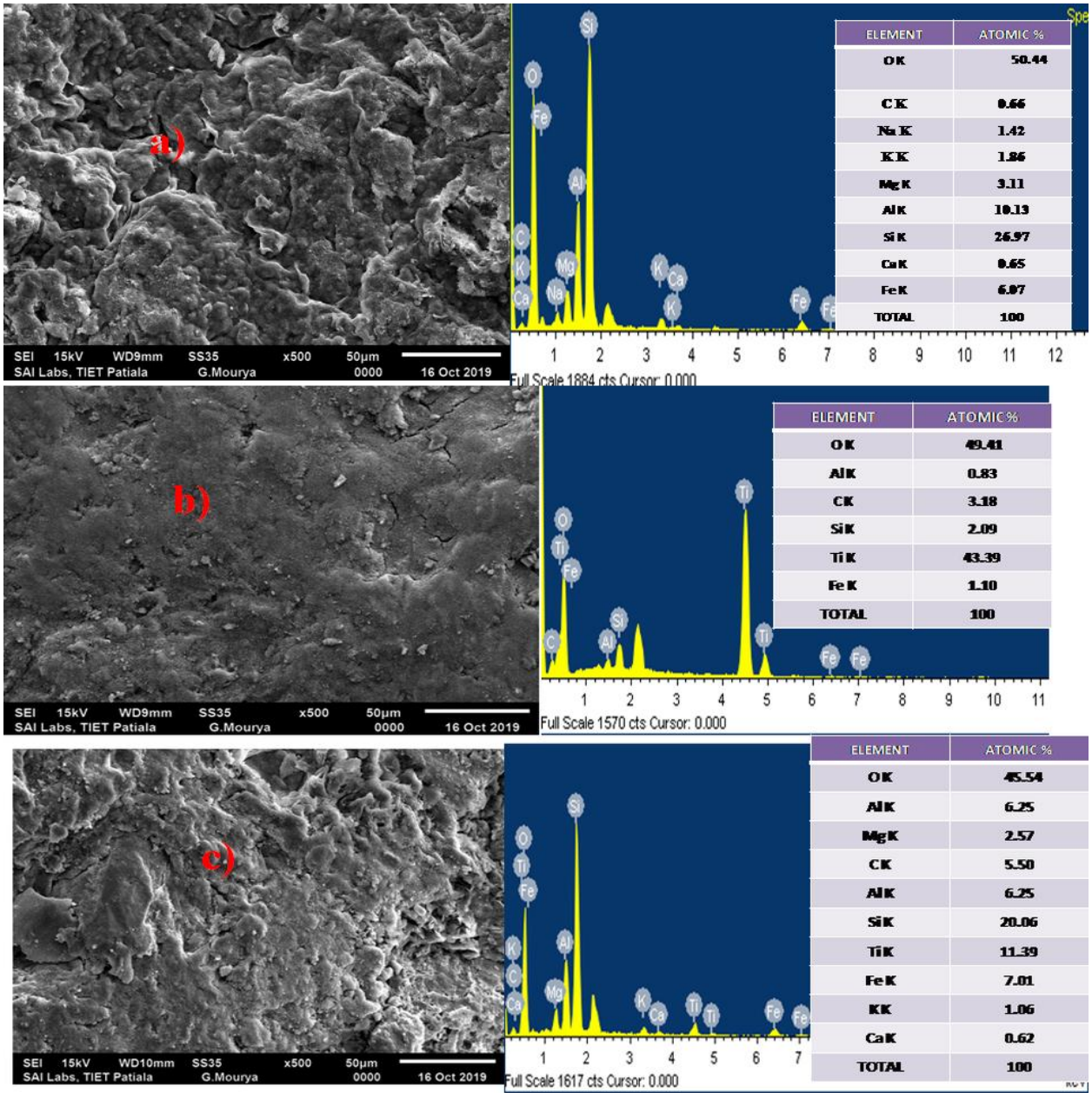

Figure 4.51: Surface morphology and the EDS analysis of the a) uncoated b) coated c) recycled bead

4.4.8.d. RAMAN SPECTROSCOPY

For the correlation between vibrational as well as structure of material, properties and composition raman spectroscopy plays an important role. The effect of concentration of Fe could be evaluated from the raman spectra as shown in Figure 4.52. The vibration modes existing in the range 210-350 cm^{-1} are basically due to the presence of Fe oxides which are not present in the spectra of TiO_2.The spectra for the fresh composite shifted upwards which further confirms the presence of Fe in the composite. Further from the analysis it was also seen that the basic peaks occurring in the P25-TiO_2 were also observed in the fresh and recycled composite.

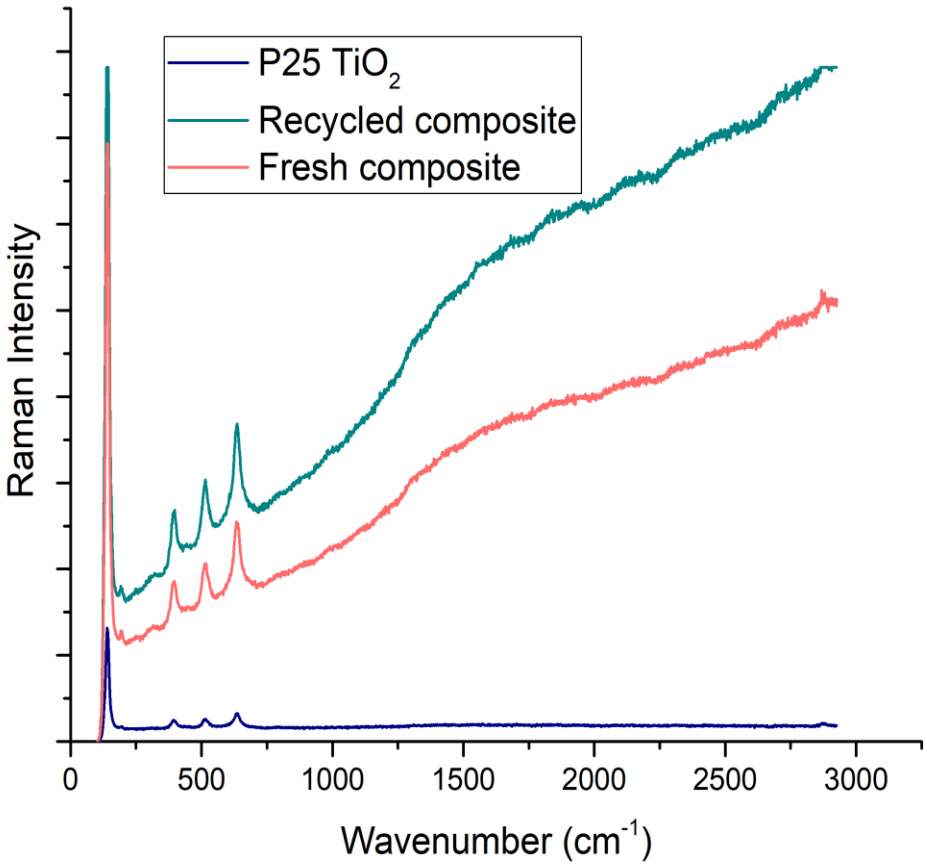

Figure 4.52: Raman analysis of the prepared composite

4.4.8.e. UV-DRS

Diffuse reflectance spectroscopy was used to determine the electron band structures of the prepared composite (Figure 4.53). The band gap energies obtained for the TiO_2, fresh composite and recycled composite were 3.14 eV, 3.01 eV, 2.87 eV respectively. The composite formed of Fe-TiO_2 leads to the reduction in the band gap energies. The decrease in the band gap shows the shift towards the visible region. Fe^{3+} metal ions have more valence electrons than Ti^{4+}. Hence, could be utilized to fill the new energy level. The iron titanium oxide composites formed as depicted from the XRD analysis also helps in the reduction of band gap energy leads to the activity of composite in visible range of light.

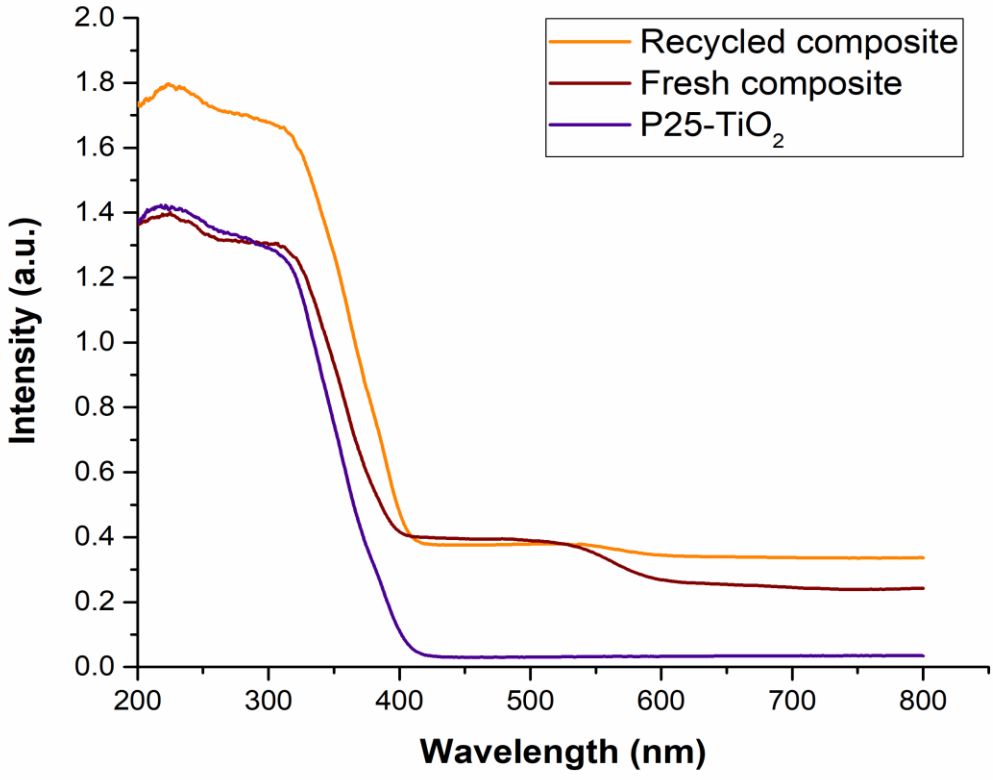

Figure 4.53: UV-DRS of the TiO_2, fresh as well as recycled composite

4.4.9. MINERALIZATION

The mineralization of PHZ was confirmed from the reduction in the TOC, and COD. Various ions including nitrates and nitrite were also examined for concluding the mineralization. The oxidation of the various nitrogen atoms present in the MTZ structure leads to the formation of these ions. The nitrate ions with time get converted into nitrites and ammonium ions (Table 4.13). Almost 35-38% reduction in COD was observed along with 28-30% reduction in TOC.

Table 4.13: The change in concentration of various ions produced during the mineralization of PHZ using reactors in series

Reactors	Concentration (mg L^{-1})		
	Nitrites (µg L^{-1})	Nitrates(mg L^{-1})	Ammonium ions(mg L^{-1})
1	2.09	3.85	3.5
2	2.87	4.79	4.3
3	3.82	4.01	5.4

For the confirmation of the by-products generated during the treatment of PHZ in once through reactors in series GCMS analysis was carried out. With the help of these, tentative pathway for the degradation of PHZ was predicted (Figure 4.54). The hydroxylation of PHZ leads to the formation of 1,2-dihydro-3-hydroxy-1-(4-hydroxyphenyl)-2-methylpyrazol-5-one. Then the formation of 4-(2H-pyrazol-1(5H)-yl) phenol takes place on the dehydroxylation of the compound. Further the fragmentation of 4-(2H-pyrazol-1(5H)-yl)phenol leads to the formation of 1-propylhydrazine and phenol. And 1-propylhydrazine might lead to the formation of propane. The Benzene ring cleavage helps in the formation of buta-1,3-diene. Further it can be concluded that the complex molecule of PHZ gets decomposed into linear and simple compounds confirming the in-situ dual effect to take place.

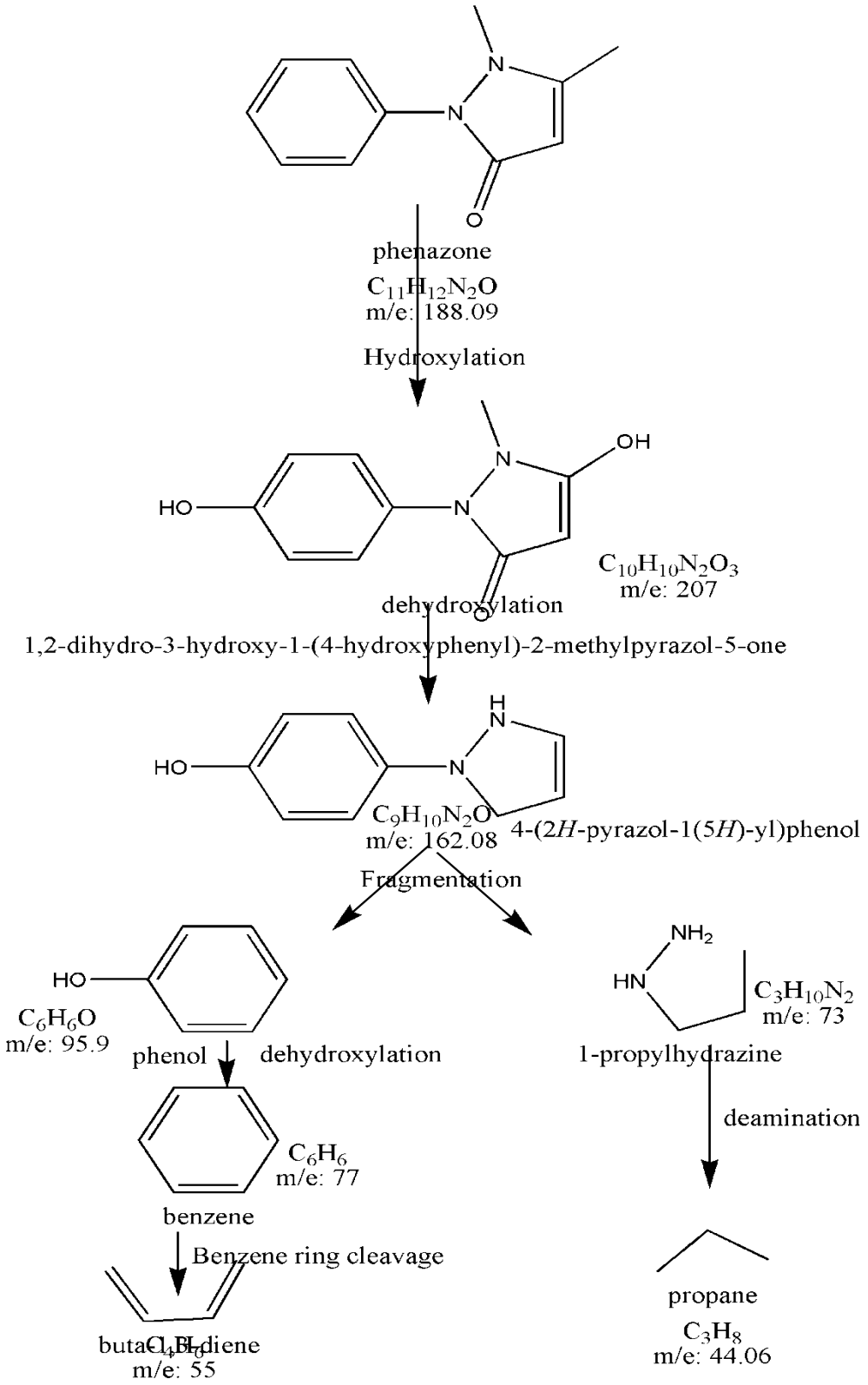

Figure 4.54: Probable expected pathway for the degradation of PHZ using reactor in series

4.4.10. COST AND ECONOMICS EVALUATIONS

The industrial applications of any process depend upon the economic analysis making it an important part. The cost of the process depends upon the results obtained from the treatment of wastewater along with the technology applied. The scale-up studies are an important part of the study as the interface between prototype and the model is created which is performed utilizing the scale-up factors. Table 4.14 presents the approximate cost/economics analysis involved for the treatment of target waste water.

Table 4.14: Economic analysis for the complete process of degradation of PHZ utilizing reactors in series

Capital Cost	**Electricity cost**
Cost of Reactor fabrication= 45$ Buffering of tank =2$ The cost of fittings and piping= 10$ Any pre treatment required = 3$ Total cost involved in fabrication = 60 $	Electricity cost = 0.011 $ kwh^{-1} Cost for baking the beads = 2×.011=.022 $ kwh^{-1}
Catalyst and raw material	**Cost of reactions**
Cost involved for catalyst Raw material cost i.e. fuller's earth =0.1$ Kg^{-1}= 0.5 $ Cost of foundry sand = 0$ Cost of TiO_2 catalyst = 5$$gm^{-1}$ Cost for beads raw material =5.5 $	Cost of UV light involved =0$ Cost of reduction of PHZ = 1.5$

Cost of oxidant involved	**Cost of pumping the wastewater**
H_2O_2 usage= 10 mL for 10L For 200 runs= 10×200=2L Cost of H_2O_2= 3$ $(0.5\ L)^{-1}$ Total cost of H_2O_2 used= 12 $	Cost of pumping the solution = Energy consumed × cost of electricity Total cost for removal = 0.015 $
Other cost involved Installing and labor charges= 5$ Installation charges =2$	Various controls involved = 1$ Various other costs = 7$ Contingency cost = 2$
Total cost Overall Total cost involved = 94.5$ for 10 L and 200 reactions Treatment cost/ L = 0.047$	
Scale up cost analysis (10,000L) Scale up cost of raw material = 347 $ Scale up cost pumping = 6.6 $ Scale up cost of Reactions = 94$ Scale up cost of oxidant= 757 $ Scale up cost of reactors fabrication =1072 $ Other miscellaneous cost and contingency = 630$ Total cost = 2906 $ (for 200 reactions handling 10,000L Volume) Cost for 1 reactions = 0.00143$/L	

4.5. COMPOUND PARABOLIC CONCENTRATOR

In this section, efforts have been done to prove the efficacy of fixed-bed in-situ dual effect towards the degradation of MTZ using fixed bed CPC reactor (approaching PFR).The complete process has been employed in once through mode.

4.5.1. KINETIC STUDIES

For the determination of the prominence of in-situ dual effect over the individual processes, kinetic studies are required to follow the changes in the MTZ concentration before and after degradation. The removal of the MTZ followed 2nd order reaction kinetics as studied according to the equation 4.33:

$$\frac{1}{C} - \frac{1}{C_0} = kt \qquad (4.33)$$

Where, k is the 2nd order rate constant (L mg^{-1} min^{-1}). From the kinetics of 1st order and 2nd order it was observed that the degradation data did not fit well in the first order whereas, best fit was observed in case of the 2nd order. This is basically due to the vast and simultaneous production of •OH from both the processes of photocatalysis and photo-Fenton in the initial phase of reaction. This can hinder the real time analysis of the appropriate kinetics rate, but with the passage of time the stabilized products are formed and the kinetics start following specified kinetics. In this study, the degradation followed 2nd order kinetics before the reaction gets stabilized. Hence, in this view we have selected 2nd order kinetics.

For the comparison of the MTZ degradation in the batch reactor with the CPC reactor, the time for reaction also depends upon the intensity of UV light in the reactor. Hence, its degradation can also be expressed as equation 4.34.

$$\frac{1}{C} - \frac{1}{C_0} = kQ_{UV,N} \qquad (4.34)$$

Where k is the 2nd order rate constant (L^2 mg^{-1} kJ^{-1}) and $Q_{UV,N}$ (Kj L^{-1}) (as shown in equation 4.33) is the amount of UV energy accumulated on any surface in the same position with regard to the sun, per unit the volume of pollutant within the CPC reactor in the interval Δt (as shown in equation 4.35, 4.36)

$$Q_{UV,N} = Q_{UV,N-1} + \Delta t\, UV_{,N} \frac{A}{V} \quad (4.35)$$

$$\Delta t = t_n - t_{n-1} \quad (4.36)$$

Where A (0.04 m^2) is the total surface area illuminated, V is the reactor volume (1.74 m^3), t_n is the time for nth sample of wastewater (45 min) and UV_N is the measured average solar irradiation during the time Δt (averaged at 30 W m^2). The equation could be used for comparison with other photocatalytic experiments by combining the experimental data.

4.5.2. PRELIMINARY STUDIES

Preliminary experiments were performed including adsorption studies in dark to further confirm the predominance of synergistic effect as compared with single processes. For these studies, only two CPC reactors were connected with recirculation and accumulated energy was calculated for 45 min (equation 4.35). Preliminary investigations revealed negligible adsorption even after 1 h due to the blockage of active sites by the pollutants of wastewater. Whereas, photolysis contributed negligible degradation. The order of the degradation efficiency of MTZ of different oxidation studies observed in this study is shown as follows:

Dual > photo-Fenton> Photocatalysis > photolysis > adsorption

Photocatalysis and photo-Fenton showed only 6% and 9% degradation respectively after 1 h due to the •OH production, contributed by individual processes (Figure 4.55). For the photo-Fenton reactions, un-coated composite beads were used at acidic pH (3.5) and H_2O_2 dose of 500 mg L^{-1}(Figure 4.56). Below pH 3.5, the reduction in the degradation was attributed to the scanning of the •OH with hydrogen ions (Bahmani P, Maleki A, Ghahramani E, 2013). Also under such high acidic conditions, the present hydrogen peroxide can capture a proton and form $H_3O_2^+$.Therefore, the used hydrogen peroxide will become electrophilic causing reduction in the reactivity between hydrogen peroxide and ferrous ions (Herney-Ramirez, Lampinen, Vicente, Costa, & Madeira, 2008). For this purpose the dual effect has been optimized in further sections in continuous once through mode.

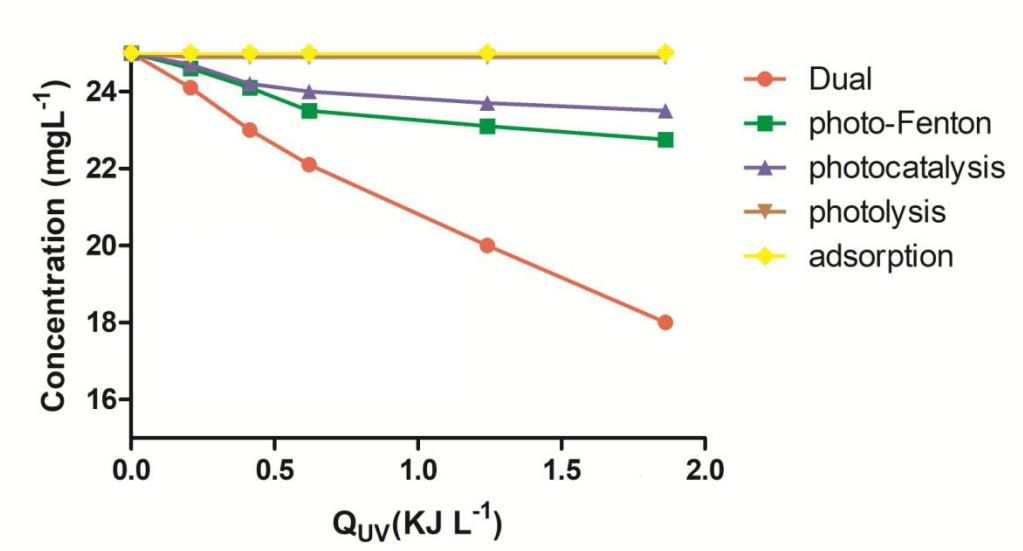

Figure 4.55: Effect of various preliminary processes on the accumulated energy (C_0=25 mg L^1, pH =3.5, covering 100% surface area)

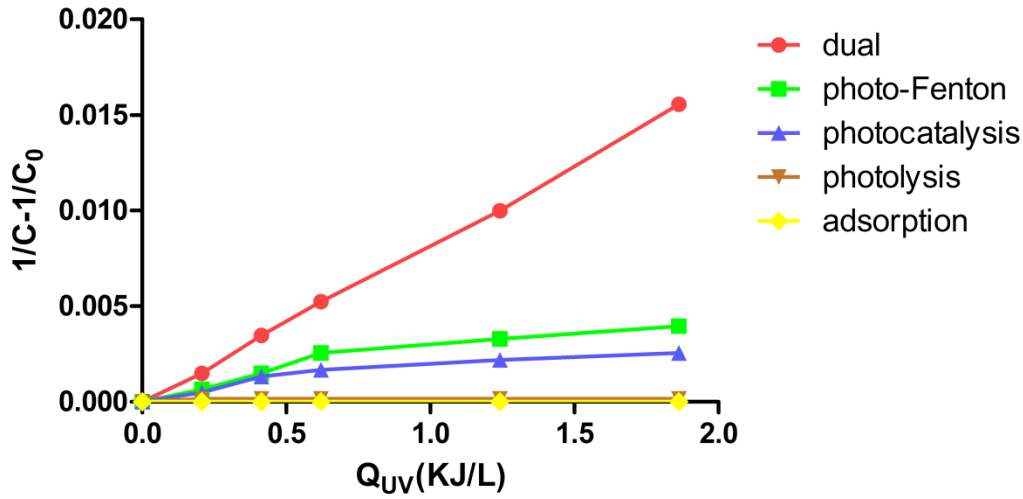

Figure 4.56: The reaction kinetics of various processes with the change in the accumulated energy (C_0=25 mg L^{-1}, pH =3.5, covering 100% surface area)

4.5.3. OPTIMIZATION OF VARIOUS INPUTS PARAMETERS AND MATHEMATICAL MODELING

BBD was employed for determining the effect of four independent parameters on the degradation of pharmaceutical drug MTZ. Accordingly 29 experiments were designed and

suggested (Table 4.15). According to the designed matrix, empirical second order polynomial equation was developed (equation 4.37). The negative and positive signs before the terms denote the opposed and encouraging effects of the parameters.

$$\%\ \text{degradation} =$$
$$-105.22310 + 3.85638 \times \text{Flow rate} + 0.97470 \times \text{Surface area covered by beads} +$$
$$0.096556 \times H_2O_2\text{dose} + 40.50278 \times \text{No. of reactors} - 0.26893 \times (\text{flow rate})^2 -$$
$$8.59259 \times 10^{-3} \times (\text{Surface area covered by beads})^2 - 1.14815 \times 10^{-4} \times$$
$$(H_2O_2\text{dose})^2 - 4.04896 \times (\text{No. of reactors})^2 - 0.029630 \times \text{flow rate} \times$$
$$\text{Surface area covered by beads} + 1.66667 \times 10^{-3} \times \text{flow rate} \times H_2O_2\text{dose} -$$
$$0.27778 \times \text{flow rate} \times \text{No. of reactor} + 3.35556 \times 10^{-4} \times$$
$$\text{Surface area covered by beads} \times H_2O_2\text{dose} + 0.050000 \times$$
$$\text{Surface area covered by beads} \times \text{No. of reactor} - 3.33333 \times 10^{-3} \times H_2O_2\text{dose} \times$$
$$\text{No. of reactor} \qquad (4.37)$$

Table 4.15: The designed set of matrix by BBD for the degradation of MTZ in CPC reactor

S.no.	Flow rate ($L\ h^{-1}$)	% Surface area covered	H_2O_2 Dose ($mg\ L^{-1}$)	No. of reactors	% degradation (Actual)	% degradation (predicted)
1	5.50	62.50	450.00	4.00	59.00	56.40
2	1.00	62.50	750.00	4.00	51.00	47.30
3	1.00	62.50	150.00	4.00	49.00	45.78
4	5.50	62.50	450.00	4.00	51.00	56.40
5	5.50	62.50	750.00	6.00	47.00	47.30
6	5.50	25.00	750.00	4.00	32.00	29.89
7	5.50	25.00	150.00	4.00	31.00	31.43
8	1.00	62.50	450.00	2.00	20.00	21.76
9	1.00	25.00	450.00	4.00	34.00	36.46
10	5.50	62.50	150.00	6.00	48.00	45.28
11	10.00	62.50	750.00	4.00	39.00	39.96
12	5.50	62.50	450.00	4.00	57.00	56.40
13	5.50	25.00	450.00	6.00	36.00	37.36
14	1.00	62.50	450.00	6.00	58.00	59.59
15	5.50	62.50	450.00	4.00	61.00	56.40
16	10.00	100.00	450.00	4.00	35.00	31.28
17	5.50	100.00	150.00	4.00	24.90	30.53
18	10.00	62.50	450.00	6.00	41.00	44.09
19	5.50	25.00	450.00	2.00	12.00	12.13
20	5.50	100.00	450.00	6.00	54.00	51.61
21	1.00	100.00	450.00	4.00	52.00	53.11
22	5.50	100.00	450.00	2.00	15.00	11.28
23	5.50	62.50	150.00	2.00	10.00	8.45
24	10.00	62.50	150.00	4.00	28.00	29.45
25	10.00	62.50	450.00	2.00	13.00	14.92
26	10.00	25.00	450.00	4.00	37.00	34.63
27	5.50	100.00	750.00	4.00	41.00	42.76
28	5.50	62.50	450.00	4.00	54.00	51.61
29	5.50	62.50	750.00	2.00	17.00	18.46

4.5.4. ANOVA

The analysis of variance (ANOVA) for the suggested model has also been studied. For the analysis of significant terms F value and p-value were important tool. Significant results

are obtained at high value of F and low value of P. Adequate precision was used for measuring the signal to noise ratio of the data. The value of ratio greater than 4 indicates the desirable results and the model could be used to navigate the design space. Model summary statistics fitted the quadratic model with high value of regression coefficient R^2. R^2 value of 0.9695 showed a good relation between predicted and adjusted R^2. The F and P value for the degradation of MTZ were shown in Table 4.16. Model F value of 31.83 is greater than 0.001 making it highly significant. The value of p being < 0.0001, i.e. < 0.05 for the model showing that there is only a 0.01% chance that a "Model F-Value" this large could occur due to noise. For testing the sufficiency of the model lack of fit value is studied. The lack of fit value is derived from noise by chance as only 58.48% ratio. The "Lack of Fit F-value" of 0.92 (Table 4.16) shows that, relative to the pure error Lack of Fit is not significant.

Table 4.16: The sequential sum of squares for the tested models for MTZ degradation using CPC reactor

Source	**Sum of Squares**	**DF**	**Sum of Square**	**F Value**	**Prob > F**	
Mean	42249.23	1	42249.23			
Linear	3895.44	4	973.86	7.88	0.0003	
2FI	274.50	6	45.75	0.31	0.9257	
Quadratic	**2483.77**	**4**	**620.94**	**41.58**	**< 0.0001**	**Suggested**
Cubic	107.77	8	13.47	0.80	0.6268	Aliased
Residual	101.30	6	16.88			
Total	49112.01	29	1693.52			

In the present study, second order effect of flow rate, number of reactors, area covered by the beads, H_2O_2 dose and the interaction between the flow rate and the area covered by beads are highly significant variables as the value of $p<0.001$ (Table 4.17). The normal plot for the degradation efficiency has also been provided in Figure 4.57a, b. The data points are close enough to the straight line confirming the analyzed assumptions to be correct. The predicted vs actual plot also confirmed the adequacy of the results as there is not much difference between the results.

Table 4.17: The variance analysis for the % degradation of MTZ for CPC

SOURCE	SUM OF SQUARES	DF	MEAN SQUARE	FVALUE	PROB > F	SIGNIFICANCE
Model	6653.71	14	475.27	31.83	< 0.0001	significant
Flow rate	420.08	1	420.08	28.13	0.0001	
Area covered	132.67	1	132.67	8.88	0.0099	
H_2O_2 dosage	108.60	1	108.60	7.27	0.0174	
Number of reactors	3234.08	1	3234.08	216.56	< 0.0001	
Flow rate^2	192.37	1	192.37	12.88	0.0030	
Area covered ^{2}	947.07	1	947.07	63.42	< 0.0001	
H_2O_2 dosage2	692.61	1	692.61	46.38	< 0.0001	
No. of reactors^2	1701.44	1	1701.44	113.93	< 0.0001	
Interaction between flow rate and area covered	100.00	1	100.00	6.70	0.0215	
Interaction between flow rateand H_2O_2 dosage	20.25	1	20.25	1.36	0.2637	
Interaction between flow rateand no. of reactors	25.00	1	25.00	1.67	0.2167	
Interaction between area covered and H_2O_2 dose	57.00	1	57.00	3.82	0.0710	
Interaction between area covered and no. of reactors	56.25	1	56.25	3.77	0.0727	
Interaction between H_2O_2 dose and no. of reactors	16.00	1	16.00	1.07	0.3182	
Residual	209.07	14	14.93			
Lack of Fit	145.87	10	14.59	0.92	0.5848	not significant
Pure Error	63.20	4	15.80			
Cor Total	6862.78	28				

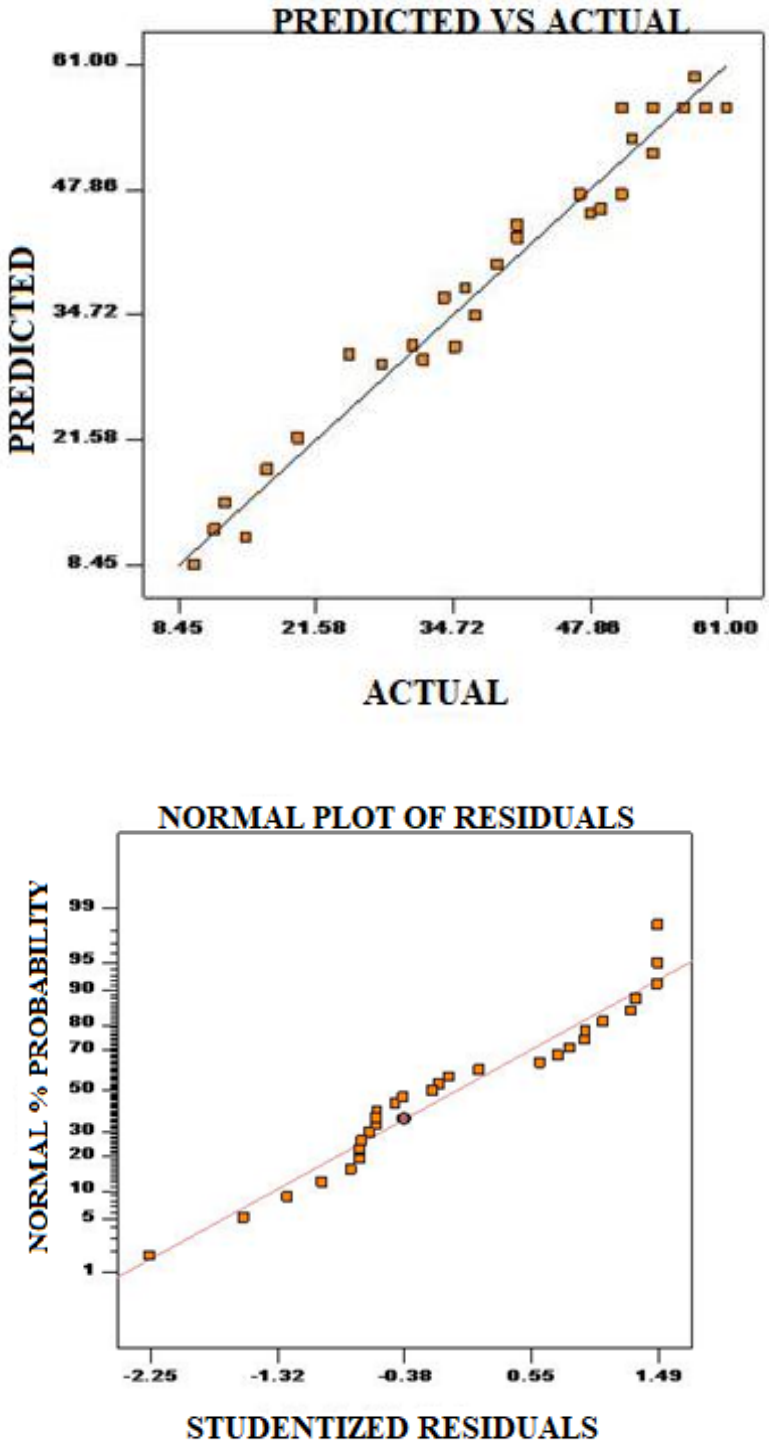

Figure 4.57: a) The plot showing the fitted range of predicted and actual values, b) The normal plot showing student residuals with probability

4.5.5. OPTIMIZATION AND RESPONSE SURFACE 3-D PLOTS

For the generation of optimum responses, 3-D surface plots along with the contour plots were generated. The effect of various interacting parameters like H_2O_2 dose, number of reactors, flow rate, and surface area covered has been studied. Among all the parameters, H_2O_2 dose came out to be the most significant parameter as it plays prominent role in both the processes i.e. in photocatalysis and photo-Fenton simultaneously. Hydrogen peroxide being the electron acceptor reacts with the electron of the activated catalyst surface to produce additional •OH (equation 4.38) (Zacharakis et al., 2013).

$$H_2O_2 + e^- \xrightarrow{h\vartheta} HO^{\bullet} + OH \qquad (4.38)$$

The 3-D interaction between the flow rate and H_2O_2 dosage for the percent degradation of MTZ has been shown in Figure 4.58a. When the dose of H_2O_2 was increased from 150 to 450 mg L^{-1}, subsequent increase in the degradation was observed i.e. from 29.12% to 57.83% which is basically due to the photon acceptance to the valance band by H_2O_2 to form •OH (equation 4.39), which helps in the reduction of the pollutant.

$$H_2O_2 + \bullet O_2 \rightarrow \bullet OH + OH^- + O_2 \qquad (4.39)$$

On further increasing the dose of H_2O_2, the production of less penetrative HO_2 radicals is formed (equation 4.40) which react with the Fe^{3+} leached out of the bead and form Fe^{2+} (equation 4.41) helping in the photo-Fenton reactions to take place.

$$HO^{\bullet} + H_2O_2 \rightarrow HO_2^{\bullet} + H_2O \qquad (4.40)$$

$$HO_2^{\bullet} + Fe^{3+} \rightarrow Fe^{2+} + O_2 \qquad (4.41)$$

At the same time, surface active TiO_2 executes the production of superoxide radicals leading to the reaction with H_2O_2 to form radicals as well. By further increasing the H_2O_2 dosage from 450 to 750 mg L^{-1} diminutions in the reduction of MTZ was observed due to scavenging effect, which might be due to the formation of hydroperoxyl radicals (Figure 4.58b). The hydroperoxyl radicals exhibits lower oxidation capacities leading to the slower degradation.

The flow rate of the influent also plays a major role in the degradation of the priority pollutant. With the Increase in flow rate, retention time of the pollutant in the reactor decreases thus efficiency is affected. Same time low flow rate, although not economically feasible, yet increase the contact time with the composite, thus leading to more efficiently pollutant degradation. The central point was obtained at 2.0±1.0 L h^{-1} with H_2O_2 dosage of 450 mg L^{-1} (Figure 4.58c).

Figure 4.58d shows the 3-D effect of oxidant dose as well as the catalyst surface area on the MTZ degradation. For this purpose, covered surface area was varied in terms of number of beads in the reactor. Taking into consideration the available shape and size of the reactor, for covering 25% area, the reactor tubes were filled with approximately one fourth portion of beads. On further increasing the surface area covered i.e. 50%, the tubes were half filled and the beads were packed tightly into the tubes for 100% coverage. Now for better contact with the compound, available surface area is an important parameter for scaling up the process. With both the processes taking place simultaneously, TiO_2 and Fe plays important role. As the number of beads increases, the exposed surface area and the iron leaching increases simultaneously. On increasing the surface area covered by the beads from 25 to 50%, the degradation of MTZ increases from 8.0 to approximately 35% (Figure 4.58d). This might be due to the increased number of available active sites on the catalyst surface and subsequent photo-Fenton reaction due to iron leaching. On further increasing the number of beads up to 80% of the reactor area, the degradation increases up to 60%. It is really uncertain to clarify which mechanism has contributed to degradation pool as both the processes are occurring simultaneously. Actually the e- from photocatalysis, which was susceptible for e^-/h^+ recombination, taken up by Fe(III) to get reduced to Fe(II) thus prompting photo-Fenton reaction (equation 4.42), leading to synergistic effect:

$$e^- + Fe(III) \rightarrow Fe(II) \qquad (4.42)$$

After the reactor was fully filled with beads, the beads got overlapped leading to the blockage of active sites and trapping of pollutant in the voidage between the beads, thus contributed to the decreased efficiency. Moreover increased amount of Fe leaching also contributed its share to the decreased efficiency due to scavenging effect.

For the continuous system, the number of reactors involved in the reaction also plays very important role. For this purpose, six reactors attached in series were evaluated by effectively assessing the concentration at the outlet of each reactor. From the Figure 4.58e, it could be seen that the concentration of MTZ decreases with subsequent increase in the reactors. At the end of 2^{nd} reactor 10% of the compound was degraded. After 4^{th} reactor the degradation was found to be nearly 40% as the compound gets in contact with the new beads every time (Figure 4.58f). On further increasing the reactor to 5, the degradation observed was 59% owing to both the processes of photocatalysis and photo-Fenton. The 6^{th} reactor didn't contribute significantly to the degradation pool as there was not much difference between the results and the degradation became constant (60%). The whole process was operated in once through mode with the space time of approximately 15 minutes. The fluorescence spectra of each reactor have been shown in Figure 4.59. The proposed study would open up new channels in the field of advanced technologies where these kinds of novel once through processes (with dual effect) can be proposed as pre/post treatment options.

The H_2O_2 is the most important source of •OH for the degradation of compounds. In the dual as well as the individual processes of photocatalysis and photo-Fenton H_2O_2 plays a very important role. The decomposition of H_2O_2 has been studied on the surface of various catalysts like Fe, TiO_2, CuO and many more (Do, Batchelor, Lee, & Kong, 2009; S. S. Lin & Gurol, 1998). For the evaluation of the degradation of H_2O_2 kinetic study was carried out using the preliminary processes i.e. adsorption, photocatalysis, photo-Fenton and dual process (Figure 4.60, 4.61). The decomposition of H_2O_2 followed pseudo first order kinetics. It was observed that in the dark there was negligible change in concentration of H_2O_2. But there was significant change in the concentration i.e. the decline in H_2O_2 concentration was observed in dual process confirming the property of dual process for the decomposition of H_2O_2 the remarkable consumption of H_2O_2 was observed in the case of dual. Thus was concluded that in the presence of light, along with the TiO_2 and the iron concentration the decomposition of H_2O_2 is accelerated with more production of •OH.

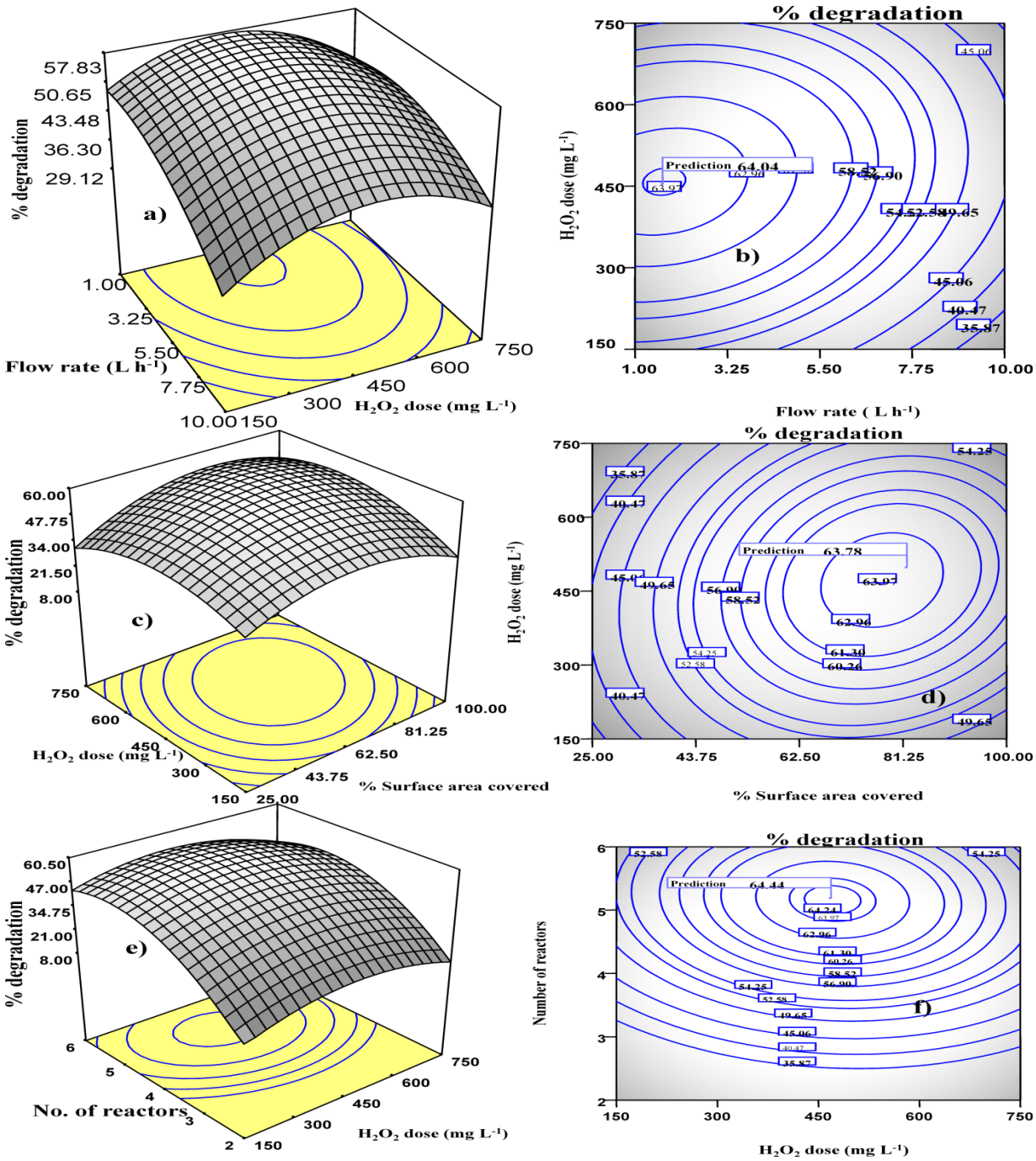

Figure 4.58: a) 3-D effect of change in H_2O_2 dosage with flow rate of the pollutant on % degradation of MTZ, b) The contour of H_2O_2 dose and flow rate with degradation of MTZ, c) Effect of change in covered surface area with H_2O_2 dose on the degradation of MTZ, d) The contour graphs of covered surface area with oxidant dose on MTZ, e) Effect of variation in number of reactors with dose of H_2O_2 on % degradation of MTZ , f) The contour graph of reactors variation with H_2O_2 dose on MTZ degradation

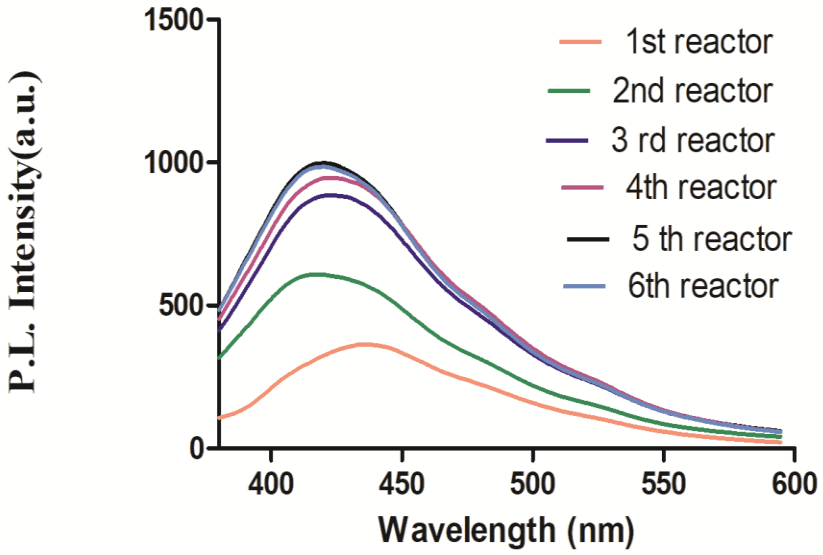

Figure 4.59: The variation in the fluorescence intensity with the each reactor

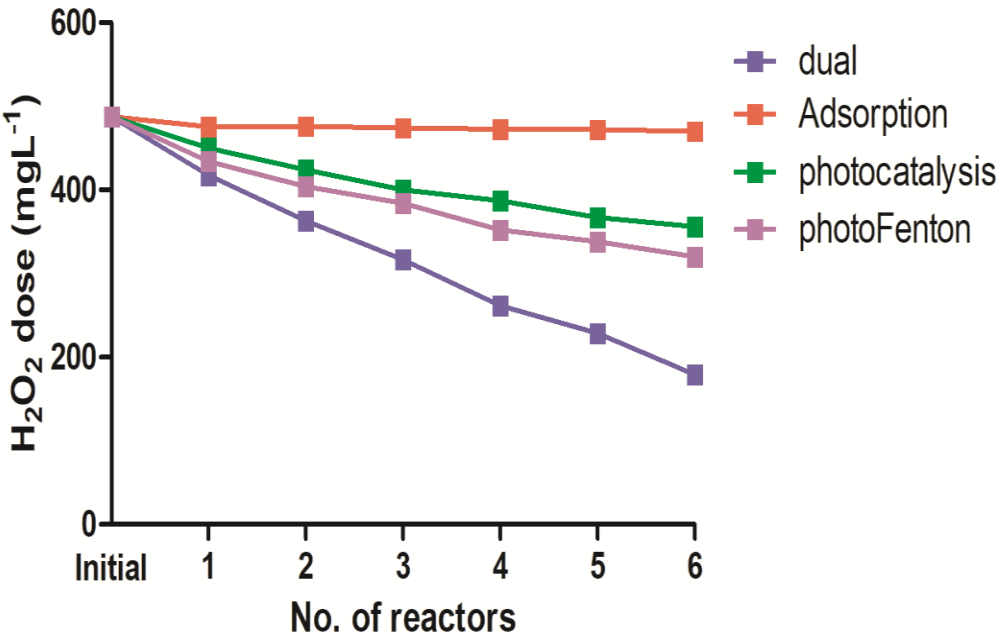

Figure 4.60: The decomposition of H_2O_2 at the end of reactors

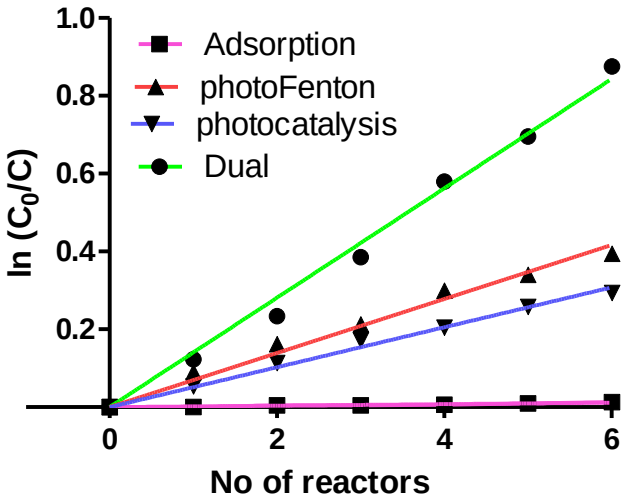

Figure 4.61: The kinetic study of the H_2O_2 decomposition

4.5.6. SYNERGISTIC EFFECT

The synergy was calculated using percentage degradation data obtained through individual rate of reactions of photocatalysis, photo-Fenton and dual process (Babu et al., 2019). The synergistic effect was observed in case of the coupled process as only 12% and 15% of the compound was degraded using photocatalysis and photo-Fenton (45 min) respectively, whereas dual process using 6 reactors contributed 59% removal in 15 min. Significant 2.19 fold synergy (equation 3.8) was observed in dual process as compared to individual processes of photocatalysis and photo-Fenton. The enhancement (E_d) of the dual process over the individual processes of photocatalysis and photo-Fenton was also evaluated using equation 4.43, at the optimized conditions and it came out to be 84.44%

$$E_d = \frac{k_{dual} - k_{photocatalysis} - k_{photo-Fenton}}{k_{dual}} \qquad (4.43)$$

The high synergy might be due to the combined effect of both the processes leading to the generation of significant amount of •OH. Moreover the prevention of electron hole recombination in photocatalysis by integrating e^- with Fe(III) for executing photo-Fenton reaction provides significant boost to synergy.

4.5.7. DURABILITY OF THE CATALYST

For the scale-up applications of the process, durability of the catalyst is a vital parameter. In fixed bed catalysis, recyclability/durability of the catalyst is still a great concern. In the present study, things have been more complicated as the process involves dual process i.e. photocatalysis and photo-Fenton occurring at same place at same time. The most challenging task here was to maintain the recyclability even in the flow conditions. The flow in the CPC being the closed channel has the main challenge as the coating might not be stabilized. Even the composite beads were not removed from the reactor and were allowed to dry inside the reactor. The main challenge was to retain the activity of TiO_2 layer coated (Figure 4.62a) on the bead while maintaining the leaching of the iron from the composite beads. In this report, the beads composed of FS and FE were reused effectively for over 40 recycles while retaining the catalytic activity of both the processes i.e iron leaching and activity of $TiO_2$was intact even after 40 recycles of continuous flow reactor (Figure 4.62b). The presence of TiO_2 was also confirmed through the SEM-EDS, XRD, FTIR analysis of the recycled beads, while presence of iron was determined by iron estimation analysis as well as from various characterizations i.e. XRD, FTIR. There was only approximately 10% loss in the degradation efficiency after 40 recycles. More importantly, the catalyst coated beads were used without any pretreatment i.e. no thermal or activation of catalyst was required, thus saving energy. To further claim the extended durability, the composite beads previously used for more than 150 recycles were tested for their dual effect in continuous flow conditions. Reasonable degradation (58%) was obtained even with these old composite beads which strengthens our claim for the commercial scale applications of the process.

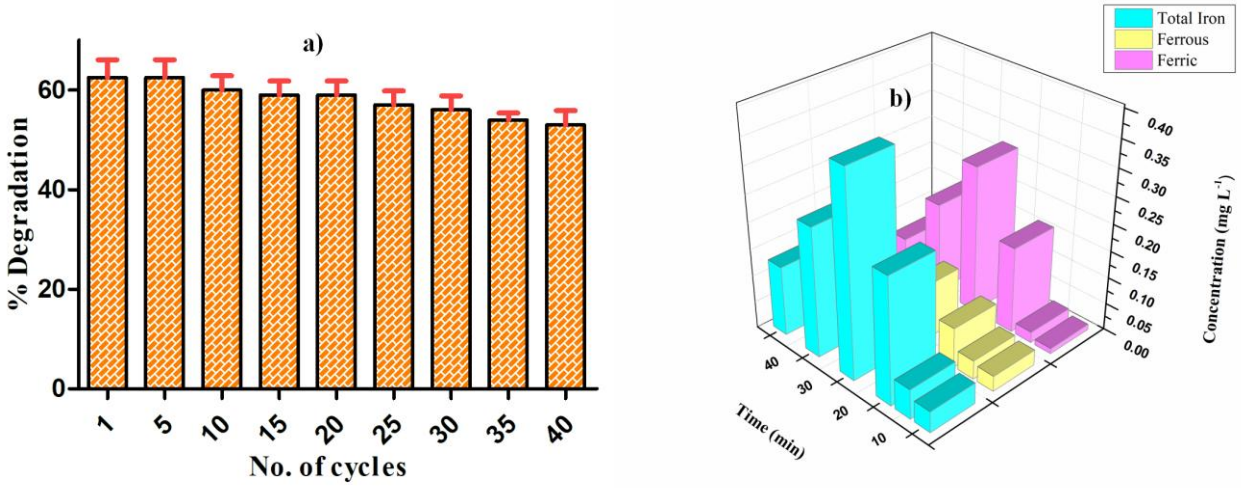

Figure 4.62: a) Durability studies of the beads, b) iron estimation analysis in terms of total, ferrous and ferric ions

4.5.8. APPROACHING TOWARDS IDEALITY

PFR has known to be the best theoretic reactor, among the other ideal flow reactors. The highest conversion of the reactants is assumed to take place with low flow rate. The PFR provides the same conversion as that of CSTR using half the size of reactor. It is ideally correct in the laminar range of flow. But still various problems like controlling the temperature, maintenance cost as well as film diffusion resistance are faced. Hence to obtain the efficiency of the reactor the behavior of the CPC reactor towards plug ideality has been studied. The theoretical plug flow calculation has been shown in equation 4.44- 4.48.

$$\frac{V}{F_{Z0}} = \int_0^{X_{Z0}} \frac{dx_Z}{-r_Z} \qquad (4.44)$$

$$\frac{V}{\nu_0} = C_{Z0} \int_0^{X_{Z0}} \frac{dX_Z}{-r_Z} \qquad (4.45)$$

Following the 2nd order kinetics,

$$-r_Z = kC_Z^2 \qquad (4.46)$$

$$X_Z = \frac{(C_{Z0} - C_Z)}{C_Z} \qquad (4.47)$$

And for 2nd order, $k\tau C_Z = \frac{1-X_Z}{X_Z}$

$$\frac{V}{\nu_0} = \frac{1}{kC_Z}\int_0^{X_{Z0}} \frac{dx_Z}{(\frac{1-X_Z}{X_Z})} \qquad (4.48)$$

Where V represents the volume of reactor in L, $\boldsymbol{\nu}_0$ (L min^{-1}) represents the volumetric flow rate, C_{Z0} = initial concentration (mg L^{-1}), C_Z= final concentration (mg L^{-1}), molar flow rate by F_{Z0} (moles min^{-1}), r_Z= reaction rate (mg $L^{-1}min^{-1}$), X_Z = conversion and k representing the rate constant ((mg $L^{-1})^{-1}min^{-1}$).

Using equation 4.47, by substituting optimized values of, 10 L of the total volume, 4 L $h^{-1}$of the flow rate and the k value of 0.0082 L mg^{-1} min^{-1}, 70 % of conversion was obtained. The actual trial results showed 72 % of conversion at these optimized conditions. There was nearly 0.8 % of error in between experimental as well as theoretical results, which is due to performance errors or due to some other limitations.

4.5.9. RESIDENCE TIME DISTRIBUTION (RTD) STUDY

For confirming the flow pattern and hydro dynamic behavior of the CPC reactor, RTD study was carried out. RTD being the characteristic approach for analyzing the ideal behavior of the reactor, could also be used to scale up designs at the optimized conditions for maximizing the efficiency. Exit age distribution (E (t)) was used for the RTD study. The distribution for E (t) was calculated using the equation 4.49.

$$E(t) = \frac{S(t)}{\int S(t)dt} \qquad (4.49)$$

Where, the tracer's concentration in (mS cm^{-1}) is denoted by S (t), and the time (min) by t. Peclet Number (Pe) is defined as (equation 4.50):

$$Pe = \frac{\vartheta L}{D} \qquad (4.50)$$

Where ϑ is the fluid velocity of fluid (m s^{-1}), L is the characteristics length (m) and dispersion coefficient (m^2 s^{-1}) is denoted by D. The tracer used for the RTD analysis was Lithium Chloride. For modeling the data axial dispersion model as well as tanks in series model

(Abu-Reesh & Abu-Sharkh, 2003) were used (Figure 4.63,4.64). The average residence time of 13.5 min as well as the actual residence time of 15 min from the experimental data was fairly similar to the theoretical value. The degree of mixing in the reactor could be related to the N (tanks in series). On using reactors in series model, it was examined that low value of N (tanks in series) showed the reactor behaved completely as continuously stirred tank reactor (CSTR) whereas high value confirms the flow regime to be approaching plug flow behavior (PFR) as shown in Figure 4.65. In this case, 10 reactors in series were optimized to be best fitted model (Figure 4.64). By fitting the axial dispersion model it was further confirmed the behavior to be as ideal plug flow. Pe was obtained to be 25. Increased value of Pe confirms the regime to be plug with less dispersion.

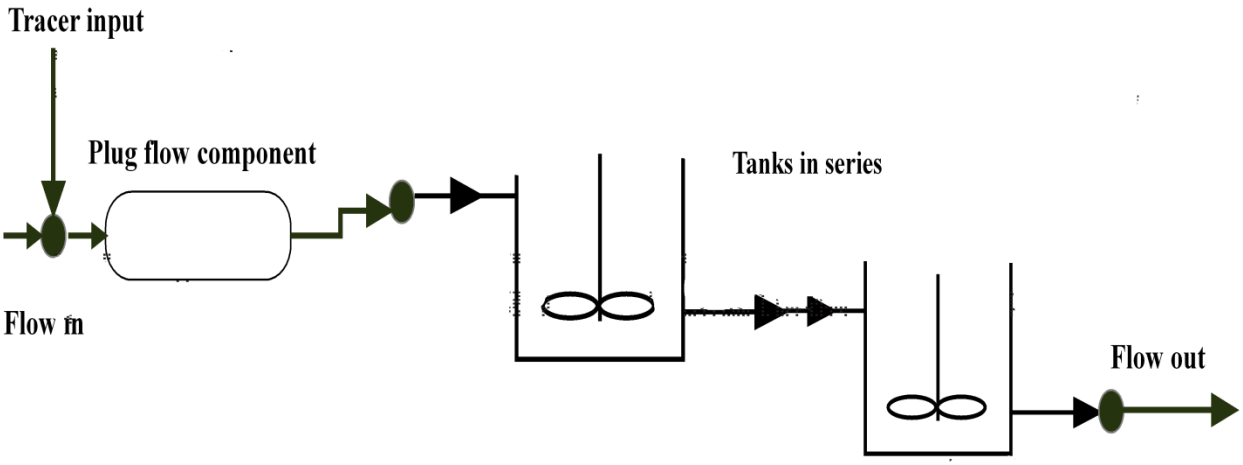

Figure 4.63: Conceptualization tanks in series model for CPC reactor

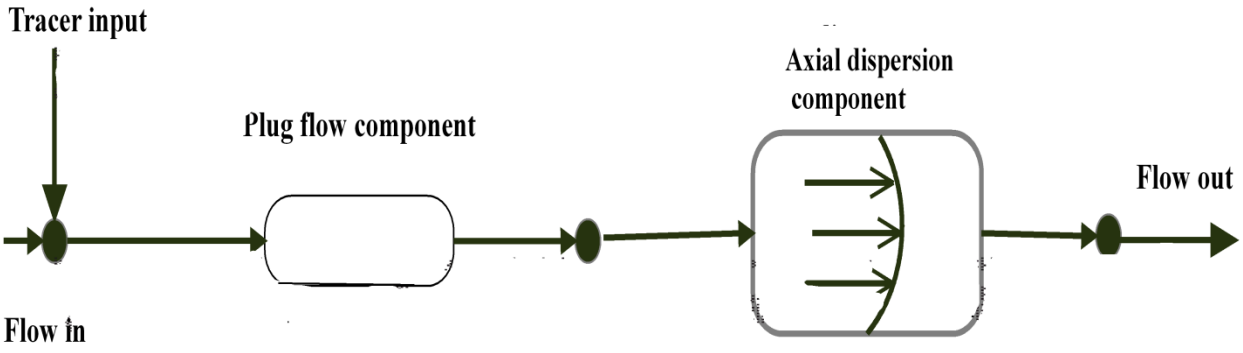

Figure 4.64: Conceptualization axial dispersion model for CPC reactor

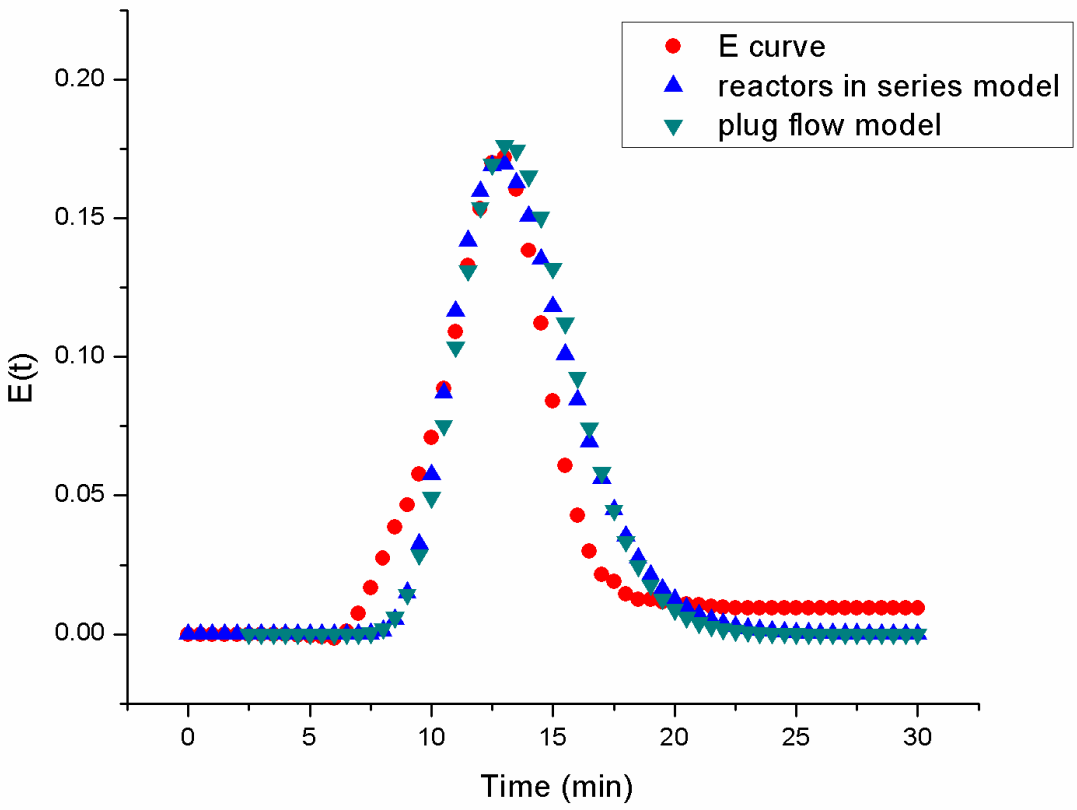

Figure 4.65: RTD study of the experimental data as well as the fitted models of reactors in series and plug flow reactor

4.5.10. CHARACTERIZATION OF CATALYST

4.5.10.a. SEM-EDS

For analyzing the morphological characteristics of the samples SEM analysis was carried out. The SEM analysis was combined with the EDS and Mapping analysis for the distribution of various elements present in the samples. For the comparison between the uncoated and coated and recycled beads Figure 4.66 depicts the SEM and EDS images at 500 magnifications. From the SEM image it was clear that the roughness of the surface was appropriate for the TiO_2 coating to be stable enough and from the EDS images it was clear that the Fe element was present even at the surface of beads along with various other elements like Si, Ca, Mg, Na. From

the SEM images of the unused coated beads it was observed that the coating was uniform without cracks and EDS confirmed the presence of Ti as well as Fe elements. Mapping of the beads also confirmed the distribution of Ti and Fe elements on the beads surface (Figure 3.8). With the subsequent recycles SEM-EDS was performed and it was confirmed that coating was still present even after recycles and Fe was also present at the surface.

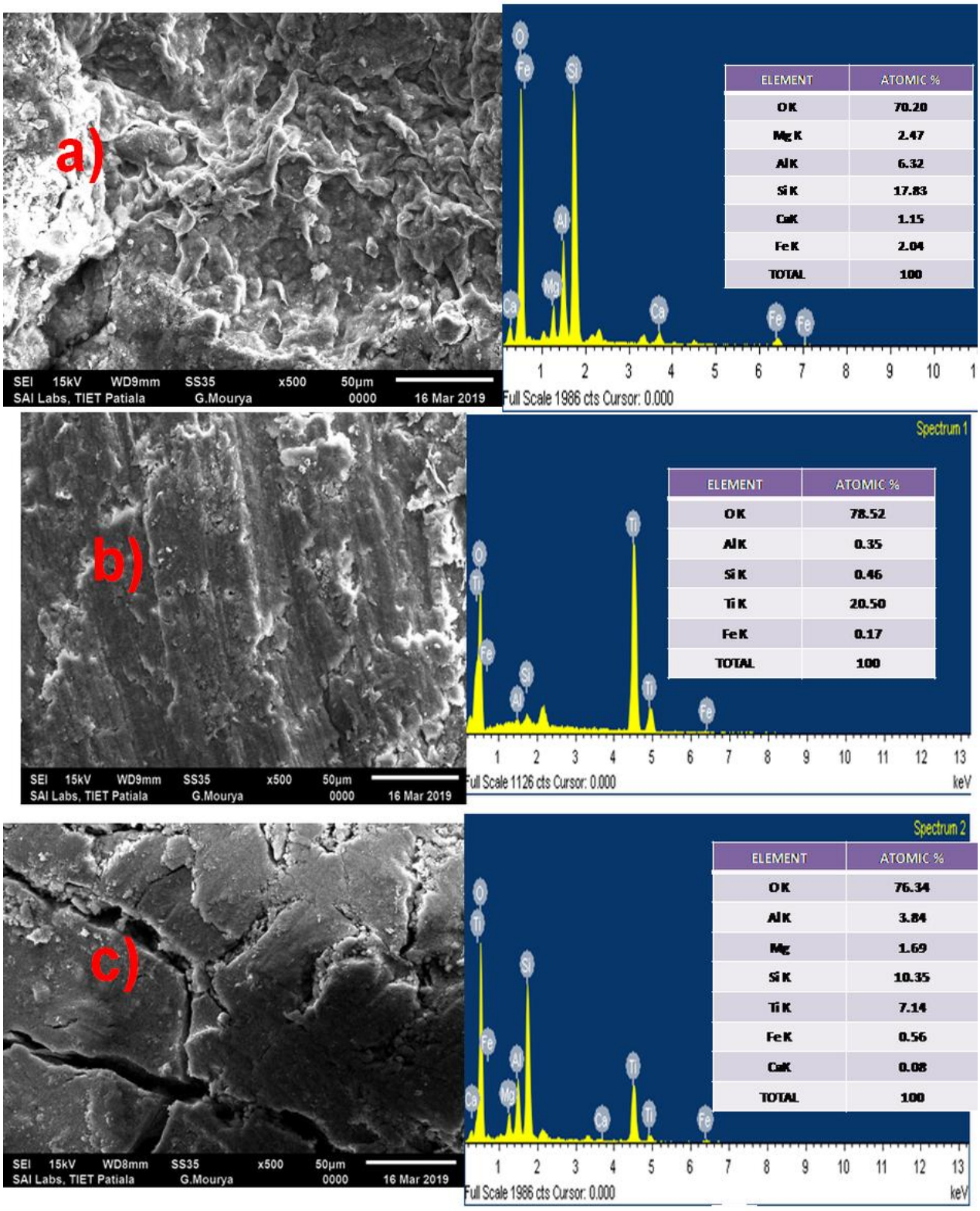

Figure 4.66: SEM-EDS analysis of a) uncoated bead b) fresh coated bead c) recycled bead

4.5.10.b. XRD

For determining the polymormhs and crystalline phases of composite X-Ray diffraction was carried out (Figure 4.67). The peaks corresponding to the basic nature of TiO_2 i.e. anatase and rutile phase (JCPDs number 01-083-2243, 01-088-1172) were detected in both the samples i.e. in unused and recycled beads. Additionally, the peaks related to the Fe oxides (JCPDs number 00-013-0534, 01-089-6466) were also observed in both the samples as shown in Figure 4.67. The oxides of iron along with the presence of TiO_2 help in both the processes i.e. photo-Fenton and photocatalysis to take place simultaneously (Bansal & Verma, 2017a). Fe^{3+} could enter the lattice structure of TiO_2 forming the Fe-TiO_2 composite.

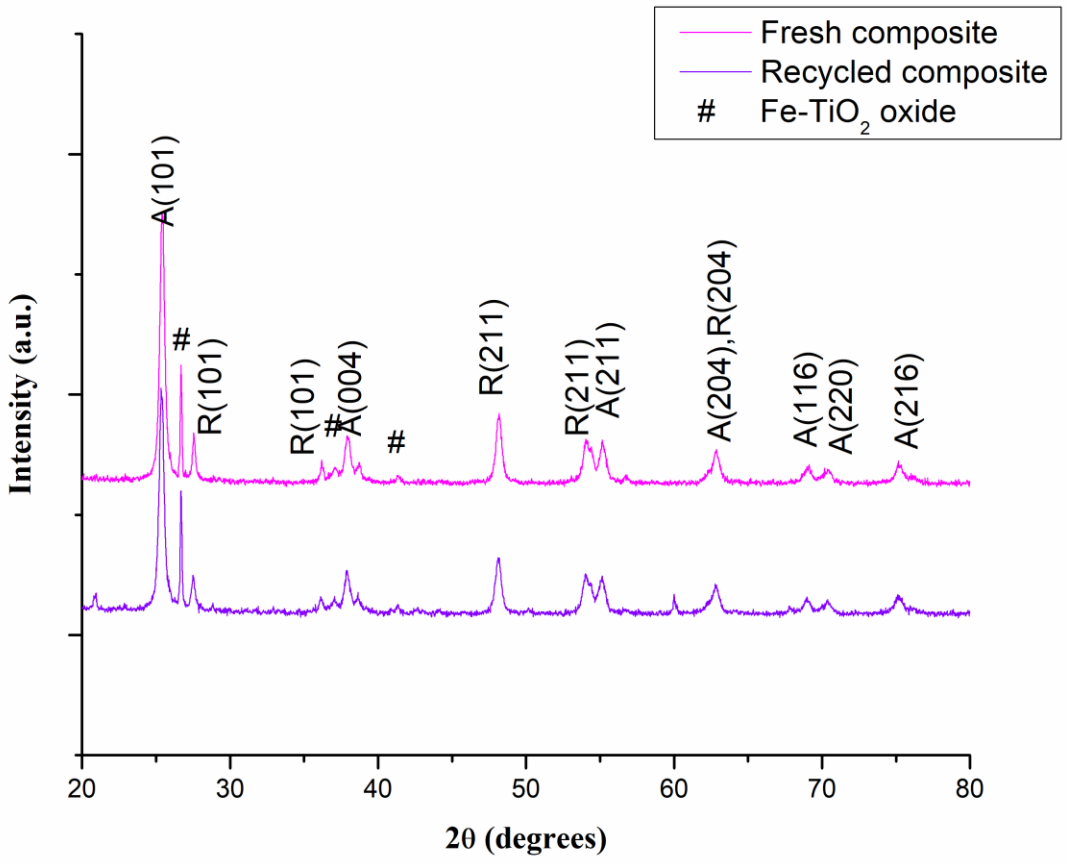

Figure 4.67: XRD analysis of fresh and recycled beads

4.5.10.c. FTIR ANALYSIS

For the analysis of molecular structure of the composite FTIR was carried out. The IR analysis of the uncoated and used composite is shown in Figure 4.68. The stretching band was observed in both the samples at 3415 cm^{-1} depicting the presence of •OH groups of H_2O which are adsorbed on the surface of the composite prepared (Jaihindh et al., 2018). Due to the presence of Fe in the composite the characteristic peak (Ali et al., 2017) was also observed in the range of 1000-1500 cm^{-1}. Peaks for Ti-O-Ti were also observed. The shift in peak was observed in the recycled composite confirming the implant of Fe on the TiO_2 composite. The peaks of Si-O were observed due to the presence of aluminium silicates in the beads (Balu, Uma, Pan, Yang, & Ramaraj, 2018).

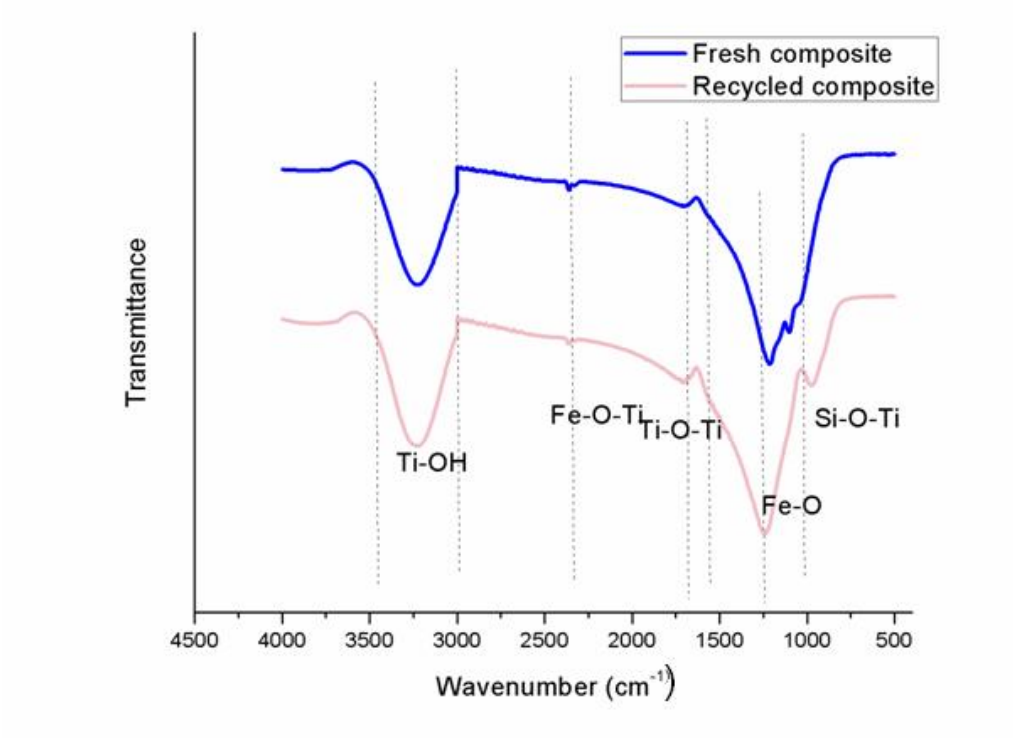

Figure 4.68: FTIR analysis of the fresh as well as recycled composite

4.5.10.d. UV-VISIBLE DIFFUSE REFLECTANCE SPECTROSCOPY

The Fe-TiO_2 composite was characterized using UV-Vis DRS for the identification of the effects caused by the Fe oxides present in the composite. It was observed that the absorbance in the visible range for the composite gave better results leading to the reduction in band gap energy

of the composite causing the TiO_2 to absorb in visible range. For quantifying the band gap energy equation 4.51, 4.52 were used.

$$E = \frac{hc}{\lambda} \qquad (4.51)$$

$$E = \frac{1240}{\lambda} \qquad (4.52)$$

Where, h = Planck's constant, c = speed of light (m s^{-1}), λ = absorption wavelength (nm) and E = band gap energy (eV),

For the prepared composite i.e. fresh and after 40 recycles band gap energy was 2.88 eV and 2.75 eV respectively.

Compared with the P25 TiO_2, the band gap energy was reduced (Figure 4.69) substantiating the claim that the catalyst prepared is predicted to utilize visible light. Under the visible light irradiation, the photocatalytic activity of prepared TiO_2 composite is enhance considerably. Fe with loaded TiO_2 photocatalysts might form a n-type semiconductor. Fe^{3+} metal ions have more valence electrons than Ti^{4+} hence, could be utilized to fill the new energy level. The iron titanium oxide composites formed as depicted from the XRD analysis also helps in the reduction of band gap energy leads to the activity of composite in visible range of light.

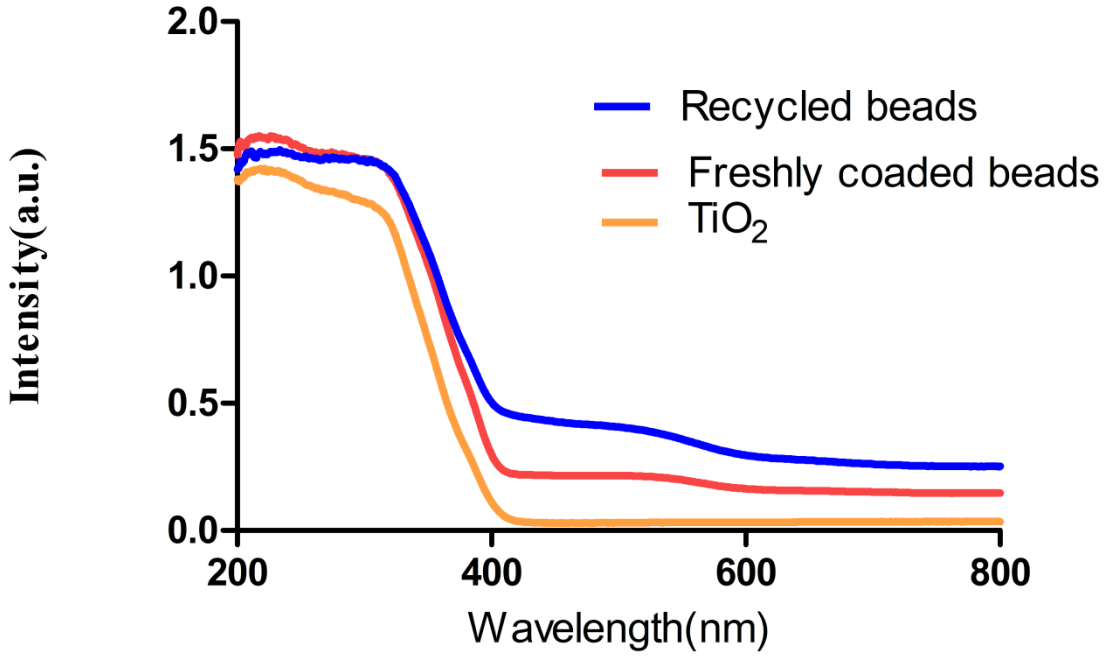

Figure 4.69: UV-DRS of the TiO_2, fresh as well as recycled composite

4.5.10.e. SURFACE CHARGE OF THE CATALYST

For the determination of the coagulation stability the surface charge is to be monitored. The surface charge is analyzed using zeta potential (Figure 4.70). The analysis showed that the zeta potential varies with change in pH. With increase in pH the zeta potential decreases. The isoelectric point was obtained at pH 5.1. When the pH is higher than isoelectric point the surface charge becomes negative i.e. the zeta potential is negative.

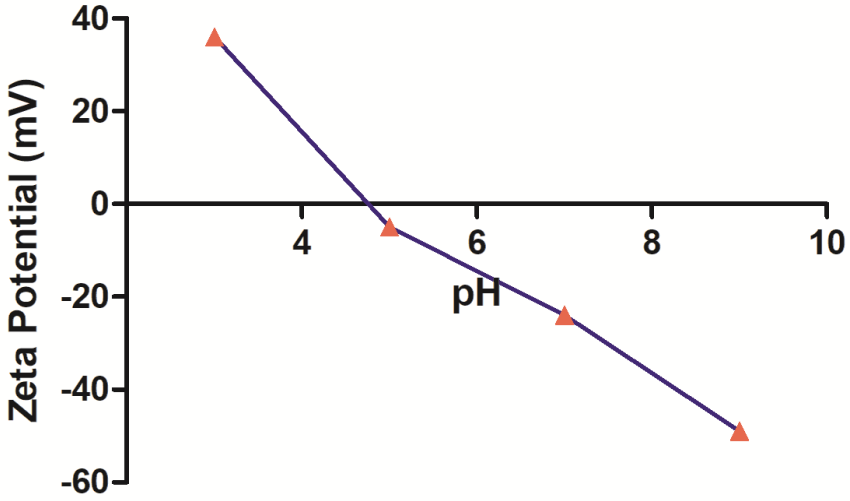

Figure 4.70: The study of zeta potential with change in pH

4.5.11. MINERALIZATION ANALYSIS

For confirming the mineralization of MTZ, reduction in the TOC, and COD was also carried out. Along with the reduction in TOC and COD, generation of ions including nitrates and nitrites were also examined. The oxidation of the various nitrogen atoms present in the MTZ structure leads to the formation of these ions. The nitrate ions with time get converted into nitrites and ammonium ions (Table 4.18). With the increase in the number of reactors the concentration of the nitrite ions increases and the concentration of nitrates first increases up to 4th reactor and then starts to decrease due to its conversion into nitrites and ammonical ions. Ammonical ions increase with increase in time and number of reactors. Almost 45-50% reduction in COD was observed along with 30-32% reduction in TOC. The effect of water matrix was also evaluated. The naturally occurring anions like Cl^-, HCO_3^-, NO_3^-, SO_4^{2-} affects the performance of the process (Figure 4.70). The effect of various anions was studied on the degradation of MTZ. It was observed that the presence of HCO_3^- had significantly higher scavenging effect on the MTZ degradation. The Cl^- presence also depicted the inhibition effect in the MTZ removal. The minor effects of SO_4^{2-} and NO_3^- were observed in the degradation of MTZ (Figure 4.71).

Table 4.18: The change in concentration of various ions produced during the mineralization of MTZ

Time (min)	Concentration (mg L^{-1})		
	Nitrites (µg L^{-1})	Nitrates(mg L^{-1})	Ammonium ions(mg L^{-1})
5	1.54	3.52	2.6
10	2.76	4.21	3.5
15	3.54	4.03	4.8

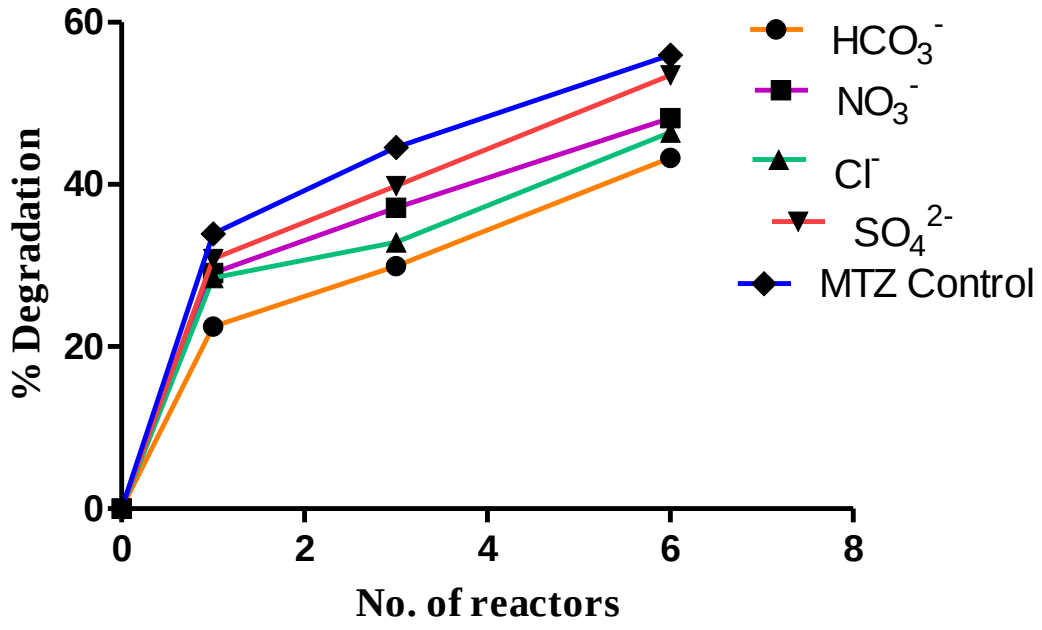

Figure 4.71: The effect of various anions (water matrix) on the degradation of MTZ

The mineralization of the MTZ was further confirmed using GCMS analysis as the intermediates formed during the degradation were predicted as depicted in the Figure 4.72. MTZ might convert into 1-(2-hydroxyethyl)-1H-imidazole-2,5-diol by the •OH produced by both the processes and in subsequent steps lead to the formation of nitrate and nitrite ions. Further

reduction of the ethyl group leads to the formation of 2-methyl-1H-imidazole. The formation of water molecules along with imidazolidine due to the reduction of the hydroxyl group attached with the MTZ structure. The attack of hydroxyl group leads to the fragmentation and formation of dimethylamine. The cleavage and the fragmentation of the ring along with the formation of ammonium ions and water loss confirm the mineralization.

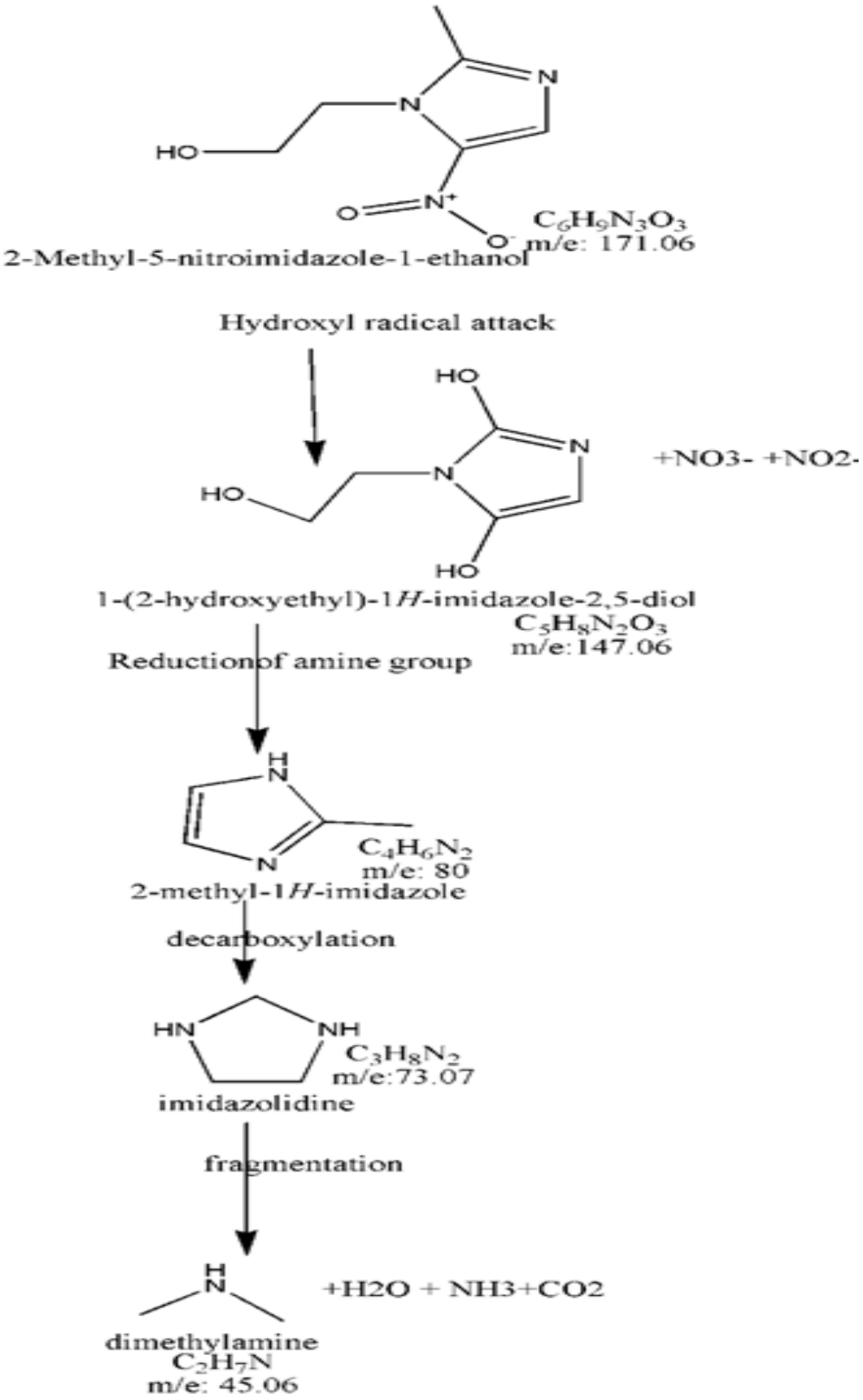

Figure 4.72: Predicted degradation pathway of the MTZ

4.5.12. COST AND ECONOMICS EVALUATIONS

The practical applications of any proposed technology depends upon the cost and economics analysis between model and prototype. The treatment cost basically depends upon the experimental results obtained from the treatment of wastewater along with scale-up factors. Table 4.19 presents the approximate cost/economics analysis involved for the treatment of target waste water and subsequent section depicts the cost factor involved for scale-up studies.

Table 4.19: Cost analysis for the complete dual process for CPC reactor

Fabrication of reactor	**Electricity cost**
Cost of Reactor fabrication= 150$ Cost of glazing of reactor = 9$ Cost involved for piping and fittings= 20$ Total cost involved in fabrication = 179$	Electricity cost = 0.015 $ kWh^{-1} Cost for baking the beads = 3×.015 =.045 $ kWh^{-1}
Catalyst and raw material	**Cost of reactions**
Cost involved for catalyst Raw material cost i.e. fuller's earth =0.1$ Kg^{-1} Cost of foundry sand = 0$ Cost of TiO_2 catalyst = 6$$gm^{-1}$ Cost for beads raw material =6.1 $	Cost of UV light involved =0$ Removal of MTZ cost = 0.25$
Cost of oxidant involved	**Pumping cost involved**
H_2O_2 usage= 15 mL for 10L For 40 runs= 15×40=600 mL =0.6 L Cost of H_2O_2= 5$ $(0.5\ L)^{-1}$	Cost of pumping the solution = Energy consumed × cost of electricity Total cost for removal = 0.262 $

Total cost of H_2O_2 used= 6$	
Other cost involved	**Annual cost**
Installing and labor charges= 1$ Designing and permitting = 2$ Various controls involved = 2$ Any pre or Post treatment = 2$ Various other costs = 7$	Contingency cost = 2$ Total annual capital cost = 26.8$ Total chemicals required = 5$ Analysis of wastewater = 5$ Maintainance cost = 5$ Electricity = 1$
Total cost	
Overall Total cost involved = 200.7$ for 10 L and 40 reactions Total annual cost =42.8$/yr Treatment cost/ L = 0.107$	

4.5.13. SCALE UP STUDIES

Scaling-up being is most important factor involved in the application of the dual process at industrial level. Various parameters involved should be taken into consideration while evaluating the cost effect/economics analysis. Modeling the scale-up of prototype is very important as there are various problems involved in the industrial version like composition, mixing, power consumption etc (Gar Alalm, Tawfik, & Ookawara, 2017). In order to estimate the treatment cost of an industry scale reactor, let us take into consideration the amount of wastewater being 10,000 L. For estimating the scaling up, 0.6 rule was used (equation 4.53).

$$\mathrm{COST_B} = \mathrm{COST_A}\left(\frac{\mathrm{SIZE_B}}{\mathrm{SIZE_A}}\right)^{\mathrm{N}} \qquad (4.53)$$

N being the size exponent, $Size_A$/ $Size_B$ being the dimensionless size factor. As discussed, we are considering scaling up reactor by 1000 times. The values for various N were reported from (Tribe & Alpine, 1986).

Table 4.20: Scale-up calculations for the real time CPC reactor system

Scale up analysis	**Total scale up cost analysis involved**
Scale up cost of raw material = 384.88 $ Scale up cost pumping = 32.98 $ Scale up cost of Reactions = 15.77 $ Scale up cost of oxidant= 378.57$ Scale up cost of reactors fabrication = 19626.95 $ Electricity cost = 2.83$ Other miscellaneous cost and contingency = 567.86 Total cost = 3309 $ (for 40 reaction handling 10,000L Volume) Cost for 1 reaction=0.0085 $/L	The cost of investment is calculated using $I = \frac{A_{illumiated}\ C_{illumated\ area}}{(\text{Treatment plant life})}$ Assuming the plant life of 10 years with illuminated area of 100 m^2. I= 3.3×10^4 $ Amortization cost $A = \frac{I}{V}$ A= 33.09$

SECTION 3

TREATMENT OF REAL PHARMACEUTICAL INDUSTRIAL WASTEWATER

4.6. REAL PHARMACEUTICAL WASTEWATER TREATMENT

The real pharmaceutical effluent was characterized for the various parameters including Biochemical Oxygen Demand (BOD), Chemical Oxygen demand (COD), Total Solids (TS), Total Dissolved Solids (TDS), and many more as shown in Table 4.21.

Table 4.21: Numerous characteristics of real pharmaceutical effluent

Parameters	**Concentration**
	Industrial pharmaceutical effluent
Total suspended solids(TSS)	880 mg L^{-1}
Total dissolved solids(TDS)	7270 mg L^{-1}
Total solids(TS)	8150 mg L^{-1}
Nitrate ions	6.85 mg L^{-1}
pH	4.8
Turbidity (NTU)	521
COD	1250 mg L^{-1}
BOD	200 mg L^{-1}
Biodegradability Index(BOD_5/COD)	0.159

4.6.1. IN-SITU DUAL EFFECT

Before confirming the prominence of the dual effect of photo-Fenton and photocatalysis, various confirmatory tests were performed on the untreated pharmaceutical effluent. Adsorption studies revealed only 3% COD reduction whereas photolysis leads to almost 10% reduction in COD after 4 h. Hence, confirming no role of adsorption and photolysis in the degradation of wastewater (Figure 4.73).

Photocatalysis using TiO_2 immobilized FE+FS beads confirmed the 60% degradation of effluent after 5 h whereas uncoated FE+FS beads in the acidic conditions were used for photo-Fenton analysis and 45% of COD reduction was obtained after 4 h for the real pharmaceutical wastewater. On the other hand, the dual concept of photo-Fenton and photocatalysis using catalyst coated composite beads lead to an 82% reduction in COD in 4 h (Figure 4.73).

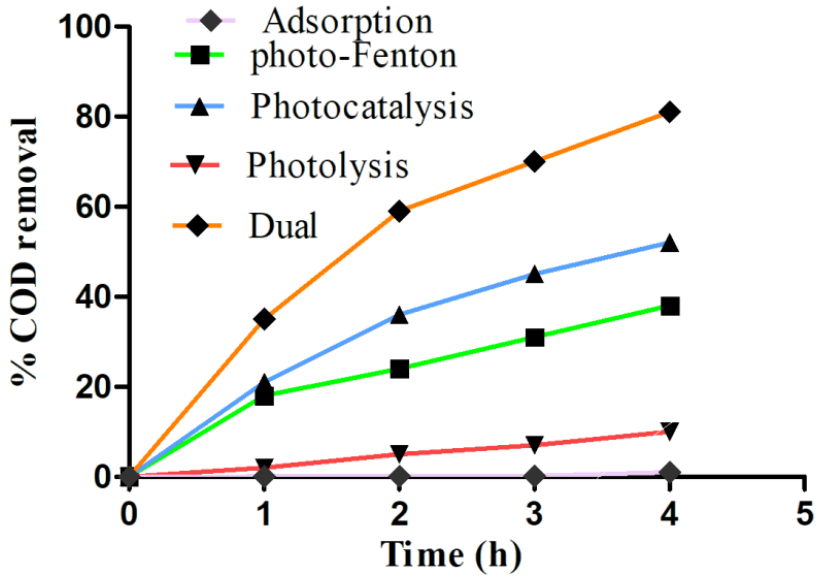

Figure 4.73: Degradation of real pharmaceutical wastewater using different processes

This might be due to the photocatalysis and photo-Fenton process taking place simultaneously. As discussed earlier, surface active TiO_2 layer, along with subsequent leaching of iron (Figure 4.74), from the composite actually lead to the proposed in-situ dual effect. From the characterization of FE+FS beads, it was clear that more amounts of ferric ions were present. The TiO_2 particles when exposed to light leads to the photocatalysis process to take place leading to the formation of electron and hole pairs. For the photo-Fenton reactions to initiate, Fe(III) is to be converted into Fe(II) (Ruales-Lonfat et al., 2015). The electron from the photocatalysis which posed the problem of recombination helped in the conversion of Fe (III) to Fe (II). When Fe (III) ions come into contact with TiO_2, some of the Ti(IV) species are replaced due to the weakening of metal oxygen bond and imbalance of the charge. This further leads to the formation of Ti(III)

species along with the vacancies of oxygen which act as the reactive species for the degradation (Y. Zhang et al., 2019).

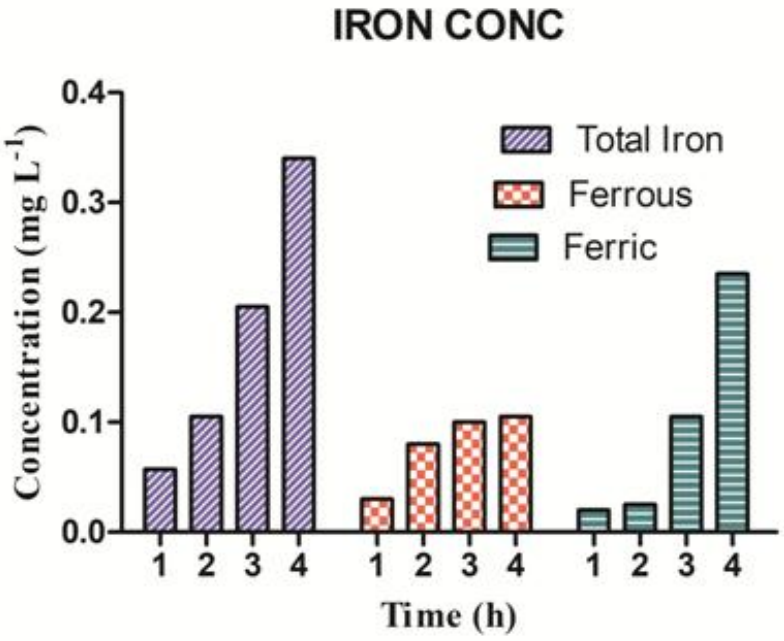

Figure 4.74: Estimation of the iron content from the beads

This lead to the electron-hole pair being separated and thus helping in the oxidation of pollutants to take place (Kim et al., 2012). This will contribute to more amount of •OH production and thus favoring the overall process (Asiltürk et al., 2009). Besides alone photo-Fenton and photocatalysis radicals generation as well as the degradation occurring at the surface of TiO_2 and the oxides of iron, synergistic effect of both the processes also helps in the removal (Mazille, Lopez, & Pulgarin, 2009b). The existence of Fe(II) and Ti(III) leads to the synergistic effect enhancing the oxidation and reduction thus leading to the increased degradation of wastewater (Mazille, Schoettl, et al., 2009). There was the significant diminution in treatment time for the degradation of industrial wastewater, thus confirming the synergy of dual effect. The treatment efficiency of various processes i.e. in-situ dual effect (82%), photo-Fenton (45%) and photocatalysis (60%) is shown in Figure 4.73. Thus the efficacy of in-situ dual process has opened up new channels in the challenging wastewater treatment technologies.

4.6.2.OPTIMIZATION AND STATISTICAL ANALYSIS

Using BBD, 17 experiments (Table 4.22) were suggested for % COD removal as output and H_2O_2 dose, time and number of beads as the input parameters (Table 4.23). Statistical results attained from the RSM suggested a quadratic model be best fitted. Fisher's test i.e. Sequential F-test was also used for the adequacy measures resulting in the F-value of 31.07 which further confirms the quadratic model to be employed. Adequate precision for the COD removal came out to be 20.598 confirming the model to be efficient. The ratio of adequate precision should be more than 4 so that the model could be navigated in design space (V. Sangal, Kumar, & Mishra, 2013). The value of probability > F was 0.002 indicating only 0.002% chance of the quadratic model F-value to occur. Value of p less than 0.01 indicated that significant correlation existed with at least one of the variable in the regression equation with the response variables.

Table 4.22: Range of the variables used for the analysis of real wastewater

	Coded levels		
Variables	-1	0	1
H_2O_2 Dose (mg L^{-1})	350	937.50	1500
Time (h)	1	2.5	4
No. of Beads	50	100	150

Table 4.23: Full factorial matrix designed utilizing BBD for the removal of real wastewater

Std	Time(h)	H_2O_2Dose (mg L^{-1})	No. of Beads	% COD Reduction
1	2.50	937.5	100	61.6
2	4.00	937.5	150	58.4
3	1.00	937.5	50	20.8
4	2.50	375	150	36.16
5	4.00	937.5	50	66
6	1.00	937.5	150	19.21
7	2.50	375	50	59.36
8	1.00	375	100	26.4
9	2.50	1500	150	36.16
10	1.00	1500	100	12.24
11	4.00	375	100	68.16
12	2.50	937.5	100	53.6
13	4.00	1500	100	48.16
14	2.50	937.5	100	58.56
15	2.50	1500	50	33.6
16	2.50	937.5	100	62.2
17	2.50	937.5	100	55.6

The summary statistics of the model for % COD reduction showed a fairly elevated value of R^2 i.e. regression coefficient R^2 Value of 0.98 and a good correlation amidst the predicted and observed values were perceived. The standard deviation was 3.51. The interaction between H_2O_2 dose and number of beads had a synergistic effect as shown in Figure 4.75. The ANOVA as concluded was based upon the quadratic model. The results of ANOVA for the % COD reduction of real industrial effluent was shown in Table 4.24, with a model F-value of 46.61 indicating the model to be highly significant. ANOVA could also be used for the identification of the factors which were more significant in the reduction of COD. The operating conditions could

be compared affecting the % COD reduction from Table 4.24. The prob>F value of time was found to be 0.0001. This showed that any change in time played a significant role in the COD reduction. As with increase in time the more amount of •OH radicals were produced leading to degradation.

The significant terms for % COD reduction were time, Number of beads, interaction between H_2O_2 dose and number of beads was perceived from the Analysis of Variance. With the increase in the number of beads the quantity of Fe(III) also increases and more amount of •OH radicals and retarding electron hole recombination.

The quadratic model equation obtained in terms of significant process parameters and interaction parameters are given below (equation 4.54). This could be used as the empirical correlation between output and input parameters.

$$\%\ \text{COD Reduction} = -26.73464 + (39.11972 \times \text{time}) + (0.34602 \times \text{Number of beads}) - (4.39767 \times \text{time}^2) - (3.05849\times10^{-5}\times H_2O_2\ \text{dose}^2) - (2.92590\times10^{-3}\times\text{No. of beads}^2) + (2.28978\times10^{-4}\times H_2O_2\ \text{dose} \times \text{Number of beads}) \quad (4.54)$$

Table 4.24: ANOVA of % COD removal of real pharmaceutical effluent

% COD Removal						
Source	Sum of Squares	DF	Mean Square	F Value	Prob>F	
Model	5184.69	9	575.24	46.63	< 0.0001	significant
Time	3282.93	1	2195.97	265.71	< 0.0001	highly significant
H_2O_2 Dose	451.95	1	25.45	36.58	0.0005	
Number of beads	112.73	1	264.07	9.12	0.0194	
Time^2	414.09	1	412.24	33.52	0.0007	
H_2O_2 Dose^2	394.50	1	394.31	31.93	0.0008	
Number of beads^2	225.27	1	225.29	18.23	0.0037	
Time ×H_2O_2 Dose	8.56	1	8.53	0.69	0.4328	
Time ×Number of beads	9.03	1	9.03	0.73	0.4209	
H_2O_2 Dose ×Number of beads	166.93	1	165.89	13.51	0.0079	
Residual	86.49	7	12.34			
Lack of Fit	31.04	3	10.28	0.75	0.5783	not significant
Pure Error	55.45	4	13.89			
Cor Total	5271.17	16				

4.6.2. BEHAVIOUR OF VARIOUS PARAMETERS AND OPTIMIZATION

The effect of various parameters i.e. treatment time, the number of catalyst coated beads and H_2O_2 dosage on the % COD reduction were studied. The interaction between various parameters has been shown in Figure 4.75 a-c. It was observed that as the treatment time was increased from 1 to 2.5 h, % COD reduction increases. After 2.5 h increase in COD reduction was not so significant and attained the steady state time at nearly 3.25 h. Moreover, from ANOVA it was

clear that treatment time was a highly significant variable for the studies of degradation of industrial effluent. Further, it was that noticed that with the increase in H_2O_2 dose from 375 mg L^{-1} degradation was found to increase up to 656 mg L^{-1}, then there was nearly constant degradation observed up to 1000 mg L^{-1}. The reason might be the production of the adequate amount of •OH for the reaction to take place. Also, the provenance might be the charge separation enhancement by H_2O_2 along with the reduction of H_2O_2 into •OH. With further increase in the dosage of H_2O_2, % COD reduction was lowered down. excess H_2O_2 indicate the scavenging effect of •OH leading to the lowered COD reduction (Nezamzadeh-Ejhieh & Khorsandi, 2014).

With an increase in the number of catalyst coated beads from 50 (50% area) to 100 (100% area), degradation increased due to the active sites enhancement further leading to the formation of appropriate •OH radicals (Figure 4.75b). With the increase in the number of beads the quantity of Fe(III) also increases which helps in retarding the electron-hole recombination in the dual effect as it acts as an electron acceptor. After a further enhancement in the beads number to 150 (150% area covered), blockage of the active sites along with the increase in the void spaces leading to dead zone area. Actually, the concentration of leached iron from the beads also increases which blocks the active sites of TiO_2 (Bokare & Choi, 2014b; Ruales-Lonfat et al., 2015) leading to the decrease in the rate of degradation as shown in Figure 4.74. This restrains the electron (present in the conduction band of TiO_2) drawing capacity of the iron and further decreasing the efficiency. The capacity of H_2O_2 and Fe to act as an electron acceptor is reduced leading to the scavenging effect.

The combined effect of H_2O_2 dose along with the number of beads played a vital role in the degradation of the wastewater. At nearly 100 beads and H_2O_2 dosage of 900 mg L^{-1}, % COD reduction was observed to be maximum (Figure 4.75c). This was basically due to the combined effect of photocatalysis and photo-Fenton, which was happening simultaneously in the system. Actually here, in this case, leached iron would lead to photo-Fenton with the existence of the varying dose of H_2O_2 along with photocatalysis employing TiO_2 coated beads. The reduction in COD, BOD, TS, TDS related values pertains to the reduction in the pollution load of the wastewater, as shown in Table 4.25.

Table 4.25: Numerous characteristics of real pharmaceutical effluent after treatment

Parameters	**Concentration**
	After Dual effect process
Total suspended solids(TSS)	110 mg L^{-1}
Total dissolved solids(TDS)	2460 mg L^{-1}
Total solids(TS)	2570 mg L^{-1}
Nitrate ions	4.98 mg L^{-1}
pH	4.80
Turbidity (NTU)	30
COD	235 mg L^{-1}
BOD	95 mg L^{-1}
Biodegradability Index(BOD_5/COD)	0.510

In-situ dual process of photocatalysis and photo-Fenton leads to the generation of more •OH which helps in increasing the rate of reaction with the decrease in the treatment time. Increasing the number of beads to 100% leads to more •OH, thus increases the degradation but further increase in the number of beads (150%) and oxidant dose, the HO_2• , and H_2O_2 (consuming •OH) are formed (as seen in equation 4.55-4.57) which lowers the degradation.

$$H_2O \rightarrow \bullet OH + H^+ + e- \quad (4.55)$$

$$2\bullet OH \rightarrow H_2O_2 \quad (4.56)$$

$$\bullet OH + H_2O_2 \rightarrow HO_2\bullet + H_2O \quad (4.57)$$

For the optimization, the targeted response i.e. % COD reduction was kept to be maximum and the optimum parameters were found to be t= 3.65 min, the number of beads as 98 (98% area covered) and H_2O_2 dose as 800 mg L^{-1} to achieve % COD reduction as 71 %. For the confirmation of the statistical optimization, experiments were executed in triplicate. The mean and standard deviation for the % COD reduction is shown in Table 4.26. Good agreement between experimental values and predicted values (70%) was found out confirming the consistency of the model suggested by RSM. In most of the reported studies (Gholami, Ghasemi,

Anvaripour, & Jorfi, 2018; S. Talwar, Sangal, & Verma, 2018) the degradation of real wastewater was performed in slurry mode leading to the removal of COD in 5-6 h (Amat, Arques, López, & Miranda, 2005; F. Deng, Zhao, Luo, Luo, & Dionysiou, 2018; Maroneze, Zepka, Vieira, Queiroz, & Jacob-Lopes, 2014). But from this present study it was proven that the treatment of real wastewater could be performed using the fixed mode in reduced time (4 h) by incorporating in-situ dual effect with enhanced rate of reaction.

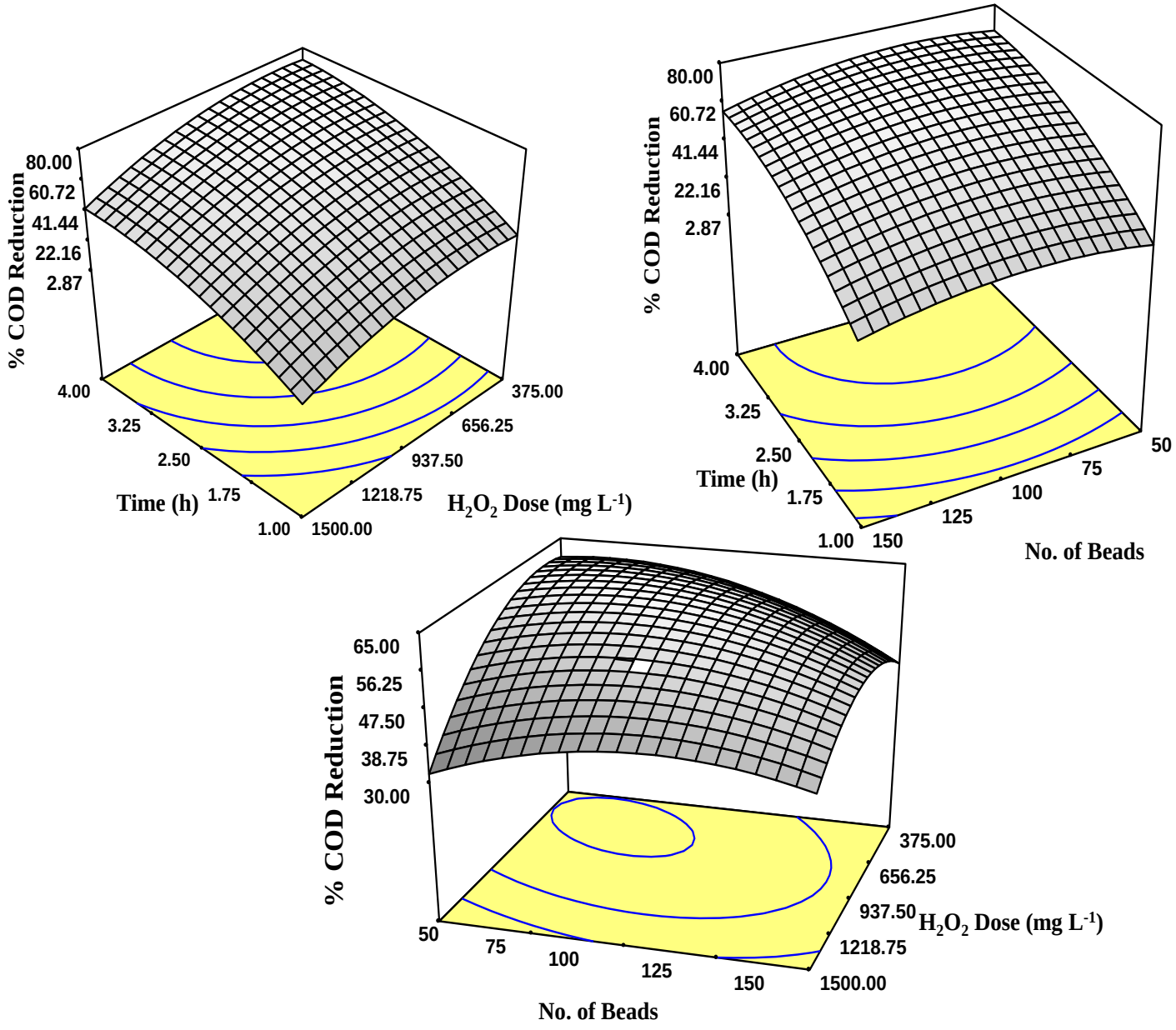

Figure 4.75: COD reduction 3-D graph of real pharmaceutical wastewater between a) time and H_2O_2 dosage, b) Time and number of beads i.e. surface area covered by beads, c) number of beads and H_2O_2 dosage

Table 4.26: Mean and Standard deviation of % COD reduction for real effluent

S.NO	Mean of % COD reduction	Standard deviation of % COD reduction
1	61.56667	0.550756
2	58.03333	0.404147
3	20.7	0.264575
4	36.18667	0.20133
5	66	0.5
6	19.84	0.852467
7	59.7	0.442267
8	26.33333	0.057735
9	36.25333	0.128583
10	12.31	0.104403
11	68.17	0.009998
12	53.56667	0.450926
13	48.35333	0.48014
14	58.55333	0.350048
15	33.86666	0.251661
16	62.33333	0.61101
17	55.6	0.300001

4.6.3. REACTION KINETICS AND SYNERGISTIC EFFECT

The degradation of the real effluent followed first order kinetics according to the equation 4.58:

$$\ln \frac{C}{C_0} = kt \qquad (4.58)$$

Where, C_0 is the initial COD reduction of the pollutant, C is the final reduction at time t (min). k is the first order rate constant(min^{-1}). Utilizing the rate constants (k) of the different processes synergy was evaluated. The rapid increment in the first order rate constant for dual effect (0.422 min^{-1}) as compared to photocatalysis (0.195min^{-1}) and photo-Fenton (0.125min^{-1}) substantiate the applicability of the dual process.

Synergistic effect of the dual process incorporating photo-Fenton and photocatalysis over the individual processes was calculated using the equations 3.5-3.7.

The synergistic effect of in-situ dual effect over photocatalysis process:

$$\% \text{ Synergy} = 100 \times \{(0.422 - 0.195)\}/0.422$$

$$\% \text{ Synergy} = 53.7\%$$

The synergistic effect of in-situ dual effect over photo-Fenton process:

$$\% \text{ Synergy} = 100 \times \{(0.422 - 0.125)\}/0.422$$

$$\% \text{ Synergy} = 70.37\%$$

The synergistic effect of in-situ dual effect over both photo-Fenton and photocatalysis process i.e overall synergy:

$$\% \text{ Synergy} = 100 \times \{(0.422 - (0.195 + 0.125))\}/0.422$$

$$\% \text{ Synergy} = 23.69\%$$

There was increment in the synergetic effects of dual process over both the processes due to the increase in the rate of reaction. With substantial synergistic effect as well as a reduction in treatment time, proposed dual effect put forward our novelty claim especially for the treatment of real pharmaceutical industry wastewater. In terms of the degradation time, results are comparatively better as compared to the cited literature (Sari, Agustina, Melwita, & Aprianti, 2017; Threrujirapapong, Khanitchaidecha, & Nakaruk, 2017).

4.6.4. CHARACTERIZATION ANALYSIS OF THE COMPOSITE BEADS

Intactness of TiO_2 coating, as well as systematic leaching of iron content, is the main challenging part of the current study as in the dual process both has a prominent role to play with. Thus, characterization of the composite beads was conducted for the confirmation of the novel dual process. Various characterizations (SEM-EDS, XRD, UV-DRS, FT-IR) of the catalyst coated composite beads were performed to further claim our novelty of the process in which both the processes take place at the same time at the same place.

For determining the surface morphology of beads SEM-EDS was used. Freshly coated beads and recycled beads were examined for confirming the changes in the morphology as shown in Figure 4.76a and b respectively. There was no significant difference between the beads even after recycle but some amount of TiO_2 was weathered from the surface. From the EDS sharp peaks of 'Ti', 'Fe' and of 'O' authenticated the iron's presence at the surface accompanied with long with the layer of TiO_2 confirming the dual effect to take place side by side. With the treatment, these solids cover the surface but they also get treated by the •OH radicals along with the ferrous ions present to form the intermediates.

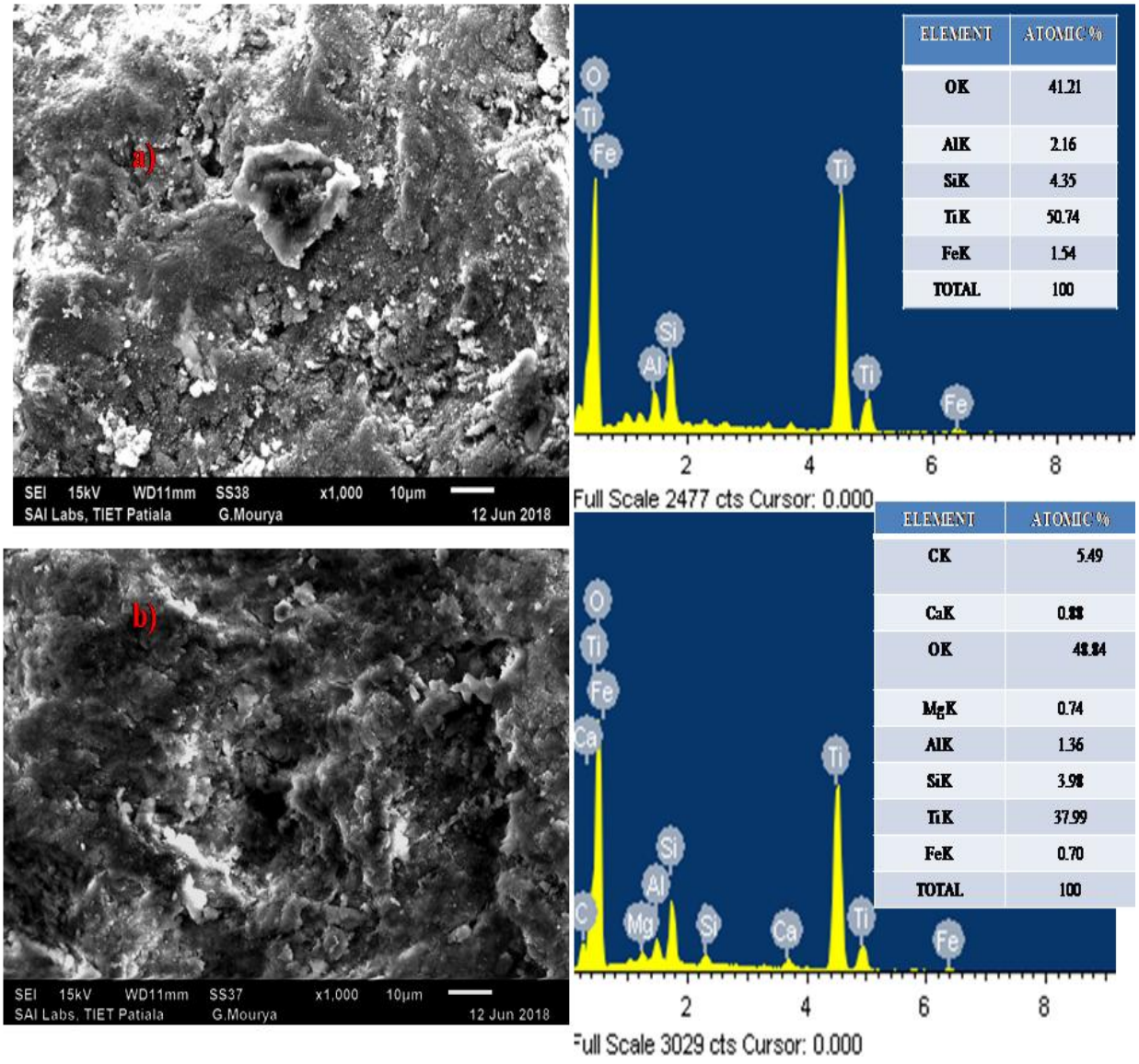

Figure 4.76: SEM-EDS analysis of a) fresh beads, b) recycled beads

The microstructural nature of catalyst was studied using XRD (Figure 4.77). Peaks corresponding to the P-25 TiO_2 were also observed as shown in the previous studies (Talwar et al., 2018b). The basic structure of TiO_2 i.e. having anatase and rutile phase was confirmed from the XRD analysis. Various peaks corresponding to the iron di-titanium oxides (IDO) and iron-titanium oxides (ITO) were also revealed which confirmed the presence of iron with TiO_2 composite in the beads. This composite helps in the validation of our claim for effective utilization of the dual process to take place at the same time.

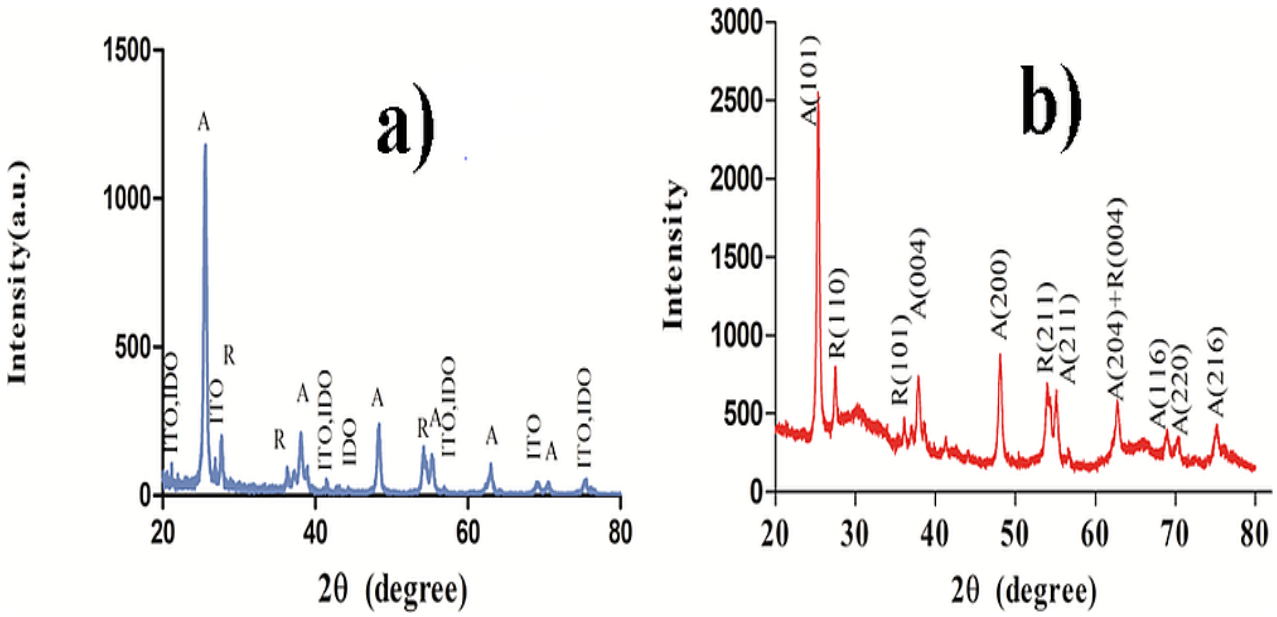

Figure 4.77: XRD plot of the fresh composite beads and Fresh P25 TiO_2

FTIR spectra of freshly coated beads, as well as recycled beads in comparison with the P-25TiO_2, are shown in Figure 4.78. The occurrence of peaks analogous to wave number ranging from 800-1200 cm^{-1} in both spectrums substantiates the presence of Ti-O-Ti (400-100 cm^{-1}) was present in both fresh as well as recycled samples thus confirming the withholding of TiO_2 lattice (Sayyar, Akbar Babaluo, & Shahrouzi, 2015). The stretching at 450 to 550 cm^{-1} (Ali et al., 2017) confirms the presence of Fe-O bonding existing in the fresh as well as recycled composite. The transmittance bands occurring at 1627.02 cm^{-1} and 1632.63 cm^{-1} with subject to composite beads and TiO_2 respectively symbolize the Ti-OH groups. Thus, FT-IR results confirm the correlation with XRD pattern which already validated the presence of several forms of iron oxide i.e. 'DO', 'DTO' and 'ITO'. The occurrence of transmittance band at 3410.82 cm^{-1} and 3407.91 cm^{-1} in case of composite beads and TiO_2 could be related with the existence of O-H groups stretching vibrations.

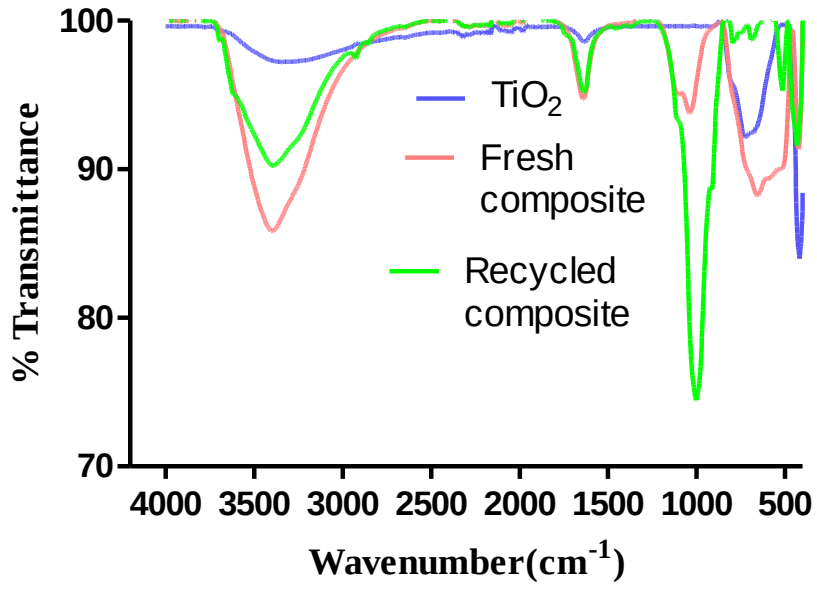

Figure 4.78: FTIR of TiO_2, Fresh TiO_2 –Fe composite and recycled TiO_2 –Fe composite

Band gap energy was evaluated using UV-visible DRS (diffuse reflectance spectroscopy). Band gap energy of the P-25 TiO_2 was compared with the fresh and recycled catalyst of the Fe-TiO_2 composite (Figure 4.79). The scan for UV-visible was conducted from 200-800 nm. A minor change was noticed in the spectra of the composite catalyst over TiO_2 composite showing the capability of the composite to absorb light even in the visible spectrum.

$$E = \hbar c/\lambda \qquad (4.59)$$

Band gap energy was evaluated to be 3.08 eV for the fresh composite (equation 4.59) and 2.9 eV for the recycled. confirming the retention of the catalyst activity as well as the photoresponse efficiency.

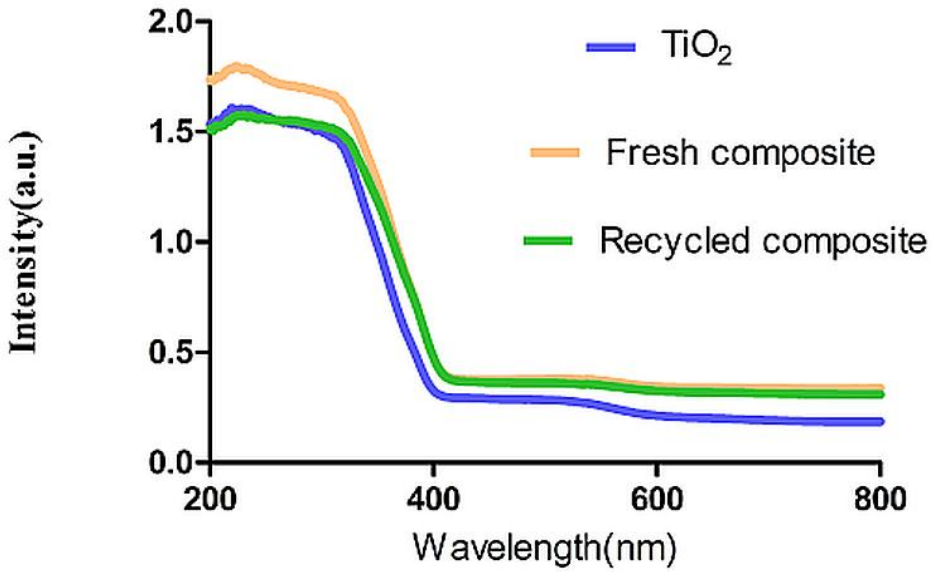

Figure 4.79: UV-Vis DRS fresh TiO_2-P25, and Fresh composite beads and Recycled composite beads

4.6.5. INTERMEDIATES ANALYSIS AND PARAMETRIC QUALITY OF TREATED EFFLUENT

The treated effluent was characterized for various parameters as shown in Table 4.25, clearly indicates the efficacy of the dual process. As per the suggested standards by the Central Pollution Control Board (CPCB) the treated wastewater was fit to be disposed of as the COD was 235 mg L^{-1} and BOD was 95 mg L^{-1}. The treated water was fit for the usage in the irrigation lands as suggested by the CPCB (CPCB, 2009). Increase in biodegradability and reduction in turbidity of the treated effluent further cementify our claim for the commercial applications of this technology. However further detailed analysis is required in terms of by-products analysis and their toxicity. In this context, GC-MS and toxicity analysis was conducted for untreated and treated effluent at the optimized conditions.

Although it was very difficult to predict the pathway of the real pharmaceutical wastewater due to the presence of various organic and inorganic compounds but the authors have tried to predict the pathway of the effluent. As the pharmaceutical industries produces drugs in various batches hence making it very difficult to evaluate the stage of the effluent. The intermediates identified

from the degradation of wastewater were shown in (Figure 4.80). The expected pathways for the degradation were explained based upon the identified intermediates from chromatograms. The fragmentation of 3-[(Trimethylsilyl) oxy] androstane-11, 17-dione 17-(O-benzyloxime) lead to the formation of by-products as shown in (A). With further reduction and fragmentation in (B) could produce a product as shown. In 6-Acetoxy-2,6,10,10-Tetramethyl-1-Oxa-Spiro(4.5)Dec-3-Ene hydroxylation could takes place (C). After that reduction of the byproducts in the form of demethylation could take place as shown in (D). Further, the reduced byproduct could be obtained (E). 6-Nitro-1h-Indazole-5-Carboxylic Acid could be reduced (F) using decarboxylation and removal of nitrate and nitrite ions. Further, the cleavage i.e. deamination could take place as shown in (G) leading to the formation of ammonium ions. Dl-3,4-Dimethyl-3,4-Hexanediol using decarboxylation lead to the by-product (H). Further demethylation in (I) could lead to the final product.

The Kirby bauer method is based on the principle of the antibiotic-impregnated disk. The previously inoculated agar placed with the test strain and the wastewater diffuses radially outward through the agar medium producing concentration gradient. A standardized inoculum was used to inoculate agar plates of the test microorganism. The test compound enclosed at the desired concentration in the filter paper discs (about 6 mm in diameter) was placed on the agar surface. The incubation of the Petri dishes was performed for 24 h at 37^0C.

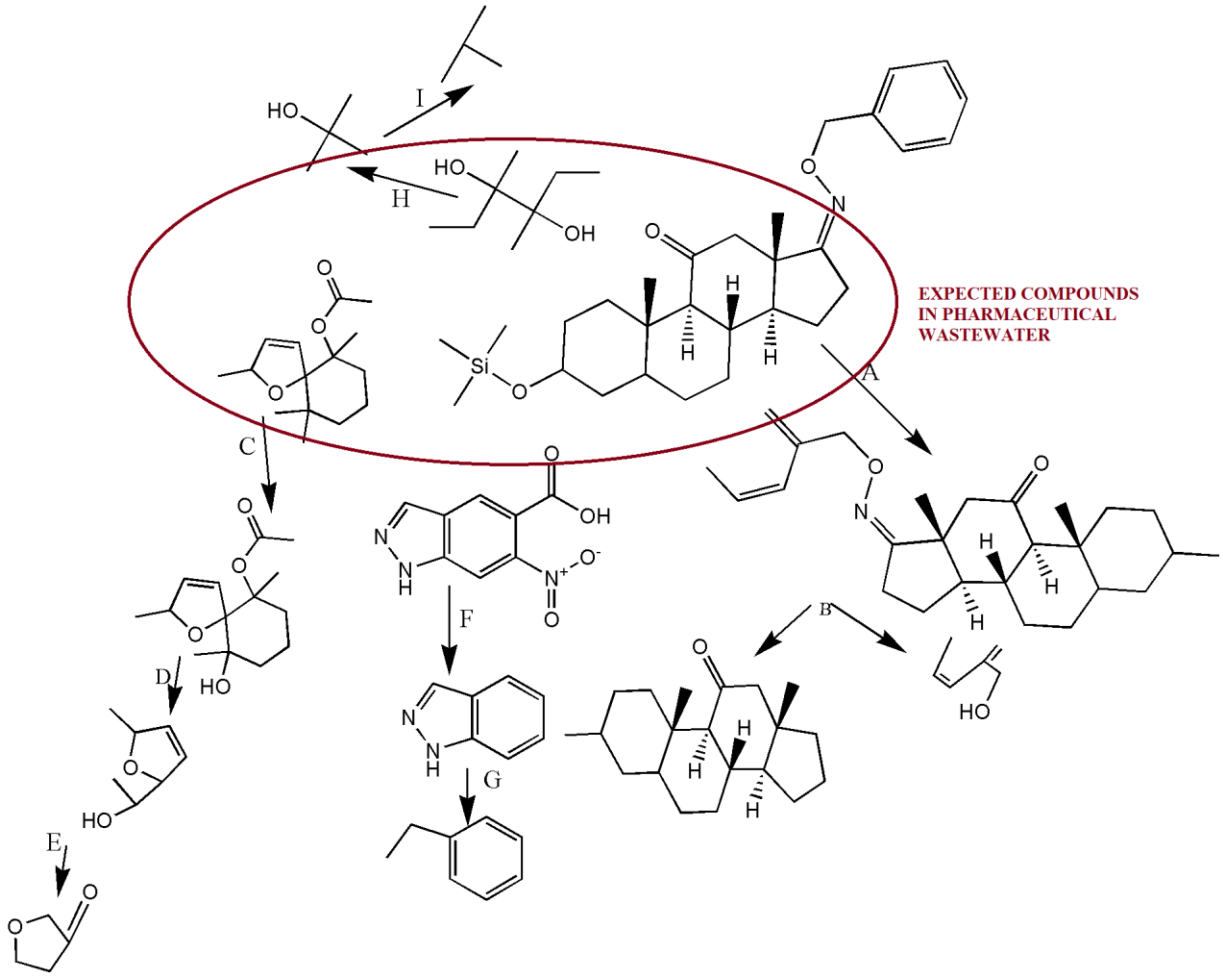

Figure 4.80: The analyzed intermediates formed during the degradation

The identified compounds by GC-MS analysis of untreated wastewater are mostly long chained compounds (Table 4.27) as confirmed earlier from the spectrophotometer spectra of wavelength 200 to 260 nm (Figure 4.81). From the GC-MS analysis, the highest matching % was found to be siloxane which is used as a covering of the capsules basically sealants, and antifoaming agents. Majority of the identified compounds exhibited in the untreated wastewater were eradicated using the in-situ dual process as clear from GC-MS analysis.

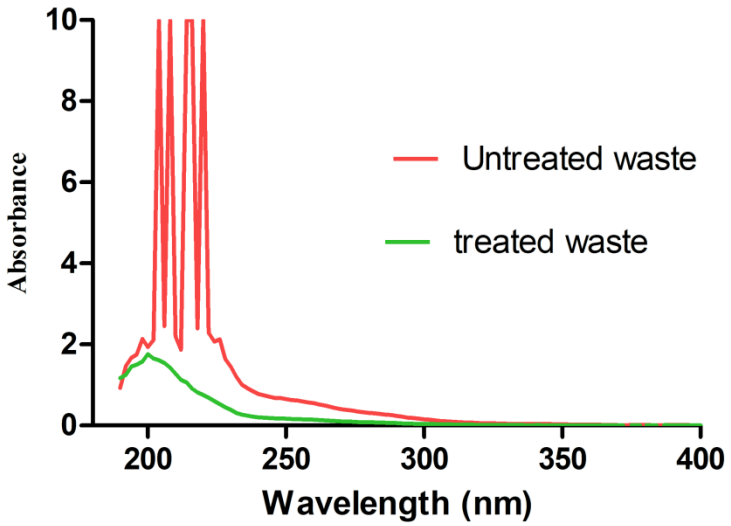

Figure 4.81: The scan of the pharmaceutical wastewater before and after treatment

Table 4.27: List of various compounds identified with GC-MS Analysis in Untreated effluent

S.No	Compound	Retention Time	Molecular Mass	Molecular Formula	Matching %	Uses and Comment
1.	6-Nitro-1h-Indazole-5-Carboxylic Acid	55.12	207	$C_8H_5O_4N_3$	71.8%	It is used in the synthesis of active pharmaceutical drugs
2.	Dl-3,4-Dimethyl-3,4-Hexanediol	55.03	146	$C_8H_{18}O_2$	80.2%	It used for encapsulation for improving flexibility and hardness
3.	6-Acetoxy-2,6,10,10-Tetramethyl-1-Oxa-Spiro(4.5)Dec-3-Ene	55.45	252	$C_{15}H_{24}O_3$	73.8%	It is used as a flavouring agent
4.	Silane, 1,4-Phenylenebis[Trimethyl	55.62	222	$C_{12}H_{22}Si_2$	65%	It is toxic in nature , may cause cancer
5.	1,3-Bis(Trimethylsilyl)Benzene	59.85	222	$C_{12}H_{22}Si_2$	86%	It is used as antineoplastic agent
6.	2,3-Anhydro-D-Galactosan	53.03	162	$C_6H_{10}O_5$	80%	Used as therapeutic agent
7.	Androstane-11,17-Dione, 3-[(Trimethylsilyl)Oxy]-, 17-[O-(Phenylmethyl)O	55.07	481	$C_{29}H_{43}O_3NSi$	65%	Anticancer, Antitumour and Antimicrobial Activity

Table 4.28: List of various compounds identified with GC-MS Analysis in treated effluent

S.No	Compound	Retention Time	Molecular Mass	Molecular Formula	Matching %	Uses and Comment
1.	Acetaldehyde	28.06	44	C_2H_4O	87.9%	It is used as the flavoring agent
2.	Decamethyl-Tetrasiloxane	48.73/52.73/59.37	310	$C_{10}H_{30}O_3Si_4$	80.2%/78%/80.7%	It used for encapsulation
3.	6-Nitro-1H-Indazole-5-Carboxylic acid	55.12	207	$C_8H_5O_4N_3$	71.8%	It is used in the synthesis of active pharmaceutical drugs

4.6.6. SCALE-UP

Although it is not exactly feasible to scale-up the lab scale trails with accurate cost analysis because of energy intensive parameters involved in scaling up studies. Attempts have been made in this work to approximate the cost involved for prototype experimentation. To further hit the approximation with some accuracy, the dual process was scaled up to check the practical feasibility at the industrial level. The conditions which were optimized at the lab scale operations were employed for the treatment of pharmaceutical wastewater at pilot-scale.

The scale-up operation utilizing FE+FS beads for assimilating in-situ dual effect was performed employing a pilot scale reactor of the handling volume of 5L. The flow rate of the effluent was kept as 2 L h^{-1}. The optimized H_2O_2 dose of 800mg L^{-1} and with the covered surface area of 98% was used for the reaction as per the available area of the reactor. The space-time for the reactor was 25 min and the system was operated in continuous mode with re-circulation.

To claim our approach for practical applications of this technology, used composite beads (more than 30 cycles) were used in the pilot-scale reactor for the degradation of wastewater. In this case, especially in flow conditions, 75% COD reduction was obtained after 5 h (Figure 4.82). Initially for the first 2 h degradation was faster due to the prominence of photocatalysis (active layer of TiO_2) and photo-Fenton (leached iron). Thus, assuring outcomes even at pilot-scale for the efficient removal of real industrial wastewater using solar light validated the pilot scale usage of an in-situ dual process in fixed-bed mode encompassing composite beads. In fact, this is one of few studies reporting the relevance of fixed-bed in-situ process for the removal of industrial wastewater.

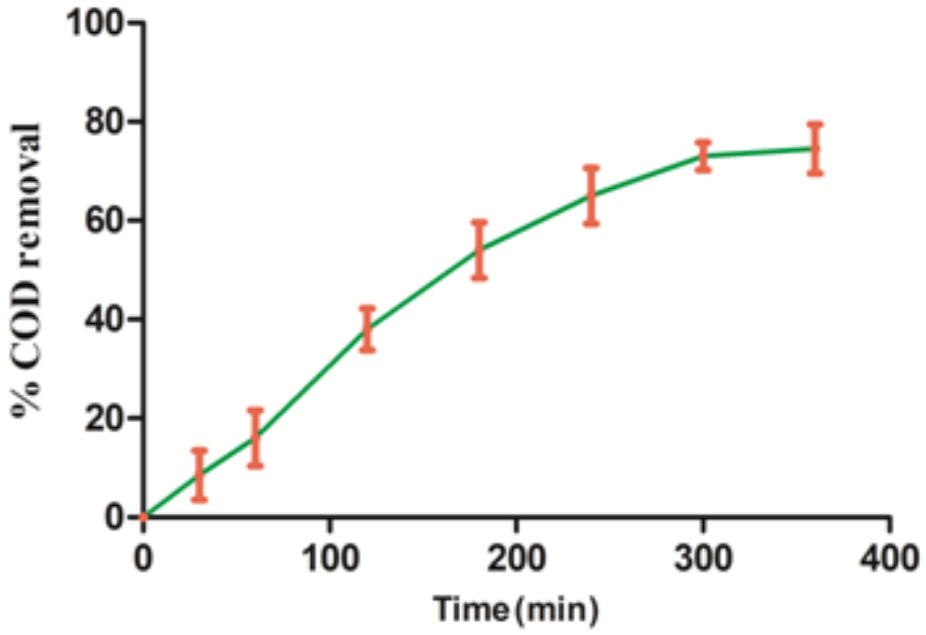

Figure 4.82: % COD reduction of real pharmaceutical wastewater using fixed bed baffled reactor

4.6.7. TREATMENT USING REACTORS IN SERIES

For providing the realistic view to this plug flow approaching reactor and the technology used, the real wastewater from the pharmaceutical industry was treated at the optimized conditions. The initial characterization of the wastewater includes the COD 1300 ±20 mg L^{-1}, BOD of 200±10 mg L^{-1},Suspended Solids of 800 mg L^{-1} and Turbidity of 74 NTU. With 55% of COD removal after 45 minutes proves the effectiveness of the process using three reactors in series model (as shown in Figure 4.83). The degradation of real effluent was fast initially as 42% COD removal was obtained after 2ndreactor, but it stabilized subsequently in the 3rd reactor. The final degradation was observed to be approximately 55%. This might be due to the formation of intermediates in between, leading to the slower removal rate. The process can be further optimized using more reactors as well as modifying the design of the reactor.

The final characterization of the treated wastewater showed the COD of 580±20 mg L^{-1}, BOD of 295±10 mg L^{-1}, suspended Solids of 800 mg L^{-1} and Turbidity of 28 NTU. The biodegradability index of 0.51 proved that the wastewater was biodegradable and could be further treated using the conventional biological treatment techniques.

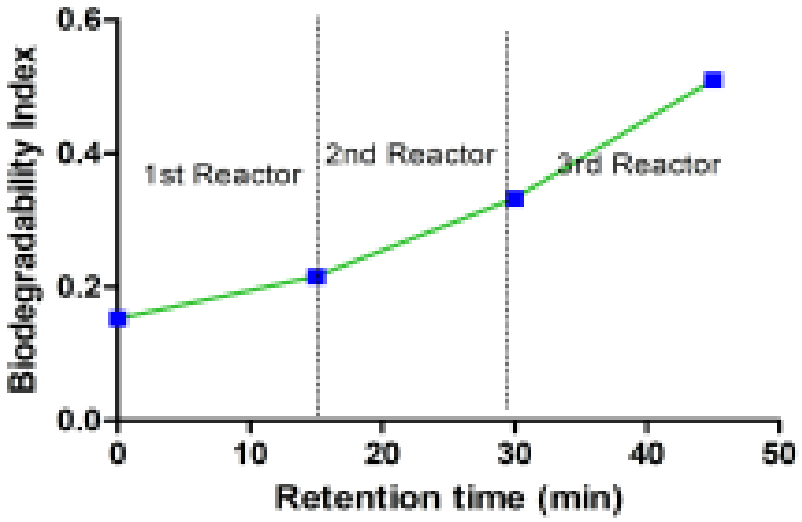

Figure 4.83: The outcome of Biodegradability Index with retention time at the optimized conditions

4.6.8. COST ANALYSIS

Efforts have also been made to approximate the total cost of the process taking into deliberation the total cost of Fe-TiO_2 composite, light source, oxidant used, the fabrication cost of the reactor and including electricity cost (Table 4.29). Dual process contributed to significant reduction of treatment cost i.e. US $ 0.14 L^{-1} of the waste water sample.

Further for the analysis at the large scale, the energy intensive parameters should be taken into consideration. The scale-up cost analyses have been carried out as shown in Table 4.29 using equation 4.60. The rule of sixth tenth was evaluated for the scale up calculations (Tribe & Alpine, 1986).

$$\mathrm{COST}_{\mathrm{prototype}} = \mathrm{COST}_{\mathrm{model}} \left(\frac{\mathrm{SIZE}_{\mathrm{prototype}}}{\mathrm{SIZE}_{\mathrm{model}}}\right)^{\mathrm{N}} \qquad (4.60)$$

This cost can be further minimized in scale-up studies by efficient designing of the reactor and other engineering modifications. Based upon the parameters involved the benefit in the cost was also evaluated. Cost being the important parameter for the field scale applicability of the process (Sharmila, Kumar, Banu, Yeom, & Saratale, 2019). From the scaling up process the cost came out to be less than 0.1 $ L^{-1} confirming the viability of the process.

Table 4.29: Cost analysis for the degradation of industrial wastewater using in-situ dual process

COST OF RAW MATERIAL
Fuller's Earth cost = 100$/ton=.1$ Kg^{-1}
Total Cost for beads=0.2$
Cost of foundry sand=0$
Cost of TiO_2 used= 0.099$(30 gm)
Electricity cost = 0.015 US $ Kwh^{-1}
Energy used by Muffle furnace for baking of beads at high temperature =3kwh
Cost of electricity=3×0.015=0.045$
Total cost for the beads=0.2+0.099+0.045=0.344$
Oxidant used for the reaction-H_2O_2
Usage of H_2O_2 = 15 mL for 5L
For 50 runs= 15×50=765 mL =0.765 L
Cost of H_2O_2= 5.86$ 0.5 L^{-1}
Total cost of H_2O_2 used=8.956$
COST OF THE Reactor and other materials
Cost of the reactor = 15$
Cost of the pipes and valves =2$
Total cost = 17 $

COST OF THE COD REDUCTION OPERATION

Cost of sunlight= 0$

Total number of reactions =50

Volume of waste water treated = 5 L × 50 = 250 L (0.25 m^3)

Cost of beads and H_20_2 for total wastewater = (0.344+8.956) $=9.3$

COD reduction =81%

Initial COD= 1250 mg L^{-1}

Final COD =235 mg L^{-1}

Removal of COD =1015 mg L^{-1} = 1.015 kgm^{-3}

Total cost for removal of COD = (0.344+8.956)/1.015=9.16$/ kg of COD removal

Pumping cost for the treatment process=Energy consumed × cost of electricity

Energy consumed by Pump =0.11KWh

Energy consumed per kg of concentration removal = 0.11/0.25 = 0.44 kWh per kg of COD removal

Cost = 0.0066 $ KWh^{-1}

Overall cost of the operation=COD removal cost + pumping cost =9.16+0.0066=9.1666$/Kg of COD removal

Total cost for 150 reactions =9.1666+17+0.344+8.956=55.46$

For 1 reaction, cost =0.37US $

4.6.9. RECYCLABILITY OF THE BEADS

The main challenging task in using composite beads is to establish the dual effect for the continuous number of cycles i.e. continuous leaching of iron from the support besides maintaining the surface activity of TiO_2. In our study, we have successfully recycled the composite beads for more than 150 runs devoid of much decrease in the efficiency of degradation. In all these recycles dual effect was maintained i.e. both iron leaching (Figure 4.84) and TiO_2 activity (Figure 4.85) was intact. The recyclability of FE+FS beads was evaluated using the % COD removal of the effluent with consequent recycles. With the subsequent usage of the same beads, nearly 14% reduction in the COD efficiency was observed after 30 runs.

For further authentication in the perspective of the industrial scale applications of the process, the extended recyclability studies were conducted on the previously used FE+FS beads for at least 150 cycles. These old composite beads were still capable for contributing 65% COD removal after 4 h. Significant reduction even with used beads proposes that the dual effect could be implemented at a large scale for commercialization and for the industrial wastewater treatment purposes. The mean and standard deviation for the % degradation is shown in Table 4.30.

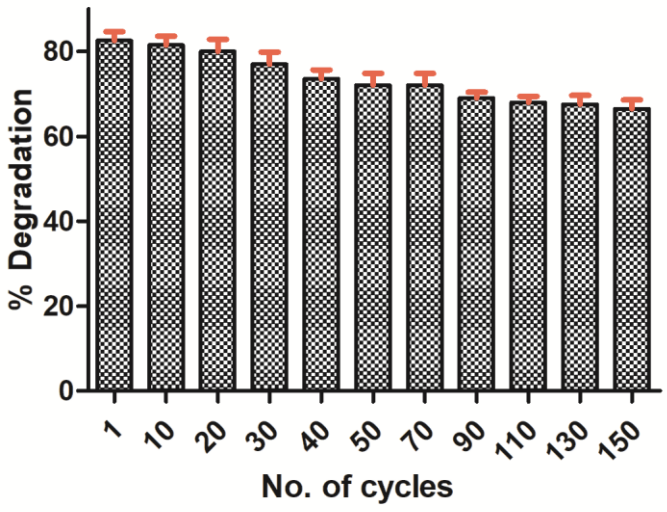

Figure 4.84: Recyclability studies of FE+FS composite beads for the degradation of effluent

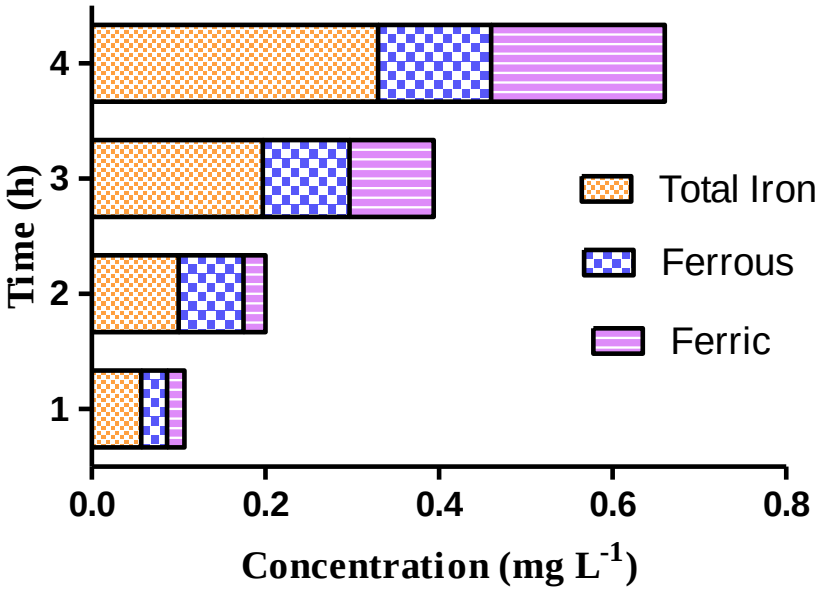

Figure 4.85: Iron content leached from the composite beads after 150 recycles

Table 4.30: Mean and Standard deviation of % degradation in recyclability for real effluent

No. of recycles	Mean of % Degradation	Standard Deviation of % Degradation
1	83.66	3.05
5	82	2.65
10	79.66	2.082
15	77.34	2.52
20	75.34	3.05
25	72.67	2.52
30	72.67	2.52
35	70.34	2.52
40	69.34	2.082
45	68.34	2.082
50	67.34	2.082

4.6.10. TOXICITY ANALYSIS

For the evaluation of the quality of the treated and untreated wastewater, toxicity analysis was performed. The toxicity test was performed using the *E-Coli* strain using the Kirby-Bauer method. The 0.5 cm well was punched in the agar plates, and addition of 30µL of the wastewater took place. Further incubating the plates at 27°C for 24 h. Cytotoxicity of the untreated and the

treated wastewater was evaluated. The cytotoxicity was evaluated in terms of the zone of inhibition. A large zone of inhibition was obtained for the untreated wastewater which disappeared after the process treatment of 4 h (Figure 4.86). The growth of the strain confirmed that the sample was non-toxic.

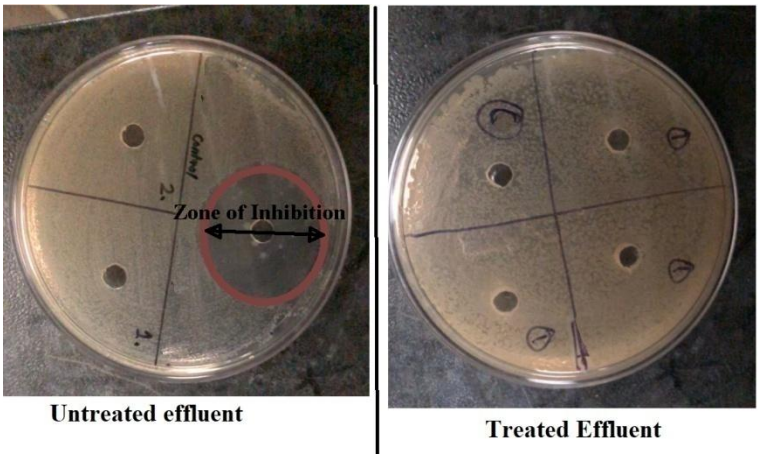

Figure 4.86: Kirby –Bauer test for the untreated and treated pharmaceutical effluent

Hence, it was finally concluded that the treated wastewater was non toxic in all respects. Thus, making the in-situ dual effect utilizing the highly durable and efficient composite beads which are highly effective for the industrial scale applications.

CHAPTER-5

CONCLUSIONS AND RECOMMENDATIONS

5.1. CONCLUSIONS

The novel concept of the application of the in-situ dual effect of photocatalysis and photo-Fenton in fixed mode has been studied for the degradation of pharmaceutical drugs i.e. phenazone (PHZ) and Metronidazole (MTZ). The application of composite materials made up of natural Fuller's Earth (FE) and waste Foundry Sand (FS) were employed for the degradation of pharmaceutical wastewater.

The fixed bed study involved the degradation of pharmaceutical compounds utilizing composite beads made up of FE and FE+FS. The composite materials wer involved in the subsequent leaching of iron prompting to in-situ photo-Fenton reactions while TiO_2 layer immobilized upon the support involved in photocatalysis. The composite support was chosen based upon the strength of beads, intactness of layer of TiO_2 and continuous iron leaching. After evaluation of these factors FE+FS beads depicted their proficiency in terms of strength, recyclability, coating and degradation of compound. For the optimization of the experiments Box Behnken Design (BBD) under Response Surface Methodology (RSM) was used. Hence, these TiO_2 coated FE+FS composite beads showed 80% of the degradation of PHZ with overall synergy of 60% over the individual processes of photo-Fenton and photocatalysis. The degradation of PHZ followed first order kinetics. The composite beads were successfully recycled for more than 35 cycles with negligible loss in degradation efficiency which was further confirmed from the characterizations including XRD, SEM, EDS, and UV-DRS. The recyclability varies invariably depending upon the phase of the study. The optimization conditions obtained for PHZ degradation were H_2O_2 dose of 45 mg L^{-1}, treatment time of 5.3 h and covered surface area of 95.7%. Further the mineralization of the PHZ was confirmed with the formation of nitrate, nitrite and ammonical ions and in terms of reduction in TOC (75%) and COD (78%). The plausible degradation pathway for the PHZ was predicted based upon the intermediates formed using GC-MS analysis.

Utilizing the same FE+FS composite beads, MTZ was treated using in-situ dual effect. 81% of the synergistic effect was observed as compared to the distinct processes with the degradation of 91%. The maximum degradation was achieved in 120 min with the oxidant dosage of 1050 mg L^{-1}, pH of 3.5, UV intensity of 25Wm^{-2} and A/V ratio of 0.273 cm^2 mL^{-1}. Modeling of the data was performed using ANN with further optimization utilizing GA. The reliability was examined with the model prediction and the validation of GE results using experimental analysis. The composites beads were successfully recycled for more than 70 cycles and without loss in the activity of catalyst as confirmed from the analysis of XRD, SEM, FT-IR, Raman spectroscopy, EDS and UV-DRS. The electrical energy consumption also substantiated the effectiveness as 70-80% less energy was consumed as compared to the individual processes. Further mineralization of the MTZ was confirmed from the reduction in COD as well as TOC with formation of ions.

For the field scale applications of the dual process, the scale up trials were also executed. Three reactors connected in series were employed in the once through mode for the degradation of MTZ. The three reactors in series approached the plug flow behavior as confirmed from the Residence time distribution studies with Pecklet number (Pe) of 18 and mean residence time (MRT) of 42.8 min. At the optimum conditions, three reactors in series with flow rate of 8L h^{-1}, 75% area covered by the beads showed a maximum degradation of 84% of MTZ. The mineralization of MTZ was confirmed with the 55% COD reduction along with formation of various ions including nitrates, nitrites. The Fe-TiO_2 composite beads were successfully recycled for more than 80 cycles with the intactness of the activity as confirmed from XRD, SEM, EDS, and DRS. For the real life applications of the process the overall cost along with the scale up cost was evaluated which came out to be less than 0.1$ confirming the commercial viability of the process.

Similarly the PHZ was effectively degraded using reactors in series. The complete reactor hydrodynamics was studied for the optimization of the configuration as well as the conditions. As confirmed from the hydrodynamics study as well as the optimized conditions suggested by BBD, three reactors with flow rate of 10.0 L h^{-1} , 100% surface area covered and 200 mg L^{-1} of H_2O_2 dose showed the maximum degradation. The composite beads were checked for the extended durability and they were durable enough even after 200 recycles as confirmed from

analysis including XRD, SEM, FTIR, Raman spectroscopy, EDS, and DRS. The intermediates analyzed were used for predicting the pathway for the degradation of PHZ.

The scale up studies were further extended by utilizing another type of reactor i.e. compound parabolic concentrator (CPC). The fixed bed CPC employing the composites made of FE+FS with TiO_2 layer immobilized was used for the degradation of MTZ. The 6 CPCs attached in series behaved as plug flow regime as confirmed from the RTD analysis of the model with reactors in series model confirming 10 reactors attached in series. 84.44% of enhancement along with the 2.19 fold of synergy was observed in case of dual effect as compared to the individual photocatalysis and photo-Fenton. With the hydraulic retention time of 15 min, 6 parabolic reactors connected in series, H_2O_2 dose of 450 mg L^{-1}, has led to maximum removal of 60%. Additionally, 45–50% COD reduction accompanying the formation of nitrate, nitrite ions confirmed the mineralization. Retention of dual catalytic activity without much deterioration even after 40 recycles confirms its applications at industrial scale. The overall economic analysis revealed the total cost approximately 0.1$ L^{-1} illustrating the field scale feasibility of the process. Furthermore the scale-up studies have substantiated the feasibility of prototype in commercial scale practical applications.

Finally, for confirming the real time applications of the in-situ dual effect, the real industrial pharmaceutical wastewater was treated. The significant reduction in Chemical Oxygen demand (COD) (81%) along with the decrease in the treatment time by 60-70 min was perceived as compared to the exclusive processes of photo-Fenton and heterogeneous photocatalysis. The optimum conditions of 3.65 h of treatment time, the 98% of the surface area covered, and H_2O_2 dose of 800 mg L^{-1} proposed to achieve % COD removal of 71%. The biodegradability index was increased from 0.15 to 0.510 making it biodegradable.The treated wastewater was evaluated to be non-toxic as verified from the GC-MS analysis as well as the Kirby-Bauer test. For the scaling up of the process, treatment of 5L of wastewater was performed in continuous mode with a COD reduction of 75% in 5 h. Various characterizations were performed to validate the importance of the dual effect (presence of iron as well as the activity of TiO_2). Recyclability of the catalyst even after 150 recycles confirmed the economic efficacy of the process. Scale up cost analysis of the prototype has been conducted for the feasible evaluation of the process.

Further the wastewater was even treated using reactors in series model and 55% of COD was removed in 45 minutes.

Hence, the extended applications of the novel composite for the degradation of real pharmaceutical wastewater even at large scale confirms the commercial scale viability of the in-situ dual effect.

5.2. RECOMMENDATIONS

The FE+FS composite beads have shown their potential in terms of the degradation efficiency of the pollutants including pharmaceuticals drugs as well as the durability of the composite. The utilization of the naturally available fuller's earth and the industrial waste foundry sand has proven to be a good option. The future research work would emphasize on the utilization of the other waste materials from the industries as a source and even act as the good binder for the effective durability of the composites. The future study would include the more scale up options based upon the cost effective and technical analysis for industrial scale applications of the in-situ dual effect. Using other reactors for the implementation of the dual effect can also be a good option. Extending the concept to the even other industries, and proving to be the boon for them in terms of cost and extended reusability of the catalyst.

REFERENCES

Abbas, S. Z., Dupont, V., & Mahmud, T. (2017). Kinetics study and modelling of steam methane reforming process over a NiO/Al_2O_3 catalyst in an adiabatic packed bed reactor. *International Journal of Hydrogen Energy*, *42*(5), 2889-2903. https://doi.org/10.1016/j.ijhydene.2016.11.093

Abdel-Maksoud, Y., Imam, E., & Ramadan, A. (2016). TiO_2 Solar Photocatalytic Reactor Systems: Selection of Reactor Design for Scale-up and Commercialization—Analytical Review, *6*(9), 138.. *Catalysts*. https://doi.org/10.3390/catal6090138

Abhishek, N., Jenamani, M., & Mahanty, B. (2017). Urban growth in Indian cities: Are the driving forces really changing? *Habitat International*, *69*,48-57. https://doi.org/10.1016/j.habitatint.2017.08.002

Abu-Reesh, I. M., & Abu-Sharkh, B. F. (2003). Comparison of Axial Dispersion and Tanks-in-Series Models for Simulating the Performance of Enzyme Reactors. *Industrial and Engineering Chemistry Research*, *42*(22), 5495-5505. https://doi.org/10.1021/ie030131j

Adams, M., Skillen, N., McCullagh, C., & Robertson, P. K. J. (2013). Development of a doped titania immobilised thin film multi tubular photoreactor. *Applied Catalysis B: Environmental*, *130-131*, 99-105. https://doi.org/10.1016/j.apcatb.2012.10.008

Adish Kumar, S., Sree lekshmi, G. S., Rajesh Banu, J., & Tae Yeom, I. (2014). Synergistic degradation of hospital wastewater by solar/TiO_2 /Fe^{2+}/H_2O_2 process. *Water Quality Research Journal of Canada*, *49*(3), 223. https://doi.org/10.2166/wqrjc.2014.026

Agatonovic-Kustrin, S., & Beresford, R. (2000). Basic concepts of artificial neural network (ANN) modeling and its application in pharmaceutical research. *Journal of Pharmaceutical and Biomedical Analysis*, *22*(5), 717–727. https://doi.org/10.1016/S0731-7085(99)00272-1

Ahmed, S., Rasul, M. G., Brown, R., & Hashib, M. A. (2011). Influence of parameters on the heterogeneous photocatalytic degradation of pesticides and phenolic contaminants in wastewater: A short review. *Journal of Environmental Management*, *92*(3), 311-

330.https://doi.org/10.1016/j.jenvman.2010.08.028

Ahmed, S., Rasul, M. G., Martens, W. N., Brown, R., & Hashib, M. A. (2010). Heterogeneous photocatalytic degradation of phenols in wastewater: A review on current status and developments. *Desalination*, *261*(1-2), 3-18. https://doi.org/10.1016/j.desal.2010.04.062

Al-Mamun, M. R., Kader, S., Islam, M. S., & Khan, M. Z. H. (2019). Photocatalytic activity improvement and application of UV-TiO_2 photocatalysis in textile wastewater treatment: A review. *Journal of Environmental Chemical Engineering*, *7*(5), 103248. https://doi.org/10.1016/j.jece.2019.103248

Ali, T., Tripathi, P., Azam, A., Raza, W., Ahmed, A. S., Ahmed, A., & Muneer, M. (2017). Photocatalytic performance of Fe-doped TiO_2 nanoparticles under visible-light irradiation. *Materials Research Express*, *4*(1), 015022. https://doi.org/10.1088/2053-1591/aa576d

Alinsafi, A., Evenou, F., Abdulkarim, E. M., Pons, M. N., Zahraa, O., Benhammou, A., … Nejmeddine, A. (2007). Treatment of textile industry wastewater by supported photocatalysis. *Dyes and Pigments*, *74*(2), 439–445. https://doi.org/10.1016/j.dyepig.2006.02.024

Alrousan, D. M. A., Polo-López, M. I., Dunlop, P. S. M., Fernández-Ibáñez, P., & Byrne, J. A. (2012). Solar photocatalytic disinfection of water with immobilised titanium dioxide in re-circulating flow CPC reactors. *Applied Catalysis B: Environmental*, *128*, 126–134. https://doi.org/10.1016/j.apcatb.2012.07.038

Amat, A. M., Arques, A., López, F., & Miranda, M. A. (2005). Solar photo-catalysis to remove paper mill wastewater pollutants. *Solar Energy*, *79*(4), 393–401. https://doi.org/10.1016/j.solener.2005.02.021

APHA/WEF/AWWA. (2018). 4500-NO_2 Nitrogen (Nitrite) (2017). In *Standard Methods For the Examination of Water and Wastewater*. doi: doi:10.2105/SMWW.2882.088.

APHA. (2017). 3500-Fe B Phenanthroline Method. *Standard Methods For the Examination of Water and Wastewater (23rd edition).*

APHA, AWWA & WEF (2005a). 4500-NH_3 Nitrogen (Ammonia). in *Standard Methods for the Examination of Water and Wastewater*.

APHA, AWWA & WEF (2005b). 4500 - Nitrate - Ultraviolet Spectrophotometric Screening Method. in *Standard Methods for the Examination of Water and Wastewater*. doi: 10.2105/AJPH.51.6.940-a.

APHA. (2000). 5220 - Chemical oxygen demand (COD). In *Standard Methods for the examination of water and wastewater*.

Asiltürk, M., Sayilkan, F., & Arpaç, E. (2009). Effect of Fe^{3+} ion doping to TiO_2 on the photocatalytic degradation of Malachite Green dye under UV and vis-irradiation. *Journal of Photochemistry and Photobiology A: Chemistry*, *203*(1), 64-71. https://doi.org/10.1016/j.jphotochem.2008.12.021

Dasaram, B., Satyanarayanan, M., Sudarshan, V., & Keshav Krishna, A. (2011). Assessment of Soil Contamination in Patancheru Industrial Area, Hyderabad, Andhra Pradesh, India. *Research Journal of Environmental and Earth Sciences*, 3(3), 214-220

Autin, O., Hart, J., Jarvis, P., MacAdam, J., Parsons, S. A., & Jefferson, B. (2013). Comparison of UV/TiO_2 and UV/H_2O_2 processes in an annular photoreactor for removal of micropollutants: Influence of water parameters on metaldehyde removal, quantum yields and energy consumption. *Applied Catalysis B: Environmental*, *138–139*, 268–275. https://doi.org/10.1016/j.apcatb.2013.02.045

Awfa, D., Ateia, M., Fujii, M., Johnson, M. S., & Yoshimura, C. (2018). Photodegradation of pharmaceuticals and personal care products in water treatment using carbonaceous-TiO_2 composites: A critical review of recent literature. *Water Research*, *142*, 26-45. https://doi.org/10.1016/j.watres.2018.05.036

Ayati, A., Ahmadpour, A., Bamoharram, F. F., Tanhaei, B., Mänttäri, M., & Sillanpää, M. (2014). A review on catalytic applications of Au/TiO_2 nanoparticles in the removal of water pollutant. *Chemosphere*, *107*, 163-174. https://doi.org/10.1016/j.chemosphere.2014.01.040

Ayoub, H., Roques-Carmes, T., Potier, O., Koubaissy, B., Pontvianne, S., Lenouvel, A.,Hamieh,

T. (2018). Iron-impregnated zeolite catalyst for efficient removal of micropollutants at very low concentration from Meurthe river. *Environmental Science and Pollution Research*, *25*, 34950-34967. https://doi.org/10.1007/s11356-018-1214-0

Babu, S. G., Karthik, P., John, M. C., Lakhera, S. K., Ashokkumar, M., Khim, J., & Neppolian, B. (2019). Synergistic effect of sono-photocatalytic process for the degradation of organic pollutants using CuO-TiO_2/rGO. *Ultrasonics Sonochemistry*, *50*, 218-223. https://doi.org/10.1016/j.ultsonch.2018.09.021

Babuponnusami, A., & Muthukumar, K. (2012). Advanced oxidation of phenol: A comparison between Fenton, electro-Fenton, sono-electro-Fenton and photo-electro-Fenton processes. *Chemical Engineering Journal*, *183*, 1-9. https://doi.org/10.1016/j.cej.2011.12.010

Babuponnusami, A., & Muthukumar, K. (2014). A review on Fenton and improvements to the Fenton process for wastewater treatment. *Journal of Environmental Chemical Engineering*, *2*(1), 557-572. https://doi.org/10.1016/j.jece.2013.10.011

Bahmani P, Maleki A, Ghahramani E, R. A. (2013). Decolorization of the dye reactive black 5 using Fenton oxidation. *African Journal of Biotechnology*, *12*(26), 4115-4122. https://doi.org/10.5897/AJB12.1226

Balakrishna, K., Rath, A., Praveenkumarreddy, Y., Guruge, K. S., & Subedi, B. (2017). A review of the occurrence of pharmaceuticals and personal care products in Indian water bodies. *Ecotoxicology and Environmental Safety*, *137*, 113-120. https://doi.org/10.1016/j.ecoenv.2016.11.014

Balu, S., Uma, K., Pan, G. T., Yang, T. C. K., & Ramaraj, S. K. (2018). Degradation of methylene blue dye in the presence of visible light using SiO_2@α-Fe_2O_3 nanocomposites deposited on SnS_2 flowers. *Materials*. *11*(6), 1030. https://doi.org/10.3390/ma11061030

Bansal, P., & Verma, A. (2017a). Novel Fe-TiO_2 composite driven dual effect for reduction in treatment time of pentoxifylline: Slurry to immobilized approach. *Materials and Design*, *125*, 135–145. https://doi.org/10.1016/j.matdes.2017.03.083

Bansal, P., & Verma, A. (2017b). Synergistic effect of dual process (photocatalysis and photo-

Fenton) for the degradation of Cephalexin using TiO_2 immobilized novel clay beads with waste fly ash/foundry sand. *Journal of Photochemistry and Photobiology A: Chemistry*, *342*, 131–142. https://doi.org/10.1016/j.jphotochem.2017.04.010

Bansal, P., Verma, A., Aggarwal, K., Singh, A., & Gupta, S. (2016). Investigations on the degradation of an antibiotic Cephalexin using suspended and supported TiO_2: Mineralization and durability studies. *Canadian Journal of Chemical Engineering*, *94*(7), 1269-1276. https://doi.org/10.1002/cjce.22512

Bejarano-Pérez, N. J., & Suárez-Herrera, M. F. (2007). Sonophotocatalytic degradation of congo red and methyl orange in the presence of TiO_2 as a catalyst. *Ultrasonics Sonochemistry*, *14*(5), 589–595. https://doi.org/10.1016/j.ultsonch.2006.09.011

Belver, C., Hinojosa, M., Id, J. B., Alvarez, M. A., Rodr, V., & Rodriguez, J. J. (2017). Ag-CoatedHeterostructures of ZnO-TiO_2/Delaminated Montmorillonite as Solar Photocatalysts. *Materials, 10*(8), 960. https://doi.org/10.3390/ma10080960

Bendesky, A., Menéndez, D., & Ostrosky-Wegman, P. (2002). Is metronidazole carcinogenic? *Mutation Research - Reviews in Mutation Research*, *511*(2),133-144. https://doi.org/10.1016/S1383-5742(02)00007-8

Bhatkhande, D. S., Pangarkar, V. G., & Beenackers, A. A. C. M. (2002). Photocatalytic degradation for environmental applications - A review. *Journal of Chemical Technology and Biotechnology,77*(1),102-116. https://doi.org/10.1002/jctb.532

Bhatti, M. S., Kapoor, D., Kalia, R. K., Reddy, A. S., & Thukral, A. K. (2011). RSM and ANN modeling for electrocoagulation of copper from simulated wastewater: Multi objective optimization using genetic algorithm approach. *Desalination*, *274*(1–3), 74–80. https://doi.org/10.1016/j.desal.2011.01.083

Blanco, J., Malato, S., Fernández, P., Vidal, a, Morales, a, Trincado, P., … Rangel, C. . (1999). Compound parabolic concentrator technology development to commercial solar detoxification applications. *Solar Energy*, *67*(4–6), 317–330. https://doi.org/10.1016/S0038-092X(00)00078-5

Blanco, M., Martinez, A., Marcaide, A., Aranzabe, E., & Aranzabe, A. (2014). Heterogeneous Fenton Catalyst for the Efficient Removal of Azo Dyes in Water. *American Journal of Analytical Chemistry*,*5*, 490-499. https://doi.org/10.4236/ajac.2014.58058

Bokare, A. D., & Choi, W. (2014). Review of iron-free Fenton-like systems for activating H_2O_2 in advanced oxidation processes. *Journal of Hazardous Materials*, *275*, 121-135. https://doi.org/10.1016/j.jhazmat.2014.04.054

Borges, M., García, D., Hernández, T., Ruiz-Morales, J., & Esparza, P. (2015). Supported Photocatalyst for Removal of Emerging Contaminants from Wastewater in a Continuous Packed-Bed Photoreactor Configuration. *Catalysts*, *5*(1), 77–87. https://doi.org/10.3390/catal5010077

Bouarioua, A., & Zerdaoui, M. (2017). Photocatalytic activities of TiO_2 layers immobilized on glass substrates by dip-coating technique toward the decolorization of methyl orange as a model organic pollutant. *Journal of Environmental Chemical Engineering*,*5*(2), 1565-1574. https://doi.org/10.1016/j.jece.2017.02.025

Bouna, L., Rhouta, B., & Maury, F. (2013). Physicochemical Study of Photocatalytic Activity of TiO_2 Supported Palygorskite Clay Mineral, *2013*, 2–7.

Bouras, P., & Lianos, P. (2008). Synergy effect in the combined photodegradation of an azo dye by titanium dioxide photocatalysis and photo-fenton oxidation. *Catalysis Letters*, *123*(3–4), 220–225. https://doi.org/10.1007/s10562-008-9466-9

Buriak, J. M., Kamat, P. V., & Schanze, K. S. (2014). Best practices for reporting on heterogeneous photocatalysis. *ACS Applied Materials and Interfaces*, *6*(15), 11815-11816. https://doi.org/10.1021/am504389z

Calza, P., Medana, C., Raso, E., Giancotti, V., & Minero, C. (2011). Characterization of phenazone transformation products on lightactivated TiO_2 surface by high-resolution mass spectrometry. *Rapid Communications in Mass Spectrometry*, *25*(19), 2923–2932. https://doi.org/10.1002/rcm.5180

Çelekli, A., Bozkurt, H., & Geyik, F. (2013). Bioresource Technology Use of artificial neural

networks and genetic algorithms for prediction of sorption of an azo-metal complex dye onto lentil straw, *129*, 396–401. https://doi.org/10.1016/j.biortech.2012.11.085

Chanda, A., Gupta, S., Vasundhara, M., Joshi, S. R., Mutta, G. R., & Singh, J. (2017). Study of structural, optical and magnetic properties of cobalt doped ZnO nanorods. *RSC Advances, 7*, 50527-50536. https://doi.org/10.1039/c7ra08458g

Chander, V., Sharma, B., Negi, V., Aswal, R. S., Singh, P., Singh, R., & Dobhal, R. (2016). Pharmaceutical compounds in drinking water. *Journal of Xenobiotics, 6*(1),5774. https://doi.org/10.4081/xeno.2016.5774

Chang, M. C., Huang, C. P., Shu, H. Y., & Chang, Y. C. (2012). A new photocatalytic system using steel mesh and cold cathode fluorescent light for the decolorization of azo dye orange G. *International Journal of Photoenergy*, *2012*, 1-9. https://doi.org/10.1155/2012/303961

Chatterjee, D., & Dasgupta, S. (2005). Visible light induced photocatalytic degradation of organic pollutants. *Journal of Photochemistry and Photobiology C: Photochemistry Reviews*, *6*(2-3), 186-205. https://doi.org/10.1016/j.jphotochemrev.2005.09.001

Chekir, N. *et al.* (2017). A comparative study of tartrazine degradation using UV and solar fixed bed reactors. *International Journal of Hydrogen Energy*, *42*(13), 8948-8954. doi: 10.1016/j.ijhydene.2016.11.057.

Chelliapan, S., & Sallis, P. J. (2011). Application of anaerobic biotechnology for pharmaceutical wastewater treatment. *IIOAB Journal*, *2*(1), 13–21.

Chen, S., & Cao, G. (2006). Study on the photocatalytic oxidation of NO^{2-} ions using TiO_2 beads as a photocatalyst. *Desalination*, *194*(1–3), 127–134. https://doi.org/10.1016/j.desal.2005.11.006

Cheng, M., Zeng, G., Huang, D., Lai, C., Xu, P., Zhang, C., & Liu, Y. (2016). Hydroxyl radicals based advanced oxidation processes (AOPs) for remediation of soils contaminated with organic compounds: A review. *Chemical Engineering Journal, 284*, 582-598. https://doi.org/10.1016/j.cej.2015.09.001

Choi, J., Park, H., & Hoffmann, M. R. (2010). Effects of single metal-ion doping on the visible-light photoreactivity of TiO_2. *Journal of Physical Chemistry C 114*(2), 783-792. https://doi.org/10.1021/jp908088x

Chong, M. N., & Jin, B. (2012). Photocatalytic treatment of high concentration carbamazepine in synthetic hospital wastewater. *Journal of Hazardous Materials*, *199–200*, 135–142. https://doi.org/10.1016/j.jhazmat.2011.10.067

Grayson, M.L.,Cosgrove, S.E.,Crowe, S.M., Hope, W., McCarthy, J.S., Mills, J., Mouton, J.W.,Paterson, D.L. (2017). Metronidazole. In *Kucers the Use of Antibiotics: A Clinical Review of Antibacterial, Antifungal, Antiparasitic, and Antiviral Drugs,7*, 1-4841. https://doi.org/10.1201/9781315152110

Clarizia, L., Russo, D., Di Somma, I., Marotta, R., & Andreozzi, R. (2017). Homogeneous photo-Fenton processes at near neutral pH: A review. *Applied Catalysis B: Environmental, 209*, 358-371. https://doi.org/10.1016/j.apcatb.2017.03.011

Cloteaux, A., Gérardin, F., Thomas, D., Midoux, N., & André, J. C. (2014). Fixed bed photocatalytic reactor for formaldehyde degradation: Experimental and modeling study. *Chemical Engineering Journal, 249,* 122-129.https://doi.org/10.1016/j.cej.2014.03.067

Coale, A. J., & Hoover, E. M. (2016). III. The Effects of Population Growth on Economic Development. In *Population Growth and Economic Development*. *Princeton University Press,1*, 1-216. https://doi.org/10.1515/9781400878598-007

CPCB. (2009). The Environment Protection Rules, 1986, *2*(ii), 469–472.

Damodhar, U., & Vikram Reddy, M. (2013). Impact of pharmaceutical industry treated effluents on the water quality of river Uppanar, South east coast of India: A case study. *Applied Water Science*, *3*(2), 501–514. https://doi.org/10.1007/s13201-013-0098-x

Daneshvar, N., Salari, D., Niaei, a, Rasoulifard, M. H., & Khataee, a R. (2005). Immobilization of TiO_2 nanopowder on glass beads for the photocatalytic decolorization of an azo dye C.I. Direct Red 23. *Journal of Environmental Science and Health. Part A, Toxic/Hazardous Substances & Environmental Engineering*, *40*(8), 1605–1617. https://doi.org/10.1081/ESE-

200060664

Dave, P. N., & Chopda, L. V. (2014). Application of iron oxide nanomaterials for the removal of heavy metals. *Journal of Nanotechnology*. https://doi.org/10.1155/2014/398569

David, C., Arivazhagan, M., & Ibrahim, M. (2015). Spent wash decolourization using nano-Al_2O_3/kaolin photocatalyst: Taguchi and ANN approach. *Journal of Saudi Chemical Society*, *19*(5), 537–548. https://doi.org/10.1016/j.jscs.2015.05.012

De-Nasri, S., Nagarajan, S., Robertson, P. K. J., & Ranade, V. V. (2018). Cavitation and immobilised photo-catalysis for effluent treatment: A comparative study of individual and combined operations. In *Environmental Division 2018 - Core Programming Area at the 2018 AIChE Annual Meeting*, 1-3.

De Araújo, K. S., Antonelli, R., Gaydeczka, B., Granato, A. C., & Malpass, G. R. P. (2016). Advanced oxidation processes: A review of fundamentals and applications in the treatment of urban and industrial wastewaters. *Revista Ambiente e Agua, 11*(2),387-401. https://doi.org/10.4136/ambi-agua.1862

Deegan, A. M., Shaik, B., Nolan, K., Urell, K., Oelgemöller, M., Tobin, J., & Morrissey, A. (2011). Treatment options for wastewater effluents from pharmaceutical companies. *International Journal of Environmental Science and Technology*, *8*(3), 649–666. https://doi.org/10.1007/BF03326250

Deng, F., Zhao, L., Luo, X., Luo, S., & Dionysiou, D. D. (2018). Highly efficient visible-light photocatalytic performance of Ag/AgIn5S8 for degradation of tetracycline hydrochloride and treatment of real pharmaceutical industry wastewater. *Chemical Engineering Journal*, *333*, 423–433. https://doi.org/10.1016/j.cej.2017.09.022

Deng, Y., & Zhao, R. (2015). Advanced Oxidation Processes (AOPs) in Wastewater Treatment. *Current Pollution Reports, 1*,167-176. https://doi.org/10.1007/s40726-015-0015-z

Destaillats, H., Colussi, A. J., Joseph, J. M., & Hoffmann, M. R. (2000). Synergistic effects of sonolysis combined with ozonolysis for the oxidation of azobenzene and methyl orange. *Journal of Physical Chemistry A, 104* (39),8930-8935. https://doi.org/10.1021/jp001415+

Devipriya, S., & Yesodharan, S. (2005). Photocatalytic degradation of pesticide contaminants in water. *Solar Energy Materials and Solar Cells*, *86*(3), 309–348. https://doi.org/10.1016/j.solmat.2004.07.013

Dewil, R., Mantzavinos, D., Poulios, I., & Rodrigo, M. A. (2017). New perspectives for Advanced Oxidation Processes. *Journal of Environmental Management 195*, 93-99. https://doi.org/10.1016/j.jenvman.2017.04.010

Dhanya, A., & Aparna, K. (2016). Synthesis and Evaluation of TiO_2/Chitosan Based Hydrogel for the Adsorptional Photocatalytic Degradation of Azo and Anthraquinone Dye under UV Light Irradiation. *Procedia Technology, 24,* 611-618. https://doi.org/10.1016/j.protcy.2016.05.141

Do, S. H., Batchelor, B., Lee, H. K., & Kong, S. H. (2009). Hydrogen peroxide decomposition on manganese oxide (pyrolusite): Kinetics, intermediates, and mechanism. *Chemosphere, 75*(1), 8-12. https://doi.org/10.1016/j.chemosphere.2008.11.075

Dudgeon, D., Arthington, A. H., Gessner, M. O., Kawabata, Z. I., Knowler, D. J., Lévêque, C., … Sullivan, C. A. (2006). Freshwater biodiversity: Importance, threats, status and conservation challenges. *Biological Reviews of the Cambridge Philosophical Society, 81*(2), 163-182. https://doi.org/10.1017/S1464793105006950

El-Sebaii, A. A., Aboul-Enein, S., Ramadan, M. R. I., Shalaby, S. M., & Moharram, B. M. (2011). Investigation of thermal performance of-double pass-flat and v-corrugated plate solar air heaters. *Energy*, *36*(2), 1076–1086. https://doi.org/10.1016/j.energy.2010.11.042

Elmolla, E. S., & Chaudhuri, M. (2010). Photocatalytic degradation of amoxicillin, ampicillin and cloxacillin antibiotics in aqueous solution using UV/TiO_2 and UV/H_2O_2/TiO_2 photocatalysis. *Desalination, 252*(1–3), 46–52. https://doi.org/10.1016/j.desal.2009.11.003

Elsalamony, R. A., & Mahmoud, S. A. (2017). Preparation of nanostructured ruthenium doped titania for the photocatalytic degradation of 2-chlorophenol under visible light. *Arabian Journal of Chemistry, 10*(2), 194-205. https://doi.org/10.1016/j.arabjc.2012.06.008

Fernández, P., Blanco, J., Sichel, C., & Malato, S. (2005). Water disinfection by solar

photocatalysis using compound parabolic collectors. *Catalysis Today*, *101*, 345–352. https://doi.org/10.1016/j.cattod.2005.03.062

Ferreira, S. L. C., Bruns, R. E., Ferreira, H. S., Matos, G. D., David, J. M., Brandão, G. C., … dos Santos, W. N. L. (2007). Box-Behnken design: An alternative for the optimization of analytical methods. *Analytica Chimica Acta*, *597*(2), 179–186. https://doi.org/10.1016/j.aca.2007.07.011

Ferro, G., Guarino, F., Castiglione, S., & Rizzo, L. (2016). Antibiotic resistance spread potential in urban wastewater effluents disinfected by UV/H_2O_2 process. *Science of the Total Environment, 560-561*, 29-35. https://doi.org/10.1016/j.scitotenv.2016.04.047

Fick, J., Soderstrom, H., Lindberg, R. H., Phan, C., Tysklind, M., & Larsson, J. D. G. (2009). Contamination of Surface, Ground, and Drinking Water From Pharmaceutical Production. *Environmental Toxicology and Chemistry*, *28*(12), 2522–2527. https://doi.org/10.1897/09-073.1

Fiorentino, A., Rizzo, L., Guilloteau, H., Bellanger, X., & Merlin, C. (2017). Comparing TiO_2 photocatalysis and UV-C radiation for inactivation and mutant formation of Salmonella typhimurium TA102. *Environmental Science and Pollution Research, 24,* 1871-1879. https://doi.org/10.1007/s11356-016-7981-6

Fu, M., Li, Y., Wu, S., Lu, P., Liu, J., & Dong, F. (2011). Sol-gel preparation and enhanced photocatalytic performance of Cu-doped ZnO nanoparticles. *Applied Surface Science*. *258*(4), 1587-1591. https://doi.org/10.1016/j.apsusc.2011.10.003

Fukahori, S., & Fujiwara, T. (2015). Photocatalytic decomposition behavior and reaction pathway of sulfamethazine antibiotic using TiO_2. *Journal of Environmental Management*, *157*, 103–110. https://doi.org/10.1016/j.jenvman.2015.04.002

Gadipelly, C., Pérez-González, A., Yadav, G. D., Ortiz, I., Ibáñez, R., Rathod, V. K., & Marathe, K. V. (2014). Pharmaceutical industry wastewater: Review of the technologies for water treatment and reuse. *Industrial and Engineering Chemistry Research 53*(29),11571-11592. https://doi.org/10.1021/ie501210j

Gar Alalm, M., Tawfik, A., & Ookawara, S. (2017). Investigation of optimum conditions and costs estimation for degradation of phenol by solar photo-Fenton process. *Applied Water Science,7*, 375-382. https://doi.org/10.1007/s13201-014-0252-0

Gholami, N., Ghasemi, B., Anvaripour, B., & Jorfi, S. (2018). Enhanced photocatalytic degradation of furfural and a real wastewater using UVC/TiO_2 nanoparticles immobilized on white concrete in a fixed-bed reactor. *Journal of Industrial and Engineering Chemistry, 62*, 291-301. https://doi.org/10.1016/j.jiec.2018.01.007

Ghosh, P., Chelli, V. R., Giri, A. S., & Golder, A. K. (2018). Steroid glycosides as potential analytes for Cu-doping on TiO_2 for photocatalytic water treatment. *Environmental Progress and Sustainable Energy, 37*(6), 1973-1981. https://doi.org/10.1002/ep.12879

Giannakis, S., Polo López, M. I., Spuhler, D., Sánchez Pérez, J. A., Fernández Ibáñez, P., & Pulgarin, C. (2016). Solar disinfection is an augmentable, in situ-generated photo-Fenton reaction—Part 1: A review of the mechanisms and the fundamental aspects of the process. *Applied Catalysis B: Environmental,199,*199-203 . https://doi.org/10.1016/j.apcatb.2016.06.009

Ginni, G., Adishkumar, S., Rajesh Banu, J., & Yogalakshmi, N. (2014). Treatment of pulp and paper mill wastewater by solar photo-Fenton process. *Desalination and Water Treatment, 52*(13-15), 2457-2464. https://doi.org/10.1080/19443994.2013.794114

Gothwal, R., & Thatikonda, S. (2017). Role of environmental pollution in prevalence of antibiotic resistant bacteria in aquatic environment of river: case of Musi river, South India. *Water and Environment Journal, 31*(4), 456–462. https://doi.org/10.1111/wej.12263

Greene, W. (2007). The emergence of india's pharmaceutical Industry and implications for the U.S. Generic drug market.*Issues and Impacts of Foreign Pharmaceuticals, 05,* 1-36.

Grosso, W. E., & Chiovetta, M. G. (2005). Modeling a fluidized-bed reactor for the catalytic polymerization of ethylene: Particle size distribution effects. *Latin American Applied Research, 35*(1), 67–76.

Guo, J., Gan, Z., Lu, Z., Liu, J., Xi, J., Wan, Y., … Xiong, R. (2013). Improvement of the

photocatalytic properties of TiO_2 by ($Fe^{+}Mo$) co-doping - A possible way to retard the recombination process. *Journal of Applied Physics*, *114*(10), 104903. https://doi.org/10.1063/1.4819449

Guo, Q., Zhou, C., Ma, Z., Ren, Z., Fan, H., & Yang, X. (2016). Elementary photocatalytic chemistry on TiO_2 surfaces. *Chemical Society Reviews*, *45*, 3701-3730. https://doi.org/10.1039/c5cs00448a

Gupta, S. K., & Garg, S. (2013). Multiobjective Optimization Using Genetic Algorithm. *Advances in Chemical Engineering*, *41*(19),4765-4776. https://doi.org/10.1016/B978-0-12-396524-0.00004-0

Halling-Sorensen, B., Halling-Sorensen, B., Nielsen, S. N., Nielsen, S. N., Lanzky, P. F., Lanzky, P. F., … S.E., J. (1998). Occurence, fate and effects of pharmaceuticals substance in the environment - A review. *Chemosphere*, *36*(2), 357–393. https://doi.org/http://dx.doi.org/10.1016/S0045-6535(97)00354-8

Haroune, L., Salaun, M., M??nard, A., Legault, C. Y., & Bellenger, J. P. (2014). Photocatalytic degradation of carbamazepine and three derivatives using TiO_2 and ZnO: Effect of pH, ionic strength, and natural organic matter. *Science of the Total Environment*, *475*, 16–22. https://doi.org/10.1016/j.scitotenv.2013.12.104

Hashemi, S. M., Badii, K., & Abdolreza, S. (2010). Study of Immobilization of Nano-TiO_2 for Environmental Aspects on Glass by Different Resin Families, *4*, 1–6. Retrieved from http://www.pccc.icrc.ac.ir/files/cu113se1up1190.pdf

Heberer, T. (2002). Occurrence, fate, and removal of pharmaceutical residues in the aquatic environment: A review of recent research data. *Toxicology Letters*, *131*(1-2),5-17. https://doi.org/10.1016/S0378-4274(02)00041-3

Hermosilla, D., Merayo, N., Gascó, A., & Blanco, Á. (2014). The application of advanced oxidation technologies to the treatment of effluents from the pulp and paper industry: A review. *Environmental Science and Pollution Research*,*22*, 168-191. https://doi.org/10.1007/s11356-014-3516-1

Herney-Ramirez, J., Lampinen, M., Vicente, M. A., Costa, C. A., & Madeira, L. M. (2008). Experimental design to optimize the oxidation of orange II dye solution using a clay-based fenton-like catalyst. *Industrial and Engineering Chemistry Research, 47*(2), 284-294. https://doi.org/10.1021/ie070990y

Holland, J. H. (1973). Genetic algorithms and the optimal allocation of trials. *SIAM Journal of Computing,2*(2), 88-105. https://doi.org/10.1109/9780470544600.ch15

Hong, S. H., Kwon, B. H., Lee, J. K., & Kim, I. K. (2008). Degradation of 2-chlorophenol by Fenton and photo-Fenton processes. *Korean Journal of Chemical Engineering*, *25*(1), 46–52. https://doi.org/10.1007/s11814-008-0008-3

Hosseini, S. N., Borghei, M., Vossoughi, M., & Taghavinia, N. (2008). Photocatalytic degradation of phenol in aqueous phase with TiO_2 immobilized on three different supports with a simple method, *3rd IASME/WSEAS Int. Conf. on Energy & Environment,* 46–50.

Huang, M., Xu, C., Wu, Z., Huang, Y., Lin, J., & Wu, J. (2008). Photocatalytic discolorization of methyl orange solution by Pt modified TiO_2 loaded on natural zeolite. *Dyes and Pigments, 77*(2), 327-334. https://doi.org/10.1016/j.dyepig.2007.01.026

Huang, W. J., Lin, H. X., Lin, H. W., & Zheng, K. W. (2018). Catalytic Ozonation Promoted by TiO2 Catalyst for the Removal of Cyanotoxin Cylindrospermopsin from Water. In *Proceedings of the World Congress on New Technologies*. 1-4. https://doi.org/10.11159/icepr18.156

Idris, A., Misran, E., Hassan, N., Jalil, A. A., & Seng, C. E. (2012). Modified PVA-alginate encapsulated photocatalyst ferro photo gels for Cr(VI) reduction. *Journal of Hazardous Materials, 227-228*, 309-316. https://doi.org/10.1016/j.jhazmat.2012.05.065

Iglesias, O., Rivero, M. J., Urtiaga, A. M., & Ortiz, I. (2016). Membrane-based photocatalytic systems for process intensification. *Chemical Engineering Journal, 305,* 136-148. https://doi.org/10.1016/j.cej.2016.01.047

Jaihindh, D. P., Chen, C. C., & Fu, Y. P. (2018). Reduced graphene oxide-supported Ag-loaded Fe-doped TiO_2 for the degradation mechanism of methylene blue and its electrochemical

properties. *RSC Advances*, *8*(12), 6488–6501. https://doi.org/10.1039/c7ra13418e

Jain, R., Mathur, M., Sikarwar, S., & Mittal, A. (2007). Removal of the hazardous dye rhodamine B through photocatalytic and adsorption treatments. *Journal of Environmental Management, 85*(4), 956-964. https://doi.org/10.1016/j.jenvman.2006.11.002

Jia, N., Horie, T., & Ohmura, N. (2011). Process intensification of water purification using taylor vortex photocatalytic reactor. In *Institution of Chemical Engineers Symposium Series, 157,* 149–154.

Kamat, P. V., & Meisel, D. (2002). Nanoparticles in advanced oxidation processes. *Current Opinion in Colloid and Interface Science, 7(*5-6), 282-287. https://doi.org/10.1016/S1359-0294(02)00069-9

Kanakaraju, D., Glass, B. D., & Oelgemöller, M. (2014a). Titanium dioxide photocatalysis for pharmaceutical wastewater treatment. *Environmental Chemistry Letters*, *12*(1), 27–47. https://doi.org/10.1007/s10311-013-0428-0

Kanakaraju, D., Glass, B. D., & Oelgemöller, M. (2014b). Titanium dioxide photocatalysis for pharmaceutical wastewater treatment. *Environmental Chemistry Letters, 12*, 27-47. https://doi.org/10.1007/s10311-013-0428-0

Kanakaraju, D., Glass, B. D., & Oelgemöller, M. (2018). Advanced oxidation process-mediated removal of pharmaceuticals from water: A review. *Journal of Environmental Management, 219*, 189-207. https://doi.org/10.1016/j.jenvman.2018.04.103

Kang, S. H., Bae, J. W., Cheon, J. Y., Lee, Y. J., Ha, K. S., Jun, K. W., … Kim, B. W. (2011). Catalytic performance on iron-based Fischer-Tropsch catalyst in fixed-bed and bubbling fluidized-bed reactor. *Applied Catalysis B: Environmental*, *103*(1–2), 169–180. https://doi.org/10.1016/j.apcatb.2011.01.024

Kasiri, M. B., Aleboyeh, H., & Aleboyeh, A. (2008). Modeling and optimization of heterogeneous photo-fenton process with response surface methodology and artificial neural networks. *Environmental Science and Technology, 42(*21), 7970-7975. https://doi.org/10.1021/es801372q

Kaur, N., Shahi, S. K., & Singh, V. (2015). Anomalous behavior of visible light active TiO_2 for the photocatalytic degradation of different Reactive dyes. *Photochemical and Photobiological Sciences, 14*, 2024-2034. https://doi.org/10.1039/c5pp00165j

Kaur, P., Kushwaha, J. P., & Sangal, V. K. (2018). Transformation products and degradation pathway of textile industry wastewater pollutants in Electro-Fenton process. *Chemosphere, 207*, 690-698. https://doi.org/10.1016/j.chemosphere.2018.05.114

Kaur, T., Toor, A. P., & Wanchoo, R. K. (2015). Parametric study on degradation of fungicide carbendazim in dilute aqueous solutions using nano TiO_2. *Desalination and Water Treatment, 54*(1), 122-131. https://doi.org/10.1080/19443994.2013.879081

Kavitha, V., & Palanivelu, K. (2004). The role of ferrous ion in Fenton and photo-Fenton processes for the degradation of phenol. *Chemosphere, 55*(9), 1235-1243. https://doi.org/10.1016/j.chemosphere.2003.12.022

Keane, D. A., McGuigan, K. G., Ibáñez, P. F., Polo-López, M. I., Byrne, J. A., Dunlop, P. S. M., … Pillai, S. C. (2014). Solar photocatalysis for water disinfection: Materials and reactor design. *Catalysis Science and Technology,4,* 1211-1226. https://doi.org/10.1039/c4cy00006d

Khan, S. J., Reed, R. H., & Rasul, M. G. (2012a). Thin-film fixed-bed reactor (TFFBR) for solar photocatalytic inactivation of aquaculture pathogen Aeromonas hydrophila. *BMC Microbiology, 12*(1), 5. https://doi.org/10.1186/1471-2180-12-5

Khan, S. J., Reed, R. H., & Rasul, M. G. (2012b). Thin-film fixed-bed reactor for solar photocatalytic inactivation of Aeromonas hydrophila: influence of water quality. *BMC Microbiology, 12*(1), 285. https://doi.org/10.1186/1471-2180-12-285

Khandegar, V., Acharya, S., & Jain, A. K. (2018). Data on treatment of sewage wastewater by electrocoagulation using punched aluminum electrode and characterization of generated sludge. *Data in Brief, 18*, 1229-1238. https://doi.org/10.1016/j.dib.2018.04.020

Kim, H. E., Lee, J., Lee, H., & Lee, C. (2012). Synergistic effects of TiO_2 photocatalysis in combination with Fenton-like reactions on oxidation of organic compounds at circumneutral

pH. *Applied Catalysis B: Environmental*, *115–116*, 219–224. https://doi.org/10.1016/j.apcatb.2011.12.027

Klamerth, N., Rizzo, L., Malato, S., Maldonado, M. I., Aguera, a., & Fernandez-Alba, a. R. (2010). Degradation of fifteen emerging contaminants at μg L^{-1} initial concentrations by mild solar photo-Fenton in MWTP effluents. *Water Research*, *44*(2), 545–554. https://doi.org/10.1016/j.watres.2009.09.059

Klavarioti, M., Mantzavinos, D., & Kassinos, D. (2009). Removal of residual pharmaceuticals from aqueous systems by advanced oxidation processes. *Environment International*, *35*(2), 402-417. https://doi.org/10.1016/j.envint.2008.07.009

Kočí, K., Matějů, K., Obalová, L., Krejčíková, S., Lacný, Z., Plachá, D., … Šolcová, O. (2010). Effect of silver doping on the TiO_2 for photocatalytic reduction of CO_2. *Applied Catalysis B: Environmental*, *96*(3-4), 239-244. https://doi.org/10.1016/j.apcatb.2010.02.030

Kositzi, M., Poulios, I., Malato, S., Caceres, J., & Campos, A. (2004). Solar photocatalytic treatment of synthetic municipal wastewater. *Water Research*, *38*(5), 1147-1154. https://doi.org/10.1016/j.watres.2003.11.024

Koumparoulis, D. N. (2015). Financial development and economic growth. In *Strategic Infrastructure Development for Economic Growth and Social Change*.1-14. https://doi.org/10.4018/978-1-4666-7470-7.ch003

Kovacic, M., Salaeh, S., Kusic, H., Suligoj, A., Kete, M., Fanetti, M., … Bozic, A. L. (2016). Solar-driven photocatalytic treatment of diclofenac using immobilized TiO_2-based zeolite composites. *Environmental Science and Pollution Research*, *23*(18), 17982–17994. https://doi.org/10.1007/s11356-016-6985-6

Kumar, P., & Bharti, R. P. (2019). Nanocomposite Polymer Electrolyte Membrane for High Performance Microbial Fuel Cell: Synthesis, Characterization and Application. *Journal of The Electrochemical Society*, *166*, F1190. https://doi.org/10.1149/2.0671915jes

Kümmerer, K. (2008). Pharmaceuticals in the Environment – A Brief Summary. In *Pharmaceuticals in the Environment, Springer, Berlin, Heidelberg*, 3-21.

https://doi.org/10.1007/978-3-540-74664-5_1

Lakatos, G. (2018). Biological wastewater treatment. In *Wastewater and Water Contamination: Sources, Assessment and Remediation*, 105-128.

Lall, S. V., Lundberg, M. K. A., & Shalizi, Z. (2008). Implications of alternate policies on welfare of slum dwellers: Evidence from Pune, India. *Journal of Urban Economics*, *63*(1), 56-73. https://doi.org/10.1016/j.jue.2006.12.001

Larsson, D. G. J., de Pedro, C., & Paxeus, N. (2007). Effluent from drug manufactures contains extremely high levels of pharmaceuticals. *Journal of Hazardous Materials*, *148*(3), 751–755. https://doi.org/10.1016/j.jhazmat.2007.07.008

Lefebvre, O., Shi, X., Wu, C. H., & Ng, H. Y. (2014). Biological treatment of pharmaceutical wastewater from the antibiotics industry. *Water Science and Technology*, *69*(4), 855–861. https://doi.org/10.2166/wst.2013.729

Levenspiel, O. (1999). *Chemical Reaction Engineering - third edition*. *3Th Edition*. https://doi.org/10.1016/0009-2509(64)85017-X

Li, H., Zhang, Z., & Liu, Z. (2017). Application of Artificial Neural Networks for Catalysis : A Review. *Catalysts*, *7*(10), 306. https://doi.org/10.3390/catal7100306

LI, Y., MA, M., WANG, X., & WANG, X. (2008). Inactivated properties of activated carbon-supported TiO_2 nanoparticles for bacteria and kinetic study. *Journal of Environmental Sciences*, *20*(12), 1527–1533. https://doi.org/10.1016/S1001-0742(08)62561-9

Lin, L., Chai, Y., Zhao, B., Wei, W., He, D., He, B., & Tang, Q. (2013). Photocatalytic oxidation for degradation of VOCs. *Open Journal of Inorganic Chemistry, 3,* 14-25. https://doi.org/10.4236/ojic.2013.31003

Lin, S. S., & Gurol, M. D. (1998). Catalytic decomposition of hydrogen peroxide on iron oxide: Kinetics, mechanism, and implications. *Environmental Science and Technology*, *32*(10), 1417-1423. https://doi.org/10.1021/es970648k

Lin, W. H., Chiu, Y. H., Shao, P. W., & Hsu, Y. J. (2016). Metal-Particle-Decorated ZnO Nanocrystals: Photocatalysis and Charge Dynamics. *ACS Applied Materials and Interfaces, 8*(48), 32754-32763. https://doi.org/10.1021/acsami.6b08132

Ling, C. M., Mohamed, A. R., & Bhatia, S. (2004). Performance of photocatalytic reactors using immobilized TiO_2 film for the degradation of phenol and methylene blue dye present in water stream. *Chemosphere 57*(7), 547-554. https://doi.org/10.1016/j.chemosphere.2004.07.011

Liu, C., Yang, Y., Wang, Q., Kim, M., Zhu, Q., Li, D., & Zhang, Z. (2012). Photocatalytic degradation of waste activated sludge using a circulating bed photocatalytic reactor for improving biohydrogen production. *Bioresource Technology*, *125*, 30–36. https://doi.org/10.1016/j.biortech.2012.08.139

Lofrano, G., Meriç, S., Zengin, G. E., & Orhon, D. (2013). Chemical and biological treatment technologies for leather tannery chemicals and wastewaters: A review. *Science of the Total Environment 461-462*, 265-281. https://doi.org/10.1016/j.scitotenv.2013.05.004

Lofrano, G., Rizzo, L., Grassi, M., & Belgiorno, V. (2009). Advanced oxidation of catechol: A comparison among photocatalysis, Fenton and photo-Fenton processes. *Desalination, 249*(2), 878-883. https://doi.org/10.1016/j.desal.2009.02.068

Lourenço, V. S., & Asencios, Y. J. O. (2018). Degradation of phenol by heterogeneous photocatalysis with TiO_2-modified black mud catalysts. In *Catalysis and Reaction Engineering Division 2018 - Core Programming Area at the 2018 AIChE Annual Meeting*.

Luna, A. J., Nascimento, C. A. O., Foletto, E. L., Moraes, J. E. F., & Chiavone-Filho, O. (2014). Photo-Fenton degradation of phenol, 2,4-dichlorophenoxyacetic acid and 2,4-dichlorophenol mixture in saline solution using a falling-film solar reactor. *Environmental Technology (United Kingdom)*, *35*(3), 364–371. https://doi.org/10.1080/09593330.2013.828762

Luo, C., Ren, X., Dai, Z., Zhang, Y., Qi, X., & Pan, C. (2017). Present Perspectives of Advanced Characterization Techniques in TiO2-Based Photocatalysts. *ACS Applied Materials and*

Interfaces, *9*(28), 23265-23286. https://doi.org/10.1021/acsami.7b00496

Madhavan, J., Grieser, F., & Ashokkumar, M. (2010). Combined advanced oxidation processes for the synergistic degradation of ibuprofen in aqueous environments. *Journal of Hazardous Materials*, *178*(1–3), 202–208. https://doi.org/10.1016/j.jhazmat.2010.01.064

Magiorakos, A. P., Srinivasan, A., Carey, R. B., Carmeli, Y., Falagas, M. E., Giske, C. G., … Monnet, D. L. (2012). Multidrug-resistant, extensively drug-resistant and pandrug-resistant bacteria: An international expert proposal for interim standard definitions for acquired resistance. *Clinical Microbiology and Infection 18*(3), 268-281. https://doi.org/10.1111/j.1469-0691.2011.03570.x

Majekodunmi, S. O. (2015). A Review on Centrifugation in the Pharmaceutical Industry. *American Journal of Biomedical Engineering*, *5*(2), 67-78. https://doi.org/10.5923/j.ajbe.20150502.03

Malato, S., Blanco, J., Vidal, A., Fernández, P., Cáceres, J., Trincado, P., … Vincent, M. (2002). New large solar photocatalytic plant: Set-up and preliminary results. *Chemosphere*, *47*(3), 235-240. https://doi.org/10.1016/S0045-6535(01)00220-X

Malato, Sixto, Blanco, J., Alarcón, D. C., Maldonado, M. I., Fernández-Ibáñez, P., & Gernjak, W. (2007). Photocatalytic decontamination and disinfection of water with solar collectors. *Catalysis Today*, *122*(1–2), 137–149. https://doi.org/10.1016/j.cattod.2007.01.034

Malato, Sixto, Blanco, J., Vidal, A., & Richter, C. (2002). Photocatalysis with solar energy at a pilot-plant scale: An overview. *Applied Catalysis B: Environmental*, *37*(1), 1-15. https://doi.org/10.1016/S0926-3373(01)00315-0

Malhotra, P., & Lofgren, H. (2004). India's pharmaceutical industry: hype or high tech take-off? *Australian Health Review : A Publication of the Australian Hospital Association, 28*(2), 182-193.

Manassero, A., Satuf, M. L., & Alfano, O. M. (2017). Photocatalytic reactors with suspended and immobilized TiO_2: Comparative efficiency evaluation. *Chemical Engineering Journal*, *326*, 29-36. https://doi.org/10.1016/j.cej.2017.05.087

Maroga Mboula, V., Héquet, V., Gru, Y., Colin, R., & Andrès, Y. (2012). Assessment of the efficiency of photocatalysis on tetracycline biodegradation. *Journal of Hazardous Materials*, *209–210*, 355–364. https://doi.org/10.1016/j.jhazmat.2012.01.032

Maroneze, M. M., Zepka, L. Q., Vieira, J. G., Queiroz, M. I., & Jacob-Lopes, E. (2014). A tecnologia de remoção de fósforo: Gerenciamento do elemento em resíduos industriais. *Revista Ambiente e Agua*, *9*(3), 445–458. https://doi.org/10.4136/1980-993X

Martínez, S., Morales-mejía, J. C., Hernández, P. P., & Almanza, R. (2014). Solar photocatalytic oxidation of Triclosan with TiO_2 immobilized on volcanic porous stones on a CPC pilot scale reactor. *Energy Procedia*, *57*(55), 3014–3020. https://doi.org/10.1016/j.egypro.2014.10.337

Matamoros, V., Arias, C., Brix, H., & Bayona, J. M. (2009). Preliminary screening of small-scale domestic wastewater treatment systems for removal of pharmaceutical and personal care products. *Water Research, 43*(1), 55–62. https://doi.org/10.1016/j.watres.2008.10.005

Matas Adams, A., Marin-Beloqui, J. M., Stoica, G., & Palomares, E. (2015). The influence of the mesoporous TiO_2 scaffold on the performance of methyl ammonium lead iodide (MAPI) perovskite solar cells: charge injection, charge recombination and solar cell efficiency relationship. *Journal of Materials Chemistry A, 3,* 22154-22161. https://doi.org/10.1039/c5ta06041a

Matilainen, A., & Sillanpää, M. (2010). Removal of natural organic matter from drinking water by advanced oxidation processes. *Chemosphere, 80*(4), 351-365. doi: 10.1016/j.chemosphere.2010.04.067.

Matsuzawa, S., Maneerat, C., Hayata, Y., Hirakawa, T., Negishi, N., & Sano, T. (2008). Immobilization of TiO_2 nanoparticles on polymeric substrates by using electrostatic interaction in the aqueous phase. *Applied Catalysis B: Environmental*, *83*(1-2), 39-45. https://doi.org/10.1016/j.apcatb.2008.01.036

Mazille, F., Lopez, A., & Pulgarin, C. (2009a). Synergistic effect of TiO_2 and iron oxide supported on fluorocarbon films. Part 2: Long-term stability and influence of reaction

parameters on photoactivated degradation of pollutants. *Applied Catalysis B: 9Environmental*, *90*(3–4), 321–329. https://doi.org/10.1016/j.apcatb.2009.05.004

Mazille, F., Lopez, A., & Pulgarin, C. (2009b). Synergistic effect of TiO2 and iron oxide supported on fluorocarbon films. *Applied Catalysis B: Environmental*, *90*(3–4), 321–329. https://doi.org/10.1016/j.apcatb.2009.05.004

Mazille, F., Schoettl, T., Klamerth, N., Malato, S., & Pulgarin, C. (2010). Field solar degradation of pesticides and emerging water contaminants mediated by polymer films containing titanium and iron oxide with synergistic heterogeneous photocatalytic activity at neutral pH. *Water Research*, *44*(10), 3029–3038. https://doi.org/10.1016/j.watres.2010.02.026

Mazille, F., Schoettl, T., & Pulgarin, C. (2009). Synergistic effect of TiO_2 and iron oxide supported on fluorocarbon films. Part 1: Effect of preparation parameters on photocatalytic degradation of organic pollutant at neutral pH. *Applied Catalysis B: Environmental*, *89*(3–4), 635–644. https://doi.org/10.1016/j.apcatb.2009.01.027

McLoughlin, O. A., Kehoe, S. C., McGuigan, K. G., Duffy, E. F., Al Touati, F., Gernjak, W., … Gill, L. W. (2004). Solar disinfection of contaminated water: A comparison of three small-scale reactors. *Solar Energy*, *77*(5), 657–664. https://doi.org/10.1016/j.solener.2004.07.004

Mehrjouei, M., Müller, S., & Möller, D. (2013). Design and characterization of a multi-phase annular falling-film reactor for water treatment using advanced oxidation processes. *Journal of Environmental Management*, *120*, 68–74. https://doi.org/10.1016/j.jenvman.2013.02.021

Mehrjouei, M., Müller, S., & Möller, D. (2015). A review on photocatalytic ozonation used for the treatment of water and wastewater. *Chemical Engineering Journal*. https://doi.org/10.1016/j.cej.2014.10.112

MiarAlipour, S., Friedmann, D., Scott, J., & Amal, R. (2018). TiO_2/porous adsorbents: Recent advances and novel applications. *Journal of Hazardous Materials*, *341*, 404–423. https://doi.org/10.1016/j.jhazmat.2017.07.070

Miranda-García, N., Suárez, S., Sánchez, B., Coronado, J. M., Malato, S., & Maldonado, M. I. (2011). Photocatalytic degradation of emerging contaminants in municipal wastewater

treatment plant effluents using immobilized TiO2 in a solar pilot plant. *Applied Catalysis B: Environmental*, *103*(3–4), 294–301. https://doi.org/10.1016/j.apcatb.2011.01.030

Mirzaei, A., Chen, Z., Haghighat, F., & Yerushalmi, L. (2017). Removal of pharmaceuticals from water by homo/heterogonous Fenton-type processes – A review. *Chemosphere, 174*, 665-688. https://doi.org/10.1016/j.chemosphere.2017.02.019

Miyawaki, A., Taira, S., & Shiraishi, F. (2016). Performance of continuous stirred-tank reactors connected in series as a photocatalytic reactor system. *Chemical Engineering Journal*, *286*, 594–601. https://doi.org/10.1016/j.cej.2015.11.007

Mohammadi-Aghdam, S., Marandi, R., Olya, M. E., & Mehrdad Sharif, A. (2014). Kinetic modeling of BB41 photocatalytic treatment in a semibatch flow photoreactor using a nano composite film. *Journal of Saudi Chemical Society*, *18*(4), 317–326. https://doi.org/10.1016/j.jscs.2013.09.012

Mohapatra, D. P., Brar, S. K., Tyagi, R. D., Picard, P., & Surampalli, R. Y. (2014). Analysis and advanced oxidation treatment of a persistent pharmaceutical compound in wastewater and wastewater sludge-carbamazepine. *Science of the Total Environment*, *470–471*, 58–75. https://doi.org/10.1016/j.scitotenv.2013.09.034

Moreira, N. F. F., Sousa, J. M., Macedo, G., Ribeiro, A. R., Barreiros, L., Pedrosa, M., … Silva, A. M. T. (2016). Photocatalytic ozonation of urban wastewater and surface water using immobilized TiO 2 with LEDs: Micropollutants, antibiotic resistance genes and estrogenic activity. *Water Research, 94*, 10-22. https://doi.org/10.1016/j.watres.2016.02.003

Mota, A. L. N., Albuquerque, L. F., Beltrame, L. T. C., Chiavone-Filho, O., Jr., A. M., & Nascimento, C. A. O. (2009). Advanced oxidation processes and their application in the petroleum industry: a review. *Brazilian Journal of Petroleum and Gas,2*(3), 1-21.

Motegh, M., Van Ommen, J. R., Appel, P. W., & Kreutzer, M. T. (2014). Scale-up study of a multiphase photocatalytic reactor - Degradation of cyanide in water over TiO_2. *Environmental Science and Technology*, *48*(3), 1574–1581. https://doi.org/10.1021/es403378e

Munter, R. (2001). Advanced Oxidation Processes - Current Status and Prospect. *Proc. Estonian Acad. Sci. Chem. 82*(1), 59-80. https://doi.org/10.1002/9780470561331.ch18

Nag, T., & Ghosh, A. (2013). Cardiovascular disease risk factors in Asian Indian population: A systematic review. *Journal of Cardiovascular Disease Research, 4*(4), 222-228. https://doi.org/10.1016/j.jcdr.2014.01.004

Nancharaiah, Y. V., Venkata Mohan, S., & Lens, P. N. L. (2016). Recent advances in nutrient removal and recovery in biological and bioelectrochemical systems. *Bioresource Technology, 215,* 173-185. https://doi.org/10.1016/j.biortech.2016.03.129

Natarajan, T. S., Natarajan, K., Bajaj, H. C., & Tayade, R. J. (2011). Energy efficient UV-LED source and TiO_2 nanotube array-based reactor for photocatalytic application. *Industrial and Engineering Chemistry Research, 50*(13), 7753–7762. https://doi.org/10.1021/ie200493k

Natarajan, T. S., Thomas, M., Natarajan, K., Bajaj, H. C., & Tayade, R. J. (2011). Study on UV-LED/TiO_2 process for degradation of Rhodamine B dye. *Chemical Engineering Journal, 169, 126-134*. https://doi.org/10.1016/j.cej.2011.02.066

Nezamzadeh-Ejhieh, A., & Khorsandi, S. (2014). Photocatalytic degradation of 4-nitrophenol with ZnO supported nano-clinoptilolite zeolite. *Journal of Industrial and Engineering Chemistry, 20*(3), 937–946. https://doi.org/10.1016/j.jiec.2013.06.026

Nickels, P., Zhou, H., Basahel, S. N., Obaid, A. Y., Ali, T. T., Al-Ghamdi, A. A., … Lynch, S. A. (2012). Laboratory scale water circuit including a photocatalytic reactor and a portable in-stream sensor to monitor pollutant degradation. *Industrial and Engineering Chemistry Research, 51*(8), 3301–3308. https://doi.org/10.1021/ie202366m

Nidheesh, P. V., Gandhimathi, R., & Ramesh, S. T. (2013). Degradation of dyes from aqueous solution by Fenton processes: A review. *Environmental Science and Pollution Research, 20,* 2099-2132. https://doi.org/10.1007/s11356-012-1385-z

Nidheesh, P. V. (2015). Heterogeneous Fenton catalysts for the abatement of organic pollutants from aqueous solution: a review. *RSC Adv.*, *5*(51), 40552–40577. https://doi.org/10.1039/C5RA02023A

Nidheesh, P. V., Zhou, M., & Oturan, M. A. (2018). An overview on the removal of synthetic dyes from water by electrochemical advanced oxidation processes. *Chemosphere, 197*,210-227. https://doi.org/10.1016/j.chemosphere.2017.12.195

Oladipo, A. A. (2018). MIL-53 (Fe)-based photo-sensitive composite for degradation of organochlorinated herbicide and enhanced reduction of Cr(VI). *Process Safety and Environmental Protection, 116*(C), 413-423. https://doi.org/10.1016/j.psep.2018.03.011

Oladipo, A. A., Ifebajo, A. O., & Gazi, M. (2019). Magnetic LDH-based CoO–$NiFe_2O_4$ catalyst with enhanced performance and recyclability for efficient decolorization of azo dye via Fenton-like reactions. *Applied Catalysis B: Environmental243,* 243-252. https://doi.org/10.1016/j.apcatb.2018.10.050

Onesios, K. M., Yu, J. T., & Bouwer, E. J. (2009). Biodegradation and removal of pharmaceuticals and personal care products in treatment systems: A review. *Biodegradation, 20,* 441-466.. https://doi.org/10.1007/s10532-008-9237-8

Oturan, M. A., & Aaron, J. J. (2014). Advanced oxidation processes in water/wastewater treatment: Principles and applications. A review. *Critical Reviews in Environmental Science and Technology, 44* (23), 2577-2641. https://doi.org/10.1080/10643389.2013.829765

Ozkal, C. B., Koruyucu, A., & Meric, S. (2016). Heterogeneous photocatalytic degradation, mineralization and detoxification of ampicillin under varying pH and incident photon flux conditions. *Desalination and Water Treatment, 57* (39), 18391-18397. https://doi.org/10.1080/19443994.2016.1155175

Pistkovi, V., Tasbihi, M., Vavrova, M., & Stangar, U. L. (2015). Photocatalytic degradation of β-blockers by using immobilized titania/silica on glass slides. *Journal of Photochemistry and Photobiology A: Chemistry*, *305*, 19–28. https://doi.org/10.1016/j.jphotochem.2015.02.014

Pal, A., Gin, K. Y. H., Lin, A. Y. C., & Reinhard, M. (2010). Impacts of emerging organic contaminants on freshwater resources: Review of recent occurrences, sources, fate and effects. *Science of the Total Environment, 408*(24), 6062-6069. https://doi.org/10.1016/j.scitotenv.2010.09.026

Pan, G., Huang, C., Chen, L., & Shiu, W. (2006). Immobilization of TiO_2 onto nonwoven fiber textile by silica sol: photocatalytic activity and duradibility studies. *Journal of Environmental Engineering and Management*, *16*(6), 413–420.

Passalía, C., Alfano, O. M., & Brandi, R. J. (2011). Modeling and experimental verification of a corrugated plate photocatalytic reactor using computational fluid dynamics. *Industrial and Engineering Chemistry Research*, *50*(15), 9077–9086.

Patel, M., Kumar, R., Kishor, K., Mlsna, T., Pittman, C. U., & Mohan, D. (2019). Pharmaceuticals of emerging concern in aquatic systems: Chemistry, occurrence, effects, and removal methods. *Chemical Reviews*, *119*(6), 3510-3673. https://doi.org/10.1021/acs.chemrev.8b00299

Pelaez, M., Nolan, N. T., Pillai, S. C., Seery, M. K., Falaras, P., Kontos, A. G., … Dionysiou, D. D. (2012). A review on the visible light active titanium dioxide photocatalysts for environmental applications. *Applied Catalysis B: Environmental*, *125*, 331-349. https://doi.org/10.1016/j.apcatb.2012.05.036

Pérez, M., Torrades, F., Domènech, X., & Peral, J. (2002). Fenton and photo-Fenton oxidation of textile effluents. *Water Research*, *36*(11), 2703–2710. https://doi.org/10.1016/S0043-1354(01)00506-1

Ping-feng, F. U., Zhuo, Z., Peng, P., & Xue-gang, D. a I. (2008). Photodegradation of Methylene Blue in a Batch Fixed Bed Photoreactor Using Activated Carbon Fibers Supported TiO_2 Photocatalyst. *The Chinese Journal of Process Engineering*, *8*(1), 65–71.

Poulios, I., Malato, S., & Mantzavinos, D. (2015). Photocatalysis: Science and applications. *Applied Catalysis B: Environmental*, *178*, 1-250. https://doi.org/10.1016/j.apcatb.2015.04.001

Prieto-Rodriguez, L., Miralles-Cuevas, S., Oller, I., Aguera, a., Puma, G. L., & Malato, S. (2012). Treatment of emerging contaminants in wastewater treatment plants (WWTP) effluents by solar photocatalysis using low TiO_2 concentrations. *Journal of Hazardous Materials*, *211–212*, 131–137. https://doi.org/10.1016/j.jhazmat.2011.09.008

Radjenović, J., Sirtori, C., Petrović, M., Barceló, D., & Malato, S. (2009). Solar photocatalytic degradation of persistent pharmaceuticals at pilot-scale: Kinetics and characterization of major intermediate products. *Applied Catalysis B: Environmental, 89*(1-2), 255-264. https://doi.org/10.1016/j.apcatb.2009.02.013

Rajeswari, R., & Kanmani, S. (2009). Degradation of pesticide by photocatalytic ozonation process and study of synergistic effect by comparison with photocatalysis and UV/ozonation processes. *Journal of Advanced Oxidation Technologies, 12*(2), 208–214.

Rao, K. D., & Peters, D. H. (2015). Urban health in India: Many challenges, few solutions. *The Lancet Global Health, 3*(12), 729-730. https://doi.org/10.1016/S2214-109X(15)00210-7

Rao, Nageswara N., & Chaturvedi, V. (2007). Photoactivity of TiO_2-coated pebbles. *Industrial and Engineering Chemistry Research, 46*(13), 4406-4414. https://doi.org/10.1021/ie0702532

Rao, Nageswara Neti, Chaturvedi, V., & Li Puma, G. (2012). Novel pebble bed photocatalytic reactor for solar treatment of textile wastewater. *Chemical Engineering Journal, 184*, 90–97. https://doi.org/10.1016/j.cej.2012.01.004

Rasheed, Q. J., Pandian, K., & Muthukumar, K. (2011). Treatment of petroleum refinery wastewater by ultrasound-dispersed nanoscale zero-valent iron particles. *Ultrasonics Sonochemistry, 18*(5), 1138-1142. https://doi.org/10.1016/j.ultsonch.2011.03.015

Rastegar, M., Shadbad, K. R., Khataee, a R., & Pourrajab, R. (2012). Optimization of photocatalytic degradation of sulphonated diazo dye C.I. Reactive Green 19 using ceramic-coated TiO_2 nanoparticles. *Environmental Technology, 33*(7–9), 995–1003. https://doi.org/10.1080/09593330.2011.604859

Rauf, M. A., & Ashraf, S. S. (2009). Fundamental principles and application of heterogeneous photocatalytic degradation of dyes in solution. *Chemical Engineering Journal, 151*(1-3), 10-18. https://doi.org/10.1016/j.cej.2009.02.026

Rauf, M. A., Meetani, M. A., & Hisaindee, S. (2011). An overview on the photocatalytic degradation of azo dyes in the presence of TiO_2 doped with selective transition metals.

Desalination, 276(1-3), 13-27. https://doi.org/10.1016/j.desal.2011.03.071

Ray, A. K. (2009). Photocatalytic Reactor Configurations for Water Purification. Experimentation and Modeling. *Advances in Chemical Engineering, 36,*1-415. https://doi.org/10.1016/S0065-2377(09)00405-0

Reddersen, K., Heberer, T., & Dünnbier, U. (2002). Identification and significance of phenazone drugs and their metabolites in ground- and drinking water. *Chemosphere, 49*(6), 539–544. https://doi.org/10.1016/S0045-6535(02)00387-9

Rizzo, L., Fiorentino, A., & Anselmo, A. (2013). Advanced treatment of urban wastewater by UV radiation: Effect on antibiotics and antibiotic-resistant E. coli strains. *Chemosphere, 92*(2), 171-176. https://doi.org/10.1016/j.chemosphere.2013.03.021

Rodríguez, A., Ovejero, G., Sotelo, J. L., Mestanza, M., & García, J. (2010). Heterogeneous fenton catalyst supports screening for mono azo dye degradation in contaminated wastewaters. *Industrial and Engineering Chemistry Research, 49*(2), 498-505. https://doi.org/10.1021/ie901212m

Romanos, G. E., Athanasekou, C. P., Katsaros, F. K., Kanellopoulos, N. K., Dionysiou, D. D., Likodimos, V., & Falaras, P. (2012). Double-side active TiO_2-modified nanofiltration membranes in continuous flow photocatalytic reactors for effective water purification. *Journal of Hazardous Materials, 211–212*, 304–316. https://doi.org/10.1016/j.jhazmat.2011.09.081

Ruales-Lonfat, C., Barona, J. F., Sienkiewicz, A., Bensimon, M., Vélez-Colmenares, J., Benítez, N., & Pulgarín, C. (2015). Iron oxides semiconductors are efficients for solar water disinfection: A comparison with photo-Fenton processes at neutral pH. *Applied Catalysis B: Environmental, 166-167,* 497-508. https://doi.org/10.1016/j.apcatb.2014.12.007

Sahoo, M. K. (2011). Degradation and mineralization of organic contaminants by Fenton and photo-Fenton processes: Review of mechanisms and effects of organic and inorganic additives. *Research Journal of Chemistry and Environment, 15*, 96-112.

Sahoo, M. K., & Sayoo, L. (2014). Removal of Acid Blue 29 in aqueous solution by Fenton and

Fenton-like processes. *Desalination and Water Treatment, 52*(16-18), 3411-3420. https://doi.org/10.1080/19443994.2013.797672

Saien, J., & Soleymani, A. R. (2012). Feasibility of using a slurry falling film photo-reactor for individual and hybridized AOPs. *Journal of Industrial and Engineering Chemistry, 18*(5), 1683–1688. https://doi.org/10.1016/j.jiec.2012.03.014

Salaeh, S., Kovacic, M., Kosir, D., Kusic, H., Lavrencic Stangar, U., Dionysiou, D. D., & Loncaric Bozic, A. (2017). Reuse of TiO_2-based catalyst for solar driven water treatment; thermal and chemical reactivation. *Journal of Photochemistry and Photobiology A: Chemistry, 333*, 117-129. https://doi.org/10.1016/j.jphotochem.2016.10.015

Saleh, R., & Djaja, N. F. (2014). UV light photocatalytic degradation of organic dyes with Fe-doped ZnO nanoparticles. *Superlattices and Microstructures, 74*, 217-233. https://doi.org/10.1016/j.spmi.2014.06.013

Sangal, V. K., Kumar, V., & Mishra, I. M. (2014). Process Parametric Optimization of a Divided Wall Distillation Column. *Chemical Engineering Communications*, *201*(1), 37–41. https://doi.org/10.1080/00986445.2012.762625

Sangal, V., Kumar, V., & Mishra, M. (2013). Optimization of a divided wall column for the separation of C4-C6 normal paraffin mixture using Box-Behnken design. *Chemical Industry and Chemical Engineering Quarterly*, *19*(1), 107–119. https://doi.org/10.2298/CICEQ121019047S

Saradamma, R. D., Higginbotham, N., & Nichter, M. (2000). Social factors influencing the acquisition of antibiotics without prescription in Kerala State, south India. *Social Science and Medicine, 50*(6), 891-903. https://doi.org/10.1016/S0277-9536(99)00380-9

Sari, M. I., Agustina, T. E., Melwita, E., & Aprianti, T. (2017). Color and COD Degradation in Photocatalytic Process of Procion Red by Using TiO_2 Catalyst under Solar Irradiation, *AIP Conference Proceedings, 1903*(1), 040017. https://doi.org/10.1063/1.5011536

Sarkar, M. B., Choudhuri, B., Bhattacharya, P., Barman, R. N., Ghosh, A., Dwivedi, S. M. M. D., … Mondal, A. (2017). Improved UV Photodetection by Indium Doped TiO_2 Thin Film

Based Photodetector . *Journal of Nanoscience and Nanotechnology*, *18*(7), 4898-4903. https://doi.org/10.1166/jnn.2018.15295

Sarkar, S., Chakraborty, S., & Bhattacharjee, C. (2015). Photocatalytic degradation of pharmaceutical wastes by alginate supported TiO_2 nanoparticles in packed bed photo reactor (PBPR). *Ecotoxicology and Environmental Safety*, *121*, 263–270. https://doi.org/10.1016/j.ecoenv.2015.02.035

Sauer, T. P., Casaril, L., Oberziner, A. L. B., José, H. J., & Moreira, R. de F. P. M. (2006). Advanced oxidation processes applied to tannery wastewater containing Direct Black 38-Elimination and degradation kinetics. *Journal of Hazardous Materials*, *135*(1-3), 274-279. https://doi.org/10.1016/j.jhazmat.2005.11.063

Sayyar, Z., Akbar Babaluo, A., & Shahrouzi, J. R. (2015). Kinetic study of formic acid degradation by Fe^{3+} doped TiO_2 self-cleaning nanostructure surfaces prepared by cold spray. *Applied Surface Science*, *335*, 1–10. https://doi.org/10.1016/j.apsusc.2015.01.014

Scott, J. P., & Ollis, D. F. (1995). Integration of chemical and biological oxidation processes for water treatment: Review and recommendations. *Environmental Progress*, *14*(2), 88–103. https://doi.org/10.1002/ep.670140212

Scotti, R., D'Arienzo, M., Morazzoni, F., & Bellobono, I. R. (2009). Immobilization of hydrothermally produced TiO2 with different phase composition for photocatalytic degradation of phenol. *Applied Catalysis B: Environmental*, *88*(3–4), 323–330. https://doi.org/10.1016/j.apcatb.2008.11.012

Sengupta, T. K., Kabir, M. F., & Ray, A. K. (2001). A Taylor Vortex Photocatalytic Reactor for Water Purification. *Industrial & Engineering Chemistry Research*, *40*(23), 5268–5281. https://doi.org/10.1021/ie001120i

Shad, M. S., Nedjati, A., & Shafiei, M. (2017). Relative Importance of Intellectual Capital Determinants, Using an Artificial Neural Network Approach: Case Study - Mellat Bank of Iran. *Journal of Business & Financial Affairs*, *6*(3), 1000285. https://doi.org/10.4172/2167-0234.1000285

Shah, V. (2012). Evolution of Pharmaceutical Industry: A global Indian & Gujarat perspective. *Journal of Pharmaceutical Science and Bioscientific Research, 2*(5), 219-229.

Shahi, S. K., Kaur, N., & Singh, V. (2016). Fabrication of phase and morphology controlled pure rutile and rutile/anatase TiO_2 nanostructures in functional ionic liquid/water. *Applied Surface Science, 360,* 953-960, . https://doi.org/10.1016/j.apsusc.2015.11.092

Shahrezaei, M., Habibzadeh, S., Babaluo, A. A., Hosseinkhani, H., Haghighi, M., Hasanzadeh, A., & Tahmasebpour, R. (2017). Study of synthesis parameters and photocatalytic activity of TiO_2 nanostructures. *Journal of Experimental Nanoscience, 12*(1), 45-61. https://doi.org/10.1080/17458080.2016.1258495

Shanmugam, G., Sampath, S., Selvaraj, K. K., Larsson, D. G. J., & Ramaswamy, B. R. (2014). Non-steroidal anti-inflammatory drugs in Indian rivers. *Environmental Science and Pollution Research, 21*(2), 921–931. https://doi.org/10.1007/s11356-013-1957-6

Sharma, J., Mishra, I. M., & Kumar, V. (2016). Mechanistic study of photo-oxidation of Bisphenol-A (BPA) with hydrogen peroxide (H_2O_2) and sodium persulfate (SPS). *Journal of Environmental Management, 166,* 12–22. https://doi.org/10.1016/j.jenvman.2015.09.043

Sharmila, V. G., Kumar, S. A., Banu, J. R., Yeom, I. T., & Saratale, G. D. (2019). Feasibility analysis of homogenizer coupled solar photo Fenton process for waste activated sludge reduction. *Journal of Environmental Management, 238,* 251-256. https://doi.org/10.1016/j.jenvman.2019.03.013

Shu, H. Y., & Chang, M. C. (2005). Pilot scale annular plug flow photoreactor by UV/H_2O_2 for the decolorization of azo dye wastewater. *Journal of Hazardous Materials, 125*(1–3), 244–251. https://doi.org/10.1016/j.jhazmat.2005.05.038

Siddique, R., Schutter, G. de, & Noumowe, A. (2009). Effect of used-foundry sand on the mechanical properties of concrete. *Construction and Building Materials, 23*(2), 976–980. https://doi.org/10.1016/j.conbuildmat.2008.05.005

Sillanpää, M., Ncibi, M. C., & Matilainen, A. (2018). Advanced oxidation processes for the removal of natural organic matter from drinking water sources: A comprehensive review.

Journal of Environmental Management, 208, 56-76. https://doi.org/10.1016/j.jenvman.2017.12.009

Singh, H., Chauhan, G., Jain, A. K., & Sharma, S. K. (2017). Adsorptive potential of agricultural wastes for removal of dyes from aqueous solutions. *Journal of Environmental Chemical Engineering, 5*(1), 122-135. https://doi.org/10.1016/j.jece.2016.11.030

Sinha, R., & Khurana, A. (2017). Antibiotics could be contributing to rise of non-communicable diseases. *Down to Earth*, 1–15. http://www.downtoearth.org.in/coverage/a-link-less-explored-59090

Sirés, I., Arias, C., Cabot, P. L., Centellas, F., Garrido, J. A., Rodríguez, R. M., & Brillas, E. (2007). Degradation of clofibric acid in acidic aqueous medium by electro-Fenton and photoelectro-Fenton. *Chemosphere, 66*(9), 11660-1669. https://doi.org/10.1016/j.chemosphere.2006.07.039

Sivagami, K., Krishna, R. R., & Swaminathan, T. (2014). Photo catalytic degradation of pesticides in immobilized bead photo reactor under solar irradiation. *Solar Energy, 103*, 488–493. https://doi.org/10.1016/j.solener.2014.02.001

Song, S., Ying, H., He, Z., & Chen, J. (2007). Mechanism of decolorization and degradation of CI Direct Red 23 by ozonation combined with sonolysis. *Chemosphere, 66*(9), 1782-1788. https://doi.org/10.1016/j.chemosphere.2006.07.090

Souzanchi, S., Vahabzadeh, F., Fazel, S., & Hosseini, S. N. (2013). Performance of an Annular Sieve-Plate Column photoreactor using immobilized TiO_2 on stainless steel support for phenol degradation. *Chemical Engineering Journal, 223*, 268–276. https://doi.org/10.1016/j.cej.2013.02.123

Spasiano, D., Marotta, R., Malato, S., Fernandez-Ibañez, P., & Di Somma, I. (2015). Solar photocatalysis: Materials, reactors, some commercial, and pre-industrialized applications. A comprehensive approach. *Applied Catalysis B: Environmental, 170-171*, 90-123. https://doi.org/10.1016/j.apcatb.2014.12.050

Stamatelatou, K., Frouda, C., Fountoulakis, M. S., Drillia, P., Kornaros, M., & Lyberatos, G.

(2003). Pharmaceuticals and health care products in wastewater effluents: The example of carbamazepine. In *Water Science and Technology: Water Supply, 3*(4), 131-137.

Stephan, B., Ludovic, L., & Dominique, W. (2011). Modelling of a falling thin film deposited photocatalytic step reactor for water purification: Pesticide treatment. *Chemical Engineering Journal, 169*(1–3), 216–225. https://doi.org/10.1016/j.cej.2011.03.016

Steter, J. R., Dionisio, D., Lanza, M. R. V., & Motheo, A. J. (2014). Electrochemical and sonoelectrochemical processes applied to the degradation of the endocrine disruptor methyl paraben. *Journal of Applied Electrochemistry, 44*(12), 1317-1325. https://doi.org/10.1007/s10800-014-0742-7

Su, T., Shao, Q., Qin, Z., Guo, Z., & Wu, Z. (2018). Role of Interfaces in Two-Dimensional Photocatalyst for Water Splitting. *ACS Cataly, 8*(3), 2253-2276. https://doi.org/10.1021/acscatal.7b03437

Su, Y., Wu, Z., Wu, Y., Yu, J., Sun, L., & Lin, C. (2015). 35-Acid Orange II degradation through a heterogeneous Fenton-like reaction using Fe-TiO_2 nanotube arrays as a photocatalyst. *Journal of Materials Chemistry A*, *3*(16), 8537–8544. https://doi.org/10.1039/C5TA00839E

Subrahmanyam, K., & Yadaiah, P. (2000). The impact of paleo-channel on groundwater contamination, Andhra Pradesh, India. *Environmental Geology, 40,* 169-183. https://doi.org/10.1007/PL00013328

Synthesis, S., & Zir-, P. P. (2018). Solvothermal Synthesis, Characterization and Photocatalytic Property of Zirconium Dioxide Doped Titanium Dioxide Spinous Hollow Microspheres with Sunflower Pollen as Bio-templates. *Journal of Colloid And Interface Science, 529,* 111-121. https://doi.org/10.1016/j.jcis.2018.05.091

Talwar, S., Sangal, V. K., & Verma, A. (2018a). Feasibility of using combined TiO_2 photocatalysis and RBC process for the treatment of real pharmaceutical wastewater. *Journal of Photochemistry and Photobiology A: Chemistry*, *353*. https://doi.org/10.1016/j.jphotochem.2017.11.013

Talwar, S., Sangal, V. K., Verma, A., Kaur, P., & Garg, A. (2018b). Modeling, Optimization and

Kinetic Study for Photocatalytic Treatment of Ornidazole Using Slurry and Fixed-Bed Approach. *Arabian Journal for Science and Engineering 43*, 6191-6202. https://doi.org/10.1007/s13369-018-3388-7

Tanaka, K., Padermpole, K., & Hisanaga, T. (2000). Photocatalytic degradation of commercial azo dyes. *Water Research, 34*(1), 327-333. https://doi.org/10.1016/S0043-1354(99)00093-7

Taylor, P., Prabhu, M. V., Karthikeyan, R., & Shanmugaprakash, M. (2015). Desalination and Water Treatment Modeling and optimization by response surface methodology and neural network – genetic algorithm for decolorization of real textile dye effluent using Pleurotus ostreatus : a comparison study, 37–41. https://doi.org/10.1080/19443994.2015.1059372

Tekbaş, M., Yatmaz, H. C., & Bektaş, N. (2008). Heterogeneous photo-Fenton oxidation of reactive azo dye solutions using iron exchanged zeolite as a catalyst. *Microporous and Mesoporous Materials, 115*(3), 594-602. https://doi.org/10.1016/j.micromeso.2008.03.001

Ternes, T. a. (1998). Occurrence of drugs in German sewage treatment plants and rivers1Dedicated to Professor Dr. Klaus Haberer on the occasion of his 70th birthday.1. *Water Research, 32*(11), 3245–3260. https://doi.org/10.1016/S0043-1354(98)00099-2

Thakur, I., Örmeci, B., & verma, A. (2020). Inactivation of E. coli in water employing Fe-TiO_2 composite incorporating in-situ dual process of photocatalysis and photo-Fenton in fixed-mode. *Journal of Water Process Engineering*. 33, 101085. https://doi.org/10.1016/j.jwpe.2019.101085

Threrujirapapong, T., Khanitchaidecha, W., & Nakaruk, A. (2017). Environmental Nanotechnology , Monitoring & Management Treatment of high organic carbon industrial wastewater using photocatalysis process. *Environmental Nanotechnology, Monitoring & Management*, *8*, 163–168. https://doi.org/10.1016/j.enmm.2017.07.006

Thu, H. B., Karkmaz, M., Puzenat, E., Guillard, C., & Herrmann, J. M. (2005). From the fundamentals of photocatalysis to its applications in environment protection and in solar purification of water in arid countries. In *Research on Chemical Intermediates, 39,* (449-461). https://doi.org/10.1163/1568567053956671

Tian, M., Su, Y., Zheng, H., Pei, G., Li, G., & Riffat, S. (2018). A review on the recent research progress in the compound parabolic concentrator (CPC) for solar energy applications. *Renewable and Sustainable Energy Reviews, 82*(1), 1272-1296. https://doi.org/10.1016/j.rser.2017.09.050

Tong, L., Pérez, S., Gonçalves, C., Alpendurada, F., Wang, Y., & Barceló, D. (2011). Kinetic and mechanistic studies of the photolysis of metronidazole in simulated aqueous environmental matrices using a mass spectrometric approach. *Analytical and Bioanalytical Chemistry, 399*(1), 421–428. https://doi.org/10.1007/s00216-010-4320-5

Toor, A. P., Verma, A., Jotshi, C. K., Bajpai, P. K., & Singh, V. (2005). Photocatalytic degradation of 3,4-dichlorophenol using TiO_2 in a shallow pond slurry reactor. *Indian Journal of Chemical Technology, 12*(1), 75-81.

Torres, R. A., Nieto, J. I., Combet, E., Pétrier, C., & Pulgarin, C. (2008). Influence of TiO_2 concentration on the synergistic effect between photocatalysis and high-frequency ultrasound for organic pollutant mineralization in water. *Applied Catalysis B: Environmental, 80*(1-2), 168-175. https://doi.org/10.1016/j.apcatb.2007.11.013

Towler, G., & Sinnott, R. (2013). Chapter 15 - Design of Reactors and Mixers. *Chemical engineering design : principles, practice, and economics of plant and process design, 1(2),* 621-640. https://doi.org/10.1016/b978-0-08-096659-5.00015-8

Tran, N., Drogui, P., Nguyen, L., & Brar, S. K. (2015). Optimization of sono-electrochemical oxidation of ibuprofen in wastewater. *Journal of Environmental Chemical Engineering, 3*(4), 2637-2646. https://doi.org/10.1016/j.jece.2015.05.001

Tran, N. H., Reinhard, M., & Gin, K. Y. H. (2018). Occurrence and fate of emerging contaminants in municipal wastewater treatment plants from different geographical regions-a review. *Water Research, 133,* 182-207. https://doi.org/10.1016/j.watres.2017.12.029

Tribe, M. A., & Alpine, R. L. W. (1986). Scale economies and the "0.6 rule." *Engineering Costs and Production Economics, 10*(1), 271-278. https://doi.org/10.1016/0167-188X(86)90053-4

Tsoumachidou, S., Antoniadis, A., & Poulios, I. (2018). Artificial and solar photocatalytic

mineralization of psychoactive drugs-loaded urban wastewater: Inorganic ions and phytotoxicity assessment. *Process Safety and Environmental Protection, 120*, 37-44. https://doi.org/10.1016/j.psep.2018.08.023

Tsoumachidou, S., Velegraki, T., & Poulios, I. (2016). TiO_2 photocatalytic degradation of UV filter para-aminobenzoic acid under artificial and solar illumination. *Journal of Chemical Technology and Biotechnology*, *91*(6), 1773-1781. https://doi.org/10.1002/jctb.4768

Tuerk, J., Sayder, B., Boergers, A., Vitz, H., Kiffmeyer, T. K., & Kabasci, S. (2010). Efficiency, costs and benefits of AOPs for removal of pharmaceuticals from the water cycle. *Water Science and Technology*, *61*(4), 985–993. https://doi.org/10.2166/wst.2010.004

Turchi, C. S. D. F. O. (1990). Photocatalytic Degradation of Organic Water Contaminants : Mechanisms Involving Hydroxyl Radical Attack, *192*, 178–192.

Vaiano, V., Sacco, O., Pisano, D., Sannino, D., & Ciambelli, P. (2015). From the design to the development of a continuous fixed bed photoreactor for photocatalytic degradation of organic pollutants in wastewater. *Chemical Engineering Science*, *137*, 152–160. https://doi.org/10.1016/j.ces.2015.06.023

Vaiano, V., Sacco, O., Sannino, D., & Ciambelli, P. (2015). Nanostructured N-doped TiO_2 coated on glass spheres for the photocatalytic removal of organic dyes under UV or visible light irradiation. *Applied Catalysis B: Environmental*, *170–171*, 153–161. https://doi.org/10.1016/j.apcatb.2015.01.039

Van Boeckel, T. P., Gandra, S., Ashok, A., Caudron, Q., Grenfell, B. T., Levin, S. A., & Laxminarayan, R. (2014). Global antibiotic consumption 2000 to 2010: An analysis of national pharmaceutical sales data. *The Lancet Infectious Diseases, 14*(8), 742-750. https://doi.org/10.1016/S1473-3099(14)70780-7

Varatharajan, B., & Kanmani, S. (2007). Treatability study of pharmaceutical wastewater by combined solar photo Fenton and activated sludge process. *Journal of Industrial Pollution Control*, *23*(1), 157–164.

Venkata Subba Rao, K., Rachel, a., Subrahmanyam, M., & Boule, P. (2003). Immobilization of

TiO_2 on pumice stone for the photocatalytic degradation of dyes and dye industry pollutants. *Applied Catalysis B: Environmental*, *46*(1), 77–85. https://doi.org/10.1016/S0926-3373(03)00199-1

Veréb, G., Ambrus, Z., Pap, Z., Mogyorósi, K., Dombi, A., & Hernádi, K. (2014). Immobilization of crystallized photocatalysts on ceramic paper by titanium(IV) ethoxide and photocatalytic decomposition of phenol. *Reaction Kinetics, Mechanisms and Catalysis*, *113*(1), 293–303. https://doi.org/10.1007/s11144-014-0734-y

Verlicchi, P., Al Aukidy, M., & Zambello, E. (2012). Occurrence of pharmaceutical compounds in urban wastewater: Removal, mass load and environmental risk after a secondary treatment-A review. *Science of the Total Environment, 429*, 123-155. https://doi.org/10.1016/j.scitotenv.2012.04.028

Verma, A., Prakash, N. T., & Toor, A. P. (2014). An efficient TiO_2 coated immobilized system for the degradation studies of herbicide isoproturon: Durability studies. *Chemosphere, 109*, 7–13. https://doi.org/10.1016/j.chemosphere.2014.02.051

Vermilyea, A. W., & Voelker, B. M. (2009). Photo-fenton reaction at near neutral pH. *Environmental Science and Technology*, *43*(18), 6927–6933. https://doi.org/10.1021/es900721x

Vetrivel, V., Rajendran, K., & Kalaiselvi, V. (2015). Synthesis and characterization of pure titanium dioxide nanoparticles by sol- gel method. *International Journal of ChemTech Research 7*(3), 1090-1097.

Vieira Dos Santos, E., Sáez, C., Cañizares, P., Martínez-Huitle, C. A., & Rodrigo, M. A. (2017). Treating soil-washing fluids polluted with oxyfluorfen by sono-electrolysis with diamond anodes. *Ultrasonics Sonochemistry, 34*, 115-122. https://doi.org/10.1016/j.ultsonch.2016.05.029

Vishnuganth, M. A., Remya, N., Kumar, M., & Selvaraju, N. (2016). Photocatalytic degradation of carbofuran by TiO_2-coated activated carbon: Model for kinetic, electrical energy per order and economic analysis. *Journal of Environmental Management, 181*, 201-207.

https://doi.org/10.1016/j.jenvman.2016.06.016

Vogna, D., Marotta, R., Napolitano, A., Andreozzi, R., & D'Ischia, M. (2004). Advanced oxidation of the pharmaceutical drug diclofenac with UV/H_2O_2 and ozone. *Water Research, 38*(2), 414-422. https://doi.org/10.1016/j.watres.2003.09.028

Vorontsov, A. V. (2019). Advancing Fenton and photo-Fenton water treatment through the catalyst design. *Journal of Hazardous Materials, 372,* 103-112. https://doi.org/10.1016/j.jhazmat.2018.04.033

Wan, T., Ramakrishna, S., & Liu, Y. (2018). Recent progress in electrospinning TiO_2 nanostructured photo-anode of dye-sensitized solar cells. *Journal of Applied Polymer Science, 135*(1), 45649. https://doi.org/10.1002/app.45649

Wang, H., Wu, Z., Zhao, W., & Guan, B. (2007). Photocatalytic oxidation of nitrogen oxides using TiO_2 loading on woven glass fabric. *Chemosphere, 66*(1), 185–190. https://doi.org/10.1016/j.chemosphere.2006.04.071

Wang, J. C., Cui, C. X., Li, Y., Liu, L., Zhang, Y. P., & Shi, W. (2017). Porous Mn doped g-C_3N_4 photocatalysts for enhanced synergetic degradation under visible-light illumination. *Journal of Hazardous Materials, 339, 43-53*. https://doi.org/10.1016/j.jhazmat.2017.06.011

Wang, J., & Wang, S. (2016). Removal of pharmaceuticals and personal care products (PPCPs) from wastewater: A review. *Journal of Environmental Management, 182,* 620-640. https://doi.org/10.1016/j.jenvman.2016.07.049

Wang, N., Zheng, T., Zhang, G., & Wang, P. (2016). A review on Fenton-like processes for organic wastewater treatment. *Journal of Environmental Chemical Engineering, 4(*1), 762-787. https://doi.org/10.1016/j.jece.2015.12.016

Wenderich, K., & Mul, G. (2016). Methods, Mechanism, and Applications of Photodeposition in Photocatalysis: A Review. *Chemical Reviews, 116*(23), 14587-14619. https://doi.org/10.1021/acs.chemrev.6b00327

Werapun, U., Werapun, W., Karrila, S. J., Phatthiya, A., Chumkaew, P., & Pechwang, J. (2018).

Synthesis, Photocatalytic Performance and Kinetic Study of TiO_2/Ag Particles. *Current Nanoscience, 14*(4), 273-279. https://doi.org/10.2174/1573413714666180115121150

WHO. (2014). Antimicrobial resistance. Global report on surveillance. *World Health Organization, 51,*171-172. https://doi.org/10.1007/s13312-014-0374-3

Winston, R., & Welford, W. T. (2008). Two-dimensional concentrators for inhomogeneous media. *Journal of the Optical Society of America, 68*(3), 289-291. https://doi.org/10.1364/josa.68.000289

Yang, Lixia, Xiao, Y., Liu, S., Li, Y., Cai, Q., Luo, S., & Zeng, G. (2010). Photocatalytic reduction of Cr(VI) on WO3 doped long TiO_2 nanotube arrays in the presence of citric acid. *Applied Catalysis B: Environmental, 94*(1-2), 142-149. https://doi.org/10.1016/j.apcatb.2009.11.002

Yang, Longkai, Wang, X., Mai, X., Wang, T., Wang, C., & Li, X. (2018). Constructing Efficient Mixed-ion Perovskite Solar Cells Based on TiO_2 Nanorod Array. *Journal of Colloid And Interface Science, 534,* 459-468. https://doi.org/10.1016/j.jcis.2018.09.045

Yu, Hua, Zhang, S., Zhao, H., Will, G., & Liu, P. (2009). An efficient and low-cost TiO_2 compact layer for performance improvement of dye-sensitized solar cells. *Electrochimica Acta, 54*(4), 1319-1324. https://doi.org/10.1016/j.electacta.2008.09.025

Yu, Hui, Nie, E., Xu, J., Yan, S., Cooper, W. J., & Song, W. (2013). Degradation of Diclofenac by Advanced Oxidation and Reduction Processes: Kinetic Studies, Degradation Pathways and Toxicity Assessments. *Water Research, 47*(5), 1909–1918. https://doi.org/10.1016/j.watres.2013.01.016

Yu, J., Xiang, Q., & Zhou, M. (2009). Preparation, characterization and visible-light-driven photocatalytic activity of Fe-doped titania nanorods and first-principles study for electronic structures. *Applied Catalysis B: Environmental, 90*(3-4), 595-602. https://doi.org/10.1016/j.apcatb.2009.04.021

Zacharakis, A., Chatzisymeon, E., Binas, V., Frontistis, Z., Venieri, D., & Mantzavinos, D. (2013). Solar photocatalytic degradation of bisphenol a on immobilized ZnO or TiO_2.

International Journal of Photoenergy, 2013, 1-9. https://doi.org/10.1155/2013/570587

Zammit, I., Vaiano, V., Ribeiro, A. R., Silva, A. M. T., Manaia, C. M., & Rizzo, L. (2019). Immobilised cerium-doped zinc oxide as a photocatalyst for the degradation of antibiotics and the inactivation of antibiotic-resistant bacteria. *Catalysts, 9*(3), 222. https://doi.org/10.3390/catal9030222

Zapata, A., Oiler, I., Gallax, R., Pulgarin, C., Maldonado, M. I., Malato, S., & Gernjak, W. (2008). Comparison of photo-fenton treatment and coupled photo-fenton and biological treatment for detoxification of pharmaceutical industry contaminants. *Journal of Advanced Oxidation Technologies, 11*(2), 261–269.

Zayani, G., Bousselmi, L., Mhenni, F., & Ghrabi, A. (2009). Solar photocatalytic degradation of commercial textile azo dyes: Performance of pilot plant scale thin film fixed-bed reactor. *Desalination, 246*(1–3), 344–352. https://doi.org/10.1016/j.desal.2008.03.059

Zazouli, M. A., & Shahmoradi, M. (2019). Efficiency of fenton process in olive oil mill wastewater treatment. *Journal of Mazandaran University of Medical Sciences, 29*(176), 1-10.

Zeng, L., Guo, X., He, C., & Duan, C. (2016). Metal-Organic Frameworks: Versatile Materials for Heterogeneous Photocatalysis. *ACS Catalysis, 6*(11), 7935-7947. https://doi.org/10.1021/acscatal.6b02228

Zhang, H., Xiao, R., Huang, H., & Xiao, G. (2009). Comparison of non-catalytic and catalytic fast pyrolysis of corncob in a fluidized bed reactor. *Bioresource Technology, 100*(3), 1428–1434. https://doi.org/10.1016/j.biortech.2008.08.031

Zhang, L., Qin, M., Yu, W., Zhang, Q., Xie, H., & Sun, Z. (2017). Heterostructured TiO_2 / WO_3 Nanocomposites for Photocatalytic Degradation of Toluene under Visible Light, *164*(14), 1086–1090. https://doi.org/10.1149/2.0881714jes

Zhang, M., Gao, J., Chen, T., Annamalai, K. P., & Tao, Y. (2018). Synthesis of carbon nanotube-supported Mn-TiO_2 as a photocatalyst under visible light. *Recent Innovations in Chemical Engineering, 11*(1), 45-49. https://doi.org/10.2174/2405520411666180219150151

Zhang, Meng hui, Dong, H., Zhao, L., Wang, D. xi, & Meng, D. (2019). A review on Fenton process for organic wastewater treatment based on optimization perspective. *Science of the Total Environment, 670*, 110-121. https://doi.org/10.1016/j.scitotenv.2019.03.180

Zhang, Y., Hu, Y., Zhao, J., Park, E., Jin, Y., Liu, Q., & Zhang, W. (2019). Covalent organic framework-supported Fe-TiO_2 nanoparticles as ambient-light-active photocatalysts. *Journal of Materials Chemistry A, 7*,16364-16371. https://doi.org/10.1039/c9ta03649k

Zhang, Z., Anderson, W. A., & Moo-Young, M. (2004). Radiation modeling of air phase corrugated plate photocatalytic reactor. In *Dynamics of Continuous, Discrete and Impulsive Systems Series B: Applications and Algorithms*, *11*, 59–68. https://doi.org/10.1016/j.cej.2004.01.001

Zhang, Zisheng, Anderson, W. A., & Moo-Young, M. (2003). Modeling of corrugated plate photocatalytic reactors and experimental validation. *Chemical Engineering Science*, *58*(3–6), 911–914. https://doi.org/10.1016/S0009-2509(02)00624-3

Zhang, Zisheng, Anderson, W. A., & Moo-Young, M. (2004). Experimental analysis of a corrugated plate photocatalytic reactor. *Chemical Engineering Journal*, *99*(2), 145–152. https://doi.org/10.1016/j.cej.2004.01.001

Zhou, H., & Smith, D. W. (2001). Advanced technologies in water and wastewater treatment. *Canadian Journal of Civil Engineering*, *1*(4), 247-264. https://doi.org/10.1139/s02-020

Ziemiańska, J., Adamek, E., Sobczak, A., Lipska, I., Makowski, A., & Baran, W. (2010). The study of photocatalytic degradation of sulfonamides applied to municipal wastewater. *Physicochemical Problems of Mineral Processing*, *45*, 127–140.

Zuehlke, S., Duennbier, U., & Heberer, T. (2007). Investigation of the behavior and metabolism of pharmaceutical residues during purification of contaminated ground water used for drinking water supply. *Chemosphere*, *69*(11), 1673–1680. https://doi.org/10.1016/j.chemosphere.2007.06.020

LIST OF PUBLICATIONS

❖ PUBLISHED ARTICLES

- Talwar, S., Sangal, V. K. & Verma, A. K. (2019). In-situ dual effect of novel Fe-TiO_2 composite for the degradation of phenazone, *Separation and Purification Technology, 211*, 391-400. doi: 10.1016/j.seppur.2018.10.007. *(Impact Factor: 5.107)*
- Talwar, S., Verma, A. K. & Sangal, V. K. (2019). Modeling and optimization of fixed mode dual effect (photocatalysis and photo-Fenton) assisted Metronidazole degradation using ANN coupled with genetic algorithm, *Journal of Environmental Management, 250,* 109428. doi: 10.1016/j.jenvman.2019.109428. *(Impact Factor: 4.865)*
- Talwar, S., Verma, A. K. & Sangal, V. K. (2020). Plug flow approaching novel reactor employing in-situ dual effect of photocatalysis and photo-Fenton for the degradation of metronidazole, *Chemical Engineering Journal, 382,* 122772. doi: 10.1016/j.cej.2019.122772. *(Impact Factor: 8.355)*
- Talwar, S., Verma, A. K., Sangal, V. K. & Štangar, U.L. (2020). Once through continuous flow removal of Metronidazole by dual effect of photo-Fenton and photocatalysis in a compound parabolic concentrator at pilot plant scale, *Chemical Engineering Journal, 388,* 124184. https://doi.org/10.1016/j.cej.2020.124184. *(Impact Factor: 8.355)*

❖ ARTICLES UNDER REVIEW

- Talwar, S., Verma, A. K. and Sangal, V. K. (2020) 'Application of waste foundry sand as iron titanium dioxide composite incorporating hybrid technology for the synergistic degradation of real industrial pharmaceutical effluent', *Journal of Cleaner Production*. (Ms. Ref. No.:JCLEPRO-D-20-02662) **(1st revision submitted)**

❖ CONFERENCE PRESENTATIONS

- Talwar, S., Verma, A. K. and Sangal, V. K. (2019) 'Dual effect of photocatalysis and photo-Fenton for the removal of pharmaceutical effluent', Oral communication in *TSEM-2019 (International Research Conference on Trends and Innovations in Technology, Sciences, Engineering & Management)* Jawaharlal Nehru University, New Delhi, India

- Talwar, S., Verma, A. K. and Sangal, V. K. (2019) ‘Fuller’s Earth and Foundry sand driven composite for the application of in-situ photo-Fenton and photocatalysis’ Oral communication in National Conference on “Pollution Control Technologies and Sustainable Development” Malaviya National Institute of Technology, Jaipur